CONTRIBUTIONS OF THE INDIVIDUAL *b* SUBUNITS TO THE FUNCTION OF THE PERIPHERAL STALK OF F_1F_0 ATP SYNTHASE

By

TAMMY WENG BOHANNON GRABAR

A DISSERTATION PRESENTED TO THE GRADUATE SCHOOL
OF THE UNIVERSITY OF FLORIDA IN PARTIAL FULFILLMENT
OF THE REQUIREMENTS FOR THE DEGREE OF
DOCTOR OF PHILOSOPHY

UNIVERSITY OF FLORIDA

2004

Copyright 2004

by

Tammy Weng Bohannon Grabar

This document is dedicated to my husband, Chuck, and my daughter, Kaia.

ACKNOWLEDGMENTS

The work illustrated in this dissertation and my growth as a scientist could not have been accomplished without the guidance, encouragement and support of several people on both the professional and personal levels. The first person I would like to thank is my mentor, Dr. Brian Cain. He allowed me to join his laboratory when I was fresh out of college, even though I had no real experiences in a scientific lab. He exhibited extreme patience while teaching me everything from how to hold and operate a pipette to pouring agarose gels to cloning my own plasmids. His evident passion and excitement about science opened my eyes to a whole new world of opportunity. Prior to joining his laboratory, I had never even dreamed of joining graduate school and pursuing a PhD; therefore, I feel extreme gratitude and consider myself very fortunate to have joined his lab. Once I joined the lab, Dr. Cain allowed me the freedom to make my own initial scientific and experimental decisions, which was an excellent teaching method for me, but he was always there for guidance and support whenever it was needed. I would also like to thank him for being so involved in his lab. On any given day, I knew I could have his undivided attention if I needed to consult with him. Over the years Dr. Cain has spent a tremendous amount of time teaching me to think critically about scientific experiments, how to communicate my data and ideas to others, how to give a professional scientific presentation, and how to write scientific papers, and for those countless hours I thank him.

I would also like to thank every person on my committee: Dr. Linda Bloom, Dr. Art Edison and Dr. Dan Purich from my department, and Dr. Julie Maupin-Furlow from the Microbiology and Cell Sciences Department. I have known Dr. Maupin-Furlow the longest. She taught one of the most challenging courses I took as an undergraduate. When an unexpected death occurred in my family, she was kind enough to allow me to postpone an exam without questioning my motive, which was very unusual for most of my professors while I was an undergraduate. Thanks to her, that was the only class in which my grade was not affected that semester. I would also like to thank her for her continual support in helping me get into graduate school and then subsequently taking the time to hike across campus to join my committee meetings. I would like to thank Dr. Purich for teaching me, in the middle of a physical biochemistry class, that sometimes we have to take some time off to go outside and get some fresh air. That was always an important lesson when endless hours in the lab led to careless mistakes. I also enjoyed his sometimes unusual stories and adventures that he had to share with me when I was spending entire days in the biochemistry library studying for exams. I would like to thank Dr. Edison for his constant support and encouragement. He has always been the first person who publicly and very kindly commended me after my journal club presentation. I believe his kind words of support through the years helped me to gain the courage I needed to believe in myself to really deliver a good presentation. I would also like to thank him for his eagerness to understand every aspect about my project. And last, but not least, I would like to thank Dr. Bloom. As a woman in my department and a new mother with a career in academia, she has been a wonderful role model. She has always had kind words and smiles to bestow on me. I would also like to thank her for

assisting me during my committee meetings when discussions of fluorescence started to go over my head.

I would also like to take the time to thank everyone that I had the pleasure of working with in the lab. These are the people I spent countless hours with during the course of the day and held many scientific and personal conversations with, and I am happy to be able to call them my friends. I could not have spent the last five years with a better group of people. Drs. Tammy Otto and Debra Zies were members of the lab when I first joined and were the ones who taught me the ways of the lab. Dr. Michelle Gumz joined the graduate program and subsequently joined Dr. Cain's lab the same time as I. I would like to thank Tammy, Debbie and Michelle for their scientific and personal support as well as sharing with me memories of pool barbeques, wedding showers and baby showers. Dr. Deepa Bhatt joined the lab as a postdoc during my graduate career. Her friendship and scientific guidance have been very valuable to me. I would like to thank her for giving me fantastic advice on all of my oral presentations and reviewing all of my papers.

And finally, I would like to thank my family for all the encouragement, love and support they have unwaveringly offered over the years. I would like to thank my dad for always finding the positive in everything that was negative and always encouraging me to overcome the many obstacles that graduate school hurled towards me. He never lost faith in me, even when I was ready to give up. I would like to thank my mom for her tremendous support as well. She spent a lot of time and energy stocking my refrigerator and freezer full of meals when I found that I did not have the time to care for myself. She has spent many weeks and weekends at my home since my daughter was born so that I

could have extra time to work on my dissertation. And last, but not least, I would like to thank my husband for his constant emotional support and belief in me. He has been with me through the thick and thin of graduate school and never once complained of my emotional torment when things were not going my way. I could not have accomplished this without him.

TABLE OF CONTENTS

Page

ACKNOWLEDGMENTS iv

LIST OF TABLES xii

LIST OF FIGURES xiii

ABBREVIATIONS xvi

ABSTRACT xx

CHAPTER

1 BACKGROUND AND SIGNIFICANCE 1

Introduction 1
Structure and Function of F_1F_0 ATP Synthase 3
The Catalytic Core 6
The αβ hexamer 8
The γ subunit 12
The Rotor Stalk 12
The γ subunit 14
The ε subunit 16
The ring of *c* subunits 21
The Stator Stalk 25
The *a* subunit 27
The δ subunit 33
The *b* subunit 37
Subunit Equivalence 51
F_1F_0 ATP Synthase Mechanism 56
Proton Translocation: Driving Rotation 57
Coupling 60
Catalysis: The Binding Change Mechanism 62
Genetic Expression and Assembly 63
Summary 65

2 INTEGRATION OF UNEQUAL LENGTH *b* SUBUNITS INTO F_1F_0 ATP SYNTHASE 67

Introduction 67
Materials and Methods 69
Materials 69
Strains and Media 70
Recombinant DNA Techniques 70
Mutagenesis and Strain Construction 75
Crude Preparative Procedures 78
Determination of Protein Concentration 80
Ni-Resin Purification 80
Assays of F_1F_0 ATP Synthase Activity 82
Immunoblot Analysis 85
Results 88
HA-Epitope Tagged *b* Subunits 88
Construction and growth characteristics of mutants 88
Effects of epitope tags 90
Expression of different *b* subunits in the same cell 91
Ni-Resin Purification 92
V5-Epitope Tagged *b* Subunits 97
Construction and growth characteristics of mutants 97
Effects of epitope tags 100
Detections of heterodimers 103
Formation of mixed length *b* subunits in F_1F_0 ATP synthase 107
Discussion 111

3 GENETIC COMPLEMENTATION BETWEEN MUTANT *b* SUBUNITS IN F_1F_0 ATP SYNTHASE 114

Introduction 114
Materials and Methods 116
Materials 116
Strains and Media 117
Recombinant DNA Techniques 117
Mutagenesis and Strain Construction 118
Preparative Procedures 120
Immunoblot Analysis 120
Assays of F_1F_0 ATP Synthase Activity 121
Results 121
Construction and Growth Characteristics of Mutants 121
Heterodimer Formation of b_{arg36} Defective Subunits with b_{wt} 123
Heterodimer formation of $b_{\Delta 153 \rightarrow end\text{-}his}$ Complemented with $b_{wt\text{-}V5}$ 128
Heterodimer Formation of $b_{+124\text{-}130\text{-}his}$ Complemented with $b_{wt\text{-}V5}$ 131

Mutual Complementation 135
Discussion 139

4 DEVELOPMENT OF CYSTEINE CHEMICAL MODIFICATIONS OF ALTERED *b* SUBUNITS 143

Introduction 143
Materials and Methods 146
Materials 146
Strains and Media 146
Recombinant DNA Techniques 147
Mutagenesis and Strain Construction 148
Crude Preparative Procedures 152
Assays of F_1F_0 ATP Synthase Activity 152
Immunoblot Analysis 153
Results 153
Construction and Growth Characteristics of Mutants 153
Effects of Cysteine Mutations 157
Discussion 158

5 MUTAGENISIS OF THE AMINO AND CARBOXYL TERMINI OF THE *b* SUBUNIT IN F_1F_0 ATP SYNTHASE 161

Introduction 161
Materials and Methods 165
Materials 165
Strains and Media 165
Recombinant DNA Techniques 166
Mutagenesis and Strain Construction 166
Crude Preparative Procedures 168
Assays of F_1F_0 ATP Synthase Activity 169
Results 169
Amino Terminal Mutations 169
Construction and growth characteristics of mutants 169
Effects of amino terminal mutations 171
Carboxyl Terminal Mutations 173
Construction and growth characteristics of mutants 173
Effects of carboxyl terminal mutation 175
Discussion 176

6 CONCLUSIONS AND FUTURE DIRECTIONS 180

Conclusions 180
Integration of Unequal Length *b* Subunits into F_1F_0 ATP Synthase 181

Genetic Complementation between Mutant *b* Subunits in F_1F_0 ATP synthase....183
Development of Cysteine Chemical Modifications of Altered *b* Subunits....185
Mutagenesis of the Amino and Carboxyl Termini of the *b* subunit in F_1F_0 ATP Synthase....186
Future Directions....188
Complementing Mutant *b* Subunits....189
Function of F_1F_0 ATP Synthase Incorporated with *b* Subunit Heterodimers....190
Positions of the Individual *b* Subunits in F_1F_0 ATP Synthase....190
Length of the Peripheral Stalk in F_1F_0 ATP Synthase Complexes Incorporated with Shortened and Lengthened *b* Subunits....191
Other Implications....195

APPENDIX

A MUTAGENIC OLIGONULCEOTIDES....202

B DEVELOPING PROTOCOL FOR PURIFYING F_1F_0 ATP SYNTHASE....206

Purification of Enzyme Complexes Incorporated with *b* Subunit Heterodimers....206
Culture....206
Disruption of Bacteria....207
Ni-Resin Purification....209
V5-Epitope Iimmunoprecipitation....210
Detection of Purified Enzyme Complexes....210
Assays of F_1F_0 ATP Synthase Activity....211

LIST OF REFERENCES....212

BIOGRAPHICAL SKETCH....237

LIST OF TABLES

Table page

1-1. F_1F_0 ATP synthase subunit equivalency....52

2-1. Aerobic growth properties and membrane-associated ATP hydrolysis activity of mutants expressing epitope tagged *uncF*(*b*) genes....90

3-1. Aerobic growth properties and membrane-associated ATP hydrolysis activity of mutants expressing epitope tagged *uncF*(*b*) genes 122

4-1. Description of *uncF*(*b*) cysteine mutations 149

4-2. Description of the *unc* operon cysteine mutations[1] 154

4-3. Aerobic growth properties and membrane-associated ATP hydrolysis activity of mutants expressing cysteine....156

5-1. Aerobic growth properties and membrane-associated ATP hydrolysis activity of mutants expressing uncF(b) mutations at the amino terminus....170

5-2. Aerobic growth properties and membrane-associated ATP hydrolysis activity of mutants expressing *uncF*(*b*) insertions or deletions throughout the *b* subunit ..175

6-1. Preliminary data of coexpressed mutant *b* subunits. 190

A-1. Oligonucleotide sequences. 203

A-2. Oligonucleotide description.....204

LIST OF FIGURES

Figure page

1-1. Timeline of developing views of F_1F_0 ATP synthase.....5

1-2. Space-filling structural model of *Escherichia coli* F_1F_0 ATP synthase.....7

1-3. Structure of the ε subunit of *E. coli* F_1F_0 ATP synthase.....19

1-4. Controversial models of the *a* subunit topology.....29

1-5. Amino acid sequence of the *E. coli* F_1F_0 ATP synthase *b* subunit.....38

1-6. Gross structure of the *E. coli* F_1F_0 ATP synthase and the domains of the *b* subunit.....40

1-7. Model for F_1F_0 ATP synthase peripheral stalk orientation dependent upon the direction of rotation during ATP synthesis or hydrolysis.....47

1-8. Speculative models for the *b*-like subunits.....55

1-9. Model of proton translocation and torque generation in F_0.....59

1-10. The binding change mechanism.....63

2-1. Oligonucleotides for epitope tags and mutagenesis of *uncF*(*b*).....74

2-2. Construction of the single transcript expression system.....77

2-3. Histidine and HA-epitope-tagged *b* subunit expression system.....89

2-4. Western blot analysis of histidine and HA-epitope tagged *b* subunits.....92

2-5. Investigation of detergent solubilization of F_1F_0 ATP synthase complexes.....94

2-6. Ni-resin purification of F_1F_0, expressing different length *b* subunits, treated with the cross-linker BS^3.....95

2-7. Ni-resin purification of histidine and HA-epitope tagged F_1F_0 treated with the cross-linker BS^3.....96

2-8. Histidine and V5-epitope-tagged *b* subunit expression system.....98

2-9. ATP-driven energization of membrane vesicles prepared from *uncF(b)* gene mutants. 101

2-10. NADH-driven acidification of membrane vesicles prepared from *uncF*(*b*) mutants 102

2-11. Ni-resin purification of F_1F_0 ATP synthase treated with the cross-linker BS^3 106

2-12. Ni-resin purification of F_1F_0 ATP synthase expressing unequal length *b* subunits....108

2-13. Quantitation of *b* subunit heterodimeric F_1F_0....110

2-14. Interactions of *b* subunits of unequal lengths 112

3-1. Oligonucleotides for epitope tags and C-terminal truncation of *uncF*(*b*) 119

3-2. Ni-resin purification of F_1F_0 ATP synthase incorporated with b_{arg36} subunit mutations 124

3-3. ATP-driven energization of membrane vesicles prepared from *uncF*(*b*) arg36 gene mutants....127

3-4. Ni-resin purification of F_1F_0 ATP synthase containing a *b* subunit carboxyl-terminal truncation 129

3-5. ATP-driven energization of membrane vesicles incorporated with F_1F_0 ATP synthase containing a *b* subunit carboxyl-terminal truncation....130

3-6. Ni-resin purification of membranes incorporated with $b_{+124\text{-}130\text{-}his}$ subunit mutation....132

3-7. ATP-driven energization of membrane vesicles incorporated with a defective $b_{+124\text{-}130}$ subunit mutation....133

3-8. Ni-resin purification of F_1F_0 ATP synthase incorporated with complementing defective *b* subunits....136

3-9. ATP-driven energization of membrane vesicles incorporated with F_1F_0 ATP synthase containing complementing defective *b* subunits 137

3-10. Interactions of defective *b* subunit with wild type *b* subunits found in intact F_1F_0 ATP synthase complexes 140

3-11. Model of F_1F_0 ATP synthase incorporated with complementing defective *b* subunits 142

4-1. Model of *E. coli* F_1F_0 ATP synthase 144

4-2. Oligonucleotides for cysteine mutagenesis of the *unc* operon 150

4-3. Expression plasmid of cysteine mutants 155

4-4. Western blot analysis of cysteine mutant *b* subunits of differing length 158

4-5. Model of F_1F_0 ATP synthase with cysteine substitutions in the *b* and δ subunits 159

5-1 Amino acid sequence and domains of the *E. coli b* subunit 162

5-2. Oligonucleotides for mutagenesis at the amino and carboxyl termini in the *unc* operon 167

5-3. ATP-driven energization of membrane vesicles prepared from *b* subunit membrane domain mutants 172

5-4. Amino acid insertion and deletion analysis of the *E. coli b* subunit 174

5-5. Mutations constructed throughout the *b* subunit 177

6-1. Design of FRET experiments to measure the peripheral stalk 193

6-2. Model of rotation inhibition due to a fusion protein on the ε subunit 195

6-3. Sequence alignments of subunits *b* and *b'* from various species with the *b* subunit of *E. coli* 200

B-1. Diagram of purification procedures for homogeneous heterodimeric b_{V5}/b_{his} F_1F_0 ATP synthase complexes 208

ABBREVIATIONS

ACMA, 9-amino-6-chloro-2-methoxyacridine

ADP, adenosine-5'-diphosphate

ala, alanine

AO, tegamineoxide WS-35

Ap, ampicillin

Ap^r, ampicillin resistant

asn, asparagine

ADP, adenosine-5'-diphosphate

ATP, adenosine-5'-triphosphate

$b_{+7\text{-his}}$, seven amino acid insertion in the *b* subunit with a 6X histidine epitope tag at the amino terminus

$b_{\Delta 7\text{-V5}}$, seven amino acid deletion in the b subunit with a V5 epitope tag at the carboxyl terminus

$b_{ser84\rightarrow cys}$, substitution of a cysteine for serine at amino acid position 84 in the *b* subunit

β-ME, β-mercaptoethanol

bp, base pair

BS^3, bis(3-sulfo-N-hydroxysuccinimide ester)

BCA, bicinchoninic acid

BSA, bovine serum albumin

Cm, chloramphenicol

Cm^r, chloramphenicol resistance

cys, cysteine

DACM, N-(7-dimethylamino-4-methyl-coumarinyl)-maleimide

DCCD, dicyclohexylcarbodiimide

$\varepsilon_{\alpha 2}$, the second α-helix in the epsilon (ε) subunit

ECD, 1-ethyl-3[3-dimethylamino]propyl carbodiimide

ECL, enhanced electrochemiluminescence

EDTA, ethylenediaminetetraacetic acid

FPLC, fast polynucleotide liquid chromatography

FRET, fluorescence resonance energy transfer

g, gravitational force

gln, glutamine

glu, glutamate

GFP, green fluorescent protein

HA, peptide epitope of hemagglutinin protein of human influenza virus

ICBR, Interdisciplinary Center for Biotechnology Research

IPTG, isopropyl-1-thio-β-D-galactopyranoside

kb, kilobase

kD, kilodalton

LB, Luria Bertani medium

LBG, Luria Bertani media supplemented with 0.2% glucose

LDAO, lauryldimethylamine oxide

LSB, Laemmli sample buffer

mG, milligram

mL, milliliter

MOPS, 3-[N-morpholino]propanesulfonic acid

NADH, β-nicotineamide adenine dinucleotide, reduced form

NFDM, nonfat dry milk

Ni-CAM, high capacity nickel chelate affinity matrix

NMR, nuclear magnetic resonance spectroscopy

PAGE, polyacrylamide gel electrophoresis

PBS, phosphate-buffered saline

PBST, phosphate-buffered saline supplemented with 0.1% tween20

PCR, polymerase chain reaction

P_i, inorganic phosphate

P/O, number of ATP's made per 2 e^- transferred to oxygen

PVDF, polyvinylidene fluoride

rms, root mean square

ser, serine

SDS, sodium dodecyl sulfate (lauryl sulfate)

TID, 3-(trifluoromethyl)-3-(m-[^{125}I]iodophenyl)diazirine

TBS, tris-buffered saline

thr, threonine

TTBS, tris-buffered saline supplemented with 0.1% tween20

TD, taurodeoxycholate

TE, tris[hydoxymethyl]aminomethane, ethylenediaminetetraacetic acid buffer, pH 8.0

T_M, tris[hydoxymethyl]aminomethane, magnesium sulfate buffer, pH 7.5

Tm, melting temperature of double stranded DNA

Tris, tris[hydoxymethyl]aminomethane

μg, microgram

μL, microliter

V5, epitope found in the P and V proteins of the paramyxovirus, SV5

v/v, volume/volume

wt, wild type

w/v, weight/volume

Abstract of Dissertation Presented to the Graduate School
of the University of Florida in Partial Fulfillment of the
Requirements for the Degree of Doctor of Philosophy

CONTRIBUTIONS OF THE INDIVIDUAL *b* SUBUNITS TO THE FUNCTION OF THE PERIPHERAL STALK OF F_1F_0 ATP SYNTHASE

By

Tammy Weng Bohannon Grabar

August 2004

Chair: Brian D. Cain
Major Department: Biochemistry and Molecular Biology

The universal molecule of biological energetics is adenosine triphosphate (ATP), and the enzyme involved in providing the majority of cellular ATP is F_1F_0 ATP synthase. Enzymes in this family utilize the electrochemical gradient of protons across membranes to synthesize ATP from ADP and inorganic phosphate in a coupled reaction. The cytoplasmic F_1 and the membrane-bound F_0 sectors are linked by two stalk structures, the rotor stalk and the peripheral stalk. Proton conduction through the F_0 sector drives the rotation of the rotor stalk within the catalytic core, which is held steadfast by the peripheral stalk. In *Escherichia coli*, the δ subunit of F_1 and a parallel homodimer of identical *b* subunits constitute the peripheral stalk of F_1F_0 ATP synthase. Work accomplished in this dissertation indicates that the bacterial enzyme does not require two identical *b* subunits to form the dimer. Two different length *b* subunits, with a size difference of at least 14 amino acids, were capable of forming the *b* dimer of an intact F_1F_0 ATP synthase complex. Also, in work presented in this dissertation, a defective

mutation in one region of the *b* subunit was overcome by dimer formation with a second *b* subunit that contained defective mutation in a different region but had a wild-type sequence in the region of the former defective *b* subunit. This mutual complementation between fully defective *b* subunits indicated that each of the two *b* subunits makes a unique contribution to the functions of the peripheral stalk, such that one mutant *b* subunit is making up for what the other is lacking. Interestingly, the equivalent of the bacterial *b* subunit in plants exists as two genetically different subunits, and the mammal counterpart exists as at least four subunits. This work suggests that the individual functions of the *b* subunits may be reflected in the fact that higher organisms evolved to encode multiple *b*-type subunits.

CHAPTER 1
BACKGROUND AND SIGNIFICANCE

Introduction

The premiere of Peter Mitchell's chemiosmotic theory in 1961 eventually resulted in the major breakthrough of the characterization of F_1F_0 ATP synthases. Basically, his theory stated that protons are pumped across energy transducing membranes, thereby creating an electrochemical gradient of protons (1). This proton gradient, also known as the proton-motive force, consists of two components: i) a chemical component due to the concentration gradient of protons and ii) an electrical component, or membrane potential, due to the positive charge of the protons (H^+). As a result, one side of the membrane is more positive than the other. The potential energy of this gradient can then be transduced to chemical energy or utilized to perform work when the protons diffuse back across the membrane from the higher to the lower potential (2). The protons can diffuse across the membrane through specific transmembrane proton conductors, which can synthesize adenosine 5'-triphosphate (ATP) or co-transport solutes, and in the case of bacteria drive flagellar rotation.

The ability to consume nutrients and convert them to energy is required of all living organisms, from microscopic bacteria to plants to humans. The universal molecule of biological energetics is ATP, and in almost all organisms, the central enzyme involved in providing the majority of cellular ATP is F_1F_0 ATP synthase (3-6). F_1F_0 ATP synthases are responsible for the production of ATP in the final step of processes called oxidative phosphorylation and photophosphorylation. They provide the bulk of cellular energy in

the majority of eukaryotes and prokaryotes. The synthesis of ATP occurs at a rate of about 100 s^{-1}, which maintains a concentration of about 3 mM ATP in *Escherichia coli* and greater concentrations in mitochondria and chloroplasts with no noticeable product inhibition (3). In eukaryotes, they are located in the inner mitochondrial membrane, or in the thylakoid membrane of chloroplasts. In most bacteria, F_1F_0 ATP synthase is located in the cytoplasmic membrane. Enzymes in this family utilize the electrochemical gradient of protons across these membranes in order to synthesize ATP from ADP and inorganic phosphate (P_i) in a coupled reaction. In bacteria, the reaction of ATP synthases can be reversed if the situation of a dissipated electrochemical proton gradient arises. In this case, ATP derived from glycolysis can be hydrolyzed in order to pump protons across the membrane, creating a membrane potential. The membrane potential can then be utilized to drive other cellular processes such as the extrusion of sodium ions, nutrient uptake and flagellar rotation.

An explosion of research concerning F_1F_0 ATP synthase has occurred during the past few decades. In particular, a great deal of knowledge of the enzyme has been solved only in the past decade. A plethora of relatively recent reviews concerning every aspect of F_1F_0 ATP synthase can be found in the special editions of *Journal of Bioenergetics and Biomembranes* (volume 32, 2000) and *Biochimica et Biophysica Acta* (volume 1458, 2000) as well as reviews authored by Noji and Yoshida (2001), Senior *et al.* (2002), Capaldi *et al.* (2002) and Weber and Senior (2004). This chapter will provide detailed explanations of what is currently known about F_1F_0 ATP synthase including the mechanism of the enzyme as a whole as well as structure and functions of individual subunits, equivalence of the bacterial enzyme to its eukaryotic equivalents and genetic

expression and assembly. The research presented in this dissertation primarily concerns the *b* subunit of the *Escherichia coli* (*E. coli*) F_1F_0 ATP synthase. Hence the *b* subunit will be discussed extensively later in this chapter.

Structure and Function of F_1F_0 ATP Synthase

The structure and function of F_1F_0 ATP synthases are remarkably similar from bacteria to humans. In *E. coli*, the simplest form of the enzyme, F_1F_0 ATP synthase is a complex enzyme composed of twenty-two polypeptides of eight different types with the stoichiometry of $\alpha_3\beta_3\delta\gamma\varepsilon ab_2c_{10}$ (Figure 1-2) (6, 7). The deduced molecular size is approximately 530 kDa. The structure of F_1F_0 ATP synthase in chloroplasts is very similar with the exception that there are two isoforms of the *b* subunit. On the other hand, the mitochondrial enzyme is more complex, including an extra 7-9 small subunits which are thought to have roles in enzyme regulation (8-10). Discussion of F_1F_0 ATP synthase is commonly divided into two portions, F_1 and F_0. The F_1 portion of the enzyme is composed of the cytoplasmic subunits, $\alpha_3\beta_3\gamma\varepsilon\delta$, and is responsible for the synthesis of ATP. The F_0 portion consists of the membrane-bound subunits, ab_2c_{10}, and is responsible for the translocation of protons through the membrane. New insights concerning the functions and the intersubunit contacts have refined the way F_1F_0 ATP synthase is perceived, dividing discussions of the enzyme into the catalytic core, the rotor (central) stalk and the stator (peripheral) stalk (3, 11-14). The catalytic core consists primarily of the $\alpha_3\beta_3\gamma$ subunits, the rotor stalk consists of the $\gamma\varepsilon c_{10}$ subunits and the stator stalk consists of the $b_2\delta$ subunits.

Over the years, F_1F_0 ATP synthase has received worldwide recognition as the tiniest rotary motor known to mankind (15, 16). Protons passing through the enzyme

complex drive the rotation of the rotor $\gamma\varepsilon c_{10}$ subunits at about 100 Hz. This rotation, which is absolutely essential for the machinery of the enzyme, transmits energy over a distance greater than 100 Å by providing the means by which conformational changes in the F_1 catalytic core, $\alpha_3\beta_3$, take place for the synthesis of ATP (3, 4).

Structural studies of F_1F_0 ATP synthase commenced in the early 1960's and persist to this day in pursuit of a complete high-resolution structure. Negative staining procedures in the early 1960's initially revealed the traditional tripartite features of the enzyme complex from sub-mitochondrial particles, consisting of what was referred to as the headpiece, stalk and basepiece (Figure 1-1) (17). Ten years later, the first electron micrograph of a detergent-solubilized F_1F_0 ATP synthase was published, confirming the existing idea of a tripartite molecule (18). Appreciably, electron microscopy (EM) in combination with other biochemical data of isolated F_1 exposed a hexagonal arrangement of alternating subunits with a seventh mass found in the center of the array (Figure 1-1) (7, 19). Based on this premise it was first suggested that F_1 consisted of an alternating hexagonal array of three α and three β subunits with the γ, δ and ε situated centrally (7). The idea did not gain favorable recognition for some twenty years until verified by x-ray crystallography (20, 21). Continuous improvements in EM technology led to numerous publications of various ATP synthases which defined the average overall dimensions of about 190 Å from top to bottom and about 37 Å assigned to the stalk structure (22-25). Using a combination of traditional biochemical, molecular biological and immunological techniques along with EM, many important discoveries were made that led to what we now understand of F_1F_0 ATP synthase. The first direct evidence for rotation of the stalk appeared in 1990 (24), but was not followed by the visualization of the peripheral stalk,

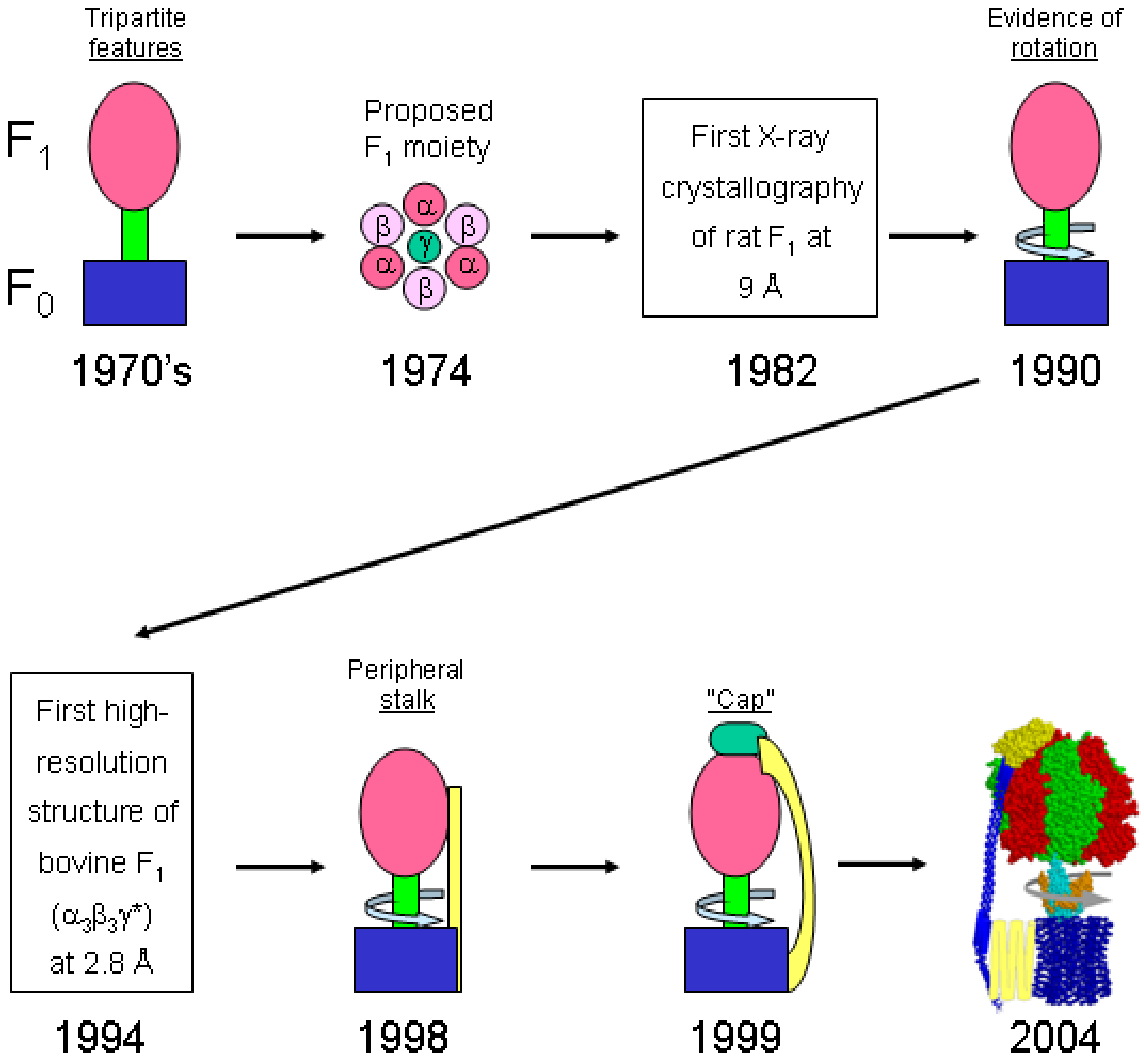

Figure 1-1. Timeline of developing views of F_1F_0 ATP synthase. Electron microscopy and biochemical analysis from the early 1970's through the 1980's allowed visualization of the classical tripartite features of F_1F_0 ATP synthase consisting of what was referred to as the headpiece, stalk and basepiece. Furthermore, the arrangement of the F_1 subunits were first proposed in 1974, though it did not gain favor until high resolution structure was obtained twenty years later. The first direct evidence for rotational catalysis appeared in 1990. Improved EM techniques showed the existence of a peripheral stalk, assigned the role of the "stator" to hold the F_1 sector in place against the proposed rotation, and a "cap" in the late 1990's. In 1994, the first high-resolution structure (2.8 Å) of F_1 appeared, consisting of the $\alpha_3\beta_3$ hexamer with partial structure of the γ subunit. Currently there is no high resolution structure for the entire F_1F_0 ATP synthase complex though many of the subunits have been solved individually or in part by model polypeptides.

assigned the task of the "stator" to hold F_1 in place against the rotation of the centrally located stalk, until many years later (26-29).

Today there is still no high-resolution structure of the entire F_1F_0 ATP synthase enzyme complex from any organism. X-ray crystallographic and NMR data of partial complex structures from rat, bovine, yeast and *E. coli* or model polypeptides deduced from nucleotide sequences have accumulated over the past twenty years to allow for a composite structural model with both high- and low-resolution structures (Figure 1-2). Currently, complete high-resolution structures are available for the α, β, γ, ε and *c* subunits and partial structures for the δ and *b* subunit. There is currently no high-resolution data for the membrane-integral *a* subunit.

The Catalytic Core

The first high-resolution structure, resolved to 2.85 Å, consisted of $\alpha_3\beta_3\gamma$ of F_1 prepared from bovine heart under inhibited conditions and in the absence of P_i and substoichiometric amounts of ADP (20). This major breakthrough was shortly followed by a 2.80 Å F_1 isolated from rat liver in the absence of the physiological cation, Mg^{2+} (21). The arrangement of the subunits in the two structures obtained were exceptionally similar and confirmed Catteral and Pedersen's proposal made two decades prior by showing the three α and three β subunits arranged alternatively with the amino and carboxyl-termini of the γ subunit, each forming an α-helix, extending up through the center of the hexamer (Figure 1-2) . The only difference in the structures, which was the occupancy of the three nucleotide binding sites located at the αβ interfaces, was likely due to the difference in preparation conditions (7) or crystal quality. In the former,

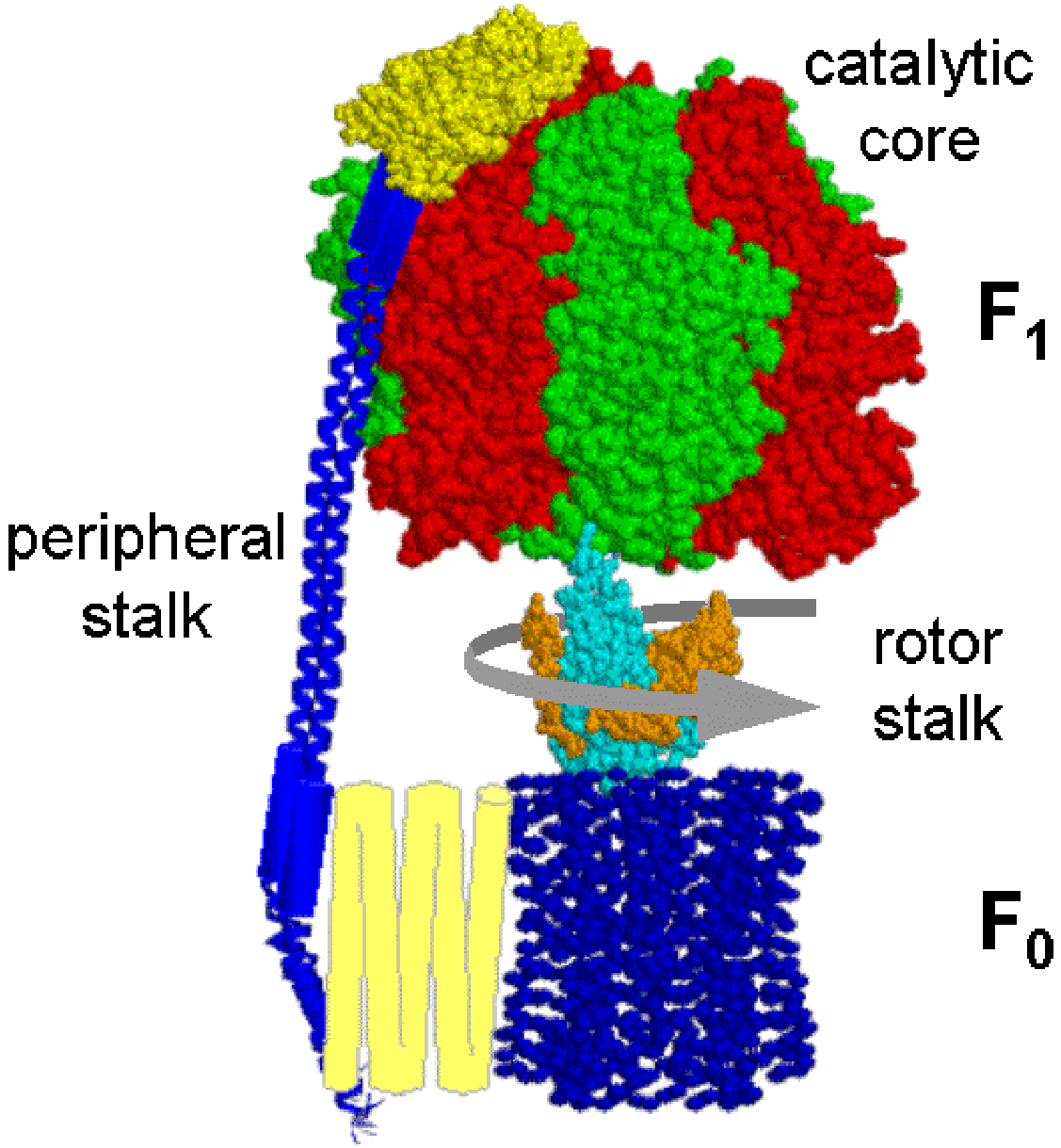

Figure 1-2. Space-filling structural model of *Escherichia coli* F_1F_0 ATP synthase. The model is based on a composite of high and low resolution structures taken from E. coli, yeast and bovine F_1F_0 ATP synthases. F_1F_0 subunits included in the model were $\alpha_3\beta_3\delta\gamma\varepsilon ab_2c_{10}$. The subunits were color coded as follows: α, red; β, green; γ, cyan; ε, orange; δ, yellow; *b*, blue; *a*, brighter yellow; *c*, darker blue. The direction of the arrow indicates the direction of rotation of $\gamma\varepsilon c_{10}$ during ATP synthesis. The yellow and blue cylinders represent the *a* subunit and portions of the *b* subunit that currently have no high-resolution structures from any species.

one of the catalytic sites was empty and in the latter, all three active sites were occupied with nucleotides (20, 21). Since the occupancy state of the three catalytic sites has been of considerable debate, a more accurate depiction of the F_1 moiety, which would give some insight about the mechanism of ATP synthesis, must be attained from crystals obtained under physiological conditions. A more accurate depiction of the structures and roles of each individual subunits of the F_1 ATPase follows.

The αβ hexamer

Homology. The α subunit of the *E. coli* F_1F_0 ATP synthase, product of the *unc*A gene, is the largest subunit consisting of 513 amino acids with a deduced molecular weight of 55,313 Da. The β subunit, a product of the *unc*D gene, is a 459 amino acid subunit, with a molecular weight of 50,325 Da. Based on the primary sequences, the α and β subunits of *E. coli* F_1 have the most obvious homologies in the chlororplast and mitochondrial enzymes (30). The highest conserved subunit from the *E. coli* F_1F_0 ATP synthase is the β subunit with approximately 70% homology with the chloroplast and mitochondria equivalents (31). The α subunits exhibit roughly 50% homology (31). A total of 6 nucleotide binding sites are housed at the αβ interfaces, three catalytic contributed primarily by the β subunit and three noncatalytic housed primarily by the α subunit (32, 33). The nucleotide binding regions have sequence homologies with other proteins that bind nucleotide or phosphate, including secA protein, N-ethylmaleimide sensitive fusion protein, herpes simplex virus UL15, Ca^{2+}-ATPase, H^+/K^+ ATPase and Na^+/K^+ ATPase (34-37). Furthermore, the nucleotide binding motif, GXXXXGKT/S, known as the Walker A motif, which was first identified in the α and β sequences of F_1, has been found to be conserved in the high-resolution structures of other proteins

including p21^{ras}, adenylate kinase, RecA, elongation factor Tu, and transducin-α (20, 38-42).

Tertiary structure. The first high-resolution structure of bovine F_1 resolved at the atomic level (2.8 Å) was solved by Walker's group a decade ago (20). It was found to be a flattened sphere approximately 80 Å high and 100 Å wide with the three α and three β subunits arranged as a hexamer of alternating subunits around a centrally located 90 Å long α-helix formed by the γ subunit. A dimple 15 Å deep is located at the top of F_1. The amino-terminal regions of the α and β subunits were once thought to be in close proximity to the membrane due to labeling experiments (43). Contrary to this early data, the crystallographic data placed the amino-terminal regions on the top of the $\alpha_3\beta_3$ hexamer over 100 Å away from the lipid bilayer.

The folds of the α and β subunits were found to be nearly identical. They each consisted of a six-stranded β-barrel at the amino terminus ($\alpha_{19\text{-}95}$, $\beta_{9\text{-}82}$), a central α-β domain containing the nucleotide-binding site ($\alpha_{96\text{-}379}$, $\beta_{83\text{-}363}$) and a bundle of seven and six helices at the carboxyl termini of the α and β subunits, respectively ($\alpha_{380\text{-}510}$, $\beta_{364\text{-}474}$) (20). The nucleotide binding domain consisted of a nine stranded β-sheet with nine associated α-helices, of which the α-carbons of the seven β-strands and the seven associated helices can be superimposed onto the RecA protein ATP binding site with an rms separation of 1.9 Å (20).

The three catalytic sites were located at the interfaces of the $\alpha_3\beta_3$ hexamer. In the original crystal structure, now commonly referred to as the reference structure, two of the three sites were occupied by nucleotide, containing MgADP ("β_{DP} site") and MgAMP-PNP ("β_{TP} site"). The third site was empty and designated "β_E." The β_{DP} and β_{TP}

subunits were in similar, closed conformations whereas the β_E adopted an open conformation, differing from the other two by a large hinge motion of the carboxyl terminal domain of greater that 20 Å. Subsequently, several high-resolution structures of crystals obtained under various nucleotide conditions gave the same overall structure of bovine F_1 with two nucleotides bound ("two nucleotide structures") (44-49). The β_{TP} site was found to occasionally contain a diphosphate nucleotide, establishing that there is no requirement for β_{TP} to be occupied by a nucleotide triphoshate to produce a conformational change (48). A more recent structure of bovine F_1 solved by the Walker group at 2.0 Å showed all three catalytic sites bound by nucleotide (50). Both the β_{TP} and β_{DP} sites contained MgADP, adopting the closed conformation, whereas the site corresponding to the β_E site in previous structures contained MgADP+P_i and adopted a half-closed conformation. It is thought that the β_{DP} site is actually the catalytic site. The structure of rat liver F_1 was solved (2.8 Å) in the presence of physiological concentrations of nucleotides but in the absence of the physiological cation, Mg^{2+}. In this structure, all three nucleotide binding sites adopted strikingly similar conformations, analogous to the β_{DP} and β_{TP} of the previously reported structure of the bovine F_1. This structure had no indication of the open conformation and showed the presence of nucleotide in all three sites (21). The structure of an $\alpha_3\beta_3$ complex from a thermophilic bacterium was solved in the absence of nucleotides and exhibited all three β subunits in the open conformation, suggesting there is a correlation between the open conformation and the absence of nucleotide (51). A low resolution crystal structure (4.4 Å) of the *E. coli* F_1 has been obtained by Capaldi's group, in which the catalytic sites are thought to be very similar to that of the bovine structure; however, the occupancy state of the nucleotide binding sites

was unclear (52). The frequent reports of "two nucleotide" structures have bewildered scientists due to the vast body of biochemical data from numerous laboratories, using a variety of techniques, which establish indisputably that all three catalytic sites are readily filled with nucleotide (32, 53). It is possible that the enzyme preferentially crystallizes in a ground state intermediate which may occur after the release of product, leaving one site empty and opened (54). Nevertheless, the accumulating structural data may be indicative of several intermediary steps that may form during the synthesis of ATP. A detailed account of the mechanism of ATP synthesis follows later in this chapter.

The crystal structure does offer some insight of the chemical mechanism of ATP synthesis (20). In the β subunit, 4.4 Å from the terminal phosphate of the bound nucleotide triphosphate, there is clearly a density for a water molecule hydrogen bonded to the carboxylate of β_{glu188}. This carboxylate is positioned to allow an inline nucleophilic attack of the water molecule on the terminal phosphate. The guanidinium of a neighboring residue, α_{arg373}, is thought to help stabilize the negative charge on the terminal phosphate during the transition state (20). This same arrangement can be found in the catalytic site of transducin-α (42). The crystal structure also provides some insight as to why the nucleotide binding sites in the α subunit are noncatalytic. There is no spacial equivalent of the carboxylate of β_{glu188} in the α subunit. The spatial equivalence in the α subunit is filled by a α_{gln208}, with the side chain pointed away from the terminal phosphate (20). The binding of the adenine to the noncatalytic site of the α subunit is highly specific, unlike the β subunit nucleotide binding site, which can accommodate GTP, ITP as well as ATP (55, 56). This specificity is due to several hydrogen bonds as well as the presence of the β_{tyr368} close to the 2-position of the adenine ring in the α

subunit, while in the β subunit the adenine is in contact with a hydrophobic interface (20). Though the binding sites in the α subunits are highly specific, the roles remain obscure.

The γ subunit

The γ subunit plays an important role in the catalytic core. Interactions between the amino- and carboxyl-terminal α-helices and the $\alpha_3\beta_3$ subunits are responsible for the conformational changes that result in ATP catalysis. The γ subunit is a fundamental part of the rotor stalk.

The Rotor Stalk

Two narrow stalks, a centrally located stalk and a peripheral stalk, have been observed to link the catalytic core of F_1 and the membrane-bound proton translocating F_0 with about of 40-45 Å in between (27). The central stalk came into view three decades ago via EM and has since become widely referred to as the rotor stalk. The rotor stalk consists of the γ and ε subunits. The bottom of the rotor stalk is connected firmly to the F_0 ring of *c* subunits located in the membrane and the top extends 90 Å within the $\alpha_3\beta_3$ hexamer of F_1 where it forms crucial interactions with both the α and β subunits (57-59).

F_1F_0 ATP synthase is an extraordinary enzyme due to its ability to couple potential energy, obtained from proton translocation through F_0 in the membrane, to the synthesis of chemical energy, over 100 Å away in F_1, by a rapid rotation of subunits. Although predicted by Boyer in the 1970's, evidence of rotation did not appear until the early 1990's. The X-ray crystal structure solved by Walker's group suggested that the γ subunit was the rotating subunit by suggesting it could distribute itself to all three β subunits as opposed to just one (20). Consistent with this idea was inhibition of the F_1

complex by crosslinking the γ subunit to one of the α or β subunits (60, 61) and recovery after photobleaching experiments (62, 63). More convincing evidence was provided when Duncan *et al*. crosslinked the γ subunit to an unlabeled β subunit by disulfide bond and then mixed the γ–β complex with ^{35}S-labeled β subunit (along with the α, δ and ε subunits). When the disulfide bond was broken and ATP was added, the γ subunit was observed to switch from labeled to unlabeled β subunit (64). Finally, direct evidence was achieved in single molecule experiments by attachment of a fluorescent actin filament to the γ subunit and observance of unidirectional rotation of the actin filament upon addition of ATP (15). Direct observation of the rotating γ subunit was soon followed by observance of the rotation of the ε and *c* subunits at the same speed and direction, indicating that these three subunits rotate in synchrony, forming the central rotary machinery of the enzyme complex (65-67). Until very recently, rotation has only been observed in the direction of ATP hydrolysis. Direct evidence for the synthesis of ATP by F_1 has been shown by attaching a magnetic bead to the γ subunit of F_1 fixed to a glass surface and the rotating the bead, in the appropriate direction, using electrical magnets (68).

The first structural information obtained for the ε subunit of *E. coli* was accomplished by nuclear magnetic resonance (NMR) studies (69) and is good agreement with the crystal structure solved at 2.3 Å (70). In all previous crystal structures of the rotor stalk, the portion of the rotor stalk's γ subunit protruding from the F_1 αβ hexamer and the ε subunit were disordered. Recently, the structure of the bovine homologs of the rotor stalk γ and ε subunits has been solved and refined to 2.4 Å (48). The structures of the *E. coli* γ and ε subunits are remarkably similar with that from bovine F_1. When

comparing the structures of the γ and ε rotor stalk obtained under different conditions or from different sources, in combination with an overwhelming amount of biochemical and immunological evidence, it is clear that the domains of the two subunits undergo major shifts in position, which reflects its fundamental role in the synthesis of ATP (20, 44, 48, 71-80).

The γ subunit

In *E. coli*, the γ subunit is the third largest subunit of F_1F_0 ATP synthase, encoded by the *unc*G gene as a 286 residue polypeptide with a deduced molecular weight of 31,563 Da. It plays an essential role in coupling proton transport to the synthesis of ATP. The first visualization of a portion of the γ subunit was a bovine F_1 partial structure solved in combination along with the $\alpha_3\beta_3$ hexamer revealing three α-helices (20). The $\gamma_{209\text{-}272}$ (residues 223-286 in the *E. coli* sequence) carboxyl terminus formed a long (90 Å) α-helix extending from the stalk structure seen by EM to about 15 Å from the top of the hexamer. The bottom half of this helix formed a left-handed anti-parallel coiled coil with a shorter α-helix composed of the amino-terminal residues $\gamma_{1\text{-}45}$ (20). The two helices protruded about 30 Å from the bottom of F_1. An approximately 20° kink in the latter helix was produced by γ_{pro40} and a similar but less pronounced kink was induced by γ_{leu217} in the former (48). A third, much smaller α-helix, composed of $\gamma_{73\text{-}90}$ (residues 83-99 in the *E. coli* sequence) was inclined at about 45 degrees from the larger helices and located directly under the F_1 hexamer.

More recently, the complete structure of the bovine rotor stalk has been solved to 2.4 Å (48). The overall length of the stalk, from the carboxyl terminus of the γ subunit to the very bottom where it contacts the ring of *c* subunits, was 114 Å. The portion that

protrudes from the $\alpha_3\beta_3$ hexamer, i.e. the part seen in electron micrographs, was 47 Å long and 54 Å wide at its largest cross-section. A completely new α/β domain, consisting of a five-strand β-sheet (1-5) and six α-helices (a-f), was identified in the complete structure of the γ subunit. Helices a and f extended into the $\alpha_3\beta_3$ hexamer to form the antiparallel coiled coil discussed previously. Strands 1-3 along with helices b and c formed a Rossman fold that forms extensive interactions with the ε subunit as well as the ring of *c* subunits in the membrane (discussed below). This fold was linked to a β-hairpin, formed by strands 4 and 5, by helix d. Overall, this α/β domain had a globular, oval shape with the dimensions 51 Å wide by 41 Å high. The positioning of the α/β domain at the base of the rotor stalk may provide stability to the structure of the rotor stalk during rotational catalysis (48).

A low-resolution crystal structure of the *E. coli* F_1F_0 ATP synthase γ subunit was solved to 4.4 Å (52). Upon comparison with the high-resolution bovine structure obtained one year later, a few differences were observed (48). Helices a and f (see above) were extended by and extra 12 and 20 residues, respectively. Four additional putative α-helices, designated B and D-F, were found in the *E. coli* structure and had little agreement with the bovine γ subunit structure. *E. coli* helix B runs parallel with the bovine β-strand 5 and may correspond to it. Helix D has no apparent equivalent in the bovine model and helices E and F appear to overlap with regions in the bovine δ (bacterial ε, see Table 1-1) and ε (no equivalent in bacteria) subunits. The remainder of the *E. coli* structure appeared similar to the bovine structure.

The crystal structure displays a strikingly asymmetrical F_1 due to differences in the domains of the α and β subunits and the interactions formed with the single γ subunit

(20). The obvious asymmetric positioning of the coiled coil of the γ subunit is a key feature to the mechanics of the binding change mechanism of F_1F_0 ATP synthase. Its large carboxyl terminus α-helix passes through a hydrophobic sleeve formed by six proline-rich loops of the α and β subunits, undoubtingly resulting in the conformational changes occurring in the catalytic sites (20). In the β_E subunit (see above), several hydrogen bonds are formed with the γ subunit, which forms a "catch", resulting in conformational changes. Specifically, residues γ_{arg254} and γ_{gln255} in the carboxyl terminal helix form hydrogen bongs with $\beta_{E\text{-}asp317}$, $\beta_{E\text{-}thr318}$ and $\beta_{E\text{-}asp319}$. Also, a second "catch" is formed between the carboxyl terminal domain of the β_T subunit and the short helix of the γ subunit. Hydrogen bonds formed between γ_{lys87}, γ_{lys90} and γ_{ala80} with $\beta_{T\text{-}asp394}$ and $\beta_{T\text{-}glu398}$. This sequence of the β subunit, DELSEED (β_{394}-β_{400}), is a portion of the binding site of amphipathic cationic inhibitors and putatively the ATPase inhibitor protein (81-83). Recently, mutations of residues involved in the "catch" loops were shown in inhibit ATP hydrolysis activity by the soluble F_1-ATPase (84). Structural information suggests the two antiparallel coiled coil α-helices of the γ subunit may unwind during rotational catalysis and the ε subunit rotates around the F_1 axis while undertaking a net translation of about 23 Å (85). It is likely that these gross changes observed in the structures revealed individual functional states of the enzyme complex during catalysis.

The ε subunit

The ε subunit of *E. coli* F_1F_0 ATP synthase consists of 138 amino acids with a molecular weight of 15, 068 Da and is encoded by the *unc*C gene. The ε subunit has several putative functions in the F_1F_0 ATP synthase complex including structural, inhibitory and coupling roles. Structurally, the binding of F_1 to F_0 has long been known

to require the presence of the ε subunit, which had implicated it as part of stalk structure (86). In isolated F_1, and in isolated F_1F_0 to a lesser extent, it has been shown to inhibit ATP hydrolysis activity (87-89). The removal of ε from isolated F_1 resulted in up to a 10-fold increase in ATP hydrolysis activity. Furthermore, a truncated version of the ε subunit lost all inhibitory functions but still promoted binding of F_1 to F_0, hence the inhibitory feature has been assigned to the extreme carboxyl terminus (90). It was speculated that it acts as an inhibitor by reducing the rate at which the product is released from the catalytic site (91). Also, the ε subunit, as part of the rotor stalk, plays a role in the coupling of proton translocation to the catalytic site. The ε subunit's diversity of functions is supported by the findings that it produces several points of interactions with the α (61, 74, 92), β (61, 88, 89, 93, 94) and γ (74, 95-97) subunits of F_1 and the *c* (98, 99) subunits of F_0.

An innovative set of experiments conducted by members of the Dunn laboratory made use of different sized fluorescent proteins, ranging from the 12 kDa cytochrome b_{562} protein to the 30 kDa flavodoxin reductase protein with a 20 residue linker (100). The proteins were fused to the carboxyl-terminus of the ε subunit. Since the ε subunit is part of the rotor stalk, according to the concept of rotational catalysis, the fusion of a large protein at this site should sterically hinder rotation due to the presence of the peripheral stalk. Cells expressing the smaller cytochrome b_{562} protein fused to the ε subunit grew on minimal media, indicating a functional F_1F_0 ATP synthase complex. However, cells expressing the larger flavodoxin reductase protein fused to the ε subunit, though found in an intact enzyme, failed to grow. These results provided the first evidence, *in vivo*, supporting rotational catalysis.

High-resolution structural data of the *E. coli* ε subunit was first solved by NMR followed by the X-ray crystal structures of the isolated ε and complexed γε subunits (69, 70, 101). The isolated ε subunit consisted of an 84 residue amino-terminal β-sandwich domain and a 48 residue carboxyl-terminal helix-turn-helix domain in which the two α-helices formed an antiparallel hairpin (70). The β-sandwich consisted of two five-stranded β-sheets folded as a rigid, flattened β-barrel. The structure of the isolated ε subunit from *E. coli* was very similar to the F_1 complex isolated from bovine, which included the $\alpha_3\beta_3\gamma\varepsilon$ subunits (48, 70). Superimposition of 127 of the amino acid Cα resulted in an rms deviation of 1.6 Å. On the other hand, in the *E. coli* γ–ε complex, resolved to 2.1 Å, the ε subunit assumed a strikingly different conformation, in which the two α-helices of the antiparallel hairpin at the carboxyl-terminus are wide apart and wrapped around the γ subunit (Figure 1-3A) (101). Subsequently, both conformations of the ε subunit have been trapped in *E. coli* F_1F_0 ATP synthase by crosslinking experiments, confirming the existence of both in an intact enzyme complex (102). Furthermore, Capaldi's group observed that when the carboxyl-terminal helices assume the hairpin conformation, bringing them closest to the F_0 sector, ATP hydrolysis was activated. Still, the enzyme was fully coupled in the direction of either hydrolysis or synthesis. In contrast, when the two helices were open, assuming a position closer to the F_1 sector, ATP hydrolysis was inhibited and the enzyme functioned only in the direction

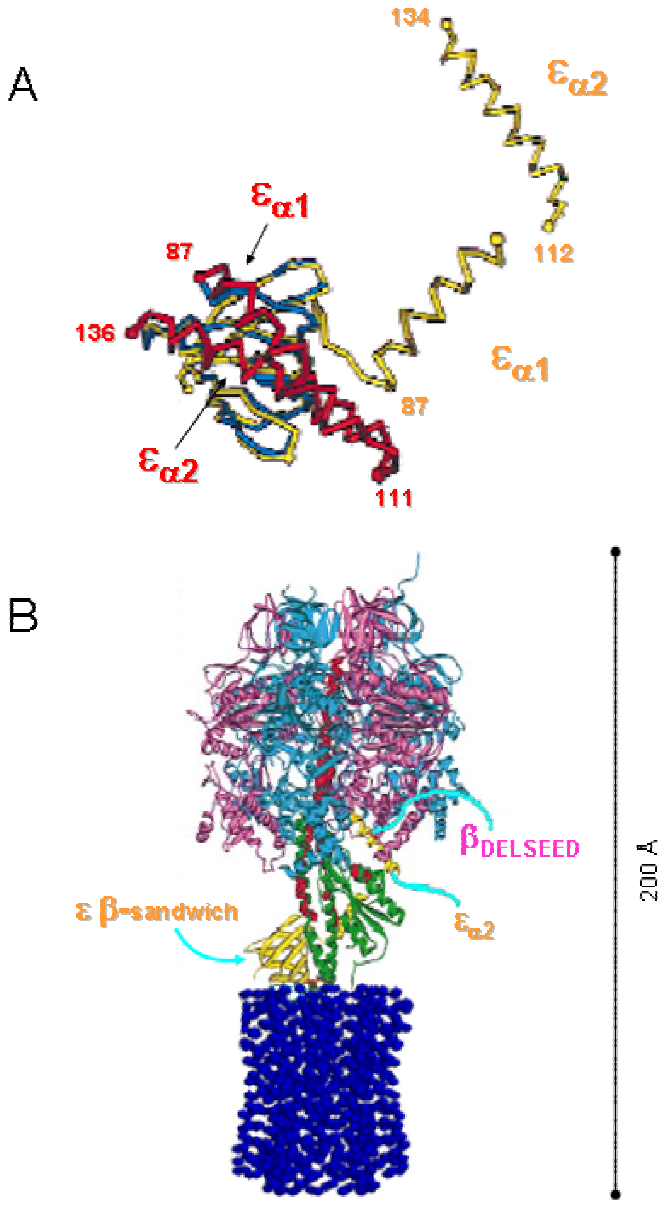

Figure 1-3. Structure of the ε subunit of *E. coli* F_1F_0 ATP synthase. The residue numbers and subunit labels are color coded to match the subunits it represents. The ε subunit has been suggested to undergo large conformational changes during catalysis from an overwhelming amount of biochemical data. Two different structures have been obtained for the ε subunit, confirming the previous data. A) Superimposition of the Cα trace of the ε structure obtained from isolated ε subunit (α-helices shown in red and the β-sandwich shown in blue) with the structure obtained from the γ–ε complex (yellow). B) Composite structural model. Rotor stalk is based on the crystal structure obtained from the γ–ε complex. The $\beta_{DELSEED}$, $\varepsilon_{\alpha 2}$ and the ε β-sandwich are indicated to show the close proximity of $\beta_{DELSEED}$ and $\varepsilon_{\alpha 2}$ as well as the relative distance between the $\varepsilon_{\alpha 2}$ and the ε β-sandwich.

of ATP synthesis. This conformational switch of the ε subunit was therefore suggested to play a key role as a selective inhibitor of ATP hydrolysis and directional regulator of rotational catalysis by acting as a ratchet (102).

Movement of the two ε α-helices was consistent with other observations. Changes in the ε subunit conformation due to nucleotide occupancy in the catalytic sites has been observed in tryptic proteolysis experiments (89). Cysteine replacements in the carboxyl-terminal α-helix ($\varepsilon_{\alpha 2}$) resulted in crosslinks with the α and β subunit (61, 103). More importantly, treatment with a zero-length crosslinker, 1-ethyl-3[3-dimethylamino]propyl carbodiimide (EDC), resulted in a high yield of crosslinks between the ε subunit and the DELSEED (β_{380}- β_{386}) region of the β subunit ($\beta_{DELSEED}$) following ATP hydrolysis in the catalytic sites, but these interactions are disrupted upon the subsequent binding of ATP. Also, in a composite structure of F_1F_0 ATP synthase incorporated with the *E. coli* ε–γ complex as solved by Rodgers and Wilce, the ε β–sandwich was at least 10 Å away from the $\beta_{DELSEED}$ region (Figure 1-3B) (101). The carboxyl-terminal $\varepsilon_{\alpha 2}$ produces several points of interactions with the α, β and γ as well as points of interactions with its own β-sandwich domain α (61, 74, 88, 89, 92-99). In order for the $\varepsilon_{\alpha 2}$ to interact with the $\beta_{DELSEED}$, $\varepsilon_{\alpha 1}$ and the ε subunit β-sandwich domain, it is clear from the structure that the ε subunit would be required to undergo large movements during the catalytic cycle.

In *E. coli*, F_1F_0 ATP synthase can act in two functional directions. In the case of a dissipated electrochemical gradient, the F_1F_0 complex acts primarily as an ATPase in order to pump protons across the membrane to provide a gradient to drive various ion transport activities in the cell. Under severe conditions where cellular ATP levels are exceedingly low the enzyme acts predominantly in the direction of ATP synthesis.

Therefore, one can imagine that the ability to selectively turn off ATP hydrolysis, while preserving ATP synthesis function, may be important for *E. coli*. In mitochondria the ability to control the F_1F_0 ATP synthase complex is essential. It is believed to act exclusively in the direction of ATP synthesis and is strictly regulated (104).

The ring of *c* subunits

The *c* subunit is one of the three membrane-bound F_0 subunits of F_1F_0 ATP synthase. Ten copies of the *c* subunit form a ring in the membrane that plays a crucial role in both proton translocation and rotation of the rotor stalk (105). It is the smallest subunit of the F_1F_0 ATP synthase enzyme complex with 79 amino acids and a molecular weight of 8,256 Da and it is encoded by the *unc*E gene.

Structure and topology. Early biochemical, genetic and immunological data had suggested the structure of the *c* subunit to be that of a helical hairpin with two lipophilic α-helices (amino acids 1-41 and 50-79) separated by a hydrophilic loop (amino acids 42-49). Both of the putative transmembrane helices in the regions of $c_{\text{leu4-leu19}}$ and $c_{\text{phe53-phe76}}$ were vulnerable to chemical modification by the nonpolar photoreactive reagent 3-(trifluoromethyl)-3-(m-[^{125}I]iodophenyl)diazirine (TID), which is a hydrophobic carbene generator that is believed to react from the nonpolar region of the lipid bilayer, indicating that these regions were in fact in the hydrophobic phase of the bilayer (106). The loop region of the hairpin is substantially more polar and antibodies against it were shown to bind to F_1-stripped inverted membrane vesicles suggesting that it resides in the cytoplasmic of the cell (107, 108). Both of the transmembrane helices are devoid of charged amino acids with the noteworthy exception of c_{asp61} in the center of the second helix, which undergoes a protonation and deprotonation cycle during proton translocation

(discussed in "F_1F_0 ATP Synthase Mechanism" below) . Dicyclohexylcarbodiimide (DCCD) reacts specifically with c_{asp61}, blocking proton translocation, and this reaction is blocked by the mutations $c_{ala24\rightarrow ser}$ or $c_{ile28\rightarrow thr}$, suggesting that the *c* subunit is folded in such a way so that the asp61 of the second helix is in close vicinity to residues 24 and 28 of the first helix (109, 110). This model was further supported by the ability to move the critical aspartate from residue 61 in the second helix to residue 24 in the first helix without disruption of enzyme function (111). Also, only one subunit in the ring of 10 *c* subunits need be modified by DCCD to inhibit activity, indicating that each one of the *c* subunits is consecutively involved in proton translocation (112, 113). Furthermore, modification of the *c* subunit by DCCD trapped the configuration of the ε subunit (discussed above), providing evidence for a connection between the *c* and ε subunits (89).

Intersubunit contacts made by the *c* subunit are evident from mutational data and gives some insight to the topology. Mutations constructed in the polar loop region can disrupt the binding of F_1 to F_0 (114-117). Three conserved amino acids, c_{arg41}-c_{gln42}-c_{pro43}, lie at the apex of the polar loop region and are predicted to interact with the F_1 ε subunit (98, 116). F_1F_0 ATP synthase complexes with the uncoupling mutation, $c_{gln42\rightarrow glu}$, were found to be recoupled with a second site suppressor mutation in the ε subunit of F_1, $\varepsilon_{glu31\rightarrow gly,\ val,\ or\ cys}$ (98) and was shortly followed by the observance of disulfide bridge formation between the *c* subunit and the ε and γ subunits (99, 118). Also, switching the essential aspartate from residue 61 in the second helix of the *c* subunit to residue 24 of the first helix (discussed above) resulted in a functional F_1F_0 ATP synthase complex though the cells were not as healthy compared to cells containing a wild-type enzyme complex (111). Eighteen third-site suppressor mutants were found that helped to

optimize this $c_{ala24\rightarrow asp,asp61\rightarrow gly}$ defect, with only five laying on the *c* subunit and 13 in the *a* subunit, all near the a_{arg210} residue, which is required for proton translocation (further discussed below) (119, 120). Early models of the organization of F_0 suggested that the ring of *c* subunits were situated on the periphery, surrounding the centrally located *a* and *b* subunits, which rotated in the center of the ring (121). This model was proved wrong by high-resolution NMR data (122) and cross-linking experiments (123, 124) which indicated that the oligomer of *c* subunits are closely packed with a lipid filled core less than 25 Å wide. The individual *c* subunits are packed front-to-back such that the second helix of each is situated towards the exterior and the first helix is located on the interior, which renders the c_{asp61} exposed to the lipid environment. The uncommonly high pKa (7.1) of the c_{asp61} carboxyl side chain is likely due to this hydrophobic environment (125). Furthermore, scanning force and cryoelectron microscopy demonstrated that F_0 is asymmetrically arranged in the membrane (27, 126, 127). For these reasons, the *a* and *b* subunits are thought to be situated to the periphery of the ring of *c* subunits.

High resolution structures of membrane-bound proteins were nonexistent for many decades past structural determination of soluble proteins and still prove difficult to this day due to their highly hydrophobic nature. The membrane intrinsic *c* subunit of *E. coli*, which was solved by NMR in an organic solvent (chloroform-methanol-water) in the 1990's, was one of the earliest high-resolution structures of a transmembrane helical protein (122, 128-130). Notable, the *c* subunit could be reconstituted from the organic solvent mixture with complete preservation of function; therefore, it was clearly not irreversibly denatured (113). As predicted two decades prior, the *c* subunit folds as a hairpin of two extended α-helices with the c_{asp61} of the second helix packed less than 5 Å

from the c_{ala24} and c_{ile28} of the first helix (122). With the exception of c_{asp61} in the second helix, both helices consist entirely of nonpolar amino acids. The first helix is greatly enriched in glycines and alanines, which led to a smaller diameter. The α-helical structure of the second helix is interrupted around c_{asp61} due to disrupted hydrogen bonds around c_{pro64} which cause the angle of the helical packing to change direction from there to the carboxyl terminus (122). A recent study, using parallax analysis of fluorescence quenching, the proton binding site c_{asp61} was found to be deeply embedded in the membrane at about 1.8 Å from the center of the bilayer (131).

Stoichiometry. The stoichiometry of *c* subunits would be valuable in determining the number of protons transported per ATP synthesized and will directly relate to the P/O ratio of oxidative phosphorylation. However, the number of *c* subunits in F_0 had been a matter of controversy for many years. The number of *c* subunits in an F_1F_0 ATP synthase complex was suggested to be between 9 and 14, but whether this number fluctuated based on the species or environmental conditions or whether it was a fixed number were the two prevailing arguments until just a few years prior. Based on a related family of vacuolar (V-type) ATPases, in which the proposed subunit *c* had evolved into a fused dimer of four transmembrane helices with a single proton-transporting glutamate in the center of the fourth helix, Fillingame *et al*. set out to genetically fuse the *E. coli c* subunit by introducing a flexible loop of similar length (123). The generated *c*-*c* dimers and *c*-*c*-*c* trimers resulted in functional enzyme complexes. In combination with crosslinking studies and normalization to the α/β content of the membranes, the favored stoichiometry was fixed to 12 *c* subunits per F_1F_0 ATP synthase complex (132). More recently, the experiment was revised to include only trimers and tetramers of the *c* subunit (105).

Partial activity was observed in complexes incorporated with eight ($c_4 + c_4$) or nine *c* ($c_3 + c_3$) subunits and crosslinked products of more than 10 *c* subunits were observed but did not purify in intact enzyme complexes. Crosslinking showed that the preferred stoichiometry of *c* subunits in intact *E. coli* F_1F_0 ATP synthase was $c_4 + c_3 + c_3$, or 10 *c* subunits. This number is consistent with the c_{10} oligomer found in the yeast crystal structure of a yeast F_1F_0 ATP synthase consisting of $\alpha_3\beta_3\gamma\varepsilon c_{10}$ resolved to 3.9 Å (58). However, the preferred number may still vary in different species. The archaebacteria *Methanococcus jannascjii* ATP synthase has a natural *c* subunit trimer and therefore cannot incorporate the *E. coli* equivalent of c_{10} in the membrane (133). With 10 *c* subunits present in the membrane 3.3 protons are required per ATP synthesized, which was compatible with the early experimentally determined ratio of 3 H^+/ATP estimated from *E. coli* whole cells (134). This value also indicates a P/O value of 2.3 from NADH-linked substrates and 1.4 for succinate, also compatible with the predicted values of 3 and 2, respectively (135).

The Stator Stalk

The *b* and δ subunits were once believed to form the central, rotating stalk of F_1F_0 ATP synthase. However, high resolution crystallographic data refuted this idea in the mid 1990's (20). The stator stalk did not come into view until improved EM technology observed a peripheral stalk in the late 1990's (26-29) and the visualization of the δ subunit, as a "cap" structure atop F_1F_0 ATP synthase, soon followed (27-29). As its name implies, the role of the stator is to hold the $\alpha_3\beta_3$ hexamer in place against the rotation of the γ subunit during rotational catalysis. Based on chemical crosslinking data, it is currently believed that the *a* subunit resides to the periphery of the ring of *c* subunits with

the membrane-spanning domain of the *b* dimer situated to one side of the *a* subunit where it is in close proximity to both the *a* and *c* subunits. The *b* dimer extends out of the membrane and in a highly elongated conformation reaches to near the top of F_1, making contacts with the α and β subunits along the way and the δ subunit at its extreme carboxyl terminus.

The stator stalk consists of the *b* subunit of F_0 and the δ subunit of F_1. Although the primary function of the *a* subunit of F_0 is considered to be a role in proton translocation along with the c_{10} subunits, it nevertheless plays the part as a stator and will be discussed in this section. Structurally, the *a* subunit plays a role in both the formation of a dynamic interface with the ring of *c* subunits as well as the formation of a secure complex with the *b* dimer. Pursuit of a high-resolution structure for the *a* subunit remains a challenge to this day. The high-resolution structure of the region of the *a* subunit that forms the interface with the c_{10} subunits is eagerly anticipated since it appears to be the crucial region for proton translocation.

In regard to the stator stalk, partial structural information has been obtained for the *E. coli b* subunit membrane spanning domain and the δ subunit amino terminus by NMR studies (136, 137). X-ray crystallography has solved the structure of a model polypeptide based on the dimerization domain of the *b* subunit (138). The binding of F_1 to the membrane-bound F_0 requires both the δ and ε subunits, suggesting that each of the subunits are involved with the stalk structures of F_1F_0 ATP synthase (87, 139, 140). In fact, the δ subunit forms an integral part of the peripheral stalk and the ε subunit functions as part of the central stalk (discussed below). The δ subunit of F_1 has been visualized seated at the very top of the F_1 $\alpha_3\beta_3$ hexamer by EM (11). However, recent

evidence has suggested that the δ subunit may actually be positioned slightly to the side of F_1 in association with only a single α subunit (Figure 1-2) (100, 141-143). The *b* subunit is the primary focus of this dissertation and will be discussed at length later in this chapter.

The *a* subunit

The *E. coli a* subunit is a large, extremely hydrophobic protein encoded by the *unc*B gene and consists of 271 amino acids with a molecular weight of 30,276 Da. All enzymes of the F_1F_0 ATP synthase family contain an *a* subunit homolog with strong primary sequence homology even among evolutionarily diverse species (144). The most highly conserved region resides in the carboxyl-terminal one-third end, amino acid residues $a_{190\text{-}263}$. Notably, in the region that is involved in proton translocation, there is a remarkable conservation of the amino acid residues a_{leu207}, a_{arg210}, $a_{leu211,}$ a_{asn214} and a_{gln252} and an evident conservation of a_{glu219} and a_{his245} at the homologous positions in all *a* subunits from different species (144). The a_{arg210} is the most strictly conserved among all species and does not tolerate substitution with any other amino acid (further discussed below) (145-147).

As mentioned above, there is no high-resolution structural data for the *a* subunit. Also, contradicting models exist concerning the number of transmembrane helices as well as the orientation in the membrane. Difficulty in studying the structure of the *a* subunit arises from its extreme hydrophobicity and the necessity to include the denaturant, trichloroacetate, in purification procedures. This is compounded by the fact that it cannot be expressed at high levels in *E. coli* and is not found in the membrane without the presence of both the *b* and *c* subunits (148-150). Furthermore, the *a* subunit is known to

be a substrate of the protease FtsH, which will rapidly degrade the subunit if it is not in its native state (151). It was readily labeled with TID, which is a hydrophobic carbene generator that is believed to react from the nonpolar region of the lipid bilayer, but its solubility properties made it unsuitable for analysis as was done with the *c* and *b* subunit (106). Consequently, the amino acids in contact with the lipid phase of the bilayer were not identified. Due to difficulties in obtaining high-resolution structural data, much of what is known of the *a* subunit arises from mutational studies.

Topology. Hydropathy analyses indicated five definite membrane-spanning regions and one putative membrane span (121, 140, 152, 153). Much of what is known of the *a* subunit structure and has come from the analysis of cysteine mutagenesis. Greater than 50 cysteine substitutions, which resulted in a functional F_1F_0 ATP synthase, were used in two kinds of experiments (154-158). Various maleimide derivatives were used to search for the surface-accessible regions (154, 155). And double cysteine mutations were used to search for disulfide formation between *a*-*a* and *a*-*c* (153). The results supported the model in which the *a* subunit spans the membrane five times and the fourth span, which includes a_{arg210} is in contact with the second transmembrane α-helix of the *c* subunit (Figure 1-4A). Additionally, residues that were originally thought to be located in the cytoplasm were not labeled, indicating that the six-membrane span model was incorrect (132, 159).

The location of the amino-terminus of the *a* subunit has also been very controversial. A substantial amount of evidence indicates that the carboxyl terminus

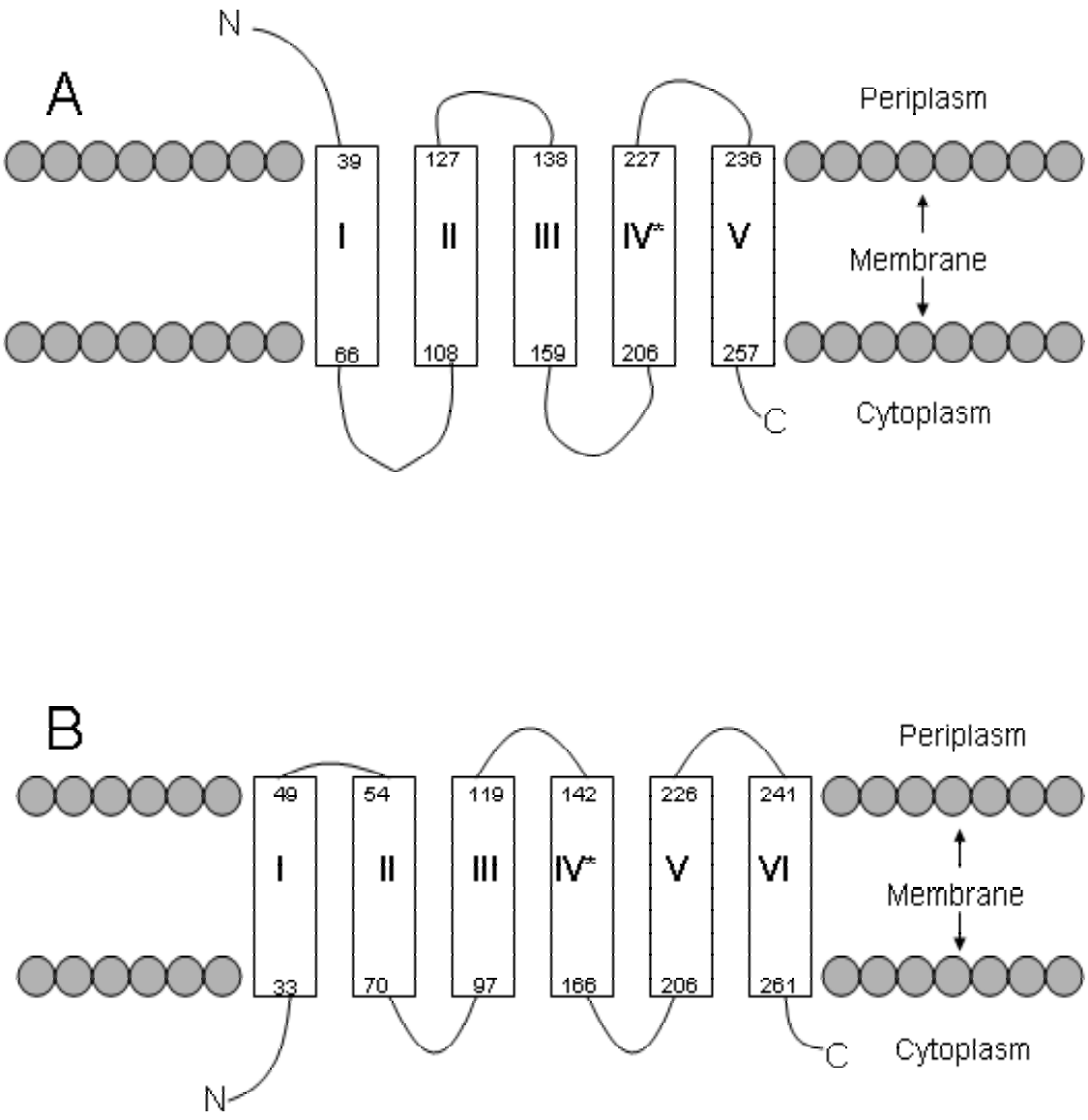

Figure 1-4. Controversial models of the *a* subunit topology. There is no high-resolution structural data for the *a* subunit. Mutagenesis, crosslinking and immunological experiments were used to study the topology. Roman numerals indicate the number of transmembrane helices. Small numbers indicate the relative position of the amino acid residue. Several crosslinking reactions were observed between the fourth helix of the *a* subunit (IV*) and the second helix of the *c* subunit in double cysteine mutants. Contradicting models exist for the topology of the *a* subunit. A) Model with five-transmembrane helices and the amino terminus residing in the periplasm. B) Model with six transmembrane helices and the amino terminus located in the cytoplasm.

resides in the cytoplasm (154, 155, 160). This observation, in combination with the five-transmembrane helices, indicates that the amino-terminus should reside in the periplasmic space. Polyclonal antibodies against a peptide model of the extreme carboxyl-terminus as well as antibodies against epitope tags constructed at the carboxyl terminus of the *a* subunit revealed this region to be located in the cytoplasm (160). Moreover, cysteine substitutions at a_{266} or a_{277} were highly reactive on the cytoplasmic side of the membrane (154, 155). The orientation of the amino and carboxyl-termini was studied by gene fusion proteins and peptide-directed antibodies, revealing a cytoplasmic location of both termini (161, 162). Insertion of epitope tags at various positions also confirmed the cytoplasmic local of both termini, arguing in favor of the controversial six-transmembrane model of the *a* subunit (Figure 1-4B) (160). In the five-transmembrane model a stretch of about 37 amino acids at the amino-terminus resides in the periplasm with only one transmembrane helix, approximately up to residue a_{66}, present (Figure 1-4A) (154-156, 158). In the six-transmembrane model the amino-terminus resides in the cytoplasm with two transmembrane helices present before the first cytoplasmic loop, which range from approximately residues $a_{33\text{-}49}$ and $a_{54\text{-}70}$ (Figure 1-4B) (160).

A series of *a* subunit amino-terminal truncations and internal deletions were constructed and the F_1F_0 ATP synthase function was tested by growth on a succinate minimal media. Assembly of intact complexes was tested by membrane-associated ATPase activity and the presence of the *a* subunit was analyzed by immunoblot analysis (163). Four sections were found to be particularly interesting. The first 33 residues at the amino terminus were shown to be necessary for the insertion of the *a* subunit into the membrane. Two internal deletions, from residues $a_{91\text{-}99}$ and $a_{163\text{-}177}$, resulted in functional

enzyme complexes, indicating that these regions were not important for function. A fourth deletion, from residues $a_{120\text{-}124}$ was concluded to be important for function, but not assemble because high levels of *a* subunit were found in the membrane, but the enzyme was not functional.

The importance of the carboxyl-terminus was also analyzed by constructing a series of early termination codons (164). Sequence alignment of the *a* subunit demonstrates that many bacterial homologues contain glutamate and histidine residues at the extreme carboxyl-terminus (glu-glu-his in *E. coli*). However, truncation of the final four residues had no effect, and truncation of the final nine residues were tolerated at 25°C, suggesting that the extreme carboxyl terminus of the *a* subunit did not significantly contribute to proton conduction or functional interactions with other subunits.

Proton translocation. The first indication that the *a* subunit was directly involved in proton translocation appeared nearly two decades ago when mutations constructed in the *a* subunit ($a_{ser206\rightarrow leu}$ and $a_{his245\text{-}tyr}$) were found to affect F_0-mediated proton pumping without influencing F_1F_0 ATP synthase assembly (165). Since then, not including the cysteine mutations described above, more than 75 missense mutations have been constructed and analyzed in or near the conserved regions of the *a* subunit to chart the amino acids involved in proton translocation. In general, mutation of a conserved amino acid residue impaired F_0-mediated proton translocation, but the severity of the defects varied (166).

The only F_1F_0 ATP synthase *a* subunit residue that is strictly conserved amongst all species, from bacteria to humans, and cannot endure any amino acid substitution, whether basic, acidic or nonpolar, was a_{arg210} (145-147). Mutations at this site abolished both

ATP-driven proton pumping and passive F_0-mediated proton translocation. Growth on succinate minimal media indicated no ATP synthesis by the mutants. The observed effects were shown not to be due to failure of F_1F_0 ATP synthase to assemble because treatment with the detergent lauryldimethylamine oxide (LDAO) released F_1 from the prepared membranes and revealed abundant ATP hydrolysis activity. The presence of assembled F_1F_0 ATP synthase complexes incorporated with an a_{arg210} mutant was later directly confirmed by Dr. James Gardner (167). Substitution with an alanine allowed passive F_0-mediated proton translocation indicating that the proton channel was intact and suggested that the a_{arg210} is not obligatorily protonated or deprotonated during proton conduction (168). A second site suppressor mutation, $a_{gln252\rightarrow arg}$, which partially compensated for the $a_{arg210\rightarrow gln}$ mutation, was identified, and suggested to be in close proximity to each other with residence on the transmembrane helix 5 and 4, respectively, in the five-transmembrane model (121). The a_{210} residue is thought to have a direct role in proton translocation. The orientation of the *a* subunit's fourth transmembrane helix had been determined relative to the orientation of the *c* subunit's second transmembrane α-helix by crosslinking double cysteine mutants (157). Crosslinking data has positioned a_{214} in close proximity to c_{62} and c_{65}, and a_{211} close to c_{69} (157). This places the putative fourth helix of the *a* subunit in contact with the second helix of the *c* subunit. Models have the a_{210} residue positioned near the center of the fourth helix at a level in the lipid bilayer very close to the essential c_{asp61} residue (14). Whether a_{210} is directly protonated/deprotonated or controls protonation of the c_{asp61} residue remain unanswered (169). Insight from a high resolution structure of an intact F_0 is greatly desired and would provide extremely valuable answers to many of the unsolved questions.

Single mutations at residues a_{218}, a_{219} or a_{245} were shown to have a considerable impact on F_0-mediated proton conduction (144, 146, 170). When comparing amino acid sequences of various mitochondria, chloroplast and bacteria, there appears to be an instance of evolutionary covariation with these three amino acids (144). This suggests that when a mutation occurred in one of the three residues, it was accompanied by a second mutation to compensate for any loss in activity. This would cause the two residues to pass through evolution as a hereditary unit. Based on this observation, double mutants were constructed in the *E. coli a* subunit to imitate other lines of evolution (144, 171). Every double mutant studied resulted in functional F_1F_0 ATP synthase complexes with considerably more activity than any of the single residue mutants. Due to the functional relationship, it is possible that these three amino acids are in close proximity to each other.

A few other strongly conserved amino acid residues located on the fourth and fifth transmembrane helices are worth mentioning. Residues a_{asp214} and a_{gln252} were both strongly conserve but found nonessential, with the effects of mutations at these residues varied widely (146, 170, 172, 173). Models of the *a* subunit have these residues lining a water-filled proton channel. Recently, the aqueous accessibility of residues along transmembrane helices 2 and 5 has been shown to extend to both sides of the membrane (174). Also, a mutation at residue 217, $a_{ala217\rightarrow arg}$, blocked proton conduction and inhibited F_1F_0 ATP synthase activity (167).

The δ subunit

The *E. coli* δ subunit is one of the F_1 subunits. It is discussed here because it is an essential part of the F_1F_0 ATP synthase stator stalk. The simplest stator stalks occur in

nonphotosynthetic prokaryotes and consist of a dimer of the F_0 *b* subunits (discussed in the following section) and a single F_1 δ subunit. The δ subunit displays a very low level of conservation across various species. It is a globular protein encoded by the *unc*H gene that consists of 177 residues with a molecular weight of 19,332 Da. It plays essential roles in both the binding of F_1 to F_0 as well as coupling of the catalytic activities of F_1 and F_0 (139, 175-180). Circular dichroism (CD) spectroscopy and sedimentation analysis studies performed on the δ subunit suggested a highly helical and elongated conformation (139).

Structure of the δ subunit. A partial high-resolution structure of the δ subunit has been solved by NMR (137). During the purification procedure, a truncated form of the δ subunit was produced by a bacterial protease. It was revealed to be the amino-terminal 134 amino acids ($\delta_{1\text{-}134}$) by mass spectroscopy and N-terminal sequencing. The same sized δ subunit fragment was often seen in F_1 preparations and could be produced in isolated *E. coli* F_1 by treatment with trypsin without liberating the $\delta_{1\text{-}134}$ from the F_1 complex (89). Furthermore, purified $\delta_{1\text{-}134}$ stably binds to δ-free F_1 preparations. The high affinity of the $\delta_{1\text{-}134}$ subunit for F_1 indicated that the conformation of the δ fragment was preserved during the purification procedure. NMR was performed on both the $\delta_{1\text{-}134}$ fragment and the intact δ subunit; however, the quality of data for the intact subunit was not sufficient enough for structural analysis due to its propensity to aggregate at high concentrations. To date, the carboxyl-terminal 43 amino acid residues ($\delta_{135\text{-}177}$) of the δ subunit is the only portion of the F_1 sector not known at the atomic level.

The amino-terminal 105 residues of the δ subunit formed a dense globular domain, while the region from residues 106-134 was mostly disordered with the exception of one

α-helix (137). The amino-terminal domain, $\delta_{1\text{-}105}$, consisted of a six α-helix bundle with the dimensions 45 x 20 x 30 Å. Helices 1 ($\delta_{4\text{-}20}$) and 2 ($\delta_{24\text{-}38}$), and helices 5 ($\delta_{70\text{-}81}$) and 6 ($\delta_{88\text{-}104}$) organized into V-shapes that intercalated to form a core. Helices 3 ($\delta_{41\text{-}47}$) and 4 ($\delta_{53\text{-}64}$) were packed compactly against this four-helix core. Following this globularly packed domain there was a loop region followed by a seventh α-helix ($\delta_{118\text{-}129}$). Comparison of the structural data for the intact δ subunit against that of the $\delta_{1\text{-}134}$ fragment illustrated the same structure for residues 1-104, but the spectral shift of residues 105-134 was very different. It was possible that the carboxyl-terminal 42 residues missing from the $\delta_{1\text{-}134}$ fragment affects this region of the δ subunit.

δ subunit topology. Taken together with biochemical and immunological data, the structure revealed by NMR revealed that the δ subunit consists of two domains, an amino terminal domain, $\delta_{1\text{-}104}$, and a carboxyl-terminal domain, $\delta_{105\text{-}177}$. Under oxidizing conditions, two native cysteines present in the amino- and carboxyl-terminal domains of the intact δ subunit, δ_{cys64} and δ_{cys140}, respectively, formed a disulfide bond. Furthermore, NMR data indicated some NOE's between the carboxyl-terminal α-helix and the amino-terminal domain. The data indicated that there is probably a close interaction between the amino- and carboxyl-terminal domains of the intact δ subunit.

Proteinase accessibility and immunological analysis were used to examine the topology of the δ subunit (89). The δ subunit was susceptible to trypsin digestion at the carboxyl-terminal 20 residues in isolated F_1, but not in intact F_1F_0 ATP synthase, indicating a protection of the amino-terminal region by F_1. Deletion analysis of the carboxyl-terminal region also implied the importance of the δ subunit in binding F_1 to F_0.

Taken together, these observations suggested that the amino-terminal domain is predominantly involved in the binding of the δ subunit to F_1 and the carboxyl-terminal domain is involved in binding to F_0.

The location of the δ subunit has had a history of being very controversial. Prior to the high resolution structure obtained by Abrahams *et al*. (1994), the *b* and δ subunits were expected to form part of the central stalk of the F_1F_0 ATP synthase enzyme, which is now known to consist of the γ and ε subunits (20). Due to the dimensions, it seemed unlikely that the *b* and γ subunits could fit as part of the central stalk, which implied that they must form a separate connection between F_1 and F_0. Improving EM technology did not allow visualization of the second stalk structure at the periphery of the F_1F_0 ATP synthase complex until many years later (27, 28). Prior to visualization by EM, several early crosslinking studies had been reported in the quest to find the location of the δ subunit binding on F_1, finding it to be on the α subunit (89, 181-184). Notably, crosslinking the δ subunit to the α subunit did not have a great impact on F_1F_0 ATP synthase function, as would be expected if the δ subunit formed part of the stator stalk (185). High-resolution structure of the F_1 $\alpha_3\beta_3$ hexamer with a partial structure of the γ subunit had revealed a dimple in the top of the hexamer approximately 15 Å deep that was adjacent to the core space where the amino- and carboxyl-terminal α-helices of the γ subunit resided (20). EM studies had revealed a "cap" structure at the very top of F_1 in both *E. coli* and mitochondrial complexes (27, 29, 186). It was thus believed that the δ subunit resided in the dimple of F_1 as the cap seen in the EM structures (187). This possibility was refuted when Prescott *et al*. demonstrated the ability to stably incorporate the green fluorescent protein (GFP), via varying length peptide linkers (0, 4 or 27 amino

acids), to the carboxyl-terminus of the γ subunit without interrupting function of the enzyme complex. GFP forms a rigid, stable structure with the dimensions 24 Å wide and 48 Å high (188). This study indicated that the putative cap structure could not possibly occupy the entire dimple atop F_1. More recent evidence has suggested that the δ subunit may actually be positioned slightly to the side of F_1 in association with only a single α subunit (Figure 1-2) (100, 141, 142, 189).

The *b* subunit

The *b* subunit is required for the normal assembly and function of F_1F_0 ATP synthase (190). The *E. coli* F_1F_0 ATP synthase has two identical *b* subunits, which form a homodimer, that are the product of a single gene (Figure 1-2). It is an elongated amphipathic polypeptide that crosses the membrane one time at its amino-terminus and has an extensive hydrophilic carboxyl-terminal domain. This pattern is characteristic of *b*-type subunits of ATP synthases, although the mitochondrial *b* has two consecutive membrane-spanning segments at the amino-terminus (191). Most ATP synthase *b*-type subunits consist of between 150 and 170 amino acid residues. The *E. coli b* subunit, encoded by the *unc*F gene, consists of 156 amino acid residues and has a deduced molecular weight of 17, 265 Da (Figure 1-5).

Domains and Structure. Currently there is no high-resolution structure of the entire *b* subunit. Several factors probably contribute to the difficulty of structural analysis. The *b* dimer is a thin, highly extended, mostly α-helical structure, its dimerization is comparatively weak and reversible (192), and it displays evidence of flexibility (193-195). This has led to alternative low-resolution approaches to study the structure of the *b* dimer such as circular dichroism (CD) spectroscopy, deletion analysis,

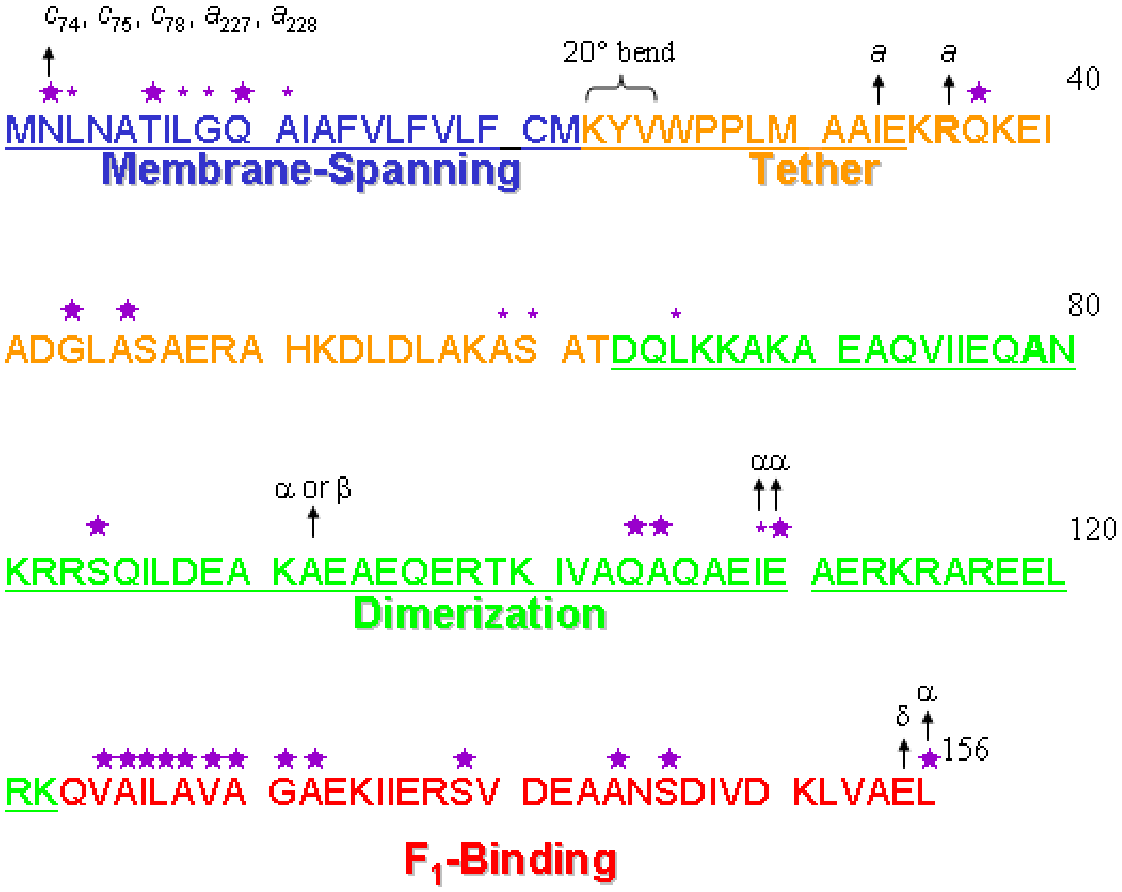

Figure 1-5. Amino acid sequence of the *E. coli* F_1F_0 ATP synthase *b* subunit. The *E. coli* *b* subunit is a 156 residue amphipathic polypeptide. The amino acid sequence and the four domains are shown. The transmembrane domain ($b_{1\text{-}22}$), tether domain ($b_{24\text{-}60}$), dimerization domain ($b_{63\text{-}122}$) and the δ-binding domain ($b_{123\text{-}156}$) are shown in blue, orange, green and red, respectively. The large purple stars indicate residues capable of forming high yields of *b*-*b* crosslinks upon cysteine substitution. The smaller purple stars indicate residues found to form low-yields of crosslinks. The arrows indicate positions crosslinked to other subunits of ATP synthase. High-resolution structures based on model polypeptides consisting of $b_{1\text{-}34}$ and $b_{62\text{-}122}$ (underlined residues) have been solved by NMR and crystallography, respectively. NMR analysis of residues 1-34 has revealed a α-helical structure with a rigid 20° bend at positions 23-26. X-ray crystallography revealed a highly α-helical structure with modeled into a right-handed coiled coil.

analytical ultracentrifugation, chemical crosslinking, and the analysis of tendencies for disulfide bond formation. CD spectroscopy analysis has predicted the secondary structure of the *b* subunit to be approximately 80% α-helical with about 14% β-turn conformation (196).

Although there is no high-resolution structure of the intact F_0 sector, an abundance of evidence suggests the necessity of the *b* subunit to exist in the dimeric state. The hydrophilic region of *b*, consisting of residues $b_{24\text{-}156}$ (also known as b_{sol}), has been expressed and shown to form highly extended dimers capable of binding to F_1-ATPase in solution (197). Sedimentation equilibrium ultracentrifugation gives a molecular weight value of about 30,000 Da for b_{sol}, consistent with a dimer of two 15,000 Da b_{sol} monomers (13). The existence of the dimeric state of the *b* subunits was confirmed by covalently cross-linking the two *b* subunits in the complex and verifying the activity of the enzyme (198). Furthermore, the ability of *b* to bind to F_1 was discovered to be directly proportional to the ability of *b* to form dimers, suggesting the necessity of the *b* dimer formation before the binding of F_1 to the complex (199).

The dimerization of the *b* subunit has been shown to be relatively weak and reversible. The monomeric and dimeric forms of b_{sol} were shown to exist in a dynamic equilibrium and the dimer was converted to the monomeric state at 40°C (192). This same melting characteristic was observed with CD spectroscopy (200). Furthermore, the similar traits were observed in photosynthetic organisms, which encode two different *b*-type subunits, *b* and *b'* (13). When the cytoplasmic regions of the *b* and *b'* subunits from the cyanobacterium *Synechocystis* were expressed individually, the polypeptides were found to only exist in the monomeric state. However, when they were mixed together,

the formation of the dimers was observed by chemical crosslinking and sedimentation equilibrium ultracentrifugation (13). Also, the dimers were observed to melt at 40°C as was the case with the *E. coli b* subunit. The striking similarity between the *E. coli b* subunit and the photosynthetic organism *b* and *b'* subunits indicate that the former is a good model in which to study the *b* subunit.

Cross-linking and deletion analysis has led to the development of a four-domain model of the *E. coli* F_1F_0 ATP synthase *b* subunit (Figures 1-5 and 1-6) (12). Amino acid

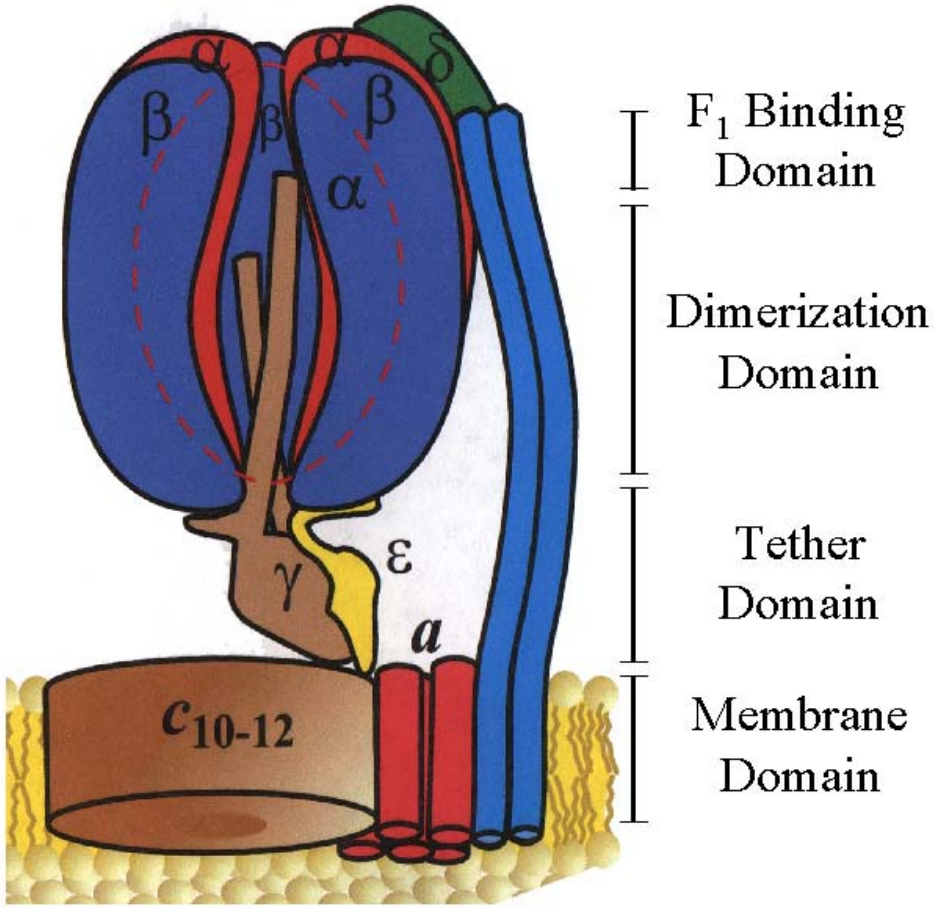

Figure 1-6. Gross structure of the *E. coli* F_1F_0 ATP synthase and the domains of the *b* subunit. The *b* subunit domains were described by Dunn *et al*. (12) The membrane-spanning domain roughly corresponds to amino acid residues 1-22, the tether domain is approximately residues 24-60, the dimerization domain is considered to be residues 60-122, and the F_1-binding domain is roughly residues 123-156.

residues $b_{1\text{-}22}$ corresponds to the hydrophilic membrane spanning domain. Residues $b_{24\text{-}60}$ roughly corresponds to the tether domain, which is the portion of the peripheral stalk often observed in electron micrographs. The dimerization domain, approximately $b_{60\text{-}122}$, is required for the dimerization of the two *b* subunits. And finally, the F_1 binding domain, roughly amino acid residues $b_{123\text{-}156}$, is required for the binding of F_1 to F_0.

The amino-terminal membrane spanning domain, $b_{1\text{-}22}$, forms a single transmembrane span while the large remainder is a polar hydrophilic domain which extends above the cytoplasmic leaflet of the lipid bilayer and reaches towards the top of F_1 (Figure 1-6) (13, 191). A wealth of evidence has suggested this proposed topology for the *b* subunit. The amino terminal region was uniformly vulnerable to chemical modification by the a nonpolar photoreactive reagent, TID, which is a hydrophobic carbene generator that is believed to react from the nonpolar region of the lipid bilayer, indicating that this region was in fact in the hydrophobic phase of the bilayer (106). This observation was consistent with other labeling procedures including the labeling of b_{cys21} by hydrophobic nitrenes (201) or the hydrophobic maleimide N-(7-dimethylamino-4-methyl-coumarinyl)-maleimide (DACM) (148). Modification of b_{cys21} interfered with intersubunit interactions within F_0. Furthermore, reconstitution of the F_0 subunits upon labeling the *b* subunit with DACM resulted in reduced proton translocation as well as F_1 binding affinities (148). TID failed to label the region $b_{asn2\rightarrow gln10}$, indicating that the first few residues at the amino-terminus protrude into the periplasm (106)

Despite attempts by several laboratories, there is presently no high-resolution structure of the entire *b* subunit. Therefore, model polypeptides have been constructed in order to elucidate the structure of the *b* subunit by domain. A model polypeptide

comparable to residues b_{1-34}, which contains the membrane-spanning domain, dissolved in a 4:4:1 v/v mixture of chloroform/methanol/water previously used for solving the structure of subunit *c*, has been solved by NMR (136). The data revealed an α-helical monomeric structure with a 20º bend at residues 23-26 (KYVW) (Figure 1-5). The hydrophobic residues, b_{4-22}, formed an α-helix, followed by the 20° bend, and then resumed with α-helical structure from residues b_{27-34}. The bend was proposed to be positioned as the *b* subunit exits the membrane. A series of cysteine substitutions resulted in a high yield of crosslinks formed at residues b_2, b_6, and b_{10} (Figure 1-5). A lower yield of crosslinks were observed to form at residues b_3, b_8, b_9 and b_{11} (Figure 1-5). No crosslinks were observed when cysteines were substituted for residues 12-21. The observance of continuous crosslinks between residues b_{6-11} were suggested to indicate a dynamic interaction between the contacting faces of the two *b* subunits in this region (132). These observations led to a dimeric model in which the extreme amino-termini of the *b* subunits crossed each other in close proximity at an angle of about 35° in the region of residues b_{4-11}, and then the two *b* subunits angled apart as they traverse the membrane towards the cytoplasmic side (Figure 1-5) (136). The region of the 20° bend, b_{23-26}, was suggested to change the direction of the second α-helix, b_{27-33}, such that it would extend into the cytoplasm at an angle perpendicular to the plan of the membrane. This model was confirmed by a systematic mutational analysis of the membrane-spanning domain performed by Hardy *et al*. (202).

The tether domain of the *b* subunit, roughly b_{24-60}, is the least defined part of the subunit domains from a structural point of view. It corresponds to the portion of the peripheral stalk often seen in electron micrographs and is called “tether” simply because

it is the section of the *b* subunit that links the more defined membrane-spanning and dimerization domains Figure 1-6). There is no high resolution structure for this region of the *b* subunit. The NMR structure of $b_{1\text{-}34}$, described above extended slightly within this domain, revealing an α-helix at least up through residue b_{34} .(136) Also, a heptad repeat, extending from just outside of the membrane and continuing without interruption up to residue b_{ala79} suggests the structure to be a coiled coil (197, 203). Though crosslinking studies showed that the tether domains of the two *b* subunits are in parallel and in close proximity, this domain contributes little to the stability of the dimerization of the *b* subunits (192).

Deletion constructs analyzed by sedimentation equilibrium experiments suggested that a form of the *b* subunit truncated in each end, $b_{53\text{-}122}$, was capable of forming dimers with an efficiency close to the complete cytoplasmic domain, $b_{24\text{-}156}$, indicating that the most pertinent intersubunit contacts of the *b* subunit was located within this central region, referred to as the dimerization domain (192). More recently, the dimerization domain has been refined to residues $b_{63\text{-}122}$; however, the amino-terminal boundary is likely to decrease even further due to the observation that deletion of residues $b_{54\text{-}64}$ or $b_{65\text{-}75}$ resulted in intact and functional F_1F_0 ATP synthase complexes (Figure 1-6) (194).

A crystal structure of a monomeric dimerization domain, based on a model polypeptide consisting of residues $b_{62\text{-}122}$, has recently been solved and refined to 1.55 Å (138). Based on an undecad repeat and crosslinking data, Dunn and coworkers have constructed a model in which the two α-helices of the $b_{62\text{-}122}$ region formed a coiled-coil with a right-handed superhelical twist. A number of previous studies supported this coiled-coil arrangement. First, the shape of the $b_{53\text{-}122}$ polypeptide was consistent with a

coiled-coil of similar length as determined from its frictional coefficient (1.60) in an ultracentrifuge and from NMR relaxation parameters (192). Secondly, small-angle X-ray scattering by $b_{52\text{-}122}$ in solution specified a maximum length to be about 95 Å, consistent with the expected coiled-coil length (13). Thirdly, CD spectroscopy indicated that this polypeptide was 100% α-helical and the similar intensities of the minima suggested the helices to be arranged in a coiled-coil (204). Fourthly, cysteine substitution and crosslinking studies suggested a periodicity consistent with a parallel coiled-coil (Figure 1-5) (204). Finally, *b* subunit sequence analysis of *E. coli* and other prokaryotes revealed a conservation of an undecad pattern, which is a distinctive characteristic of a right-handed coiled coil. Mutation of amino acid residue $b_{arg\text{-}83}$, which interrupts the undecad repeat, markedly stabilized the dimer, as expected for the proposed two-stranded, right-handed coiled-coil structure.

The carboxyl-terminal F_1-binding domain, $b_{124\text{-}156}$, also referred to as the δ-binding domain, has a more globular conformation and is required for the binding of F_1 to F_0 (205, 206). Work accomplished by Futai and coworkers two decades ago revealed that truncation of the extreme carboxyl-terminus of the F_1-binding domain by only a few amino acids resulted in assembly defects in F_1F_0 ATP synthase (206). Subsequently, work performed by Dunn and coworkers demonstrated that the final two to four amino acids of the *b* subunit were necessary for binding the δ subunit of F_1 (205). An addition of a cysteine at the carboxyl-terminus was chemically crosslinked to a cysteine introduced at δ_{158}.

A close association of the two *b* subunits in the F_1-binding domain was indicated by crosslinks formed between cysteines individually substituted at positions b_{124}, b_{125},

b_{126}, b_{127}, b_{128}, b_{129}, b_{130}, b_{131}, b_{132}, b_{139}, b_{144}, b_{146}, or b_{156} (Figure 1-5) (198, 200, 207). Hydrodynamic evidence favors a folded structure for this domain of the *b* subunit as opposed to the highly elongated structure of the remainder of the *b* subunit. Also, several studies have shown that either a $b_{ala128\rightarrow glu}$ mutation, deletion of the last four residues, or cold temperature dramatically decreased the sedimentation coefficient, by 23%, suggesting that the F_1-binding domain underwent a conformational change from a globular structure to a less folded more extended conformation (192, 205, 208)**.** The mutation, $b_{ala128\rightarrow glu}$, may have caused an electrostatic repulsion that would cause the two *b* subunits to push apart. The carboxyl-terminal residues may form an amphipathic helix, so the deletion would have disrupted essential interactions. And cold temperatures have been shown to weaken hydrophobic interactions in proteins, suggesting the importance of the hydrophobic amino acids in the folding of this domain (13). Dunn *et al.* suggested that these observations implied that the carboxyl-terminus of the *b* subunit has a weakly folded structure in which the hydrophobic amino acids are arranged to impart structural stability and create hydrophobic patches on the surface (13). The folded conformation appears to be required for the exposed hydrophobic patches to interact with F_1.

Mutagenesis. Several mutant searches and site-directed mutagenesis studies have been performed in the membrane-spanning domain of the *b* subunit. However, only a single mutation, $b_{gly9\rightarrow asp}$, located near the periplasmic side of the lipid bilayer, resulted in a defective proton pore in an intact F_1F_0 ATP synthase complex (209). Second site suppressors of this mutation have been found in the *a*($a_{pro240\rightarrow ala}$ or $a_{pro240\rightarrow leu}$) and *c* ($c_{ala62\rightarrow ser}$) subunits that partially repaired the defect, indicating an interaction between the *b* subunit and both the *a* and *c* subunits (210, 211). The membrane-spanning domain

contains one charged residue, b_{lys23}, but mutations generated at this site did not influence proton translocation, suggesting that this domain of the *b* subunit did not have a direct function in proton conduction, although it was required for the maintenance of a functional F_0 complex (212). A systematic mutational study of the membrane-spanning domain conducted by Hardy *et al.* was described above and a triple mutant, $b_{N2A,T6A,Q10A}$, is described in Chapter 5 of this dissertation (202).

A couple notable characteristics can be attributed to the tether region of the *b* subunit. Relatively large deletions and insertions of up to 11 and 14 amino acids, respectively, were accommodated in this region and the altered *b* subunits still assembled into fully functional F_1F_0 ATP synthase complexes (193, 194). In fact, decreases observed in enzyme activity paralleled the decrease of *b* subunit found in the membrane, suggesting that the alterations affected assembly of the enzyme, but not the function. Assuming α-helical structure, an 11 amino acid deletion would shorten the *b* subunit tether region by approximately 16.5 Å and a duplication of 14 amino acids would increase the length by about 21 Å. This implies that the *b* subunit is highly flexible and the altered *b* subunits may compensate for the lost or gained distance via that flexibility. The fact that the peripheral stalk must extend from within the membrane to up near the top of F_1 suggests that some part of the stalk must be flexible enough to stretch or straighten in the shortened *b* subunits, or in the case of the lengthened *b* subunits, bend to take up the slack. Prior to these observations, the *b* subunit was often viewed as a rigid, rod-like structural feature during rotational catalysis. Also, though the *b* subunit is the least conserved subunit of F_1F_0 ATP synthase, gaps are rarely found in sequence alignments of numerous organisms (213, 214). Therefore, the ability to manipulate the

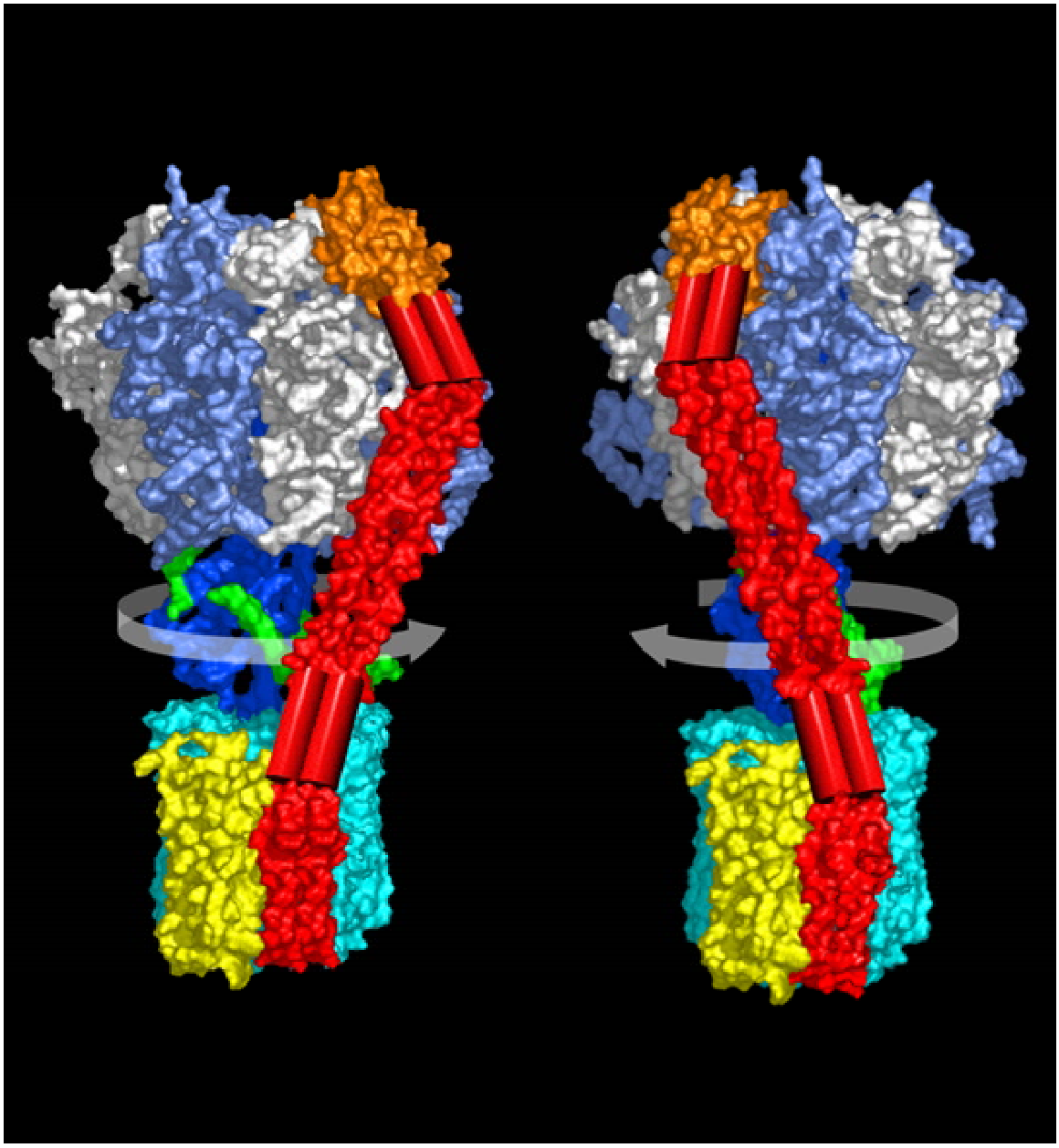

Figure 1-7. Model for F_1F_0 ATP synthase peripheral stalk orientation dependent upon the direction of rotation during ATP synthesis or hydrolysis. The subunits are color coded as follows: α, light blue; β, grey; γ, dark blue; ε, green; δ, orange; *a*, yellow; *b*, red; *c*, cyan. The panel on the left indicates the orientation of the b_2 dimer if the enzyme is actively synthesizing ATP. The panel on the right represents the position of the b_2 dimer during ATP hydrolysis. The arrows indicate the direction of rotation of the rotor stalk subunits ($\gamma\varepsilon c_{10}$). The red cylinders indicate regions of the *b* subunits for which there is no high-resolution structure.

length of the peripheral stalk was an unexpected surprise to the field. The length of the wild-type *b* subunit is probably the optimum length for assembly of F_1F_0 ATP synthase. The apparent flexibility has been proposed to help alleviate torsional strain brought about by rotational catalysis (193). Another hypothesis concerning the flexibility of the tether domain is that this region of the b_2 dimer serves as a hinge, allowing reorientation of the stator depending on the direction of rotation as the enzyme carries out ATP synthesis or hydrolysis (Figure 1-7) (195, 202).

Another important feature of the tether domain is the evolutionarily conserved b_{arg36}, that has been implicated in a structural role influencing proton conduction through F_0. Mutational studies at this amino acid residue led to numerous defects from failure to assemble or function to uncoupling phenotypes (215). Amino acid substitutions, $b_{arg26\rightarrow ile}$ or $b_{arg26\rightarrow glu}$, resulted in assembled F_1F_0 ATP synthase complexes that displayed defects in F_0-mediated proton translocation or a disruption of coupling activity, respectively. Substitution with a cysteine at this residue led to a crosslink product with the *a* subunit of F_0 (216, 217). The close proximity of this conserved residue to the *a* subunit indicates that it may play a role in aligning the proton exit channel.

Protein-protein interactions between the two *b* subunit dimerization domains have been shown to be essential for forming the peripheral stalk (13). Mutations at a conserved residue, b_{ala79}, resulted in major F_1F_0 ATP synthase assembly defects (203, 218). The b_{ala79} mutations were modeled in the b_{sol} polypeptide to investigate the affects of the mutations. The model polypeptides were shown to retain α-helical structure, but chemical crosslinking and sedimentation experiments suggested that the b_{ala79} mutants were incapable of forming dimers (199).

In the F_1-binding domain, a mutation was found, $b_{ala128\rightarrow asp}$, that had little effect on the dimerization of the *b* subunits but led to an assembly defect of F_1F_0 ATP synthase (208). However, the mutant was found to have a reduced tendency to interact with F_1 and sedimentation equilibrium ultracentrifugation experiments revealed a 12% decrease in the sedimentation coefficient, indicating a structural perturbation (discussed above). The studies suggested that the b_{ala128} residue was not important in *b* subunit dimerization, but it had an important structural role in the F_1-binding domain.

Intersubunit interactions. The formation of disulfide bonds between cysteine residues introduced in the membrane-spanning domain of the *b* subunit and the *a* subunit as well as second site suppressors of the $b_{gly9\rightarrow asp}$ found in the *a* subunit (discussed above) strongly suggests an interaction between the two stator subunits (209-211). The $b_{gly9\rightarrow asp}$ mutation was also partially suppressed by a mutation in the *c* subunit (discussed above), but it is not known whether it is due to a direct interaction between the *b* and *c* subunits or if the suppression is mediated through the *a* subunit.

The *b* subunit has also been shown to interact with the α, β and δ subunits of F_1 (198, 216). The interaction of the F_0 *b* subunit with the F_1 δ subunit has been well documented (200, 205, 219, 220). The interaction is mediated by the carboxyl-termini of both subunits and is essential for the binding of F_1 and F_0. The critical role of the δ subunit mediating the interaction between the *b* subunit and the bulk of F_1 has been demonstrated by the inability of δ-depleted F_1 to bind to F_0 (219). Crosslinking the *b* and δ subunits via introduced cysteines did not affect F_1F_0 ATP synthase activity, which was consistent with the proposed role of the $b_2\delta$ peripheral stalk as a stator and demonstrated that the *b*-δ interaction need not be dynamic (221). Though it is believed that the binding

of F_1 to F_0 heavily relies on the *b*-δ interaction, evidence of other subunit contacts may also influence binding. Furthermore, the binding of *b* to δ was shown to be relatively weak by analytical ultracentrifugation, indicating that other subunit contacts may contribute to binding (220). Many crosslink formations were found when cysteines were introduced into the *b* and α or β subunits (Figure 1-5). A cysteine introduced to the carboxyl-terminus of the *b* subunit has been shown to crosslink to α_{cys90} (198). Also, cysteines positioned at b_{92} or b_{109} formed crosslinked products with the α subunit or both the α and β subunits, respectively (216). These results confirm that the *b* subunit is proximal to the $\alpha_3\beta_3$ hexamer, but a direct interaction has not been confirmed.

Stator stalk function. The necessity of a stator in F_1F_0 ATP synthase was recognized after the realization that rotation was a fundamental feature of ATP catalysis. The current view of the peripheral stalk is primarily that of the stator which forms a connection the *a* subunit and the $\alpha_3\beta_3$ hexamer, holding these subunits in place against the rotation of the rotor subunits, $c_{10}\gamma\varepsilon$. The idea of a flexible stator stalk has led to other proposed features of the *b* subunit. The apparent flexibility of the *b* subunit has been suggested to transiently store energy during rotational catalysis which could be potentially be expended to force the conformational change that allows the release of ATP(222). Another model describes the flexibility of the tether region as a hinge that could reorient the *b* subunit when switching between ATP synthesis and hydrolysis (discussed above) (Figure 1-7) (202). However, there is no direct evidence of whether the *b* subunit is actually acting in a flexible manner. Finally, the *b* subunit has recently been suggested to influence the nucleotide binding sites in the β subunits (223). In these experiments, a spin label was incorporated at residue β_{331}. Upon addition of b_{sol}, the

spectrum of this spin label was observed to change in a way that implied that the catalytic sites were in a more open conformation. These results indicate that the current view of the stator stalk as a structural feature may soon be revised such that the *b* subunit has a more direct role during rotational catalysis.

Subunit Equivalence

The *E. coli* ATP synthase complex has, by far, the simplest architecture of all the F_1F_0 ATP synthase enzyme complexes. It is composed of twenty-two polypeptides of eight different types with the stoichiometry $\alpha_3\beta_3\gamma\delta\varepsilon ab_2c_{10}$ (Figure 1-2, Table 1-1) (112, 224). The $\alpha_3\beta_3\gamma\delta\varepsilon$ subunits comprise the F_1 sector and the ab_2c_{10} subunits comprise the F_0 sector. In the *E. coli* enzyme, all eight subunits are necessary for the function of F_1F_0 ATP synthase (225, 226). Chloroplasts also have a relatively simple architecture with the exception that they have nine different subunits (227) due to the fact that the two *b* subunits are products from two different genes and are not identical (Figure 1-8). In contrast, the F_1F_0 ATP synthase from mammalian mitochondria is composed of at least thirty-one polypeptides of sixteen different types with the F_1 stoichiometry of $\alpha_3\beta_3\gamma\delta\varepsilon$ and a much more complex F_0 consisting of *a*, b_2, $c_{10\text{-}14}$, *d*, *e*, *f*, *g*, $(F_6)_2$, A_6L, OSCP, IF_1 (7, 228-230). Yeast mitochondria F_1F_0 ATP synthase has an extra three subunits compared to the mammalian enzyme, *stf1p*, *i*, and *k*.

The F_1 sector. In the F_1 sectors, homologues of the *E. coli* F_1F_0 ATP synthase have been identified for the α, β and γ subunits, based on amino acid sequence homology, in the chloroplast and mitochondrial enzymes (30). Based on the primary sequences, the highest conserved subunit from the *E. coli* F_1F_0 ATP synthase is the β subunit with approximately 70% homology with the chloroplast and mitochondria

Table 1-1. F_1F_0 ATP synthase subunit equivalency

Bacteria	Chloroplast	Mitochondria		*Function*
		Yeast	**Bovine**	
α	α	α	α	catalytic site
β	β	β	β	catalytic site
γ	γ	γ	γ	rotor
δ	δ	OSCP	OSCP	stator
ε	ε	δ	δ	rotor
-	-	ε	ε	stabilization?
a	*a* (or IV)	*a* (or 6)	*a*	proton channel, stator
b	*b* (or I)	*b* (or 4)	*b*	stator
-	*b'* (or II)	9	-	stator
c	*c* (or III)	*c* (or 8)	*c*	proton channel, rotor
-	-	*d*	*d*	stator?
-	-	8	A6L	stator?
-	-	*e*	*e*	?
-	-	*f*	*f*	?
-	-	*g*	*g*	?
-	-	*h*	F6	stator
-	-	*inh*1*p*	IF1	inhibitor
-	-	*stf*1*p*	-	?
-	-	*j*	-	?
-	-	k	-	?

equivalents (31). The α subunits exhibit roughly 50% homology (31). The nucleotide binding regions of these two subunits also have sequence homologies with other proteins that bind nucleotide or phosphate, including the *E. coli* secA protein, N-ethylmaleimide sensitive fusion protein, herpes simplex virus UL15, Ca^{2+}-ATPase, H^+/K^+ ATPase and Na^+/K^+ ATPase (34-37). Furthermore, the nucleotide binding motif, GXXXXGKT/S, which was first identified in the α and β sequences of F_1, has been found to be conserved in the high-resolution structures of other proteins including $p21^{ras}$, adenylate kinase, RecA, elongation factor Tu, and transducin-α (20, 38-42).

Interestingly, the γ subunit in the chloroplast F_1F_0 ATP synthase complex contains an insert of about 35 amino acids that is not present in the mitochondrial or

nonphotosynthetic eubacteria (231). This loop contained two cysteine residues that were found to be reduced in the active enzyme complex during photosynthesis and oxidized to a disulfide bond in the inactive enzyme while in the dark (232). The *E. coli* ε subunit is unfortunately known as the δ subunit in the mitochondrial enzyme (233) and also shares primary sequence homology with the mitochondrial IF_1 inhibitor protein. The *E. coli* ε and bovine δ subunits share 60% sequence identity, which had suggested that they are functionally equivalent (191, 234). The availability of high resolution structures for these subunits has revealed that they are strikingly similar. Superimposition yields a 1.64 Å rms deviation (48). The bacterial ε subunit has been suggested to be an inhibitor of ATP hydrolysis, undergoing large, ratchet-like conformational changes to selectively switch off ATP hydrolysis (102). In mitochondria, this inhibitor action of the bacterial ε subunit is ascribed to the IF_1 protein of the F_0 sector. It was suggested that the bacterial ε subunit was separated into the two polypeptides in the mitochondrial enzyme complex, ε and IF_1. Finally, the bacterial and chloroplast δ subunits of F_1 share a significant sequence homology (234). The δ subunit's equivalent in the mitochondrial F_1F_0 ATP synthase is known as oligomycin-sensitivity-conferring protein (OSCP) (235-237). The carboxyl-terminal region of the mitochondrial *b* subunit was been demonstrated to bind to the OSCP subunit (*E. coli* δ subunit) through subunit interactions (Collinson *et al*., 1994) and chemical crosslinking analysis (Soubannier *et al*., 1999).

The F_0 sector. The F_0 sectors of the F_1F_0 ATP synthase family is by far more diverse than the F_1 sector with an additional eight different subunit types in mammalian and an extra ten different subunits in yeast mitochondria (Table 1-1). The *E. coli a* and *c* subunits are respectively equivalent to the chloroplast IV and III subunits and the

mitochondrial ATPase-6 and ATPase-8 subunits. In every case, both subunits are hydrophobic proteins required for proton translocation (120, 140). Unlike the *a* and *c* subunits, the *E. coli b* subunit does not have any obvious homologues in chloroplasts or cyanobacteria F_1F_0 ATP synthases. However, both of them have two distinct subunits with similar hydrophobic and hydrophilic residue distribution (238). These subunits are referred to as subunits *b* and *b'* in cyanobacteria and subunits I and II in chloroplasts. It is believed that only one of each of these subunits is present in the F_1F_0 ATP synthase complex, incorporating into the enzyme as a *b-b'* heterodimer as opposed to the *b* subunit homodimer present in *E. coli*. No obvious homologue of the *E. coli b* subunit has been found in the mitochondrial F_1F_0 ATP synthase, even upon analysis of sequence, function or three-dimensional structure (239). However, hydropathy plot analysis does indicate that the mammalian mitochondrial *b* subunit that may be analogous to the *E. coli b* subunit (240, 241). Proteolysis studies and crosslinking data supported the location of the mitochondria *b* subunit at a position analogous to the *E. coli b* subunit (242, 243). At least three other subunits may play the role of the *E. coli b* dimer including subunit 8 (or A6L), *d* and F6. The mitochondrial *b* subunit is believed to have two α-helical transmembrane spans at its amino-terminus arranged in an antiparallel configuration. The extreme amino-terminus of the mitochondrial *b* subunit is thought to begin on the cytoplasmic side of the membrane, traverses the membrane to the periplasmic leaflet of the membrane as an α-helix, then turn back and traverses the membrane again as it exits the membrane in the cytoplasm and reaches towards the top of F_1 (Figure 1-8). The remainder of what would be equivalent to the *E. coli b* dimer is highly speculative, though the overall shape and characteristics of the *b*8*d*F6 subunits favor this explanation

(Figure 1-8). In this model, the mitochondrial subunit 8 contributes to a third membrane spanning region, and a combination of subunit *d* and subunit F6 forms the hydrophilic domain.

The F_0 subunit known as the ε subunit in mitochondrial F_1F_0 ATP synthase has no counterpart in the bacterial or chloroplast enzymes. It is a small polypeptide (50 amino acids) folded into a helix-loop-helix. It is believed to play a role in the stabilization of the central stalk and its absence in the bacterial and chloroplast enzymes may explain why

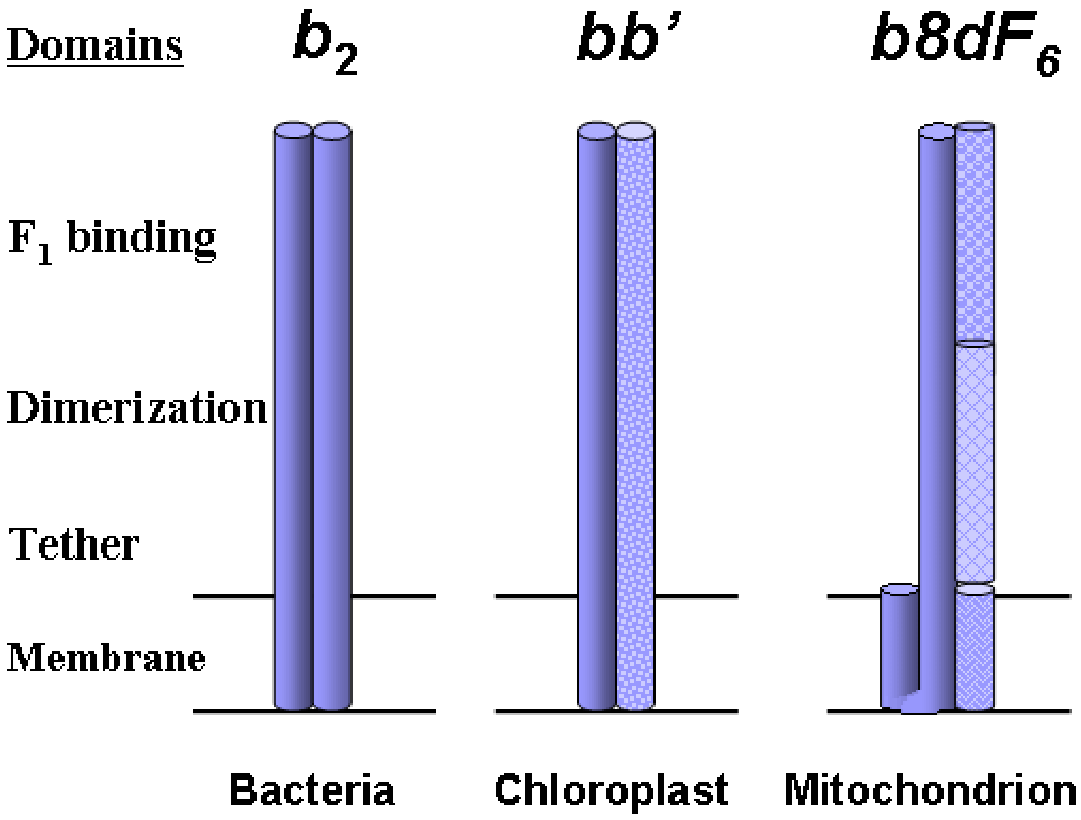

Figure 1-8. Speculative models for the *b*-like subunits. Shown are models for the bacterial, chloroplast and mitochondrial *b* subunits. The membrane-spanning regions are indicated by the black lines. An abundance of evidence supports the parallel arrangement of the bacterial b_2 homodimer and the chloroplast *bb'* heterodimer. The mitochondrial analogue of the *b* subunit is believed to consist of up to four polypeptides. The model shown for the mitochondrial $b8dF_6$ structure is highly speculative.

the bacterial ε subunit of the F_1 sector (equivalent to the δ subunit in mitochondria) easily dissociates from the F_1 complex whereas this has not been observed for the mitochondrial enzyme. Mitochondrial F_0 consists of several additional subunits not found in the *E. coli* or chloroplast enzymes including the *e*, *f* and *g* subunits as well as an extra three in yeast, *stf*1*p*, *j*, and *k* subunits.

***E. coli* F_1F_0 ATP synthase as a model.** Initial studies of the F_1F_0 ATP synthase complex were achieved with enzymes isolated from mitochondria or chloroplast. Although the bacterial, chloroplast and mitochondrial enzymes differ in oligomeric complexity, the enzymes show acceptable overall structural resemblance and primary sequence homology that it is widely accepted that the mechanism of action is the same in all organisms (240, 244). Therefore, studies using the bacterial model became widely accepted since it was more versatile and offered a large range of research that could not be readily undertaken with the more complex organisms. Other advantages include ease of genetic techniques, the ability of bacteria to grow via glycolysis, which allowed characterization of defective F_1F_0 ATP synthases, and ease of large-scale purification procedures due to a practically unlimited supply of bacteria.

F_1F_0 ATP Synthase Mechanism

The overall function of F_1F_0 ATP synthase can be divided into three distinct parts: proton conduction, coupling, and catalysis. The *a* and *c* subunits of F_0 are responsible for the translocation of protons through the membrane. The F_1 γ and ε subunits of the rotor stalk are responsible for coupling the energy acquired from the proton gradient to the F_1 catalytic sites. And the three catalytic sites located at the interfaces of the three α and β

subunits are responsible for the synthesis of ATP or sometimes, as in the case of bacteria, ATP hydrolysis. All three functions must be tightly integrated for the production of ATP.

Proton Translocation: Driving Rotation

The demonstration that the electrochemical gradient of protons drives the rotation of bacterial flagella (245) in combination with Peter Mitchell's chemiosmotic theory (2) began the search for evidence of rotation in F_1F_0 ATP synthesis. At the same time, a model for proton transport was suggested by Cox *et al.* (212) and Boyer developed his ideas for the binding change mechanism (discussed below) (246). But an indication of rotational catalysis was not evident until the high-resolution crystal structure of F_1 became available (20). This was followed a few years later by the first direct observation of rotation when Noji *et al.* fixed the top of F_1 to a glass coverslip and attached a fluorescently labeled actin filament to the γ subunit (15). Upon addition of ATP, rotation of the actin filament was observed under an optical microscope at 0.2-10 revolutions per second. At low concentrations of ATP (<600 nM), the actin filaments were observed to rotate in a step-wise manner at 120° intervals, which reflects the three catalytic sites in the F_1 $\alpha_3\beta_3$ hexamer (247). Experiments, in which two phenylalanine residues in the nucleotide binding pocket were mutated to reduce the binding affinity of ATP, indicated that the binding and hydrolysis of ATP is initially accompanied by a 90° substep followed by a 30° substep attributed to product release (248, 249). These observations were consistent with the two proposed "catches" observed between the β and γ subunits in the high resolution structure (see "The γ subunit" above) (20). The observance of the rotation of the ε and *c* subunits at the same speed and direction, indicating that these three subunits rotate in synchrony, forming the central rotary machinery of the enzyme

complex (65-67). The concept of rotational catalysis with the rotation of the $\gamma\varepsilon c_{10}$ subunits relative to the $\alpha_3\beta_3$ hexamer is now well accepted.

Several models have been proposed for proton translocation. One of the earliest models suggested a series of side chains spanning the lipid bilayer formed a "proton wire", involving amino acid residues c_{asp61}, a_{arg210}, a_{glu219} and a_{his245}, in which the protons "hop" from one side chain to another until it passes through the membrane (212, 226, 250). Other models include a water-filled "proton channel" model, formed by the charged residues of the *a* and *c* subunits, in which hydronium ions (H_3O^+) pass through the lipid bilayer (251) and a "proton carrier" model, in which a proton binds on the exterior of the membrane followed by a conformational change that brings the complex through the membrane and releases the proton on the outer surface (252, 253).

The current prevailing model suggests that protons, in the form of H_3O^+, enter a half channel created by the *a* subunit (Figure 1-9) (254, 255). The H_3O^+ is then believed to protonate one of the c_{10} subunits at residue c_{asp61}, which is positioned near the center of the lipid bilayer (131). Besides forming the proposed half channel, the *a* subunit is thought to play another crucial role in the protonation of the c_{asp61}. The pKa of the c_{asp61} carboxyl side chain is uncommonly high, which is likely due to its lipid environment (125). The essential a_{arg210} residue is thought to facilitate a pKa shift of the c_{asp61} carboxyl side chain to a lower pKa form during proton translocation (14, 132). Either the protonation of the carboxylate, or possibly the release of a proton from a previously protonated c_{asp61} into an exit channel housed by the *a* subunit, somehow promotes the generation of torque (Figure 1-9). The torque produced by proton translocation is believed to drive the rotation of the ring of c_{10} subunits relative to the *a* and *b* subunits

during rotational catalysis. Translocation of three to four protons generates enough torque energy to rotate the c_{10} ring by 120° and results in the synthesis of a single molecule of ATP.

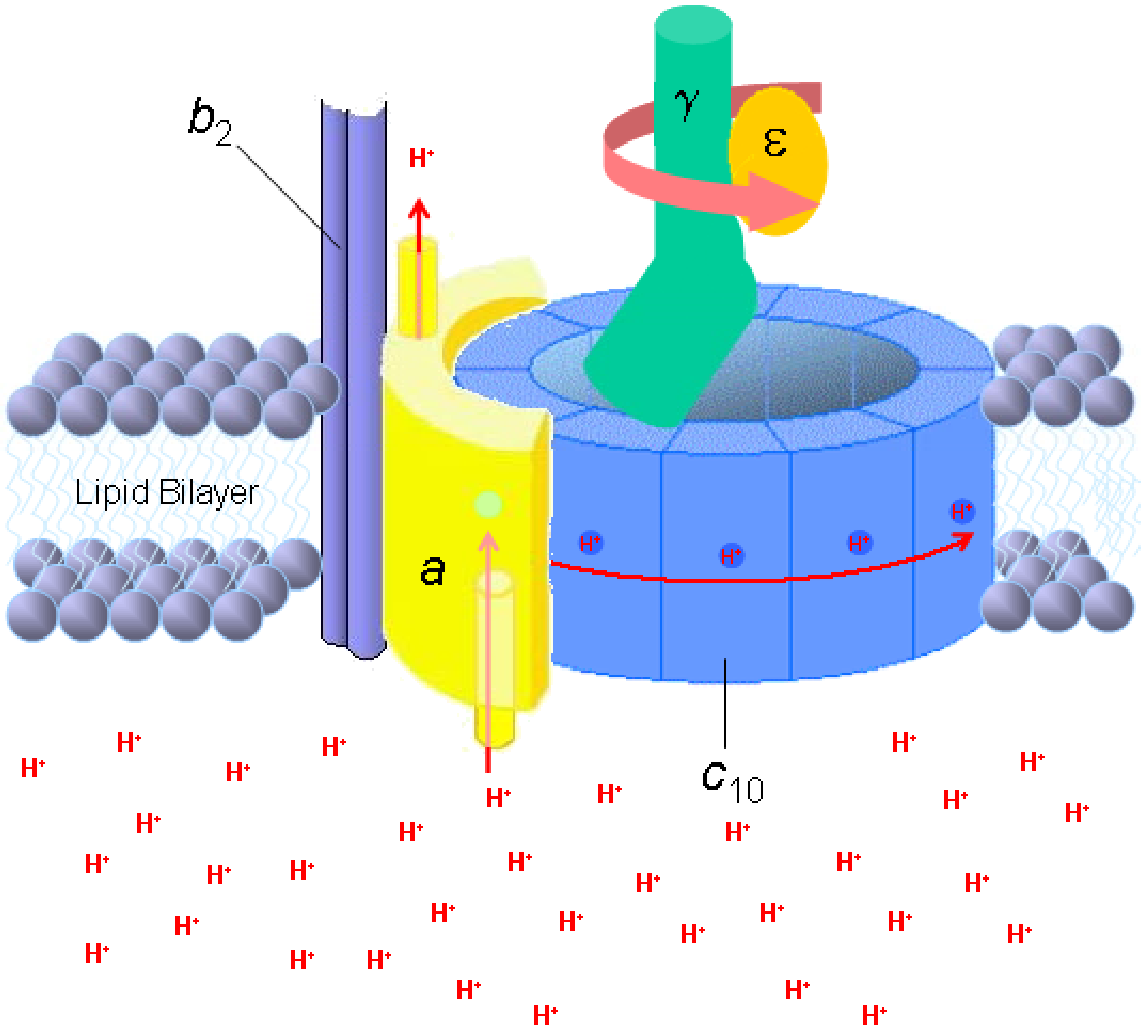

Figure 1-9. Model of proton translocation and torque generation in F_0. Subunits included are γ (green), ε (orange), *a* (yellow), b_2 (purple), c_{10} (blue). Protons (red) are traveling in the direction of ATP synthesis. Protons are believed to travel through a half channel housed in the *a* subunit as hydronium, H_3O^+. An essential residue located near the center of the lipid bilayer in the *c* subunit, c_{asp61}, is thought to be protonated as another proton exits through another "exit" half channel located on the cytoplasmic side of the membrane. The protonation/deprotonation drives the rotation of the c_{10} ring. The model was drawn from schemes proposed by Junge (254) and Vik and Antonio (255).

Coupling

In F_1F_0 ATP synthase, the mechanism of energy coupling requires both the rotor stalk and the peripheral stalk. Rotation of the ring of c_{10} subunits consequently results in the rotation of the entire rotor stalk, which is essential in coupling the energy obtained from proton translocation to the synthesis of ATP in the catalytic sites of the $\alpha_3\beta_3$ hexamer located over 100 Å away. The role of the peripheral stalk is to hold the hexamer in place while the amino- and carboxyl-terminal α-helices of the γ subunit rotates within. In a fully functional and coupled enzyme, the kinetics of proton translocation and ATP synthesis are linked so that one cannot proceed without the other, and vise versa (256).

Mutational studies suggested that the polar loop of the c_{10} subunits was involved in the coupling function. In F_1F_0 ATP synthases incorporated with the $c_{gln42\rightarrow glu}$ subunit mutant, F_1 was found to bind normally to the F_0 mutant, but the passive leakage of protons through this complex was not prevented as in must be in coupled enzyme complexes (257). Also, ATP was hydrolyzed normally by this mutant, but hydrolysis was not coupled to active proton translocation. A similar uncoupled phenotype was found in complexes incorporated with a $c_{arg41\rightarrow lys}$ mutant (258). Another mutation at the same site, $c_{arg41\rightarrow his}$, was found to prevent the binding of F_1 to F_0. Thus, this loop region in the *c* subunit appears to play essential roles in both the binding of F_1 and the coupling of proton translocation to ATP synthesis. Second site suppressor mutations to the $c_{gln42\rightarrow glu}$ mutation were found in the ε subunit, specifically, $\varepsilon_{glu31\rightarrow gly,val,lys}$, that recouped proton translocation and ATP synthesis (98). Crosslinking studies of cysteine double mutants found cross-linked products between ε_{cys31} and c_{cys40}, c_{cys42} and c_{cys43} (99). Moreover, a functional contribution of the γ subunit in energy coupling was demonstrated

by γ subunit mutants that uncoupled proton transport and ATP hydrolysis (259). Second site suppressor mutations were found in other regions of the γ subunit (260, 261). Cysteine substitutions formed crosslinks between the γ subunit, γ_{cys205}, and c_{cys40}, c_{cys42} and c_{cys43} (118). Crosslinking studies also provided evidence for an interaction between γ and β (75, 77). In addition, the ε subunit has been cross-linked to both the F_1 and F_0 subunits, via introduced cysteines, indicating that it spans the entire length of the stalk with the γ subunit (60, 99). Combined, these observations had suggested that the coupling mechanism occurred by direct interactions of the *c* subunit loop regions and the γ and ε rotor stalk of F_1, which convey the proton gradient energy to the catalytic sites, probably by direct interactions.

The crystal structure later confirmed these interactions (20). The crystal structure displayed a strikingly asymmetrical F_1 due to differences in the domains of the α and β subunits and the interactions formed with the single γ subunit (20). The obvious asymmetric positioning of the coiled coil of the γ subunit is a key feature to the mechanics of the binding change mechanism (discussed below) of F_1F_0 ATP synthase. Its large carboxyl terminus α-helix passes through a hydrophobic sleeve formed by six proline-rich loops of the α and β subunits, presumably resulting in the conformational changes occurring in the catalytic sites (20). In the β_E subunit (see above), several hydrogen bonds are formed with the γ subunit which forms a "catch", resulting in conformational changes. Specifically, residues γ_{arg254} and γ_{gln255} in the carboxyl terminal helix form hydrogen bongs with $\beta_{E\text{-}asp317}$, $\beta_{E\text{-}thr318}$ and $\beta_{E\text{-}asp319}$. Also, a second "catch" is formed between the carboxyl terminal domain of the β_T subunit and the short helix of the

γ subunit. Hydrogen bonds form between γ_{lys87}, γ_{lys90} and γ_{ala80} within the $\beta_{DELSEED}$ region, $\beta_{T\text{-}asp394}$ and $\beta_{T\text{-}glu398}$. Structural information suggests the two antiparallel coiled coil α-helices of the γ subunit may unwind during rotational catalysis and the ε subunit rotates around the F_1 axis while undertaking a net translation of about 23 Å (85). It is likely that these gross changes observed in the structures revealed individual functional states of the enzyme complex during catalysis.

Catalysis: The Binding Change Mechanism

F_1F_0 ATP synthases house three catalytic sites, located at the $\alpha_3\beta_3$ interfaces, with the predominate sites positioned in the β subunit and some contributions made by the α subunits (20). The minimal complex capable of normal ATP hydrolysis activity is the $\alpha_3\beta_3\gamma$ complex (262)**.** Boyer predicted that ATP synthesis requires a chronological involvement of the three catalytic sites, each of which changes its binding affinity for the substrates and products as it continues through a cyclical mechanism, referred to as the "binding change mechanism" (246, 263). The mechanism of ATP synthesis, in terms of the α_3, β_3 and γ subunits and the substrates, ADP and P_i, is described here (Figure 1-10).

The principles of the binding change mechanism have become the most commonly used model for recounting the means of ATP synthesis by F_1F_0 ATP synthase. The three distinct catalytic sites were described as the tight (T) site containing ATP, an empty open (O) site, and the loose (L) site illustrated with ADP and P_i bound (Figure 1-10). According to Boyer, catalysis starts with the binding of ADP and P_i at the open site. The energy input from proton translocation drives the rotation of the rotor stalk, which ultimately results in the conformational changes responsible for ATP synthesis such that the tight site is converted to an open site, the open site assumes a loose site conformation,

and the loose sites becomes a tight sight. ATP is formed in the new tight site and the molecule of ATP that was found in the original tight site is released and the binding change mechanism starts fresh (Figure 1-10). Boyer's mechanism included three proposals: i) only one site is actively synthesizing ATP at any given moment, ii) the reaction occurs reversibly at this site, and iii) energy input is required to bind the substrates, ADP and P_i, into the catalytic sites and to release the synthesized ATP, but not for the actual reaction to occur. Strong evidence for this model has come from the crystal structure of F_1 (20) and the observance of rotation via an attached fluorescent actin filament (discussed previously) (15, 65-67).

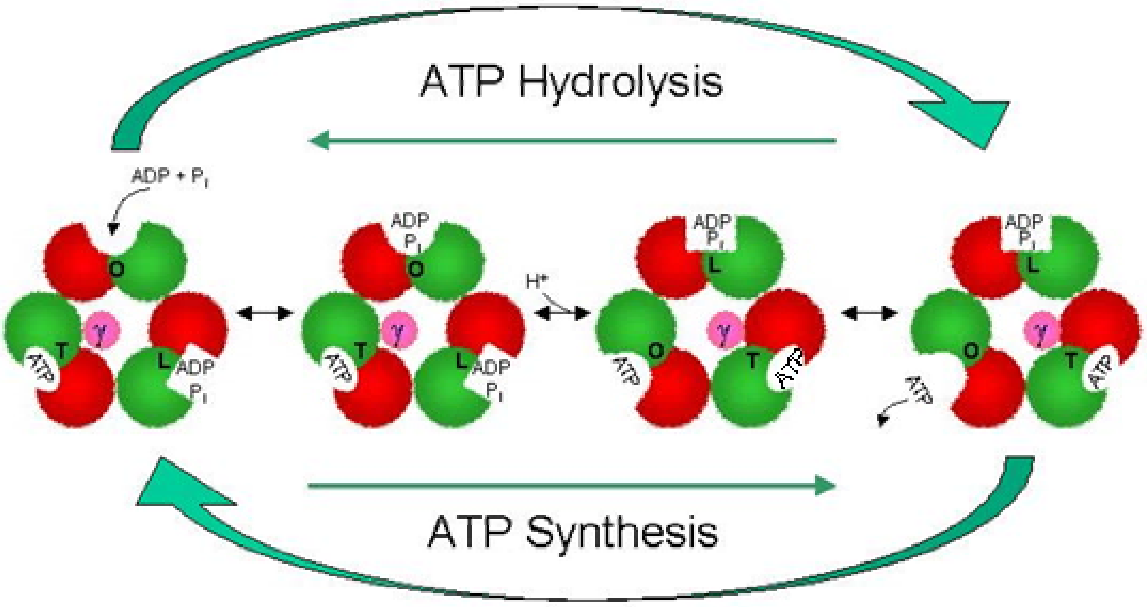

Figure 1-10. The binding change mechanism. This is a simplified model of a more detailed enzymatic mechanism described by Weber and Senior (189) in which all three catalytic sites are transiently filled with nucleotide during ATP synthesis. Subunits included are α (red), β (green) and γ (pink).

Genetic Expression and Assembly

The *E. coli* F_1F_0 ATP synthase is encoded in the 7 kb *unc* operon, which was cloned and sequenced in its entirety (224, 264). The genes encoded are called the *unc*B,

*unc*E, *unc*F, *unc*H, *unc*A, *unc*G, *unc*D and *unc*C coding for the *a*, *c*, *b*, δ, α, γ, β and ε subunits, respectively. A single copy of each gene is transcribed into a single polycysternic mRNA transcript, from which multiple polypeptides can be translated (265-267). The synthesis of the correct number of subunits, resulting in the stoichiometry of $\alpha_3\beta_3\delta\gamma\varepsilon ab_2c_{10}$, is thought to occur by translational regulation (264, 268). The efficiency at which the individual subunits are synthesized were observed to be variable and roughly corresponded to the stoichiometry of the intact enzyme complex (269, 270).

Far less is understood about the assembly of the complex F_1F_0 ATP synthase enzyme compared to the structural and mechanistic studies. Some have proposed that no particular pathway is necessary based on the observation that the complex can be dissembled into individual subunits and then reconstituted *in vitro* (113, 148, 271). On the contrary, some believe that the assembly follows an integrated pathway *in vivo* (272). The idea of an assembly pathway appealed to many since it would prevent a newly assembled F_1 sectors from freely hydrolyzing cellular ATP in the cytoplasm, and newly assembled F_0 sectors from acting as open proton pores in the membrane. If assembly were a random event, the potential to create isolated F_1 and F_0 sectors would exist. Some evidence supporting the integrated pathway does exist. The ε subunit is thought to function as an inhibitor of ATP hydrolysis activity, undertaking large conformational changes to allow the enzyme to switch from ATP synthesis to ATP hydrolysis under conditions of low ATP or low proton gradient, respectively (102, 177, 273-276). Its inhibitory action may possibly act to inhibit free ATPase activity in the partially assembled state. Some have speculated that the binding of the F_1 subunits to F_0 may

influence the opening of the F_0 proton channel *in vivo* (176, 277-279). The *a* subunit was observed to be absent from membranes of cells lacking the *b* or *c* subunits (150). Furthermore, work accomplished in our laboratory has showed that the *b* subunit monomer does not integrate into the membrane has no affinity for F_1, indicating that the formation of the *b* dimer in the membrane is an early event in F_1F_0 ATP synthase assembly (199, 203, 218).

Summary

There is now ample evidence indicating that F_1F_0 ATP synthases are composed of three functional parts, the catalytic core, the rotor stalk and the stator stalk. In the *E. coli* enzyme complex, the catalytic core consists of the $\alpha_3\beta_3\gamma$ subunits and functions as an ATP synthase or an ATPase. The rotor stalk consists of the $\gamma\varepsilon c_{10}$ subunits and couples the energy of proton conduction to the synthesis of ATP by rotating within the $\alpha_3\beta_3$ hexamer. Finally, the stator stalk consists of the $\delta a b_2$ subunits and remains in a fixed position, anchored to the membrane by the *a* and b_2 subunits and to the $\alpha_3\beta_3$ hexamer via interactions made by the δ subunit. Much of what was known of F_1F_0 ATP synthase has been irrefutably confirmed by high resolution structures of partial complexes or model polypeptides. To date, a high resolution structure of the complete enzyme, or at least the complete F_0 is eagerly anticipated.

Since the visualization of the peripheral stalk less than a decade ago a plethora of data characterizing the b_2 homodimer has emerged. The observation that the b_2 homodimer was likely not a rigid structure, and possibly more of an elastic structure, created the foundation for the work described in the following chapters. The work illustrated in Chapters 2, 3, 4, 5 and 6 of this dissertation will characterize the role of the

peripheral stalk's dimer of identical *b* subunits in the *E. coli* F_1F_0 ATP synthase by using a combination of site-directed mutagenesis and biochemical methods. Chapter 2 demonstrates the ability of the *E. coli b* subunit to form heterodimers and the capability of F_1F_0 ATP synthase complex to tolerate the incorporation of two different length *b* subunits with a size difference of at least 14 amino acids (195). Chapter 3 demonstrates the formation of *b* heterodimers including at least one and up to two defective *b* subunits and documents indisputable evidence that F_1F_0 ATP synthases incorporated with *b* subunit heterodimers are functional (280). Furthermore, the work accomplished in the chapter indicates, for the first time, that each of the two *b* subunits makes a unique contribution to the functions of the peripheral stalk, such that one mutant *b* subunit is making up for what the other is lacking. Chapter 4 describes cysteine chemical modifications constructed in the δ subunit and shortened, lengthened and wild-type length *b* subunits. The *unc* operon expression plasmids generated in this study will be used in future fluorescent labeling experiments. Chapter 5 documents mutagenesis experiments conducted on the extreme amino- and carboxyl termini of the *b* subunit (202) (Bhatt *et al.*, manuscript in preparation, 2004). Finally, Chapter 6 summarizes the conclusions of this study and suggests the future directions that the work described in this dissertation has offered.

CHAPTER 2
INTEGRATION OF UNEQUAL LENGTH *b* SUBUNITS INTO F_1F_0 ATP SYNTHASE

Introduction

F_1F_0 ATP synthases provide the bulk of cellular energy production in both eukaryotes and prokaryotes (3, 5, 6). Enzymes in this family utilize the electrochemical gradient of protons across membranes in order to synthesize ATP from ADP and inorganic phosphate in a coupled reaction (16). In *Escherichia coli*, F_1F_0 ATP synthase is a complex enzyme composed of approximately twenty-two polypeptides with the stoichiometry of $\alpha_3\beta_3\gamma\delta\varepsilon ab_2c_{10}$ (6, 7). The F_1 portion is composed of the subunits $\alpha_3\beta_3\gamma\delta\varepsilon$ and is responsible for enzymatic catalysis. The F_0 portion of the enzyme consists of the ab_2c_{10} subunits and is responsible for the translocation of protons through the membrane.

Electron microscopy has shown that the F_1 and F_0 sectors are linked by two slender stalk structures (11). During ATP synthesis proton translocation drives the rotation of the central stalk, which consists of subunits $\gamma\varepsilon$, within the $\alpha_3\beta_3$ hexamer held stationary by the peripheral stalk. This rotation propagates the conformational changes in the active sites located at the $\alpha\beta$ interfaces driving catalytic activity (3, 15, 62, 65, 281, 282). The δ subunit of F_1 and a dimer of two identical *b* subunits from F_0 comprise the peripheral stalk acting as the stator. The δ subunit has been visualized seated at the top of the F_1 $\alpha_3\beta_3$ hexamer (187). However, recent evidence has suggested that the δ subunit may be positioned slightly to the side of F_1 in association with a single α subunit (100, 141-143).

The C-terminal region of the δ subunit is in direct contact with the extreme C-terminal end of the *b* dimer (3, 185, 200, 219, 220). The *b* subunit dimer constitutes the majority of the peripheral stalk stretching from within the membrane to near the top of F_1 (12).

Dimerization of the *b* subunits is required for the normal assembly and function of F_1F_0 ATP synthase (199). The two *b* subunits are believed to exist in parallel as an extended structure spanning from the periplasmic side of the membrane to near the top of F_1. Each has a N-terminal transmembrane domain, a tether domain extending from the surface of the membrane to the bottom of F_1, a dimerization domain and a δ-binding domain (13). The ability of *b* to bind to F_1 was proportional to the ability of *b* to form dimers, suggesting the necessity of the *b* dimer formation before the binding of F_1 to the complex (199). Presently, there is no high-resolution structure of the entire *b* subunit. A model polypeptide of the first 34 residues of the N-terminus has been solved by NMR, revealing a hydrophobic membrane-spanning α-helix (136). A crystal structure of a monomeric dimerization domain, consisting of residues 62-122, has been solved and refined to 1.55 Å (138). Dunn and coworkers have constructed a model in which the two α-helices of the $b_{62\text{-}122}$ region form a right-handed coiled coil. Much of the structural information on the *b* dimer has been gleaned from classical biochemical approaches such as CD-spectroscopy, crosslinking and sedimentation experiments (30, 166, 192, 196, 197, 203, 283). These studies revealed that the overall structure of the *b* subunit dimer is a highly extended conformation with approximately 80% α-helix.

Previous studies have shown that *b* subunits with deletions of up to eleven amino acids and insertions of up to fourteen amino acids, corresponding to approximately 16 Å and 21 Å, respectively, formed functional F_1F_0 complexes (193, 194). When *b* subunits

with either a seven amino acid deletion or an insertion, $b_{\Delta 7}$ or b_{+7}, respectively, were incorporated into the F_1F_0 ATP synthase complex, the properties of the enzymes were essentially wild type. These observations suggested that the role of the *b* dimer is more of a flexible structural feature. However, it was not known whether this flexibility extended to the dimerization of two *b* subunits of unequal lengths and their incorporation into an enzyme complex. In the present study an experimental system was developed to allow expression of two different *b* subunit genes and determine whether the differing *b* subunits were assembled into an F_1F_0 ATP synthase complex. Here, we demonstrate that the F_1F_0 ATP synthase complex can tolerate *b* subunits with a size difference of at least 14 amino acids.

Materials and Methods

Materials

Molecular biology enzymes and mutagenic oligonucleotides were obtained from Invitrogen (Carlsbad, CA), Life Technologies, Inc. (Grand Island, NY), New England Biolabs (Beverly, MA) and Stratagene (La Jolla, CA). Reagents were obtained from Sigma (St. Louis, MO), BioRad Laboratories (Hercules, CA) and Fisher Scientific (Pittsburgh, PA). Plasmid purification kits were acquired from Qiagen Inc. (Valencia, CA). The anti-rabbit immunoglobulin horseradish peroxidase-linked whole antibody (from donkey), anti-mouse immunoglobulin horseradish peroxidase-linked whole antibody (from sheep), Hybond ECL Nitrocellulose membrane, electrochemiluminescence Western blotting reagents and high performance chemiluminescence film were purchased from Amersham Biosciences (Piscataway, NJ). Polyclonal antibodies against SDS-denatured *b* subunit (284, 285) were generously

provided by Dr. Karlheinz Altendorf (Universität Osnabrück, Osnabrück, Germany). Mouse monoclonal antibodies against the peptide epitope of hemagglutinin protein of human influenza virus (HA epitope tag) were purchased from Roche Molecular Biochemicals (Indianapolis, IN). Monoclonal antibodies against the epitope found in the P and V proteins of the paramyxovirus, SV5 (V5 epitope tag) were purchased from Invitrogen.

Strains and Media

The bacterial strains used to create the epitope tagged *b* subunits include the wild type *b* subunit expression plasmid, pKAM14, and plasmids used to express *b* subunits shortened or lengthened by 7 amino acids, pAUL3 and pAUL19, respectively, and have been described previously (193, 194, 203). The plasmids encoding the different *uncF*(*b*) genes were used to compliment *E. coli* strain KM2 (Δ*b*) carrying a chromosomal deletion of the gene (218). All strains were streaked onto plates containing Minimal A media supplemented with succinate (0.2% w/v), to determine enzyme viability. Cells harvested for membrane preparation were grown in Luria Bertani media supplemented with glucose (0.2% w/v) (LBG). Isopropyl-1-thio-β-D-galactopyranoside (IPTG)(40 μg/ml), ampicillin (Ap) (100μg/ml), and chloramphenicol (Cm) (25 μg/ml) were added to media as needed. All cultures were incubated at 37˚C for the appropriate duration.

Recombinant DNA Techniques

Plasmid purification. Plasmid DNA was purified with the Qiagen Mini-Prep and Maxi-Prep kits according to the protocols provided from the manufacturer. Mini-preps required 4 mL (high copy plasmid) or 6 mL (low copy plasmid) of an overnight bacterial culture carrying the desired plasmid. Maxi-preps required a 500 mL culture grown

overnight. Final elution volumes for the mini-prep kit was 30 or 50 μL, for low copy and high copy plasmids, respectively, and 200-250 μL for the maxi-prep kit. Final concentrations of 0.5 and 1.0 μg/μl plasmid were routinely obtained with the Qiagen mini and maxi-prep kits.

Digestions, ligations, and transformations. Restriction endonuclease digestions, ligations, and transformations were performed according to the recommendations of the manufacturers (New England Biolabs, Stratagene and Invitrogen). For analytical purposes, restriction endonuclease digestions were normally prepared in a total volume of 20 μL, including plasmid DNA, enzyme, buffer, ddH_2O and occasionally BSA, and then incubated for an hour at the temperature specified by the manufacturer. Ligations required two purified double-stranded DNA fragments, a vector and an insert, of known length and concentration (ng/μL). DNA fragments were routinely separated in a 0.8 % agarose gel by electrophoresis and the appropriate sized fragment was excised and purified using a Qiagen, Inc. QIAquick Gel Extraction kit. The vector fragment contained the antibiotic resistance gene and the origin of replication. The insert typically contained the desired gene or a site specific mutation. Two control reactions and two ligation reactions were set up. The typical reaction was set up in 20-40 μL and included vector, insert, ATP, T4 DNA ligase buffer, T4 DNA ligase and ddH_2O. The first control reaction was a control for uncut plasmids, containing no insert and no ligase, and the second, containing no insert, was a control for the vector's ability to ligate with itself. The femptomolar concentration (fmol/μL) was determined from the known size and measured concentration. Two ligation reactions were then set up, the first had 1 part vector to 3 parts insert and the second was 1:10. Typically 5-15 fmol of vector was used.

The four reactions were incubated for 5 minutes at room temperature if T4 High Concentration DNA ligase was used or overnight at 16 ºC if T4 DNA ligase was used and then transformed into competent *E. coli*. Transformations were performed in one of three different *E. coli* strains. DH5α competent cells and XL10-Gold Ultracompetent cells were competent bacteria purchased from Invitrogen and Stratagene. These bacteria were used for purposes of plasmid preparations or to transform with a mutagenesis reaction such as Quikchange or ligations. The DH5α and XL10-Gold bacteria were stored at –80 ˚C. Basically, 25 μL pre-aliquoted cells were thawed on ice and 1-5 μL plasmid DNA was added and mixed by gentle stirring with the pipette tip. The bacteria were incubated on ice for 30 minutes, heat shocked at 42 ˚C for 45 seconds, and then incubated on ice for 2 minutes. 1 mL LBG was added and then incubated at 37 ˚C taped to a roller drum. The cells were harvested by centrifugation for 1 minute, the supernatant was discarded, the bacteria were resuspended in the remaining media, spread onto a LBG plate supplemented with the appropriate antibiotic and incubated at 37 ˚C overnight. XL10-Gold cells required treatment with β-mercaptoethanol (β-ME) before transformation to increase the efficiency. 2 μL of the provided β-ME mix was added to 45 μL pre-aliquoted cells and incubated on ice for 10 minutes prior to transformation with gentle swirling every 2 minutes. The transformation proceeded as described above. KM2 (Δ*b*) was a strain of *E. coli* generated by a previous lab member (218) and maintained in our laboratory. This strain was used for purposes of plasmid expression and the study of the *b* subunit of F_1F_0 ATP synthase. Before transformation, KM2 had to be made competent. Sterile technique was important since KM2 cells cannot be selected for by an antibiotic. All reagents and supplies were pre-chilled unless otherwise noted. A culture of KM2

cells was grown overnight at 37 ºC in 5 mL LBG. The overnight culture (100 μL) was inoculated into 10 mL pre-warmed (37 ºC) LBG and allowed to grow for 2-4 hours. The fresh culture was poured into sterile polypropylene tubes and incubated on ice for 10 minutes. The bacteria were then harvested by centrifugation (6,000 rpm in a ss-34 rotor) for 10 minutes. The supernatant was discarded and the tubes were inverted on a Kimwipe for 1 minute to allow excess LBG to drain. The bacteria pellet was resuspended in 10 mL cold, sterile 50 mM $CaCl_2$ and incubated on ice for 45-60 minutes. The bacteria were harvested as described above, resuspended in 1 mL of the 50 mM $CaCl_2$, and stored at 4 ºC until use. Generally, the competent KM2 cells could be used after two hours on ice but were most efficient for transformation at 24 hours and expired at 72 hours. For transformation, 100-200 μL of cells were used as previously described.

Site-directed mutagenesis. Site-directed mutagenesis was performed either by means of a Stratagene Quikchange XL kit or by ligation-mediated mutagenesis. Oligonucleotides containing the desired mutation(s) were designed to anneal to the same sequence on opposite strands of the plasmid (sense and antisense primers) (Appendix A) (Figure 2-1). When possible, a silent mutation was encoded to add or delete a restriction endonuclease recognition sequence to allow for easy screening of the mutation. Primers were optimally designed by ensuring the mutation was in the middle of the sequence, a cytosine (C) or guanine (G) flanked both ends of the sequence, and the melting temperature (T_m) was greater than or equal to 78 ºC. The T_m was calculated as T_m=81.5+0.41(%GC)-675/N-%mismatch, where N was the primer length (bases). When introducing insertions or deletions, "%mismatch" was dropped from the formula.

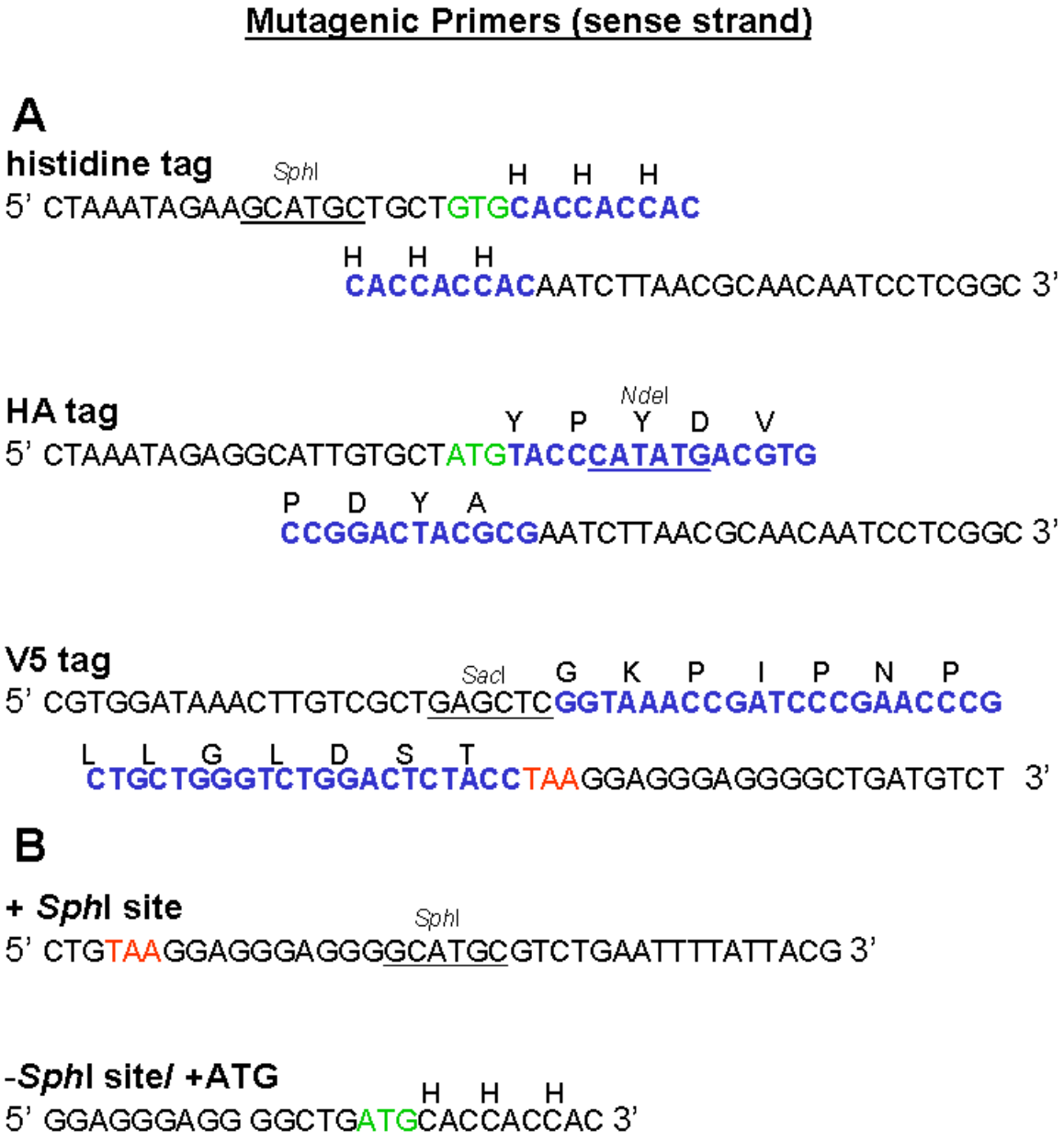

Figure 2-1. Oligonucleotides for epitope tags and mutagenesis of *uncF*(*b*). Shown are the sense strands of the mutagenic primer pairs. Green and red codons specify translation start and stop sites, respectively. A) Mutagenic primers encoding the sequence of the desired epitope tag insertion along with a silent mutation that introduced a new endonuclease recognition sequence. Epitope tags were inserted as described in the Materials and Methods. The oligonucleotides sequences specifying the histidine, HA or V5 epitope (bold blue) tag are labeled with the corresponding amino acid. The *Sph*I, *Nde*I and *Sac*I restriction sites (underlined) were added along with the histidine, HA and V5 tags, respectively, to facilitate screening. B) Oligonucleotides designed to construct the one-plasmid expression system.

Primers were not fast polynucleotide liquid chromatography (FPLC) or polyacrylamide gel electrophoresis (PAGE) purified as called for in the protocol. The reaction mixture consisted of 5 μL Stratagene's 10X *Pfu* buffer, 3 μL QuikSolution, 50 ng wild type plasmid, 125 ng each of the sense and antisense oligonucleotides, 1 μL of 25 mM dNTP's, and 1 unit *Pfu* turbo polymerase. The total volume was brought up to 50 μL with ddH_2O and PCR was performed in a Perkin Elmer GeneAmp PCR System 2400 thermocycler according to the following cycling parameters: 95°C 1 minute presoak; 18 cycles of 95°C 50 seconds, 60°C 50 seconds, 68°C 1 minute per kb of plasmid length; 4°C 7 min. Upon completion of the thermocycling, 1 μL *Dpn*I restriction endonuclease was added to the reactions in order to digest the methylated (nonmutated) plasmid DNA. The plasmids carrying the desired mutation were then transformed into competent DH5α cells, purchased from Life Technologies, and grown on LBG plates supplemented with the appropriate antibiotic. Plasmids carrying the desired mutation(s) were screened for by restriction endonuclease analysis and then the nucleotide sequences were directly determined by automated sequencing in the core facility of the University of Florida Interdisciplinary Center for Biotechnology Research (ICBR).

Mutagenesis and Strain Construction

Plasmids pKAM14 (*b*, Ap^r) (203), pAUL3 ($b_{\Delta 7}$, Ap^r) (194) or pAUL19 (b_{+7}, Ap^r) (193) were used to construct the epitope tagged *b* subunits. Epitope tags were inserted into each of the plasmids using the Stratagene Quikchange kit. A histidine epitope tag was inserted at the N-terminus by mutagenesis between the first and second codons of the *uncF*(*b*) gene to express b_{his} or $b_{+7\text{-}his}$ (Appendix A) (Figure 2-1). Plasmids pTAM37 (b_{his}) and pTAM35 ($b_{+7\text{-}his}$) were created by digesting both of the recombinant histidine-

tagged *b* subunit plasmids with *Pst*I and *Nde*I and subsequently ligating the genes into a plasmid conferring the chloramphenicol resistance gene and the pACYC184 origin of replication (Table 2-1). Likewise, an HA epitope tag was inserted at the N-terminus by mutagenesis between the first and second codons of the *uncF(b)* gene to generate plasmids pTAM36 (b_{HA}) or pTAM34 ($b_{\Delta 7\text{-}HA}$). A V5 epitope tag was added to the C-terminus by site-directed mutagenesis before the termination codon of the *uncF*(*b*) gene to express b_{V5} or $b_{\Delta 7\text{-}V5}$ from plasmids pTAM46 and pTAM47 (Figure 2-1). The recombinant HA-tagged and V5-tagged *b* subunit plasmids included the ampicillin resistance gene and the pUC18 origin of replication. Unique restriction enzyme sites *Sph*I, *Nde*I and *Sac*I were constructed near the histidine, HA and V5 epitope tag sequence, respectively, for an initial detection of the insertions, and then the nucleotide sequence was subsequently confirmed by automated sequencing in the ICBR core facility. Additionally, a set of plasmids was designed in order to express two different-tagged *b* subunits from a single transcript (Figure 2-2). As an example, a unique restriction enzyme site, *Sph*I, was created in conjunction with the histidine tag between the Shine Dalgarno sequence and the first codon of *uncF(b)* to create pTAM35 (Figure 2-2A). In a separate site-directed mutagenesis reaction, an *Sph*I site was added to the pTAM34 plasmid downstream of the HA-tagged *b* subunit and behind another favorable Shine Dalgarno sequence (Figure 2-2B). The two plasmids were digested with *Sph*I and *BstE*II restriction endonucleases. The 3.2 kb vector fragment from pTAM34 and the 623 bp insert fragment from pTAM35 were isolated and then excised from a 0.8 % (w/v) agarose gel and purified with a QIAquick gel extraction kit. The vector and insert fragments were then allowed to ligate overnight at 16 ˚C. It was then crucial to mutate an

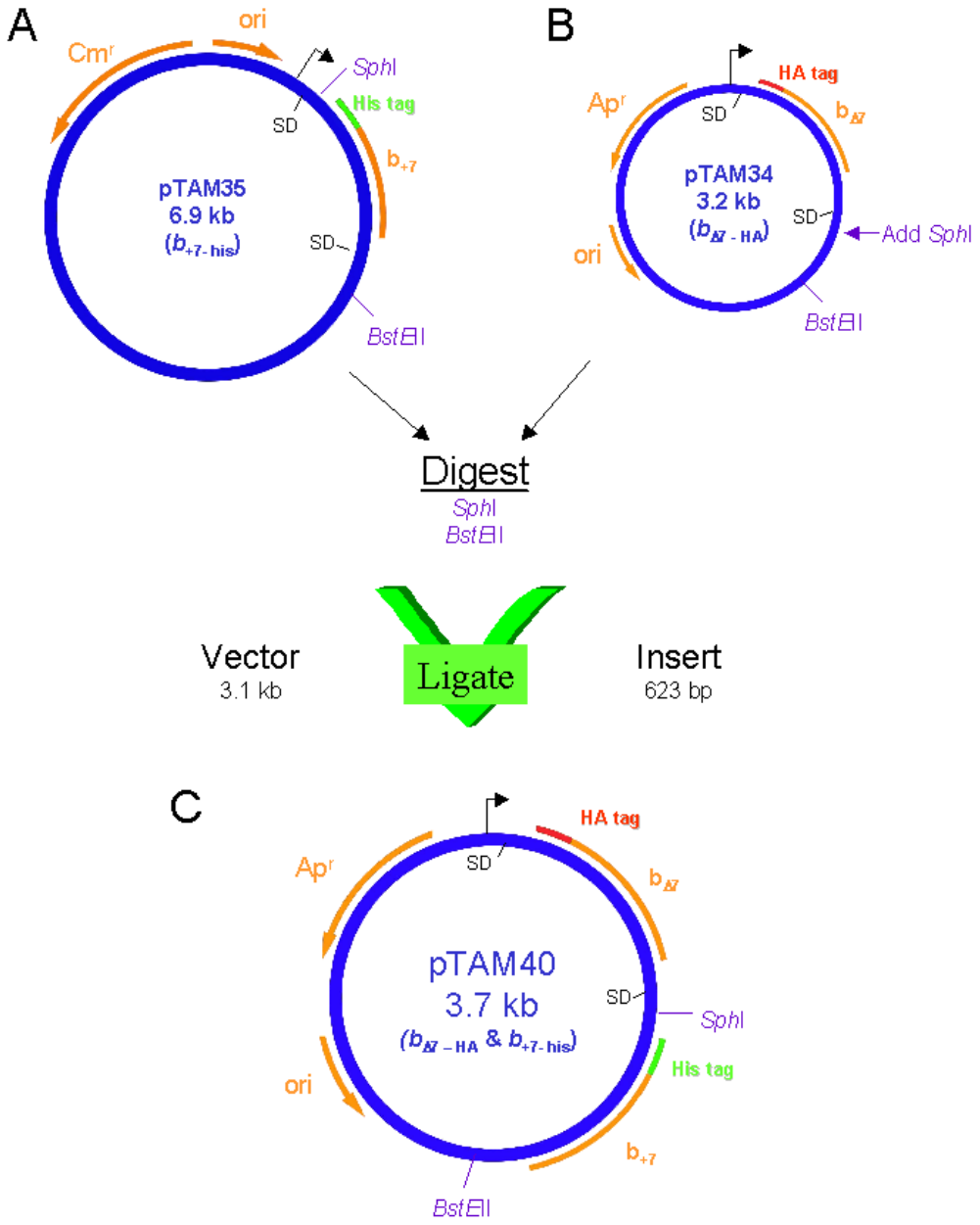

Figure 2-2. Construction of the single transcript expression system. A) A unique restriction enzyme site, *Sph*I, was created in conjunction with the histidine tag between the Shine Dalgarno sequence and the first codon of *uncF*(*b*) to create pTAM3. B) An *Sph*I site was added to pTAM34 downstream of the HA-tagged *b* subunit and behind another favorable Shine Dalgarno sequence. The two plasmids were digested with *Sph*I and *BstE*II. The 3.2 kb vector fragment from pTAM34 and the 623 bp insert fragment from pTAM35 were ligated. Additional mutagenesis (see Materials and Methods) resulted in C) a 3.7 kb plasmid, pTAM40, which expressed $b_{\Delta 7\text{-HA}}$ and $b_{+7\text{-his}}$ from the same promoter and included the ampicillin resistance gene and the pUC18 origin of replication. In similar constructions, plasmids pTAM41 ($b_{\text{wt-HA}}$ and $b_{+7\text{-his}}$) and pTAM42 ($b_{\text{wt-HA}}$ and $b_{\text{wt-his}}$) were created.

intrinsic added start codon, which is in the *Sph*I recognition sequence, to prevent a missense mutation. The mutagenic oligonucleotide was designed to accomplish three tasks in one reaction: 1) mutate the "ATG" found in the *Sph*I recognition sequence, 2) add a new Shine Dalgarno sequence in a favorable position from the true start codon, and 3) mutate the "GTG" start codon to a more favorable "ATG" start site (Figure 2-1). The resulting 3.7 kb plasmid, pTAM40, expressed $b_{\Delta 7\text{-HA}}$ and $b_{+7\text{-his}}$ from the same promoter and included the ampicillin resistance gene and the pUC18 origin of replication (Figure 2-2C). In similar constructions, plasmids pTAM41 ($b_{\text{wt-HA}}$ and $b_{+7\text{-his}}$) and pTAM42 ($b_{\text{wt-HA}}$ and $b_{\text{wt-his)}}$ were created (Table 2-1). Throughout this dissertation, the insertion or deletion and the epitope tag are indicated after the plasmid name for clarity, for example plasmid pTAM35 ($b_{+7\text{-his}}$). Each plasmid and the control plasmids pKAM14 (*b*) and pBR322 were expressed in the *E. coli* cell line KM2 (Δ*b*) for study, so that the only *b* subunits in the cells were the product of the plasmid genes.

The two plasmid expression system successfully allowed expression of various combinations of histidine tagged and V5-tagged *b* subunits in the same cell (Figure 2-7). Appropriate antibiotics were added to the growth medium, and in the case of the coexpressed plasmids, both ampicillin and chloramphenicol were added to select for cells expressing both plasmids.

Crude Preparative Procedures

Inverted membrane vesicles from KM2(Δ*b*) strains expressing the desired *b* subunit epitope tagged F_1F_0 ATP synthase complex were prepared for activity assays, Ni-resin purification and Western Blot analysis. Unless otherwise noted, all reagents, rotors and materials were kept at 4 ˚C. The membrane preparations were prepared by inoculating a

10 mL starter culture, grown overnight, into a 2 L Erlenmeyer flask containing 500 mL LBG, supplemented with the appropriate antibiotic, ampicillin (Ap) and/or chloramphenicol (Cm). Similarly, 1 mL of a starter culture was inoculated into a nephalo flask containing 50 mL LBG (Ap and/or Cm). The bacteria were grown at 37 ˚C in a New Brunswick Scientific incubator shaker (220 rpm) and the turbidity was monitored using a Klett-Summerson photoelectric colorimeter. IPTG (40 μM) was added when the turbidity reached 75 Klett units and the cells were collected when the turbidity reached 150 Klett units. The bacteria were harvested by centrifugation for 10 minutes at 8,000Xg in a Sorvall GSA rotor. The pellets were rinsed once with TM buffer (50 mM tris-HCl, 10 mM $MgSO_4$, pH 7.5) and then resuspended in a final volume of 10 mL TM buffer. DNaseI (10 mg/mL) was added to a final concentration of 10 μg/mL and the bacteria were broken by passing through a French Pressure Cell one time at 14,000 psi. Cellular debris and unbroken cells were removed by centrifuging twice at 10,000Xg for 10 minutes. Membranes were then collected by ultracentrifugation at 150,000Xg in a Beckman 70.1 Ti rotor for 1.5 hours. The membrane pellets were rinsed once with TM buffer and then resuspended in TM buffer to a final volume of 2 mL using a 2 mL Wheaton tissue grinder. For the purposes of Western blot analysis or Ni-resin purification, one ultracentrifugation step sufficed. However, activity analysis required an additional ultracentrifugation step in order to remove nonspecifically bound ATPases. In this case, the membrane pellets were resuspended in a final volume of 10 mL using a 10 mL Wheaton tissue grinder and the ultracentrifugation step was duplicated.

Determination of Protein Concentration

Total membrane protein concentrations were determined by the bicinchoninic acid (BCA) assay (286). The membrane preparations were diluted 1:10 for this assay. For each sample, triplicates of 10 μL, 20 μL and sometimes 30 μL of the diluted samples were aliquoted for the assay. Bovine serum albumin (BSA) was used to generate a standard curve. A stock of 1 mg/mL BSA was prepared and stored in microcentrifuge tubes at –20 ºC. The exact BSA concentration was determined from the OD_{280} (1.0 mg/mL BSA OD_{280}=0.667). The BSA was aliquoted in triplicates ranging from 0 to 100 μg (0, 5, 10, 20, 40, 60, 80, and 100 μL) of protein. All of the samples were incubated in 3 mL of standard working reagent (SWR), consisting of 50 parts solution A (1% BCA-Na_2, 2% $Na_2CO_3 \cdot H_2O$, 0.16% sodium potassium tartrate, 0.95% $NaHCO_3$, pH 11.25 and filtered) to one part solution B (4 % $CuSO4 \cdot 5H_2O$) plus 1% sodium dodecyl sulfate (SDS) mixed fresh as needed, for 30 minutes at 37 ºC and then for 10 minutes at room temperature. The absorbance at 562 nm was recorded for each sample with an LKB Biochrom Ultrospec II spectrophotometer. The standard curve was generated from the BSA OD readings, with a typical correlation coefficient of at least 0.997, and then protein concentrations were determined using linear regression. A typical concentration range of the total membrane protein prepared from 500 mL of media was 5-20 μg/μL.

Ni-Resin Purification

Ni-resin purification was achieved using the High Capacity Nickel Chelate Affinity Matrix (Ni-CAM) purchased from Sigma. It became necessary to optimize conditions and the ratio of protein to packed Ni-resin volume for each type of experiment. Determining the optimal ratio of protein to Ni-resin was critical because F_1F_0 ATP

synthase complexes with two histidine-tagged *b* subunits bind with a higher affinity than the complexes containing a *b* subunit heterodimer, which has only one histidine epitope tag. For the purposes of Western blot analysis, a total of 5 mg of membrane protein was brought up to 1 mL with final concentrations of 0.2% tegamineoxide WS-35, 0.15 M NaCl, and 1 mM imidazole. The purification procedure was accomplished using the trial scale miniprep method essentially described by the manufacturer. The 1 mL of clarified membrane protein was divided up equally into 5 microcentrifuge tubes, containing 100 μL of packed Ni-resin that had been washed one time with 500 μL equilibration/wash buffer (50 mM $NaH_2PO_4 \cdot H_20$, 0.3 M NaCl, 10 mM imidazole, 0.2% tegamineoxide WS-35, pH8.0), and allowed to mix on a nutator for 5 minutes. The samples were centrifuged for 30 seconds at 5,000Xg and the supernatant was discarded. The resin was washed 8 times with 1 mL wash buffer by gently mixing for 1 minute, centrifuging for 30 seconds at 5,000Xg and discarding the supernatant. The histidine-tagged proteins were eluded by mixing 50 μL elution buffer (50 mM $NaH_2PO_4 \cdot H_20$, 0.3 M NaCl, 250 mM imidazole, 0.2% tegamineoxide WS-35, pH8.0) in each microcentrifuge tube for 1 minute, centrifugation, and then the supernatant was extracted. The elution step was repeated one more time to recover more of the target protein. Finally, the target protein was pooled together and then concentrated from 500 μL to about 50 μL by centrifugation with a Millipore Amicon Bioseparations Microcon YM-10 (14,000Xg for 30 minutes). To control for possible enzyme disruption during the solubilization and purification procedures, the tagged wild-type length *b* subunits were either mock treated or treated with the homobifunctional crosslinker, bis(3-sulfo-N-hydroxysuccinimide ester) (BS^3), after the addition of detergent. Membrane preparations were chemically crosslinked by

treating with 1mM BS^3 for 30 minutes at room temperature. The cross-linking reaction was stopped by addition of 100 mM ethanolamine HCl, pH 7.5, for 10 minutes.

For the purposes of densitometric analysis, a total of 15 mg membrane protein was solubilized and clarified as described above. The clarified protein was divided into 10 samples and then Ni-resin purified (1 ml packed resin volume divided into 10 microcentrifuge tubes) as described previously, and the final eluate was concentrated with a Microcon YM-10. Attempts to purify the heterodimers with the batch method (15 mg membrane protein to 1 mL packed resin volume in a 15 mL corning conical tube, undivided) proved unsuccessful; therefore division into several microcentrifuge tubes was necessary.

Assays of F_1F_0 ATP Synthase Activity

Growth on a minimal succinate medium was used as an initial, *in vivo*, assay for enzyme viability. ATP hydrolysis activity was assayed by the acid molybdate method (146), which measures the release of P_i from ATP, in order to determine the specific activity of the epitope tagged F_1F_0 ATP synthase enzyme complexes. Membranes were assayed to determine the linearity with respect to time and enzyme concentration. Prior to the assay, all supplies and reagents were distributed, labeled and placed on ice or 37 ºC as specified below. For each membrane sample, duplicates of 60 μg membrane protein were incubated in 4.0 mL of the reaction buffer (50 mM Tris-HCl, 1 mM $MgCl_2$, pH9.1) at 37 ˚C. Stop buffer, which acts to prevent further hydrolysis of ATP, was prepared as needed and consisted of 1.3 part ddH_2O to 0.6 part HCl/molybdate solution (2.5% $NH_4Mo_4O_{24}\cdot 4H_2O$, 4.0 N HCl) to 0.4 part 10% SDS. The stop buffer was divided into 2 mL aliquots in 13x100 mm disposable borosilicate glass tubes and kept on ice throughout

the assay. Tubes of stop buffer were required for each time point of each sample, phosphate standard curve, and "ATP only" control. Prior to the beginning of the time course, two measures are taken to subtract background phosphate. First, a zero time point was taken by removing 435 μL of the reaction buffer, containing the membranes before the addition of ATP, and adding it to 2 mL of stop buffer. Also, to account for spontaneous hydrolysis, ATP was incubated in 4 mL of reaction buffer with no membrane protein and then 435 μL was removed and added to stop buffer. The time course was started by the addition of 80 μL ATP (0.15 M in 25 mM Tris-HCl, pH 7.5) to the reaction buffer and additional time points were taken at 2, 5, 7, 10 and 12 minutes. A phosphate standard curve was generated by preparing duplicates of 1 mL reaction buffer containing 0, 0.02, 0.1, 0.2, 0.4 and 0.6 μmol phosphate (KH_2PO_4), and then adding 435 μL of each to 2 mL stop buffer. Once the time course and the standard curve were completed, all of the samples in stop buffer were removed from the ice and allowed to come to room temperature. The inorganic phosphate concentration was determined by adding 100 μL of Eikonogen solution (1 M $NaHSO_3$, 0.1 M Na_2SO_3, 0.01 M 4-amino-3-hydroxy-1-naphthalenesulfonic acid), diluted 1:10, and incubating at room temperature for 30 minutes to allow color development. The absorbance of each time point at 700 nm was recorded with an LKB Biochrom Ultrospec II spectrophotometer and the amount of free phosphate in each sample was determined using linear regression. The rate of ATP hydrolysis was determined and the apparent specific activity was expressed as μmol P_i/min/mg membrane protein.

Membrane energization was detected by the fluorescence quenching of 9-amino-6-chloro-2-methoxyacridine (ACMA) (271). First, F_1F_0 ATP synthase-mediated ATP-

driven proton pumping activity in inverted membrane vesicles prepared from the epitope-tagged mutants was used as an indication of coupled activity. Acidification of the inverted membrane vesicles upon addition of ATP was directly examined by fluorescence quenching. Membrane protein (250 μg) was suspended in 3 ml of assay buffer (50 mM MOPS, 10 mM $MgCl_2$, pH 7.3) in a quartz cuvette. The fluorescent dye ACMA was added to a final concentration of 1 μM, and fluorescence was monitored with a Perkin-Elmer LS-3B Fluorescence Spectrometer with excitation at 410 nm and emission at 490 nm and directly recorded with a Perkin-Elmer GP-100 Graphics Printer. After several seconds, the fluorescent emission stabilized and was manually set to 85% for the purpose of the scale. The emission was graphically recorded for 1.5 minutes, ATP was added to a final concentration of 0.4mM and the emission was recorded for and additional 10-12 minutes.

The level of β-nicotinamide adenine dinucleotide, reduced form, (NADH)-driven fluorescence quenching was monitored for all membrane preparations to demonstrate that the vesicles were intact and closed. Membrane protein (250 μg) was suspended in 3 ml of assay buffer (50 mM MOPS, 10 mM $MgCl_2$, pH 7.3). ACMA was added to a final concentration of 1 μM, and fluorescence was recorded excitation set at 410 nm and emission set at 490 nm. After several seconds, the fluorescent emission stabilized and was manually set to 95%. The emission was recorded for 1 minute, 5 μL NADH (0.1 mM) was added and the emission was continually recorded. Over time, membrane vesicle acidification peaked and the fluorescence quenching reached a maximum. As the fluorescence began to rise, 5 μL of 0.3 mM KCN was added and the emission was recorded for a total time of about 10-15 minutes.

Immunoblot Analysis

Electrophoresis and transfer. Proteins were mixed with 2X Laemmli sample buffer (LSB) (62.5 mM tris-HCl, pH 6.8, 2% w/v SDS, 720 mM β-mercaptoethanol, 20% glycerol, and 0.1% Bromophenol blue) and incubated for 5 minutes at 95 ºC. The proteins were then loaded on either a 15 cm 15% tris-glycine SDS gel or a purchased SDS-PAGE 15% Tris-HCl Ready Gel purchased from BioRad Laboratories and then transferred onto a nitrocellulose (anti-*b* or anti-V5 antibody incubation) or polyvinylidene fluoride (PVDF) (anti-HA antibody incubation) microporous membrane by electroblot. The proteins were separated in electrode buffer (25 mM tris, 192 mM glycine, and 0.1% SDS) by electrophoresis in a Mini-PROTEAN II cell (small gels) or a PROTEAN II (large gels). When it was necessary to distinguish two different tagged *b* subunits from the same immunoblot, a maximal separation was required. The proteins were run on a 15 cm 15% polyacrylamide tris-glycine gel at 100 mamp, with current held constant, until the dye reached the stacker and then at 24 mamp for 12 hours. It was necessary to double the amperage when two gels were running at the same time. The protein transfer was accomplished in transfer buffer (25 mM tris, 192 mM glycine, 20% methanol) at 4 ºC at either 100 V, 0.25 amp limit for 1 hour (small gels) or 100 V, 0.36 amp limit for 4 hours (large gels).

Anti-*b* subunit antibody. The *b* subunit antibody incubation was performed essentially as described previously by Tamarappoo *et al*. (287). The current lab stock of anti-*b* subunit antibodies were diluted 1:40 (long-term stock) and 1:40,000 (short-term stock) for storage on a non-frost-free shelf at –20 ˚C and required and additional 1:40 dilution of the short-term stock for the working concentration. Upon completion of

electrophoresis to a nitrocellulose membrane, the protein was visualized, for loading comparison, with fast green stain (50% methanol, 10% glacial acetic acid, 0.01% fast green) by incubation at room temperature with gentle shaking on a Bellco Biotechnology Orbital Shaker for 15 minutes followed by three 2-5 minute (depending on strength of stain) destain washes (50% methanol, 10% glacial acetic acid). The fast green stain was recycled for repetitive use and the destain was discarded. The membrane was washed three times for 5 minutes with tris-buffered saline (TBS) (10 mM tris-HCl, 150 mM NaCl, pH7.2) supplemented with 0.1% polyoxyethylenesorbitan monolaurate (tween 20) (TTBS) and then blocked for 1 hour at room temperature or overnight at 4 ˚C in TBS supplemented with 5% nonfat dry milk (NFDM). The primary antibody incubation was performed with the anti-*b* subunit antibody (1:40) in TTBS supplemented with 2% BSA for 1 hour followed by three 5 minute washes with TTBS. The anti-*b* antibody was restored at –20 ˚C and thawed for reuse up to 3-5 times. Finally, secondary antibody incubation was performed with horseradish peroxidase-linked donkey anti-rabbit antibody (1:50,000 in TTBS-BSA), washed 4 times in TTBS (two 5 minute washes, two 10 minute washes) and then the antibody was detected by enhanced chemiluminescence (ECL). Signals were visualized on high performance chemiluminescence film using a Kodak X-Omat. Typical exposure times for the anti-*b* antibody ranged from 1-5 minutes for strong signals and 30-60 minutes for weaker signals.

Anti-HA antibody. The HA-epitope tag antibody was performed essentially as described by the manufacturer followed by a secondary antibody incubation with horseradish peroxidase-linked anti-mouse (from sheep) antibody (1:10,000). Several initial attempts to visualize the HA-epitope tagged *b* subunit on a nitrocellulose

membrane failed to give a clean signal. It was essential to enhance the sensitivity of the antibody by transfer onto a PVDF membrane for a higher signal to noise ratio. Before electrotransfer, it was crucial to prepare the membrane by immersion in 100% methanol for 15 seconds , ddH_2O for 2 minutes and then transfer buffer for 5 minutes. The wash buffer consisted of a phosphate buffered saline (PBS) (1% NaCl, 0.025% KCl, 0.18% Na_2HPO_4, 0.03% KH_2PO_4, pH 7.4) supplemented with 0.1% tween 20 (PBST), membranes were blocked in PBS with 5% NFDM, and the primary and secondary antibody incubation was performed in PBST supplemented with 2.5% NFDM. Typical exposure times for the anti-HA antibody were about 1 hour. Occasionally, a stronger detection reagent, ECL Plus (Amersham Biosciences), was required for detection. ECL Plus is an extremely sensitive detection system; therefore it was necessary to follow protocol carefully, using optimal primary and secondary antibody conditions. The detection reagents were brought to room temperature before opening and then solutions A and B were mixed in a 40:1 ration. The final volume required was 0.1 mL per cm^2 of membrane. Excess wash buffer was allowed to drip off the membrane and then the detection solution was pipetted onto the membrane and incubated at room temperature for 5 minutes. Finally, it was critical to drain off excess detection reagent by touching the corner of the membrane onto a kimwipe before exposure to film.

Anti-V5 antibody. The V5-epitope tag antibody incubation was performed as described by the manufacturer followed by secondary antibody incubation with horseradish peroxidase-linked sheep anti-mouse antibody (1:10,000). The wash buffer consisted of TTBS, membranes were blocked in TBS with 5% NFDM, and the primary and secondary antibody incubation was performed in TBS supplemented with 2.5%

NFDM. Typical exposure times for the anti-V5 antibody were about 30 seconds to 1 minute for membrane proteins and about 1 hour to overnight to visualize Ni-resin purified proteins.

Results

HA-Epitope Tagged *b* Subunits

To investigate whether it is possible for two *b* subunits of unequal length to dimerize to form the peripheral stalk in a functional enzyme complex, a collection of plasmids expressing two different epitope tagged *b* subunits were generated by site-directed mutagenesis. Initially a histidine-epitope tag and a HA-epitope tag were employed.

Construction and growth characteristics of mutants

The first approach developed to express two different *b* subunits in the same cell was a two plasmid expression system (Figure 2-2). A total of four plasmids were constructed expressing $b_{\text{wt-his}}$ (Cm^r), $b_{\text{+7-his}}$ (Cm^r), $b_{\text{wt-HA}}$ (Ap^r) or $b_{\Delta 7\text{-HA}}$ (Ap^r) (Table 2-1). The histidine and HA epitope tags were needed to facilitate enzyme purification and subunit detection on Western blot, respectively. Coexpression of both *b* subunits was selected for by media that contained both ampicillin and chloramphenicol.

A previous analysis of F_1F_0 ATP synthase complexes with *b* subunits shortened and lengthened by 7 amino acids found the mutants to be essentially wild-type (193, 194). Functional F_1F_0 ATP synthase complexes have been studied with epitope tags positioned on many of the subunits, however, an epitope tag on the *b* subunit had not been attempted. It was possible that the epitope tags would affect enzyme assembly or function. The effects of the added epitope tags were studied by the ability of the plasmids to complement the *E. coli* strain KM2 (Δ*b*) (218). Growth on succinate minimal

medium was used as an initial qualitative gauge of enzyme activity *in vivo* since *E. coli* strains lacking F_1F_0 ATP synthase cannot derive energy from nonfermentable carbon sources. In each case, the strains expressing the histidine and HA-epitope tagged *b* subunits grew comparably to the wild type strain (Table 2-1).

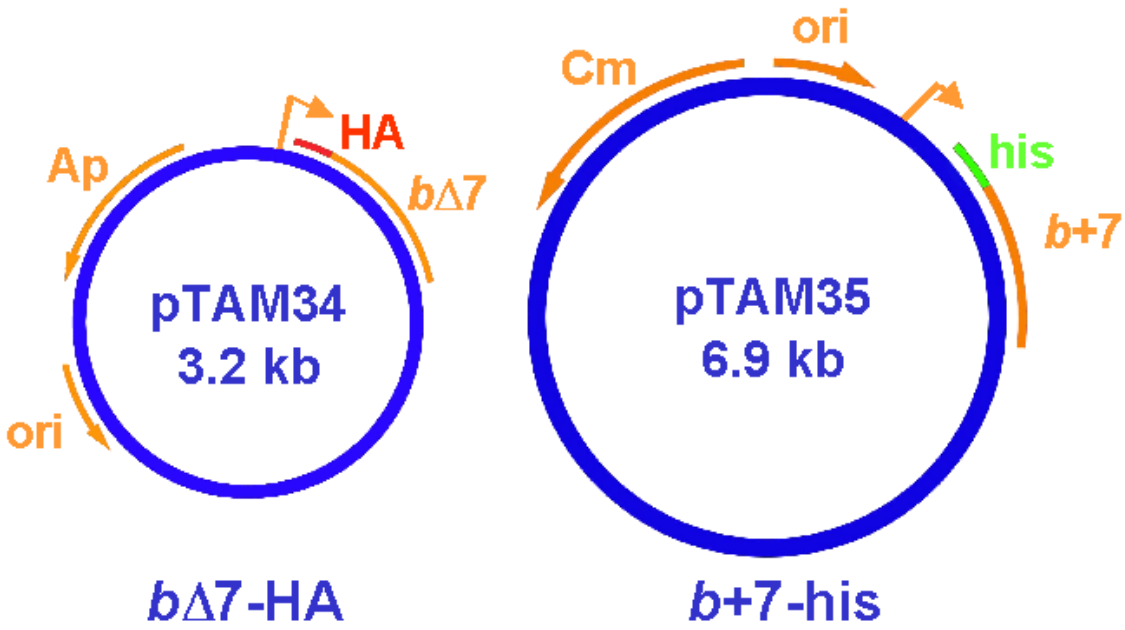

Figure 2-3. Histidine and HA-epitope-tagged *b* subunit expression system. We employed an epitope-tag system in order to determine whether *b* subunits of unequal length can interact to form the dimer in an intact and functional enzyme complex. B) Both $b_{\Delta 7\text{-HA}}$ and $b_{+7\text{-his}}$ were expressed together in KM2 (Δb) cells using a two-plasmid expression system. Plasmid pTAM34 was designed to express high levels of HA-tagged $b_{\Delta 7}$. This plasmid contains the genes conferring ampicillin resistance and the pUC18 origin of replication. Plasmid pTAM35 includes the chloramphenicol resistance gene, the pACYC184 origin of replication and expresses histidine-tagged b_{+7}. In similar constructions, plasmids pTAM37 ($b_{\text{wt-his}}$, Cm^r) and pTAM36 ($b_{\text{wt-HA}}$, Ap^r), or pTAM35 ($b_{+7\text{-his}}$, Cmr) and pTAM46 ($b_{\text{wt-HA}}$, Ap^r) were developed for coexpression experiments.

Table 2-1. Aerobic growth properties and membrane-associated ATP hydrolysis activity of mutants expressing epitope tagged *uncF*(*b*) genes

Strains	Description	Growth[1]	Specific activity[2]
KM2/pKAM14 (+)	b_{wt}, Ap^r	+++	1.72 ± 0.04
KM2/pBR322 (-)	Δ*b*, Ap^r	-	0.50 ± 0.01
KM2/pTAM37	$b_{wt\text{-}his}$, Cm^r	+++	1.53 ± 0.08
KM2/pTAM35	$b_{+7\text{-}his}$, Cm^r	+++	1.35 ± 0.03
KM2/pTAM36	$b_{wt\text{-}HA}$, Ap^r	+++	1.48 ± 0.03
KM2/pTAM34	$b_{\Delta 7\text{-}HA}$, Ap^r	+++	1.39 ± 0.04
KM2/pTAM37/pTAM36	$b_{wt\text{-}his}$ + $b_{wt\text{-}HA}$, Cm^r & Ap^r	+++	nd
KM2/pTAM35/pTAM36	$b_{+7\text{-}his}$ + $b_{wt\text{-}HA}$, Cm^r & Ap^r	+++	nd
KM2/pTAM35/pTAM34	$b_{+7\text{-}his}$ + $b_{\Delta 7\text{-}HA}$, Cm^r & Ap^r	+++	1.41 ± 0.04
KM2/pTAM42	$b_{wt\text{-}his}$ + $b_{wt\text{-}HA}$, Ap^r	+++	nd
KM2/pTAM41	$b_{+7\text{-}his}$ + $b_{wt\text{-}HA}$, Ap^r	+++	nd
KM2/pTAM40	$b_{+7\text{-}his}$ + $b_{\Delta 7\text{-}HA}$, Ap^r	+++	nd
KM2/pTAM46	$b_{wt\text{-}V5}$, Ap^r	+++	1.63 ± 0.02
KM2/pTAM47	$b_{\Delta 7\text{-}V5}$, Ap^r	+++	1.40 ± 0.05
KM2/pTAM37/pTAM46	$b_{wt\text{-}his}$ + $b_{wt\text{-}V5}$, Cm^r & Ap^r	+++	1.70 ± 0.03
KM2/pTAM35/pTAM46	$b_{+7\text{-}his}$ + $b_{wt\text{-}V5}$, Cm^r & Ap^r	+++	1.58 ± 0.02
KM2/pTAM35/pTAM47	$b_{+7\text{-}his}$ + $b_{\Delta 7\text{-}V5}$, Cm^r & Ap^r	+++	1.53 ± 0.03

[1] *E. coli* strains were grown aerobically on succinate minimal medium. Colony size was scored after 72-hr incubation at 37ºC as: +++, ≥ 1.0 mm; ++, 0.3-0.5 mm; +, ~0.1 mm; -, no growth.

[2] ATPase activities were measured as described under "Materials and Methods." Units of specific activity = μmol of PO_4 released per mg of protein/min ± S.D. Units were calculated from the slope of the line based on three measurements with incubations for 12 minutes.

Effects of epitope tags

Since F_1 has little affinity for the membrane in the absence of intact F_0, total membrane associated F_1-ATP hydrolysis activity was used as a test of F_1F_0 ATP synthase complex assembly. Under conditions of high pH, F_1 can be released from the influence of F_0 (146), so the amount of ATPase activity in the solution was used as a measure of the amount of intact enzyme complex located in the membrane vesicles. The histidine and HA-epitope tags had a slight, but not vitally significant affect on enzyme assembly. Membrane preparations with a $b_{wt\text{-}HA}$ or $b_{\Delta 7\text{-}HA}$ incorporated into the F_1F_0 ATP synthase complex had specific activities of about 86% and 81% of the wild type strain, respectively (Table 2-1). The latter value was comparable to the effect of the seven

amino acid deletion in the absence of the epitope tag. Similar activities were observed in membrane vesicles isolated from cells with a histidine epitope tag was incorporated onto the enzyme. F_1F_0 ATP synthase complexes with a $b_{wt\text{-}his}$ or $b_{+7\text{-}his}$ dimer had specific activities of about 90% and 79% of the wild type strain, respectively (Table 2-1).

Expression of different *b* subunits in the same cell

The ability to express two different *b* subunits in the same cell in roughly equal quantities was crucial to the success of the experiment. Therefore it was necessary to establish whether two separate plasmids could be used to direct production of two different *b* subunits. Two *b* subunits, expressed from pTAM35 ($b_{+7\text{-}his}$) and pTAM34 ($b_{\Delta 7\text{-}HA}$), were expressed in the same KM2 (Δb) cell and their ability to exist in the same cell was determined by Western blot analysis (Figure 2-4A). As expected, immunoblot analysis of crude membrane preparations using anti-*b* antibodies showed the presence of the *b* subunit in all strains complemented with an epitope-tagged *b* subunit (Figure 2-4A, Lanes 3-6). As shown in the first lane, KM2 cells did not express *b* subunit. After transforming with plasmid pKAM14 (b_{wt}), the KM2 cells expressed the wild type *b* subunit (Lane 2). The third and forth lanes represented KM2 cells expressing the $b_{\Delta 7\text{-}HA}$ and $b_{+7\text{-}his}$ subunits, respectively. In lane 5, individual membrane preparations representing lanes 3 and 4 were mixed together. Finally, lane 6 represented the KM2 expressing both the short and long *b* subunits in the same cell. This figure demonstrated our ability to separate the short and long subunits enough to be sufficiently distinguishable. Notably, the KM2 cells successfully expressed the two different *b* subunits in roughly equal quantities from the same cell.

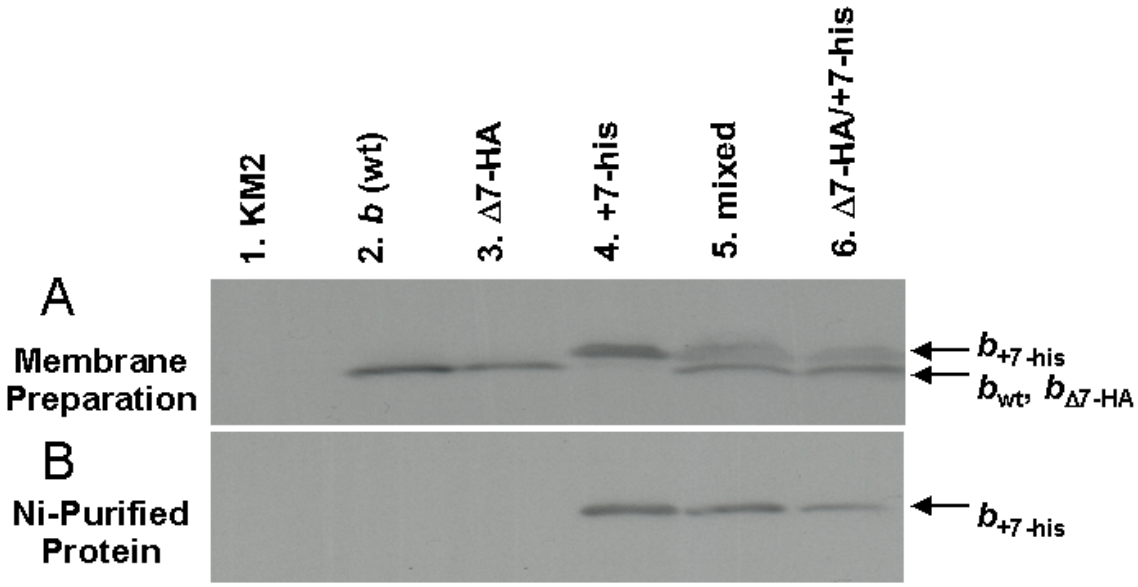

Figure 2-4. Western blot analysis of histidine and HA-epitope tagged *b* subunits. A) KM2 (Δ*b*) cells were transformed with pKAM14 (b_{wt}), pTAM34 ($b_{\Delta 7\text{-HA}}$), pTAM35 ($b_{+7\text{-his}}$), or both pTAM34 and pTAM35. Crude membrane preparations were made and proteins separated on a 15% polyacrylamide Tris-HCl-SDS BioRad Ready gel. The proteins were transferred to a nitrocellulose membrane and probed with anti-*b* anitbodies. Lane 5 represents a mixture of membranes in lanes 3 and 4. B) The crude membrane preparations were solubilized with 0.2% LDAO and then subjected to Ni-resin purification under native conditions (see Materials and Methods). The purified proteins were then separated with SDS-PAGE and Western blotted with anti-*b* antibodies.

Ni-Resin Purification

Initial experiments utilizing the two plasmid expression system approach indicated that the two different *b* subunits were incorporated into F_1F_0 ATP synthase in a segregated manner, suggesting that the *b* subunit dimer must form in parallel during F_1F_0 ATP synthase assembly. The two *b* subunits, expressed from pTAM35 ($b_{+7\text{-his}}$) and pTAM34 ($b_{\Delta 7\text{-HA}}$), were expressed in the same KM2 (Δ*b*) cell and their ability to exist in the same F_1F_0 ATP synthase enzyme complex was determined by Ni-resin purification followed by Western blot analysis (Figure 2-4B). Upon Ni-resin purification, only enzyme containing the histidine epitope tagged *b* subunit should have been present. As

anticipated, KM2 cells did not express *b* subunit. Western blot analysis confirmed that *b* subunits without a histidine epitope tag were washed off the resin during the wash steps (Figure 2-4B, Lanes 2 and 3) whereas $b_{+7\text{-his}}$ was retained by the Ni-resin (Figure 2-4B, Lane 4). In lane 5, when individual membrane preparations of KM2 individually expressing either the short or long subunit were mixed together, as expected, only the histidine epitope tagged *b* subunit was purified from the Ni-resin. In the KM2 cells expressing both $b_{+7\text{-his}}$ and $b_{\Delta 7\text{-HA}}$, only the histidine-tagged long *b* subunit appeared, suggesting the different *b* subunits were segregated into separate enzyme complexes. However, there were two important caveats: the enzyme complex may have dissociated before coming off the Ni-resin, and a difference of fourteen amino acids may have simply been too much for the stability of the enzyme. Both issues were studied. First, two additional detergents to solublize the membrane were investigated. The capability of the detergents to allow the enzyme to come off the resin intact was investigated by cross-linking the *b* subunits after solubilization and Ni-resin purification and then visualized by Western blots. Secondly, the size difference of the two *b* subunits was decreased by testing for the ability of the $b_{+7\text{-his}}$ subunit to dimerize with a $b_{\text{wt-HA}}$ subunit.

Membrane preparations of KM2 (Δb) expressing $b_{+7\text{-his}}$ were solubilized with 0.2% solutions of tegamineoxide WS-35 (AO), taurodeoxycholate (TD), lauryldimethylamine oxide (LDAO) or SDS and allowed to incubate at room temperature for 30 minutes. AO, TD and LDAO were detergents commonly used to solubilize membrane proteins. LDAO was likely to dissociate F_1 from F_0. In theory, however, F_0 should have remained intact through the purification. The solubilized proteins were then mock treated (-) or treated (+) with the homobifuctional crosslinker, BS^3. The cross-linking reaction was stopped by

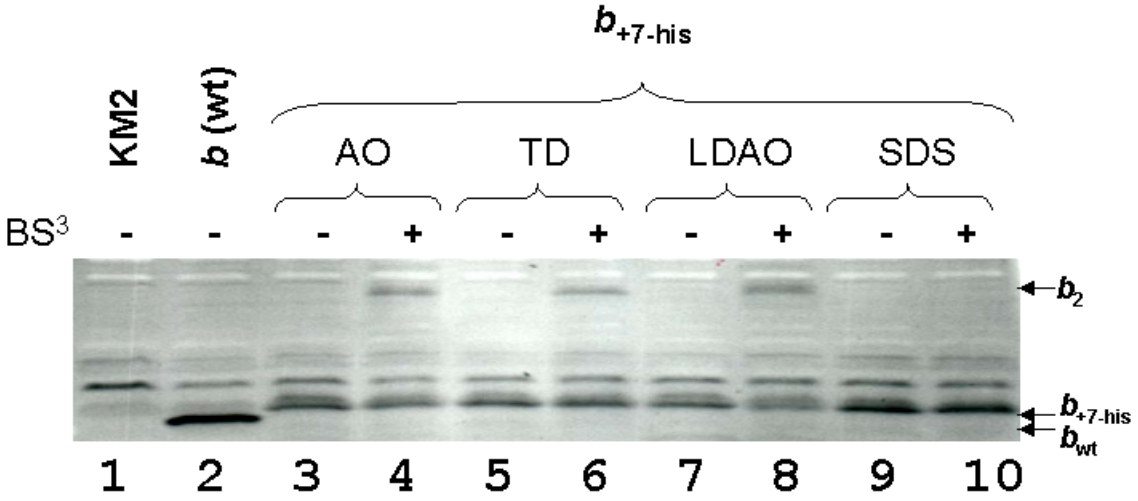

Figure 2-5. Investigation of detergent solubilization of F_1F_0 ATP synthase complexes. Membrane preparations of KM2 (Δ*b*) expressing $b_{+7\text{-his}}$ were solubilized with 0.2% solutions of detergents: tegamineoxide WS-35 (AO), taurodeoxycholate (TD), lauryldimethylamine oxide (LDAO) or SDS. The solubilized proteins were then mock treated (-) or treated (+) with 1mM bis(3-sulfo-N-hydroxysuccinimide ester) (BS^3) for 20 minutes at room temperature. The cross-linking reaction was stopped by addition of 100 mM ethanolamine HCl, pH 7.5 for 10 minutes. The products were separated by SDS-PAGE, transferred to nitrocellulose, and probed with anti-*b* antibodies.

addition of ethanolamine HCl, pH 7.5 and then the products were separated by SDS-PAGE, transferred to nitrocellulose, and probed with anti-*b* antibodies for Western blot analysis (Figure 2-5). The $b_{+7\text{-his}}$ dimers were detected in membrane preparations treated with BS^3 after solubilization, therefore, the crosslinked product showed that the $b_{+7\text{-his}}$ subunit dimer was stable during solubilization with AO, TD and LDAO (Figure 2-5, Lanes 4,6, and 8), but not with SDS (Figure 2-5, Lane 10), which was expected to denature the proteins. Once the detergent conditions were determined to be safe for the enzyme complex, the ability of the different *b* subunits, $b_{+7\text{-his}}$ and $b_{\Delta 7\text{-HA}}$, to heterodimerize was reevaluated by a slightly different approach. This time, membrane preparations were treated with the crosslinker, BS^3, prior to Ni-resin purification to ensure no disruption of the dimers (Figure 2-6). Immunoblot analysis of crude membrane

preparations using anti-*b* antibodies showed the presence of the *b* subunit in all strains complimented with a *b* or an epitope-tagged *b* subunit (Figure 2-6A, Lanes 2-5). As expected, only *b* subunits with a histidine tag were retained by Ni-resin purification (Figure 2-6A, Lanes 6-11). F_1F_0 complexes with only the HA-tagged *b* subunits were completely washed off the resin (Figure 2-6A, Lanes 6-7). To detect a heterodimer formation, immunoblot analysis using the anti-HA antibody was performed (Figure 2-6B). When the two plasmids were coexpressed in the same cell the anti-HA antibody did not detect the presence of $b_{\Delta 7\text{-HA}}$ after Ni-resin purification, indicating the two different

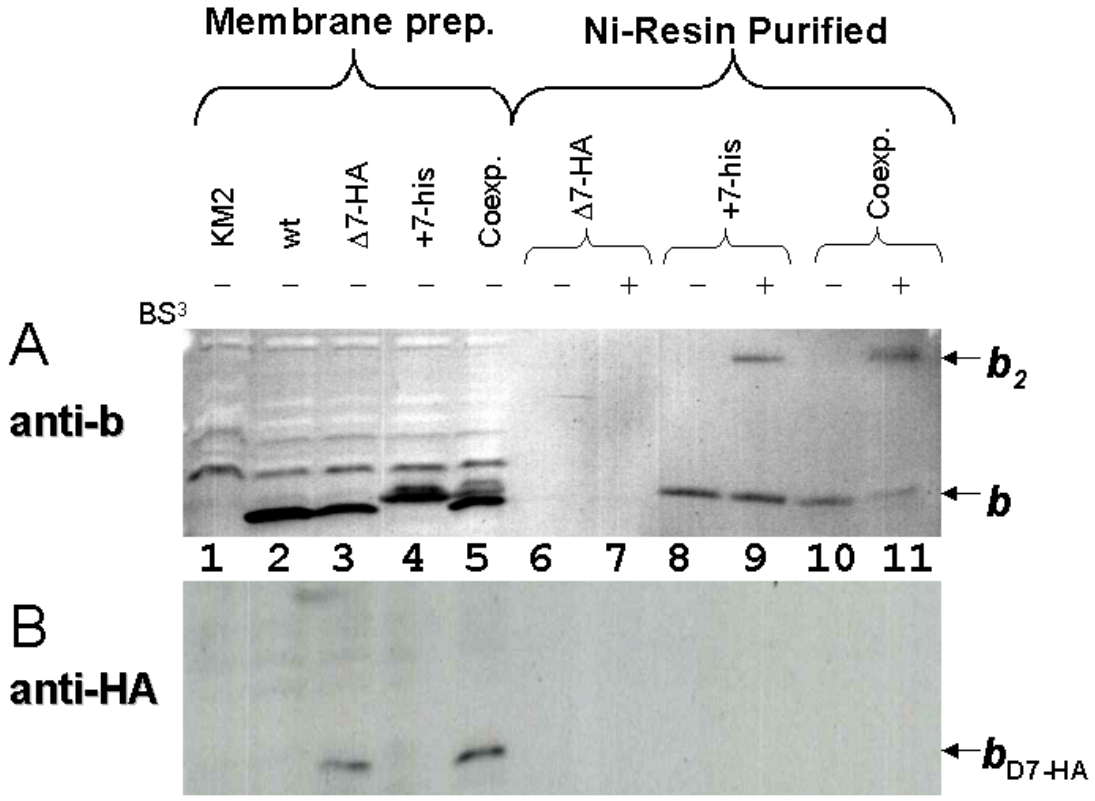

Figure 2-6. Ni-resin purification of F_1F_0, expressing different length *b* subunits, treated with the cross-linker BS^3. Crude membrane preparations of KM2 expressing the different *b* subunits were cross-linked (Materials and Methods). The products were then solubilized and subjected to Ni-resin purification before separation by SDS-PAGE and subsequent Western blot analysis. A) Proteins were transferred to a nitrocellulose membrane and probed using a polyclonal anti-*b* antibody. B) Proteins were transferred to a PVDF membrane and probed using an anti-HA mouse monoclonal antibody.

b subunits, $b_{+7\text{-his}}$ and $b_{\Delta 7\text{-HA}}$, did not dimerize. Similar experiments were performed with a seven amino acid size difference as opposed to the fourteen amino acid difference just attempted (data not shown). The immunoblot analysis gave identical results to the previous data, $b_{+7\text{-his}}$ and $b_{\text{wt-HA}}$ dimerization was not detected, suggesting the two different *b* subunits had incorporated into F_1F_0 ATP synthase in a segregated manner. However, further experimentation utilizing this experimental approach indicated that dimerization was not detected between two wild type length *b* subunits, $b_{\text{wt-his}}$ and $b_{\text{wt-HA}}$,

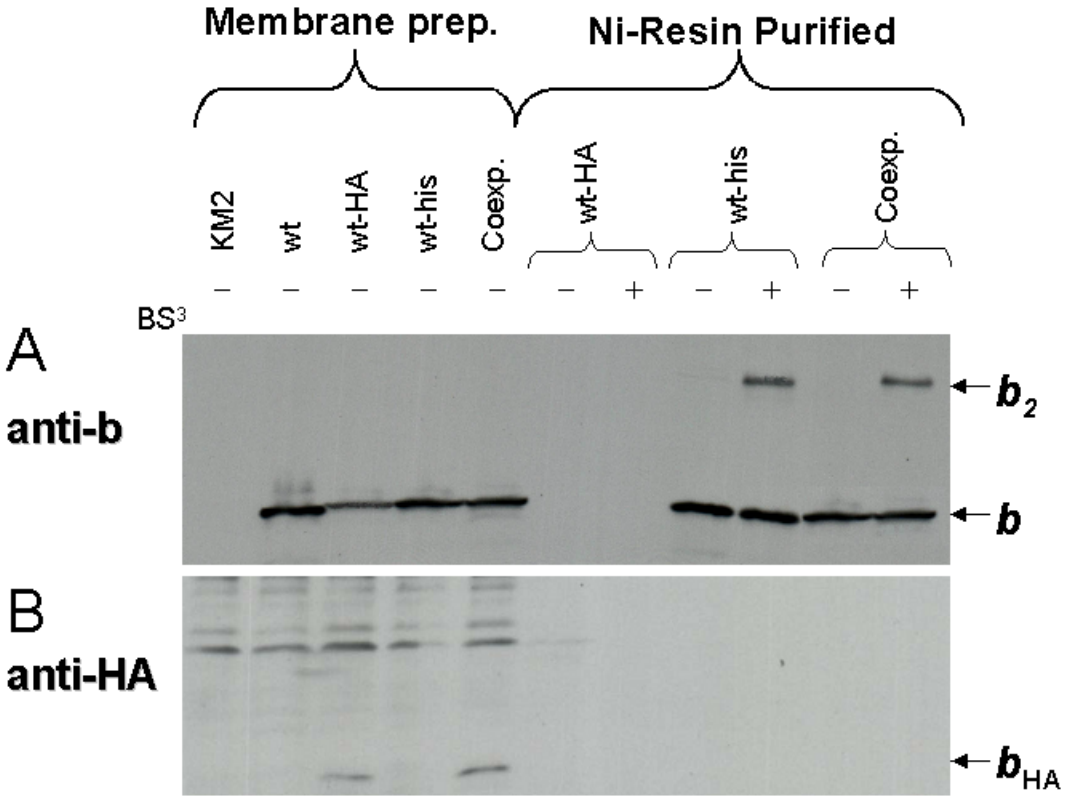

Figure 2-7. Ni-resin purification of histidine and HA-epitope tagged F_1F_0 treated with the cross-linker BS^3. Crude membrane preparations of KM2 expressing the different *b* subunits were cross-linked (Materials and Methods). The products were then solubilized and subjected to Ni-resin purification before separation by SDS-PAGE and subsequent Western blot analysis. A) Proteins were transferred to a nitrocellulose membrane and probed using a polyclonal anti-*b* antibody. B) Proteins were transferred to a PVDF membrane and probed using an anti-HA mouse monoclonal antibody.

rendering the previous data worthless (Figure 2-7). In order to conclude that the different *b* subunits formed F_1F_0 ATP synthase complexes in a segregated manner, it was necessary to detect an interaction between two wild type length *b* subunits.

Several factors may have contributed to the failure of the first experimental system: unknown interactions between the HA- and histidine-epitope tag may have hindered an interaction between the two *b* subunits, the anti-HA antibody was not sensitive enough or the signal-to-noise ratio was too small for detection, or expression from two different plasmids may have placed an early, detrimental affect on the experimental system. The latter was considered first. Dimerization of the *b* subunits is thought to be an early event in enzyme assembly, making the requirement for immediate dimerization of *b* via co-translation of a single *b* subunit transcript feasible. Therefore, three plasmids were designed to express two different tagged *b* subunits from a single transcript (Figure 2-3C, and Table 2-1). All three plasmids, pTAM40, pTAM41 and pTAM42, successfully expressed two different *b* subunits, nevertheless, an interaction between $b_{\text{wt-his}}$ and $b_{\text{wt-HA}}$ was not found.

V5-Epitope Tagged *b* Subunits

Several attempts to visualize an interaction between two different wild type length *b* subunits with a histidine and a HA-epitope tag failed. Attention was then focused on the types of epitope tags used and we decided to replace the HA tag with a V5-epitope tag.

Construction and growth characteristics of mutants

In a third attempt to investigate whether it is possible for two *b* subunits of unequal length to dimerize to form the peripheral stalk in a functional enzyme complex, a collection of plasmids expressing histidine or V5 epitope-tagged *b* subunits were

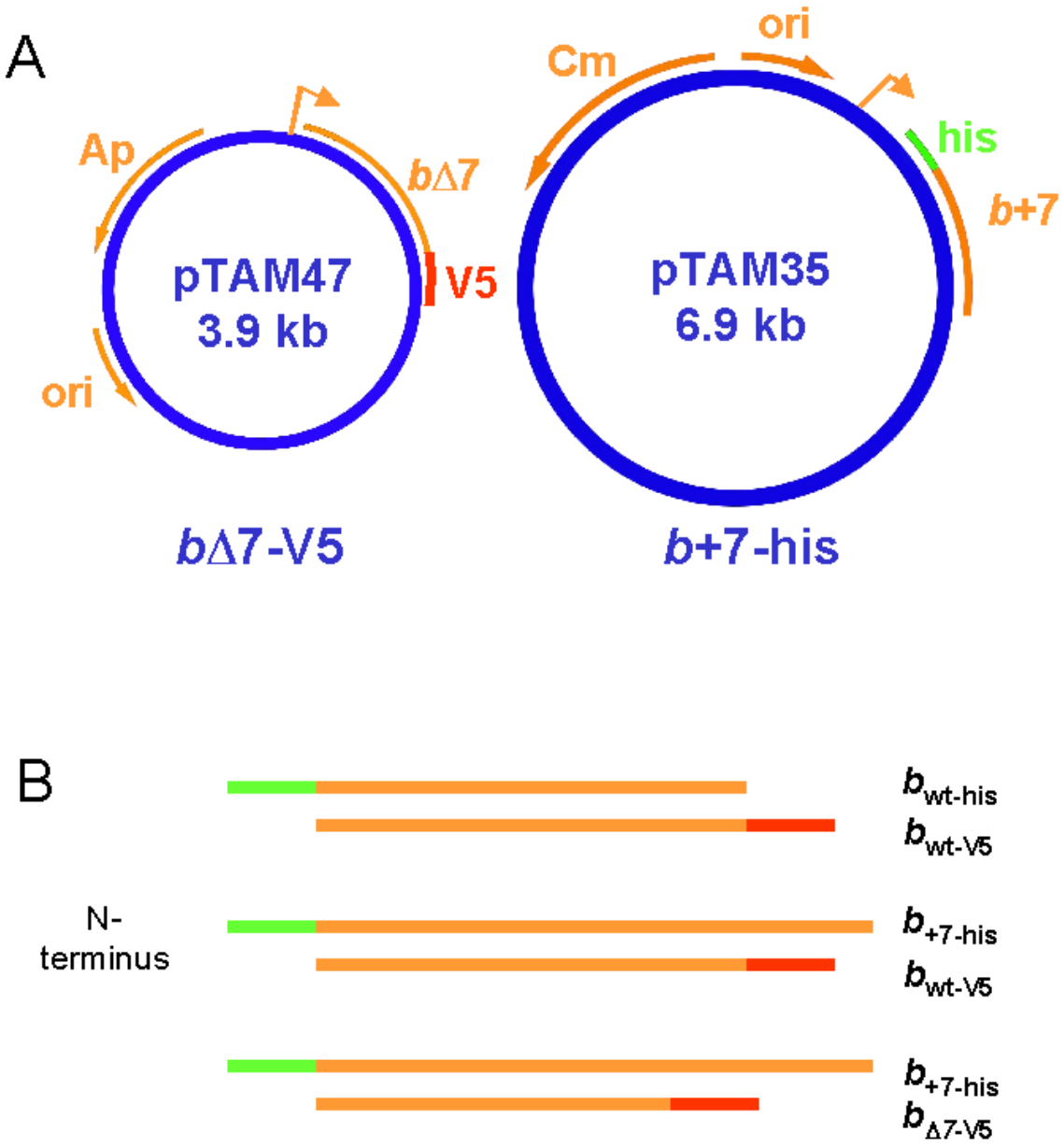

Figure 2-8. Histidine and V5-epitope-tagged *b* subunit expression system. A) Both $b_{\Delta 7\text{-V5}}$ and $b_{+7\text{-his}}$ were expressed together in KM2 (Δ*b*) cells using a two-plasmid expression system. Plasmid pTAM47 was designed to express high levels of V5-tagged $b_{\Delta 7}$. This plasmid contains the genes conferring ampicillin resistance and the pUC18 origin of replication. Plasmid pTAM35 includes the chloramphenicol resistance gene, the pACYC184 origin of replication and expresses histidine-tagged b_{+7}. In similar constructions, plasmids pTAM37 ($b_{\text{wt-his}}$, Cm^r) and pTAM46 ($b_{\text{wt-V5}}$, Apr), or pTAM35 ($b_{+7\text{-his}}$, Cm^r) and pTAM46 ($b_{\text{wt-V5}}$, Apr) were developed for coexpression experiments. B) Line diagram of the different *b* subunits that were coexpressed in the same cell. Interactions between $b_{\text{wt-his}}$ / $b_{\text{wt-V5}}$, $b_{+7\text{-his}}$ / $b_{\text{wt-V5}}$, and $b_{+7\text{-his}}$ /$b\Delta_{7\text{-V5}}$ were investigated.

generated by site-directed mutagenesis. Again, the epitope tags were needed to facilitate enzyme purification and subunit detection on a Western blot, respectively. In order to express two different *b* subunits in the same cell, we first used the two-plasmid expression system (Figure 2-8A). A total of four plasmids were constructed expressing $b_{wt\text{-}his}$ (Cm^r), $b_{+7\text{-}his}$ (Cm^r), $b_{wt\text{-}V5}$ (Ap^r) or $b_{\Delta 7\text{-}V5}$ (Ap^r) (Table I). The deletion removed the segment from *Leu*54-*Ser*60, and the insertion resulted in duplication of the same series of amino acids.

Previous work had shown that F_1F_0 ATP synthase complexes with *b* subunits shortened and lengthened by 7 amino acids were essentially wild-type (193, 194). However, it was possible that the epitope tags would affect enzyme assembly or function. This was particularly a concern at the C-terminus where small deletions at the extreme C-terminal end of the subunit had been shown to inhibit F_1F_0 ATP synthase function (206, 288). Addition of the fourteen amino acid V5-epitope tag to the C-terminus of *b* might have impinged on enzyme assembly. The effects of the added epitope tags were studied by the ability of the plasmids to complement the *E. coli* strain KM2 (Δ*b*) (218). Growth on succinate minimal medium was used as an initial qualitative gauge of enzyme activity *in vivo* since *E. coli* strains lacking F_1F_0 ATP synthase cannot derive energy from nonfermentable carbon sources. In each case, the strains expressing the epitope-tagged *b* subunits grew comparably to the wild type strain (Table I). Hence, even though deletion of as few as two amino acids affected the ability of the *b* dimer to interact with the F_1 δ subunit (41,42), addition of fourteen amino acids to the C-terminus did not interfere with the interaction of the *b* and δ subunits.

Effects of epitope tags

Since F_1 has little affinity for the membrane in the absence of intact F_0, total membrane associated F_1-ATP hydrolysis activity was used as a test of F_1F_0 ATP synthase complex assembly. Under conditions of high pH, F_1 can be released from the influence of F_0 (146), so the amount of ATPase activity in the solution was used as a measure of the amount of intact enzyme complex located in the membrane vesicles. The V5-epitope tag did not have a significant affect on enzyme assembly. Membrane preparations with a $b_{wt\text{-}V5}$ or $b_{\Delta 7\text{-}V5}$ incorporated into the F_1F_0 ATP synthase complex had specific activities of about 95% and 82% of the wild type strain, respectively (Table I). The latter value was comparable to the effect of the seven amino acid deletion in the absence of the epitope (194). A slightly greater decrease in specific activity was reproducibly observed in membrane vesicles isolated from cells when a histidine epitope tag was incorporated onto the b_{wt} or b_{+7} subunit, about 90% and 79% of wild type, respectively. Nevertheless, abundant activity was retained, suggesting very limited effects resulting from addition of the epitope tags. Furthermore, comparable activities were observed in samples when the histidine-tagged and V5-tagged *b* subunits were coexpressed.

F_1F_0 ATP synthase-mediated ATP-driven proton pumping activity in membrane vesicles prepared from the epitope-tagged mutants was used as an indication of coupled activity. Acidification of inverted membrane vesicles was examined by fluorescence of ACMA (Figure 2-9). The level of NADH-driven fluorescence quenching was monitored for all membrane preparations to demonstrate that the vesicles were intact and closed. The levels of NADH-driven fluorescence quenching were strong and directly comparable in every case (Figure 2-10). Membranes isolated from cells with a V5 epitope tag

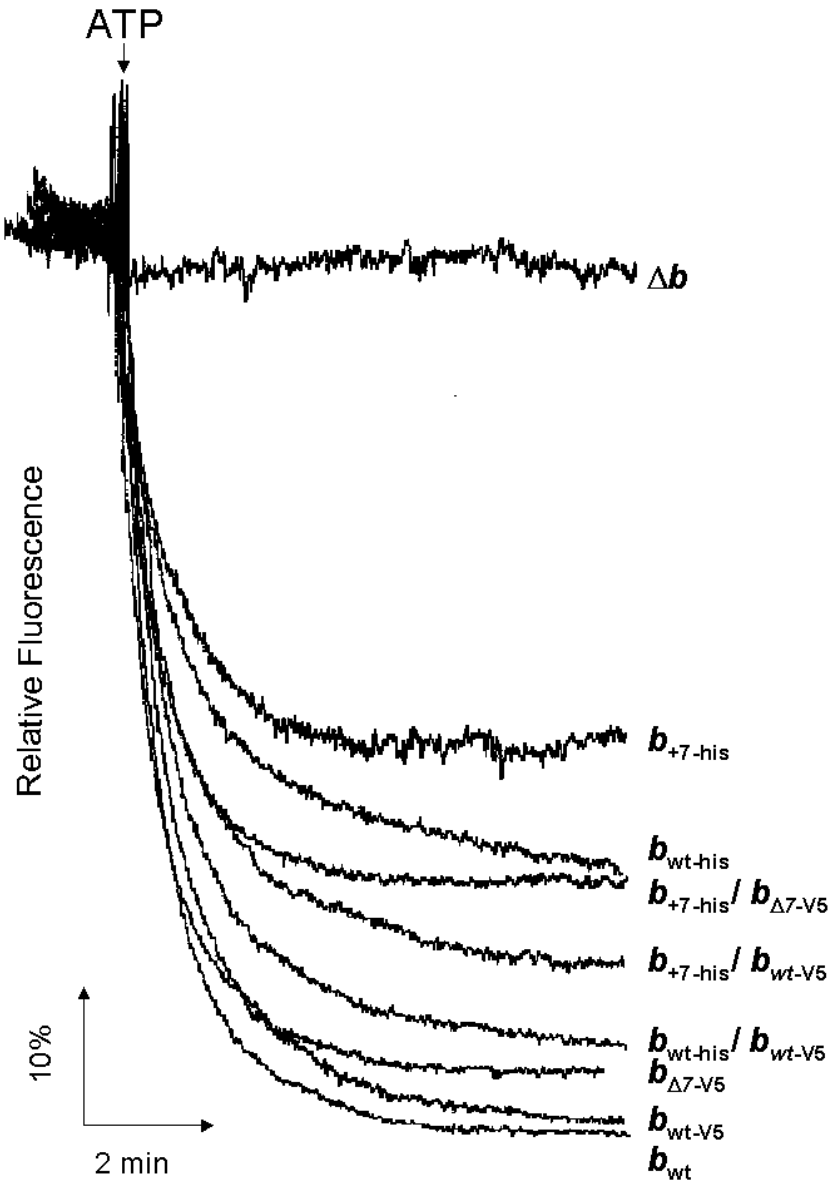

Figure 2-9. ATP-driven energization of membrane vesicles prepared from *uncF(b*) gene mutants. Cell membrane vesicles were prepared by differential centrifugation (see Materials and Methods). Membrane protein (200 μg) was suspended in 3 ml of assay buffer (50 mM MOPS, 10 mM $MgCl_2$, pH 7.3). The fluorescent dye ACMA was added to a final concentration of 1 μM, and fluorescence was recorded with excitation at 410 nm and emission at 490 nm. ATP was added as indicated to a final concentration of 1mM. The samples for each trace have been labeled according to the amino acid insertion or deletion and the epitope tag, so the strains used as the sources of the samples were as follows: b_{wt}, KM2/pKAM14; $b_{wt\text{-}V5}$, KM2/pTAM46; $b_{\Delta7\text{-}V5}$, KM2/pTAM47; $b_{wt\text{-}his}$, KM2/pTAM37; $b_{+7\text{-}his}$, KM2/pTAM35; $b_{wt\text{-}his}/ b_{wt\text{-}V5}$, KM2/pTAM37/pTAM46; $b_{+7\text{-}his}/b_{wt\text{-}V5}$, KM2/pTAM35/pTAM46; b_{+7}-his/$b_{\Delta7\text{-}V5}$, KM2/ pTAM35/pTAM47.

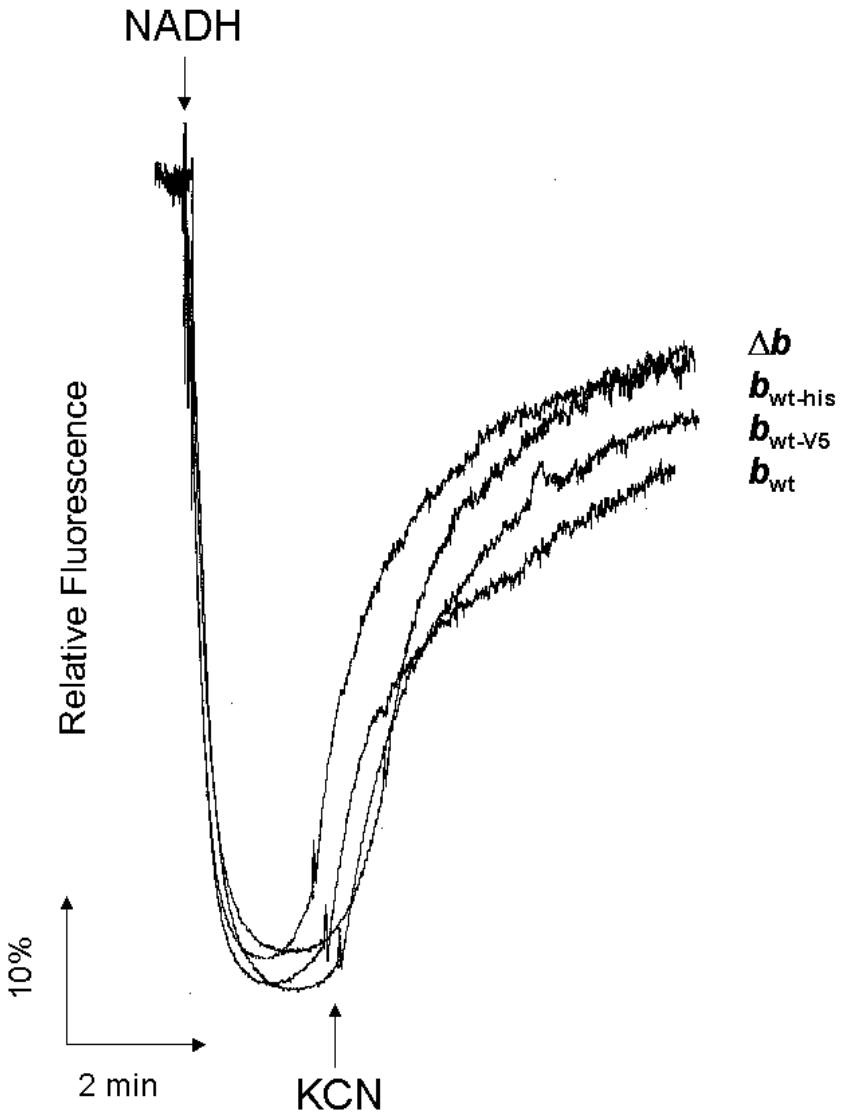

Figure 2-10. NADH-driven acidification of membrane vesicles prepared from *uncF*(*b*) mutants. Membrane protein (250 μg) was suspended in 3 ml of assay buffer (50 mM MOPS, 10 mM $MgCl_2$, pH 7.3). The fluorescent dye ACMA was added to a final concentration of 1 μM, and fluorescence was recorded with excitation at 410 nm and emission at 490 nm. 5 mL NADH (0.1 mM) was added and the emission was continually recorded. Over time, membrane vesicle acidification peaked and the fluorescence quenching reached a maximum. As the fluorescence began to rise, 5 mL of 0.3 mM KCN was added and the emission was recorded for a total time of about 10-15 minutes. The samples for each trace have been labeled according to the amino acid insertion or deletion and the epitope tag, so the strains used as the sources of the samples were as follows: b_{wt}, KM2/pKAM14; $b_{wt\text{-}V5}$, KM2/pTAM46; $b_{\Delta 7\text{-}V5}$, KM2/pTAM47; $b_{wt\text{-}his}$, KM2/pTAM37; $b_{+7\text{-}his}$, KM2/pTAM35; $b_{wt\text{-}his}$/ $b_{wt\text{-}V5}$, KM2/pTAM37/pTAM46; $b_{+7\text{-}his}/b_{wt\text{-}V5}$, KM2/pTAM35/pTAM46; $b_{+7\text{-}his}/b_{\Delta 7\text{-}V5}$, KM2/ pTAM35/pTAM47.

incorporated onto the b_{wt} or $b_{\Delta 7}$ subunit, KM2/pTAM46 or KM2/pTAM47, respectively, displayed a very slight reduction in coupled activity (Figure 2-9). The reduction in coupled activity correlated very well with the minor reduction in F_1-ATP hydrolysis activity. A larger reduction in coupled activity, of about 20-25%, was observed in membrane vesicles isolated from cells when a histidine epitope tag was incorporated onto the b_{wt} or b_{+7} subunit, KM2/pTAM37 or KM2/pTAM35, respectively. The decrease in coupled activity also paralleled with the reduction seen in F_1-ATP hydrolysis activity. Moreover, the coupled activities observed in membranes isolated from cells coexpressing histidine-tagged and V5-tagged *b* subunits were, as expected, intermediary between the V5-tagged species and the histidine-tagged species. The larger reduction seen in the cells expressing a histidine epitope tag arose in part from the plasmid vector. The moderate-copy plasmid vector pACYC184 was used to express the histidine-tagged *b* subunits. When histidine-tagged *b* subunits were expressed from the pUC18 plasmid vector, both coupled activity and ATP hydrolysis activity were similar to untagged *b* subunits (data not shown). Hence the reductions in activity observed in membranes from the histidine-tagged strains reflected reduced amounts of intact F_1F_0 ATP synthase incorporated into the membranes. For the purposes of this study, the important parameters were the presence of an intact and functional F_1F_0 ATP synthase enzyme complex and the ability to distinguish the two different tagged *b* subunits via Western blot.

Detections of heterodimers

Dimerization of the *b* subunits is thought to occur early during enzyme assembly, making the requirement for immediate dimerization of *b* via co-translation of a single *b* subunit transcript, feasible. Therefore, it was necessary to establish whether a two-

plasmid expression system could be utilized in order to direct production of two different *b* subunits that will dimerize to form an intact F_1F_0 enzyme complex. Two wild-type length *b* subunits, expressed from plasmids pTAM37 ($b_{wt\text{-}his}$, Cm^r) and pTAM46 ($b_{wt\text{-}V5}$, Ap^r), were expressed in the same cell and studied for their ability to dimerize. Under the appropriate conditions, the histidine-tagged *b* subunits allowed for the easy purification of enzyme from a crude membrane preparation using a nickel affinity resin. Via immunoblot analysis, the presence or absence of the V5 epitope tag provided a means to determine whether the two different tagged *b* subunits are interacting to form a heterodimer. Immunoblot analysis of crude membrane preparations using anti-*b* antibodies showed the presence of the *b* subunit in all strains complemented with an epitope-tagged *b* subunit (Figure 2-11A, Lanes 2-4). As expected, only *b* subunits with a histidine tag were retained by Ni-resin purification (Figure 2-11A, Lanes 5-12). Importantly, F_1F_0 complexes with only the V5-tagged *b* subunits were completely removed from the resin during the wash steps (Figure 2-11A, Lanes 7-8). To detect a heterodimer formation consisting of wild-type length *b* subunits, $b_{wt\text{-}his}$ and $b_{wt\text{-}V5}$ expressed from two plasmids, immunoblot analysis using the anti-V5 antibody was performed (Figure 2-11B). When the two plasmids were coexpressed in the same cell the anti-V5 antibody detected the presence of $b_{wt\text{-}V5}$ after Ni-purification, indicating that the expression system was successful and the tags do not hinder hetero-dimerization (Figure 2-11B, lanes 11-12).

To confirm that the F_1F_0 ATP synthase complex did not rupture during the solubilization and purification procedures, the tagged *b* subunits were either mock treated or treated with the homobifunctional crosslinker, BS^3, after the addition of detergent. As

expected, crosslinked *b* subunits were readily observed only in samples that had undergone BS^3 treatment and survived Ni-resin purification (Figure 2-11A, Lanes 6, 10, 12). BS^3 chemical crosslinking had also demonstrated that the $b_{+7\text{-his}}$ subunit dimer was stable during solubilization with tegamineoxide WS-35, taurodeoxycholate and lauryldimethylamine oxide, but not with sodium dodecyl sulfate (SDS) (Figure 2-5).

As an added precaution to ensure there was no nonspecific aggregation of *b* subunits after membrane solubilization or during Ni-resin purification, two independent membrane preparations were mixed together (Figure 2-11, Lanes 9-10). Membrane vesicles derived from strains KM2/pTAM37 ($b_{\text{wt-his}}$) and KM2/pTAM46 ($b_{\text{wt-V5}}$) were mixed, the membranes were solubilized with 0.2% tegamineoxide and allowed to incubate at room temperature for 30 minutes, and the treated with BS^3 before performing Ni-resin purification. Immunoblot analysis with anti-*b* antibodies showed normal levels of histidine-tagged *b* subunit upon Ni-resin purification (Figure 2-11A, Lanes 9-10). No V5-epitope was present after Ni-resin purification indicating nonspecific aggregation was not a factor in the observed results (Figure 2-11B, Lanes 9-10). Therefore, any observed interactions of *b* subunits must have been due to heterodimers integrating within an intact F_1F_0 ATP synthase complex in a cell expressing both *b* subunits. Importantly, immunoblotting using the anti-V5 antibody clearly detected V5 epitope tagged *b* subunits in Ni-resin purified samples when the two were coexpressed (Figure 2-11B, Lanes 11-12).

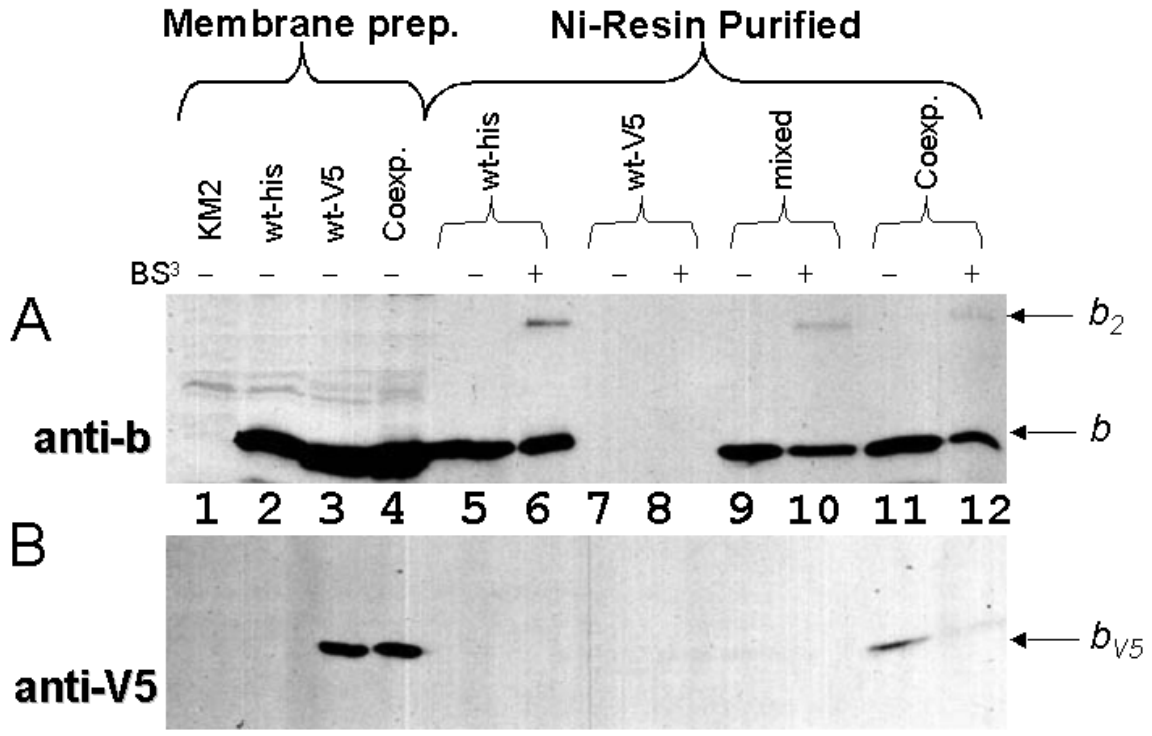

Figure 2-11. Ni-resin purification of F_1F_0 ATP synthase treated with the cross-linker BS^3. Crude membrane preparations of KM2 expressing the normal length *b* subunits with epitope tags were mock treated (-) or treated (+) with 1mM bis(3-sulfo-N-hydroxysuccinimide ester) (BS^3) for 20 minutes at room temperature. The cross-linking reaction was stopped by addition of 100 mM ethanolamine HCl, pH 7.5 for 10 minutes. The products were then solubilized with 0.2% tegamineoxide WS-35 and subjected to Ni-resin purification before separation on a 15% polyacrylamide Tris-glycine SDS gel and subsequent Western blot analysis. A) Proteins were transferred to a nitrocellulose membrane and probed using a polyclonal anti-*b* antibody. B) Proteins were transferred to a nitrocellulose membrane and probed using an anti-V5 mouse monoclonal antibody.

Formation of mixed length *b* subunits in F_1F_0 ATP synthase

The two plasmid expression system was used to study whether unequal length *b* subunits could form a dimer or, alternatively, whether the *b* subunits dimerize and incorporate into enzyme complexes in a segregated manner. In order to determine if there is a direct protein-protein interaction between the different length *b* subunits, we investigated the ability of $b_{+7\text{-his}}$ to retain an interaction with a $b_{\text{wt-V5}}$ or a $b_{\Delta 7\text{-V5}}$ subunit following Ni-purification (Figure 2-12). All membranes prepared from strains expressing a *b* subunit were readily detectable and distinguishable by size on an immunoblot (Figure 2-12, Lanes 1-7). Only *b* subunits with a histidine tag were retained by Ni-resin purification (Figure 2-12A, Lanes 8-12). Immunoblot analysis using an anti-V5 antibody was performed on the membrane preparations and Ni-purified products (Figure 2-12B). The V5-epitope tag was detected only in membrane vesicles derived from KM2 strains expressing either the V5-tagged *b* subunit or the coexpressed V5-tagged and his-tagged *b* subunits (Figure 2-12B, Lanes 1-7). As expected, upon Ni-resin purification, the V5 epitope was not detected in samples containing only histidine-tagged *b* subunit (Figure 2-12B, Lane 8). Likewise, samples containing only the V5-tagged *b* subunits were not detected upon Ni-resin purification, signifying that they were efficiently removed from the resin during wash steps (Figure 2-12B, Lanes 9-10). Finally, we investigated the ability of $b_{+7\text{-his}}$ to dimerize to form intact F_1F_0 ATP synthase complexes with $b_{\text{wt-V5}}$ or $b_{\Delta 7\text{-V5}}$. The $b_{\text{wt-V5}}$ was detected with anti-V5 antibodies and was readily observed to dimerize with the $b_{+7\text{-his}}$ indicating a $b_{wt\text{-his}}/b_{\text{wt-V5}}$ interaction (Figure 2-12B, Lane 11). To a much lesser extent, the $b_{\Delta 7\text{-V5}}$ subunit was also distinguishable with anti-V5 antibodies (Figure 2-12B, Lane 12). The data indicated that the F_1F_0 ATP synthase enzyme

complex could tolerate *b* subunit heterodimers with a size difference of at least 14 amino acids.

Detection of *b* subunit heterodimers led directly to two additional questions. How many *b* subunit heterodimer F_1F_0 ATP synthase complexes were formed? Were they active? We had not yet purified a heterodimeric complex to homogeneity so the direct assay has not been performed. However, an indication of activity could be assessed based on the percentage of homodimeric and heterodimeric F_1F_0 complexes. Therefore,

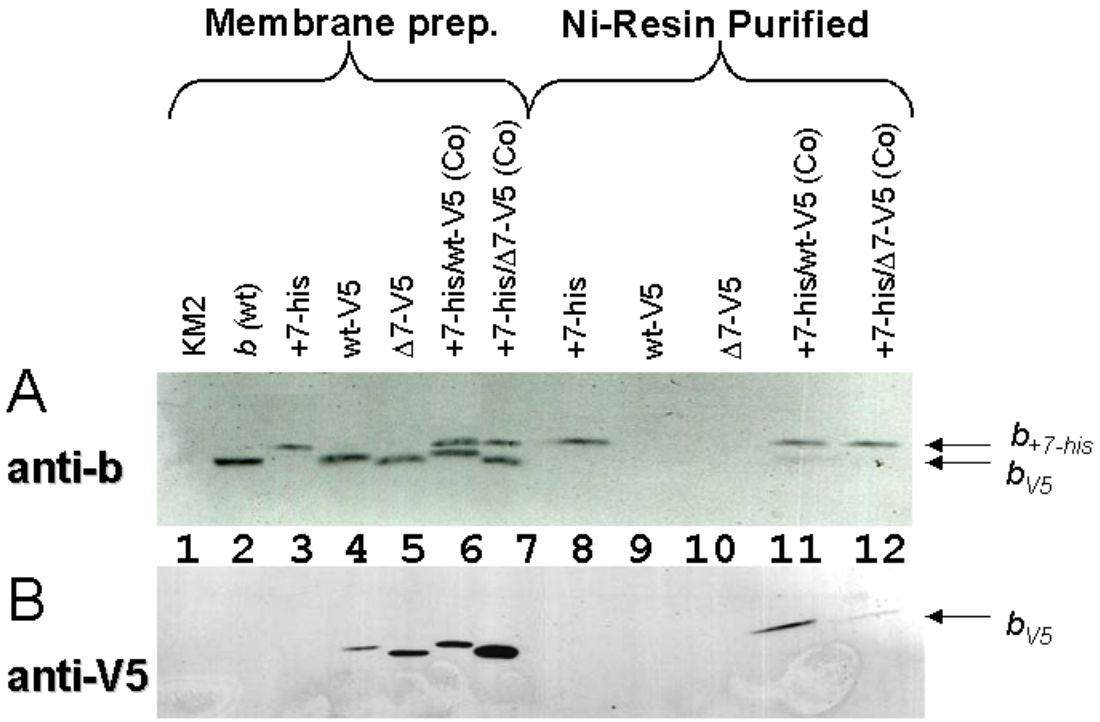

Figure 2-12. Ni-resin purification of F_1F_0 ATP synthase expressing unequal length *b* subunits. IPTG-induced cells were lysed in a French pressure cell, and membrane vesicles were isolated by differential ultra-centrifugation. The crude membrane preparation was solubilized with 0.2% tegamineoxide WS-35 and subjected to Ni-resin purification before separation on a 15% polyacrylamide Tris-glycine SDS gel and subsequent Western blot analysis. A) Proteins were transferred to a nitrocellulose membrane and probed using a polyclonal anti-*b* antibody. B) Proteins were transferred to a nitrocellulose membrane and probed using an anti-V5 mouse monoclonal antibody.

membranes were prepared from strains KM2/pTAM37/pTAM46 ($b_{wt\text{-}his}/b_{wt\text{-}V5}$), KM2/pTAM35/pTAM46 ($b_{+7\text{-}his}$ /$b_{wt\text{-}V5}$) and KM2/pTAM35/pTAM47 ($b_{+7\text{-}his}/b_{\Delta 7\text{-}V5}$). All membranes prepared from strains expressing an epitope-tagged *b* subunit were readily detectable and distinguishable by size on an immunoblot of a 15 cm 15% SDS-PAGE gel (Figure 2-13A). Densitometry was used to determine the relative amounts of histidine-tagged and V5-tagged *b* subunits in samples coexpressing the different subunits (Figure 2-13B). Relative amounts of the histidine- and V5-tagged *b* subunits were determined from crude membrane preparations that contained the different coexpressed *b* subunits. In each case, expression of the various length b_{his} and b_{V5} subunits led to nearly equal incorporation into F_1F_0 ATP synthase complexes (Figure 2-13B). Relative amounts of the b_{his} and b_{V5} subunits were also determined from Ni-resin purified samples coexpressing both *b* subunits. Upon Ni-resin purification, all of the b_{V5} subunit seen on a Western blot must necessarily be incorporated into the enzyme complex as a heterodimer along with a b_{his} subunit. Hence, when the two different wild-type length *b* subunits were coexpressed, there was at least 15% heterodimer formation (Figure 2-13B). It is possible that further manipulation of subunit expression and optimization of the purification procedure might result in a higher percentage of heterodimers found in the membranes. Somewhat lower percentages of heterodimer formation were found when $b_{+7\text{-}his}$ was coexpressed with $b_{wt\text{-}V5}$ or $b_{\Delta 7\text{-}V5}$ (Figure 5B). Based on the percentage of heterodimer formation and the activities observed when the different *b* subunits were coexpressed in the same cell (Figure 2-13, Table 2-1), it is likely that the heterodimeric F_1F_0 ATP synthase species are functionally active.

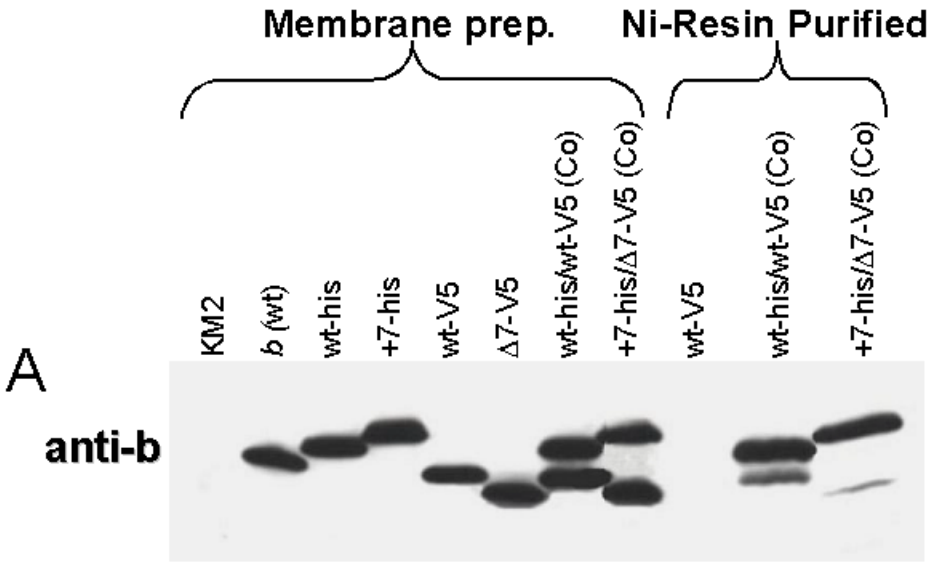

B

	% membrane *b*-his	% membrane *b*-V5	% Ni-Purified heterodimer
wt/wt	51 ± 4	49 ± 4	15 ± 1
+7/wt	46 ± 4	54 ± 4	11 ± 2
+7/Δ7	44 ± 6	56 ± 6	4 ± 1

Figure 2-13. Quantitation of *b* subunit heterodimeric F_1F_0. Membranes were prepared from IPTG-induced cells by differential centrifugation. A total of 15 mg membrane protein was solubilized, Ni-resin purified (1 ml packed resin volume), concentrated with a Microcon YM-10 and separated on a 15 cm 15% polyacrylamide Tris SDS gel to allow maximal separation. A) Proteins were transferred to a nitrocellulose membrane and probed using a polyclonal anti-*b* antibody. This Western blot was deliberately overexposed to allow easy visualization of the V5-tagged *b* subunits in the Ni-resin purification lanes. B) Densitometric analysis of lower exposures was used to determine the relative amounts of histidine-tagged and V5-tagged *b* subunits in samples coexpressing the different subunits. Reletive amounts of *b* subunits were determined for crude membrane preparations and Ni-resin purified samples coexpressing both *b* subunits. The percent of heterodimer formation was calculated based on three independent membrane preparations as well as three separate exposure times.

Discussion

In the present chapter, we have developed an expression system that facilitates production, purification and detection of *b* subunits of unequal lengths within *E. coli*. The experiments involved an epitope tag system that allowed us to determine if the different *b* subunits segregated into homodimers, or alternatively, if a heterodimer of long and short *b* subunits can be incorporated into an F_1F_0 ATP synthase complex. The histidine and V5 epitope tags introduced into the *b* subunits did not appreciably affect enzyme assembly or function. Expression of two different wild-type length *b* subunits led to three distinct F_1F_0 ATP synthase complexes in the same cell; 1) a homodimer of histidine-tagged *b* subunits, 2) a homodimer of V5-tagged *b* subunits and 3) a heterodimer consisting of a histidine-tagged *b* and a V5-tagged *b* subunit.

More importantly, three different F_1F_0 ATP synthase complexes were present even when the *b* subunits were not of identical length. We observed dimerization of *b* subunits between $b_{+7\text{-his}}$ and both $b_{\text{wt-V5}}$ and $b_{\Delta 7\text{-V5}}$. This demonstrates that *b* subunits that differ in length by at least 14 amino acids can be incorporated into an enzyme complex. Given that the tether domain is likely an α–helix, the difference in length between the *b* subunits would be approximately 21 Å. Dimerization could occur in two ways. First, assuming that the transmembrane domains were in parallel, the hydrophilic domains could be out of register. Alternatively, we favor a conformation in which both the transmembrane domains and the dimerization domains as defined by Dunn and coworkers (13) exist in parallel. This would require that a section of the tether domain in the longer *b* subunit be out of contact with the shorter *b* subunit (Figure 2-14). It is likely that a parallel alignment of the dimerization domain is required for enzyme assembly.

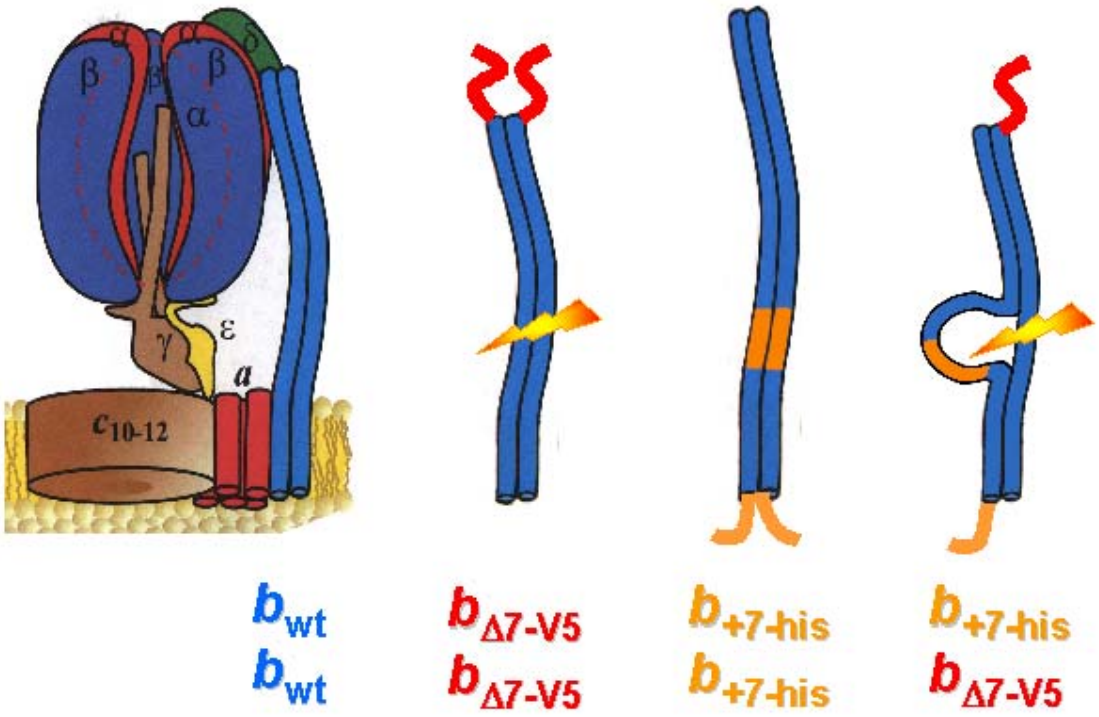

Figure 2-14. Interactions of *b* subunits of unequal lengths. An epitope-tag system novel to F_1F_0 ATP synthase studies was established in order to determine whether *b* subunits of unequal length could interact to form the dimer in an intact and functional enzyme complex. The $b_{\Delta 7}$ subunit was expressed with a V5-epitope tag at its C-terminus (represented by the 's' shaped red line) and b_{+7} was expressed with a histidine tag at its N-terminus (represented by the curved oragnge line). The lightning bolt indicates a deletion and the orangte patch represents an insertion of amino acids. The histidine tag allowed for purification on a Nickel affinity column and the V5-tag allowed us to detect the presence of the $b_{\Delta 7}$ subunit after Ni-purification using Western blot analysis. Expression of the two different epitope-tagged *b* subunits in the same cell leads to three distinct interactions within an F_1F_0 ATP synthase complex – (1) a homodimer of $b_{\Delta 7\text{-V5}}$, (2) a homodimer of $b_{+7\text{-his}}$ and (3) a heterodimer consisting of both the shortened and lengthened *b* subunit.

Recent electron microscopy and NMR studies have revealed a distinctive 20º bend in the *b* dimer within the tether domain (27, 136, 196). The research presented here suggests the possibility of straightening or further bending of the two *b* subunits within the peripheral stalk and lends support to the concept of a flexible peripheral stalk.

This raises the question, why should the tether domain be so flexible as to allow insertions, deletions and dimerization of *b* subunits of unequal lengths? If one views the peripheral stalk to be a rope-like structure linking F_1 to F_0, then its position holding F_1 against the rotation of the central stalk would not be expected to be the same for counterclockwise and clockwise rotation. Flexibility of the tether domain might facilitate reorienting the peripheral stalk to act as a stator for rotation in either direction during ATP synthesis and ATP hydrolysis.

The ability to generate and purify F_1F_0 complexes with two genetically different *b* subunits provides a potentially useful experimental tool. It is now feasible to specifically label a single *b* subunit within a purified complex. This will facilitate biochemical modification experiments and the use of physical methods.

CHAPTER 3
GENETIC COMPLEMENTATION BETWEEN MUTANT *b* SUBUNITS IN F_1F_0 ATP SYNTHASE

Introduction

In the F_1F_0 ATP synthase enzyme complex, the peripheral stalk consists of a parallel dimer of identical *b* subunits. Dimerization of the *b* subunits is thought to be an early event necessary for enzyme assembly and function (199). The two *b* subunits exist in an extended α-helical conformation, spanning from the periplasmic side of the membrane to near the top of F_1. However, due to the asymmetric nature of the enzyme complex the two *b* subunits cannot participate in identical protein-protein interactions with the other subunits. In the amino-terminal membrane spanning region, the peripheral stalk contacts a single *a* subunit. Similarly, at the carboxyl end of the peripheral stalk, the two *b* subunits interact with a single δ subunit. The *b* dimer has been studied by a variety of traditional biochemical approaches such as CD spectroscopy, cross-linking, and sedimentation experiments (30, 166, 192, 196, 197, 203, 283). Limited structural information is available from studies of polypeptides modeling functionally defined domains of the *b* subunit. Dmitriev *et al*. studied the amino-terminal membrane spanning domain by NMR using a 34 amino acid polypeptide, revealing an α-helix with a 20° bend at *pro*-27 and *pro*-28 (136). A systematic mutagenesis approach supported the model described in the NMR paper suggesting that the extreme amino-termini of the two *b* subunits were in close contact and then the subunits flare apart as they traverse the membrane (136, 202). X-ray crystallography of a model polypeptide reflecting residues

62-122, corresponding to the dimerization domain, showed an extended, highly α-helical structure (138). The structures of the tether domain contributing to the segment between the membrane surface and the bottom of F_1, and the F_1 binding domain in the carboxyl terminal region have yet to be determined.

Previously we showed that *b* subunits with deletions and insertions in the tether region of up to eleven and fourteen amino acids, respectively, formed functional F_1F_0 complexes (193, 194). These observations suggested that flexibility is an inherent characteristic of the peripheral stalk. This apparent flexibility also extended to the dimerization of the *b* subunits. When two *b* subunits with unequal length tether domains were expressed together, F_1F_0 ATP synthase complexes containing heterodimeric peripheral stalks were assembled (195). F_1F_0 complexes were able to tolerate the incorporation of two different *b* subunits with a size difference of at least fourteen amino acids. Although activity evidence suggested the heterodimeric F_1F_0 complexes were likely functional, the earlier study was not design to rigorously demonstrate that these were active.

A major problem that plagued all previous mutagenesis studies of the *b* subunit was that mutations constructed in the *uncF*(*b*) gene affected both subunits of the *b* homodimer. One missense mutation led to two amino acid replacements. Our ability to express two different *b* subunits in the same cell and detect *b* subunit heterodimer formation provided an approach to study the individual functional roles of the *b* subunits. In the present study, three different *b* subunit mutations were studied. Mutation of an evolutionarily conserved arginine, b_{arg36}, to an isoleucine or glutamate has previously been shown to result in an intact, completely defective F_1F_0 ATP synthase complex

(215). Second, deletion of the last four amino acids at the C-terminus has been shown to affect the ability of the *b* dimer to form a stable interaction with the δ subunit F_1 resulting in a major defect in F_1F_0 ATP synthase assembly (205, 206). Thirdly, insertions or deletions constructed in a cytoplasmic region of the *b* dimer that contains a stretch of hydrophobic amino acids, $b_{I24\text{-}130}$ (VAILAVA) has been shown to completely affect the ability of the *b* subunit to form a stable dimer and insert into the membrane. Here, we demonstrate functional activity for F_1F_0 ATP synthase complexes containing a heterodimeric peripheral stalk, with major defects occurring in the different domains of each *b* subunit.

Materials and Methods

A thorough account of many of the procedures used in Chapter 4 can be found in previous chapters. Many of the techniques, including recombinant DNA techniques, site directed mutagenesis, western blotting, as well as assays of protein concentration and F_1F_0 ATP synthase activity have been described in detail in Chapter 2. A detailed description of purification of F_1F_0 ATP synthases containing *b* subunit heterodimers to homogeneity can be found in Chapter 3.

Materials

Molecular biology enzymes and mutagenic oligonucleotides were obtained from Invitrogen (Carlsbad, CA), Life Technologies, Inc. (Grand Island, NY), New England Biolabs (Beverly, MA) and Stratagene (La Jolla, CA). Reagents were obtained from Sigma (St. Louis, MO), BioRad Laboratories (Hercules, CA) and Fisher Scientific (Pittsburgh, PA). Plasmid purification kits were acquired from Qiagen Inc. (Valencia, CA). The anti-rabbit immunoglobulin horseradish peroxidase-linked whole antibody (from donkey), anti-mouse immunoglobulin horseradish peroxidase-linked whole

antibody (from sheep), Hybond ECL Nitrocellulose membrane, electrochemiluminescence Western blotting reagents and high performance chemiluminescence film were purchased from Amersham Biosciences (Piscataway, NJ). Polyclonal antibodies against SDS-denatured *b* subunit (284, 285) were generously provided by Dr. Karlheinz Altendorf (Universität Osnabrück, Osnabrück, Germany. Monoclonal antibodies against the epitope found in the P and V proteins of the paramyxovirus, SV5 (V5 epitope tag) were purchased from Invitrogen. The Seize® Primary Immunoprecipitation Kit was purchased from Pierce Biotechnology (Rockford, IL).

Strains and Media

The wild type *b* subunit expression plasmid, pKAM14, and plasmids used to express *arg*36 mutatations *b* subunits have been described previously (203, 215). The plasmids encoding the *uncF*(*b*) gene were used to complement *E. coli* strain KM2 (Δ*b*) carrying a chromosomal deletion of the gene (218). All strains were streaked onto plates containing minimal A media supplemented with succinate (0.2% w/v), to determine enzyme viability. Cells harvested for membrane preparation were grown in Luria Broth supplemented with glucose (0.2% w/v) (LBG). Isopropyl-1-thio-β-D-galactopyranoside (IPTG)(40 μg/ml), ampicillin (Ap) (100μg/ml), and chloramphenicol (Cm) (25 μg/ml) were added to media as needed. All cultures were incubated at 37˚C for the appropriate duration.

Recombinant DNA Techniques

Plasmid DNA was purified with the Qiagen Mini-Prep and Maxi-Prep kits. Restriction endonuclease digestions, ligations, and transformations were performed

according to the recommendations of the manufacturers (New England Biolabs, Stratagene and Life Technologies, Inc.). Site-directed mutagenesis was performed either by means of a Stratagene Quikchange kit or by ligation-mediated mutagenesis. DNA fragments were separated in 0.8 % agarose gel by electrophoresis and purified using a Qiagen, Inc. QIAquick Gel Extraction kit. Plasmid sequences were determined by automated sequencing in the core facility of the University of Florida ICBR.

Mutagenesis and Strain Construction

Plasmid pKAM14 (*b*, Ap^r) (203) was used to construct *b* subunits with a deletion of the last four amino acids. Plasmids pKAM14 (*b*, Ap^r) (203), pTLC11 ($b_{arg36\rightarrow ile}$, Ap^r), or pTLC15 ($b_{arg36\rightarrow glu}$, Ap^r) (215) were used to construct the epitope tagged *b* subunits. Epitope tags were inserted into each of the plasmids using the Stratagene Quikchange kit. A four amino acid carboxyl-terminal truncation was accomplished by deletion of the final four codons of the *uncF*(*b*) gene to express $b_{\Delta 153\rightarrow end}$ (Appendix A) (Figure 3-1A). The restriction endonuclease recognition sequence for *Hind*III was constructed near the deleted sequence for an initial detection of the truncation. A histidine epitope tag was inserted at the N-terminus by mutagenesis between the first and second codons of the *uncF*(*b*) gene to express b_{his}, $b_{\Delta 153\rightarrow end\text{-}his}$ or $b_{+124\text{-}130\text{-}his}$ (Figure 3-1B). All of the recombinant histidine-tagged *b* subunit plasmids were then digested with *Pst*I and *Nde*I and subsequently ligated into a plasmid conferring the chloramphenicol resistance gene and the pACYC184 origin of replication (Table 3-1). A V5 epitope tag was added to the C-terminus by site-directed mutagenesis before the termination codon of the *uncF*(*b*) gene to express b_{V5}, $b_{arg36\rightarrow ile\text{-}V5}$, or $b_{arg36\rightarrow glu\text{-}V5}$ (Figure 3-1B). The recombinant V5-tagged *b* subunit plasmids included the ampicillin resistance gene and the pUC18 origin

of replication. Unique restriction enzyme sites *Sph*I and *Nde*I were constructed near the histidine and V5 epitope tag sequence, respectively, for an initial detection of the insertions, and then the nucleotide sequence was subsequently confirmed by automated sequencing in the ICBR core facility. Throughout the paper, the mutation and the epitope

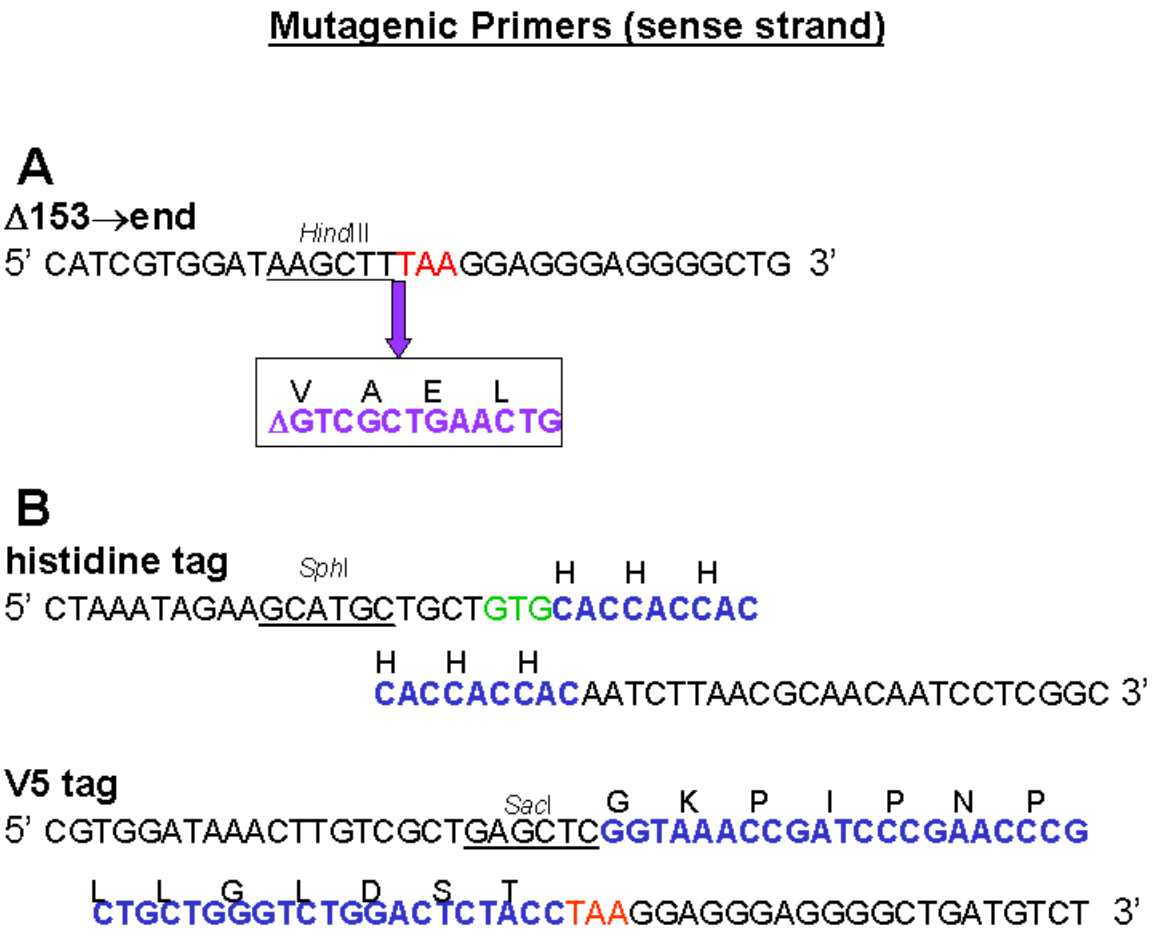

Figure 3-1. Oligonucleotides for epitope tags and C-terminal truncation of *uncF*(*b*). Shown are the sense strands of the mutagenic primer pairs. Mutagenesis was accomplished as described in the Materials and Methods. Green and red codons specify translation start and stop sites, respectively. The amino acids encoded in the sequences are labeled above the codons. A) Mutagenic primer encoding a four amino acid deletion (codons shown in purple) along with a silent mutations that introduced a new endonuclease recognition sequence, *Hind*III (underlined). B) Oligonucleotides designed to insert a histidine or V5-epitope tag (bold blue). The *Sph*I and *Sac*I restriction sites (underlined) were added along with the histidine and V5 epitope tag to facilitate screening.

tag are indicated along with the plasmid name for clarity, for example plasmid pTAM51 ($b_{\Delta 153 \rightarrow \text{end-his}}$). Each plasmid and the control plasmids pKAM14 (*b*) and pBR322 were expressed in the *E. coli* cell line KM2 (Δ*b*) for study, so that the only *b* subunits in the cells were the product of the plasmid genes. The two plasmid expression system allowed expression of various combinations of histidine tagged and V5-tagged *b* subunits in the same cell (Figures 2C, 4C, 6C, 8C). Appropriate antibiotics were added to the growth medium, and in the case of the coexpressed plasmids, both ampicillin and chloramphenicol were added to select for cells expressing both plasmids.

Preparative Procedures

Inverted membrane vesicles from KM2 (Δ*b*) strains expressing the desired *b* subunits were prepared essentially as described previously (194). Protein concentrations were determined by the bicinchoninic acid (BCA) assay (289). Ni-resin purification was achieved using the High Capacity Nickel Chelate Affinity Matrix (Ni-CAM) purchased from Sigma. A total of 5 mg of membrane protein was brought up to 1 mL with final concentrations of 0.2% tegamineoxide WS-35, 0.15 M NaCl, and 1 mM imidazole. The purification procedure was accomplished using the batch method as described by the manufacturer.

Immunoblot Analysis

Proteins were loaded on a 15% tris-glycine SDS gel and transferred onto nitrocellulose by electroblot. The *b* subunit antibody incubation was performed essentially as described previously (195), using a 1:25,000 dilution of the anti-*b* subunit antibodies. Secondary antibody incubation was performed with horseradish peroxidase-linked donkey anti-rabbit antibody (1:50,000), and the antibody was detected by

enhanced chemiluminescence. The V5-subunit antibody incubation was performed as described by the manufacturer followed by a secondary antibody incubation with horseradish peroxidase-linked sheep anti-mouse antibody (1:10,000). Signals were visualized on high performance chemiluminescence film using a Kodak X-Omat.

Assays of F_1F_0 ATP Synthase Activity

Growth on a minimal succinate medium was used as an initial, *in vivo*, assay for enzyme viability. ATP hydrolysis activity was assayed by the acid molybdate method (146). Membranes were assayed in buffer (50 mM Tris-HCl, 1 mM MgCl2, pH 9.1) to determine the linearity with respect to time and enzyme concentration. Membrane energization was detected by the fluorescence quenching of 9-amino-6-chloro-2-methoxyacridine (ACMA) (271).

Results

Construction and Growth Characteristics of Mutants

To investigate the function of individual *b* subunits in a F_1F_0 ATP synthase enzyme complex, plasmids expressing defective *b* subunits with either a histidine or a V5 epitope-tag were generated by site-directed mutagenesis. A total of five plasmids were constructed expressing the $b_{\text{wt-his}}$, $b_{\Delta 153 \rightarrow \text{end-his}}$, $b_{\text{wt-V5}}$, $b_{\text{arg36} \rightarrow \text{ile-V5}}$, or $b_{\text{arg36} \rightarrow \text{glu-V5}}$ subunits (Table 3-1). The epitope tags were needed to facilitate enzyme purification and subunit detection on a Western blot, respectively. In order to express two different *b* subunits in the same cell, we used the two-plasmid expression system described previously in Chapter 2(195). Enzyme complexes incorporated with a histidine or V5 epitope-tagged *b* subunit homodimer have been studied previously and were shown to result in a functional enzyme complex (195). *E. coli* strain KM2 (Δ*b*) was used as the host because the *uncF*(*b*) gene has been deleted, eliminating any background *b* subunit.

Table 3-1. Aerobic growth properties and membrane-associated ATP hydrolysis activity of mutants expressing epitope tagged *uncF*(*b*) genes

Strains	Description	Growth[1]	Specific activity[2,3]
KM2/pKAM14 (+)	b_{wt}, Ap^r	+++	1.18 ± 0.05
KM2/pBR322 (-)	Δ*b*, Ap^r	-	0.24 ± 0.03
KM2/pTAM37	$b_{wt\text{-}his}$, Cm^r	+++	1.08 ± 0.08
KM2/pTAM51	$b_{\Delta 153 \rightarrow end\text{-}his}$, Cm^r	-	0.22 ± 0.05
KM2/pTAM46	$b_{wt\text{-}V5}$, Ap^r	+++	1.22 ± 0.04
KM2/pTAM53	$b_{arg36 \rightarrow ile\text{-}V5}$, Ap^r	-	0.80 ± 0.02
KM2/pTAM54	$b_{arg36 \rightarrow glu\text{-}V5}$, Ap^r	-	0.75 ± 0.08
KM2/pTAM38	$b_{+124\text{-}130\text{-}his}$, Cm^r	-	0.21 ± 0.04
KM2/pTAM37/pTAM46	$b_{wt\text{-}his} + b_{wt\text{-}V5}$	+++	1.16 ± 0.03
KM2/pTAM51/pTAM46	$b_{\Delta 153 \rightarrow end\text{-}his} + b_{wt\text{-}V5}$	+++	1.00 ± 0.05
KM2/pTAM37/pTAM53	$b_{wt\text{-}his} + b_{arg36 \rightarrow ile\text{-}V5}$	+++	1.12 ± 0.04
KM2/pTAM37/pTAM54	$b_{wt\text{-}his} + b_{arg36 \rightarrow glu\text{-}V5}$	+++	1.10 ± 0.05
KM2/pTAM38/pTAM54	$b_{+124\text{-}130\text{-}his} + b_{wt\text{-}V5}$	+++	1.20 ± 0.03
KM2/pTAM51/pTAM53	$b_{\Delta 153 \rightarrow end\text{-}his} + b_{arg36 \rightarrow ile\text{-}V5}$	+	0.51 ± 0.02
KM2/pTAM51/pTAM54	$b_{\Delta 153 \rightarrow end\text{-}his} + b_{arg36 \rightarrow glu\text{-}V5}$	-	0.37 ± 0.07

[1] *E. coli* strains were grown aerobically on succinate minimal medium. Colony size was scored after 72-hr incubation at 37ºC as: +++, ≥ 1.0 mm; ++, 0.3-0.5 mm; +, ~0.1 mm; -, no growth.

[2] ATPase activities were measured as described under "Materials and Methods." Units of specific activity = μmol of PO_4 released per mg of protein/min ± S.D. Units were calculated from the slope of the line based on three measurements with incubations for 12 minutes.

[3] Previously reported ATPase activities resulted from an abbreviated membrane preparation protocol. Activities reported here resulted from an additional wash step to remove nonspecifically bound ATPases.

Previous analyses of F_1F_0 ATP synthase complexes incorporated with the mutant $b_{arg36 \rightarrow ile}$, $b_{arg36 \rightarrow glu}$, $b_{\Delta 153 \rightarrow end}$ or $b_{+124\text{-}130\text{-}his}$ subunits found the mutants to be completely defective (205, 206, 215). Therefore, our ability to form F_1F_0 complexes containing *b* heterodimers offered an approach to study activity in a complex with only a single functional *b* subunit protein. First, the effects of the $b_{arg36 \rightarrow ile\text{-}V5}$, $b_{arg36 \rightarrow glu\text{-}V5}$, $b_{\Delta 153 \rightarrow end\text{-}his}$ and $b_{+124\text{-}130\text{-}his}$ mutations were studied for dimerization with a wild type epitope tagged *b* subunit in order to complement the *E. coli* strain KM2 (Δ*b*) (218). Growth on succinate minimal medium was used as an initial qualitative gauge of enzyme activity *in vivo* since *E. coli* strains lacking F_1F_0 ATP synthase cannot derive energy from nonfermentable carbon sources (Table 3-1). As expected, when any one of the mutants was expressed

alone in the cells no growth was detected. In each case, the strains coexpressing the mutant epitope-tagged *b* subunits with a wild-type epitope-tagged *b* subunit grew comparably to the wild type strain.

Heterodimer Formation of b_{arg36} Defective Subunits with b_{wt}

Although two unequal length *b* subunits formed a heterodimer in an intact F_1F_0 ATP synthase complex (195), it was possible that a single amino acid substitution could affect dimerization, preventing assembly of a complex. To consider whether a V5 epitope-tagged b_{arg36} subunit, $b_{arg36\rightarrow ile\text{-}V5}$ or $b_{arg36\rightarrow glu\text{-}V5}$, could form a heterodimer with a wild type histidine epitope-tagged *b* subunit, $b_{wt\text{-}his}$ each pair of subunits were expressed in strains KM2/pTAM37/pTAM53 and KM2/pTAM37/pTAM54 (Δ*b*) (Figure 3-2A and B). The *b* subunits were detected in membranes prepared from strains expressing a *b* subunit by immunoblot analysis (Figure 3-2A, Lanes 1-9). However, only *b* subunits in complexes with at least one histidine tag were retained by Ni-resin purification (Figure 3-2A, lanes 10-13). Immunoblot analysis using an anti-V5 antibody was performed on the membrane preparations and Ni-purified products (Figure 3-2B). The V5-epitope tag was detected only in membrane vesicles derived from KM2 strains expressing either the V5-tagged *b* subunit or the coexpressed V5-tagged and his-tagged *b* subunits (Figure 3-2B, Lanes 1-9). When only V5-tagged *b* subunits were expressed alone in a cell, no F_1F_0 complexes were recovered from the Ni-resin purification (Figure 3-2B, Lane 10). Finally, we investigated the ability of $b_{wt\text{-}his}$ to dimerize to form intact F_1F_0 ATP synthase complexes with $b_{arg36\rightarrow ile\text{-}V5}$ or $b_{arg36\rightarrow glu\text{-}V5}$. Both $b_{arg36\rightarrow ile\text{-}V5}$ and $b_{arg36\rightarrow glu\text{-}V5}$ were detected with anti-V5 antibodies after Ni-resin purification (Figure 3-2B, Lanes 12-13). The only mechanism for recovery of defective V5-tagged *b* subunits was through

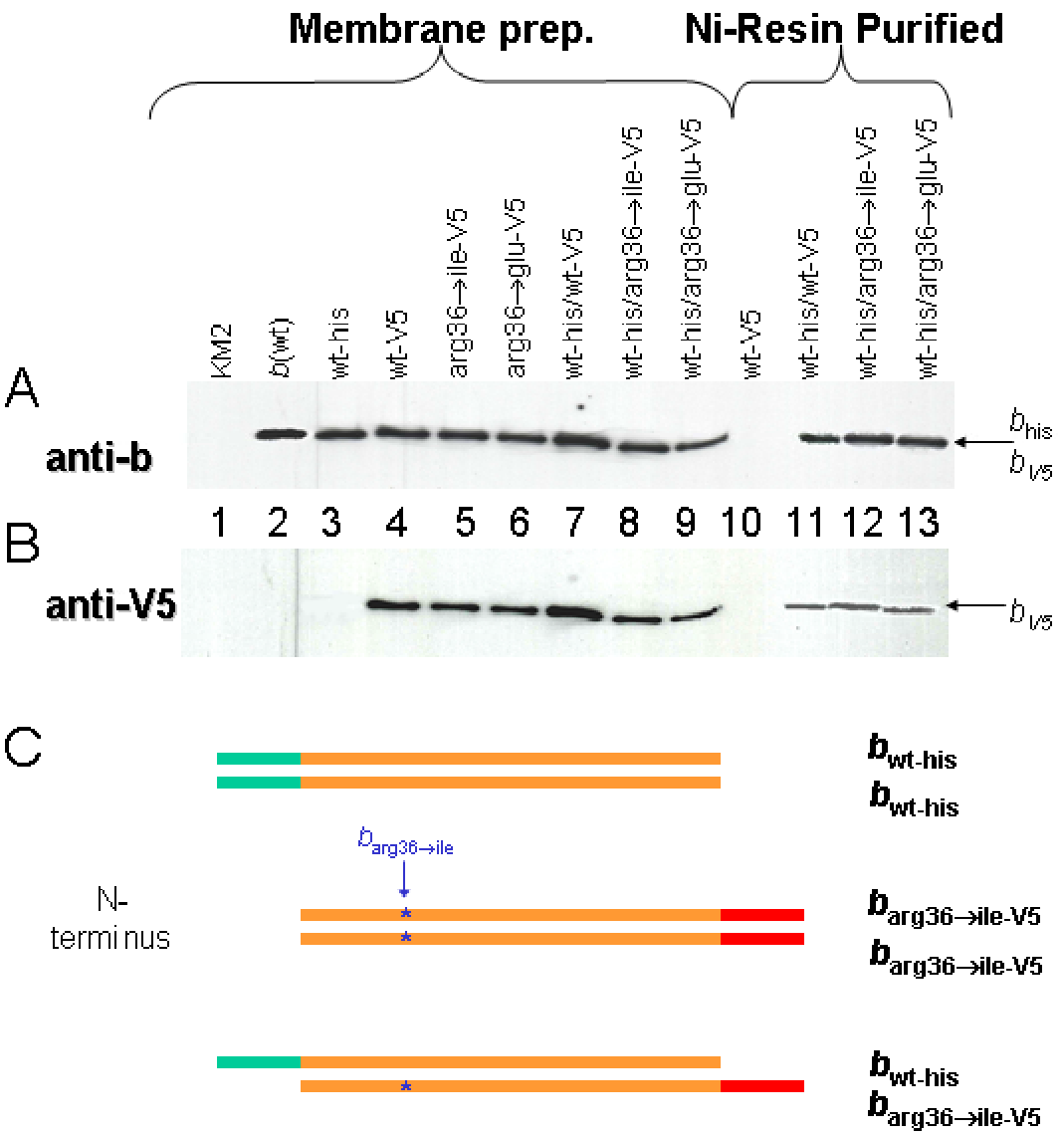

Figure 3-2. Ni-resin purification of F_1F_0 ATP synthase incorporated with b_{arg36} subunit mutations. Cells expressing recombinant *b* subunits were lysed in a French pressure cell, and membrane vesicles were isolated by differential ultracentrifugation. The crude membrane preparation was solubilized with 0.2% tegamineoxide WS-35 and subjected to Ni-resin purification before separation on a 15% polyacrylamide Tris-glycine SDS gel for subsequent anti-*b*, or on a mini BioRad 15% Ready Gel for anti-V5 Western blot analysis (see Materials and Methods). A) Proteins were transferred to a nitrocellulose membrane and probed using a polyclonal anti-*b* antibody. B) Proteins were transferred to a nitrocellulose membrane and probed using an anti-V5 mouse monoclonal antibody. C) Line diagram of the different *b* dimers found in the cell. Green and red lines represent the histidine and V5 epitope tags, respectively. Orange represents the *b* subunit and the blue star represents the b_{arg36} mutation.

dimerization with $b_{wt\text{-}his}$ indicating formation of heterodimeric F_1F_0 ATP synthase complexes. Therefore, coexpression of the two different *b* subunits in the same cell led to three distinct interactions within an intact F_1F_0 ATP synthase complex (Figure 3-2C): 1) a homodimer of $b_{wt\text{-}his}$, 2) a homodimer of $b_{arg36\rightarrow ile\text{-}V5}$ or $b_{arg36\rightarrow glu\text{-}V5}$, and 3) a heterodimer consisting of both the defective and wild type *b* subunit.

Since F_1 displays reduced affinity for the membrane in the absence of intact F_0, total membrane associated F_1-ATP hydrolysis activity was used as a test of F_1F_0 ATP synthase complex assembly. Under conditions of high pH, F_1 can be released from the influence of F_0 (146), so the amount of ATPase activity in the solution was used as a measure of the amount of intact enzyme complex located in the membrane vesicles. Previous data indicated minimal affects on specific activity due to the epitope tags (195). Confirming these observations, the V5-epitope tag did not have an apparent affect on enzyme assembly. Membrane preparations with a $b_{wt\text{-}V5}$ incorporated into the F_1F_0 ATP synthase complex had virtually the same specific activity of the wild type strain (Table 3-1). A small decrease in specific activity was reproducibly observed in membrane vesicles isolated from cells when a histidine epitope tag was incorporated onto the b_{wt}, about 89% of the wild type strain. Furthermore, comparable activities were observed in samples when the histidine-tagged and V5-tagged b_{wt} subunits were coexpressed. Also verifying previous data (215), when $b_{arg36\rightarrow ile\text{-}V5}$ or $b_{arg36\rightarrow glu\text{-}V5}$ was expressed alone in strains KM2/pTAM53 and KM2/pTAM54, the membranes retained abundant activity, about 60% and 54%, of the wild type strain, respectively (Table 3-1), indicating considerable amounts of intact F_1F_0 ATP synthase complexes found in the membranes. When $b_{arg36\rightarrow ile\text{-}V5}$ or $b_{arg36\rightarrow glu\text{-}V5}$ were coexpressed with $b_{wt\text{-}his}$ by construction of strains

KM2/pTAM37/pTAM53 or KM2/pTAM37/pTAM54 specific activities of about 94% and 91%, respectively, were observed indicating a quantity of intact F_1F_0 ATP synthase complexes approaching the wild type strain levels.

F_1F_0 ATP synthase-mediated ATP-driven proton pumping activity in membrane vesicles prepared from the epitope-tagged mutants was used as an indication of coupled activity. Acidification of inverted membrane vesicles was examined by fluorescence of ACMA (Figure 3-3). Membranes isolated from cells with a V5 epitope tag incorporated onto the b_{wt} subunit, KM2/pTAM46 ($b_{wt\text{-}V5}$), reproducibly displayed a very small reduction in coupled activity, correlating very well with the F_1-ATP hydrolysis activity. Consistent with previous observations, a larger reduction in coupled activity of about 20% was observed in membrane vesicles isolated from strain KM2/pTAM37 ($b_{wt\text{-}his}$). The coupled activities observed in membranes isolated from cells coexpressing histidine-tagged and V5-tagged *b* subunits were intermediary between the V5-tagged species and the histidine-tagged species. Strains expressing either $b_{arg36\rightarrow ile\text{-}V5}$ or $b_{arg36\rightarrow glu\text{-}V5}$ displayed no ATP-dependent proton pumping activity as expected. Significantly, when either one of the $b_{arg\text{-}36}$ mutants was coexpressed with $b_{wt\text{-}his}$, KM2/pTAM37/pTAM53 ($b_{wt\text{-}his}/b_{arg36\rightarrow ile\text{-}V5}$) or KM2/pTAM37/pTAM54 ($b_{wt\text{-}his}/b_{arg36\rightarrow glu\text{-}V5}$), the coupled activity observed was essentially the same as strain KM2/pTAM37/pTAM46 ($b_{wt\text{-}his}/b_{wt\text{-}V5}$). When expressed alone, the strains with $b_{arg\text{-}36\text{-}V5}$ mutants had no activity and the strains expressing $b_{wt\text{-}his}$ displayed less activity than the $b_{wt\text{-}his}/b_{arg\text{-}36\text{-}V5}$ mutant enzyme. As a consequence, it was most likely that the F_1F_0 ATP synthase complexes with either the $b_{wt\text{-}his}/b_{arg36\rightarrow ile\text{-}V5}$ or $b_{wt\text{-}his}/b_{arg36\rightarrow glu\text{-}V5}$ peripheral stalks were active. To demonstrate that the

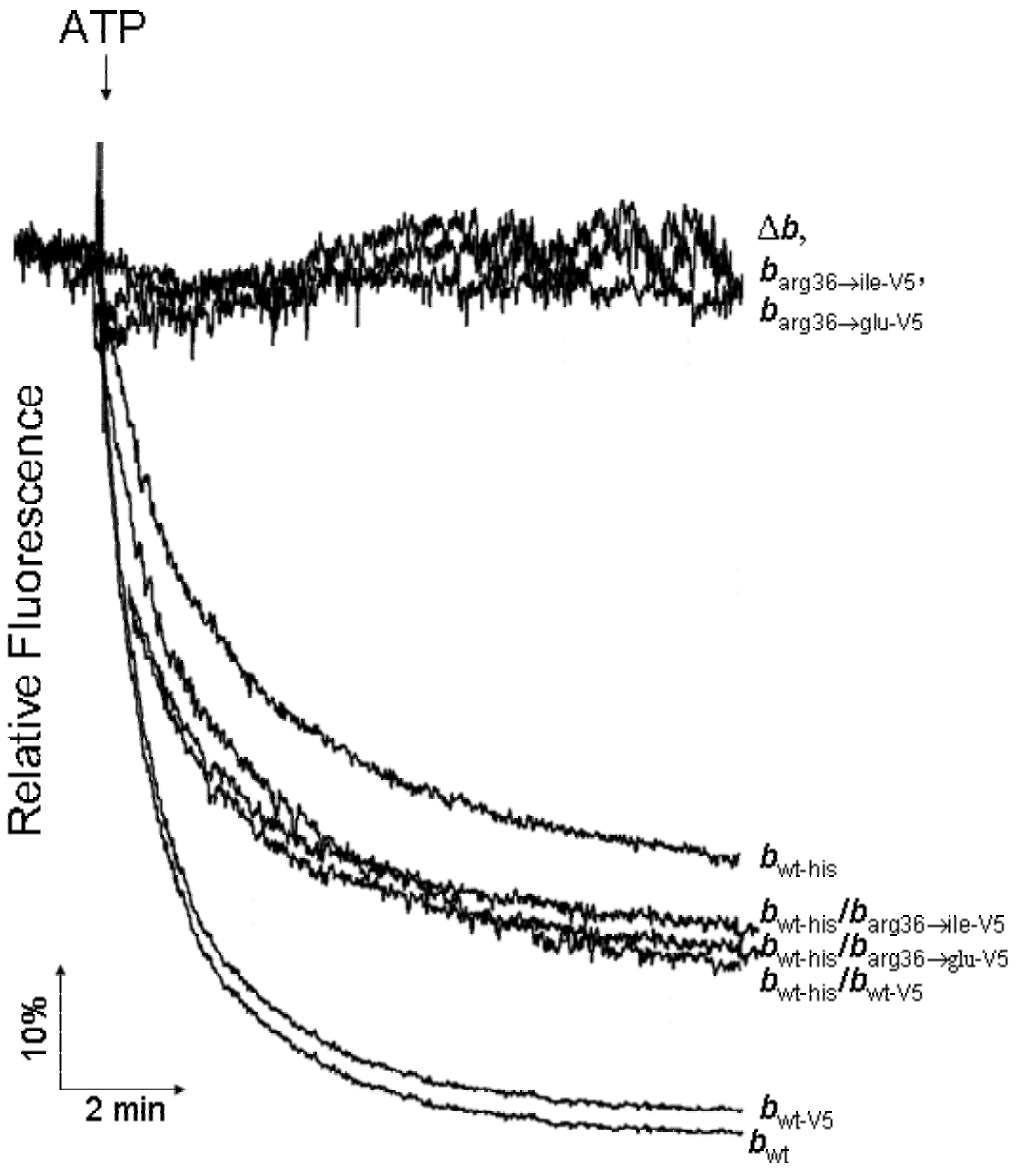

Figure 3-3. ATP-driven energization of membrane vesicles prepared from *uncF*(*b*) arg36 gene mutants. Membrane vesicles were prepared by differential centrifugation. Membrane protein (200 μg) was suspended in 3 ml of assay buffer (50 mM MOPS, 10 mM $MgCl_2$, pH 7.3). The fluorescent dye ACMA was added to a final concentration of 1 μM, and fluorescence was recorded with excitation at 410 nm and emission at 490 nm. ATP was added as indicated to a final concentration of 1mM. The samples for each trace have been labeled according to the *b* subunit mutation and the epitope tag, so the strains used as the sources of the samples were as follows: Δ*b*, KM2/pBR322; b_{wt}, KM2/pKAM14; $b_{wt\text{-}V5}$, KM2/pTAM46; $b_{wt\text{-}his}$, KM2/pTAM37; $b_{arg36\rightarrow ile\text{-}V5}$, KM2/pTAM53; $b_{arg36\rightarrow glu\text{-}V5}$, KM2/pTAM54; $b_{wt\text{-}his}/b_{wt\text{-}V5}$, KM2/pTAM37/pTAM46; $b_{wt\text{-}his}/b_{arg36\rightarrow ile\text{-}V5}$, KM2/pTAM37/pTAM53; $b_{wt\text{-}his}/b_{arg36\rightarrow glu\text{-}V5}$, KM2/ pTAM37/pTAM54.

membrane vesicles were intact and closed, the level of NADH-driven fluorescence quenching was monitored for all membrane preparations. The levels of NADH-driven fluorescence quenching were strong and directly comparable in every case (data not shown, for a representative figure, see Figure 2-10).

Heterodimer formation of $b_{\Delta 153 \rightarrow end\text{-}his}$ Complemented with $b_{wt\text{-}V5}$

Deletion of the last four amino acids at the C-terminus has been shown to dramatically affect the ability of the *b* dimer to form a stable interaction with the δ subunit F_1 resulting in a major F_1F_0 ATP synthase assembly defect (205, 206). Immunoblot analysis was performed in order to detect a heterodimer interaction between $b_{\Delta 153 \rightarrow end}$ and b_{wt} (Figure 3-4A and B). Coexpression of pTAM51 ($b_{\Delta 153 \rightarrow end\text{-}his}$) and pTAM46 ($b_{wt\text{-}V5}$) in the same cell resulted in the appearance of a weak signal representing $b_{wt\text{-}V5}$ in Ni-resin purified material (Figure 3-4B, Lane 8). Although there was no attempt to be quantitative in this assay, the appearance of the band suggested relatively inefficient assembly of these heterodimers. Nevertheless, when the two different *b* subunits are expressed in the same cell, three distinct F_1F_0 complexes were assembled (Figure 3-4C). These included a homodimer of $b_{wt\text{-}V5}$ in an intact F_1F_0 ATP synthase complex, a homodimer of $b_{\Delta 153 \rightarrow end\text{-}his}$ in a partially assembled defective enzyme, and a heterodimeric F_1F_0 ATP synthase consisting of both subunits. Apparently, the $b_{wt\text{-}V5}$ subunit stabilized the $b_{\Delta 153 \rightarrow end\text{-}his}$ subunit within an intact F_1F_0 ATP synthase complex.

Total membrane associated F_1-ATP hydrolysis activity was used as a test of F_1F_0 ATP synthase complex assembly (Table 3-1). As expected, membranes with enzyme complexes incorporated with $b_{\Delta 153 \rightarrow end\text{-}his}$ displayed a specific activity similar to the negative control, indicating virtually no interaction with F_1. Coexpression of pTAM51

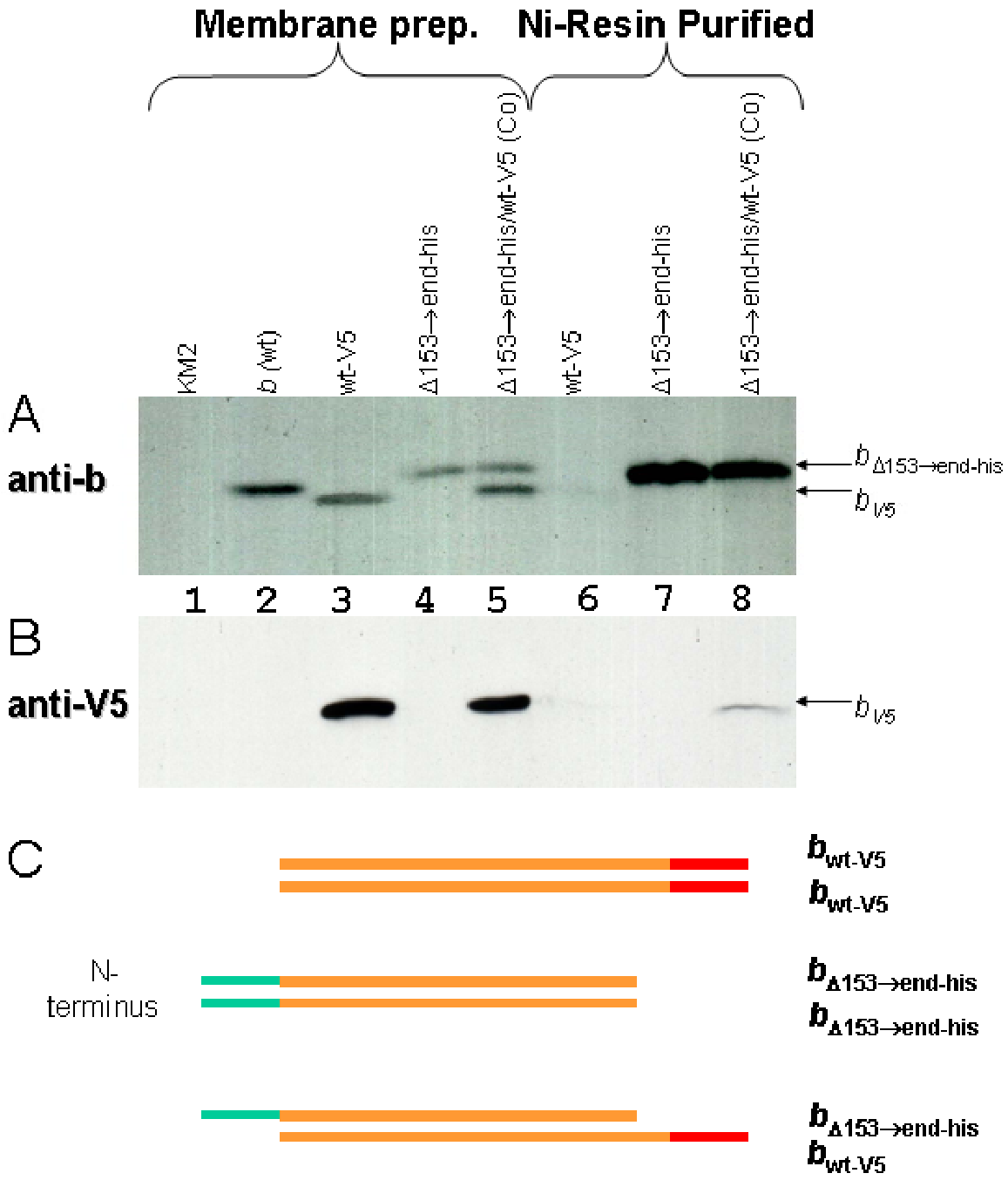

Figure 3-4. Ni-resin purification of F_1F_0 ATP synthase containing a *b* subunit carboxyl-terminal truncation. Membrane preparation and Ni-resin purification and Western blot analysis were accomplished as described in Materials and Methods. A) Proteins were transferred to a nitrocellulose membrane and probed using a polyclonal anti-*b* antibody or B) an anti-V5 mouse monoclonal antibody. C) line diagram of the different *b* dimers found in the cell.

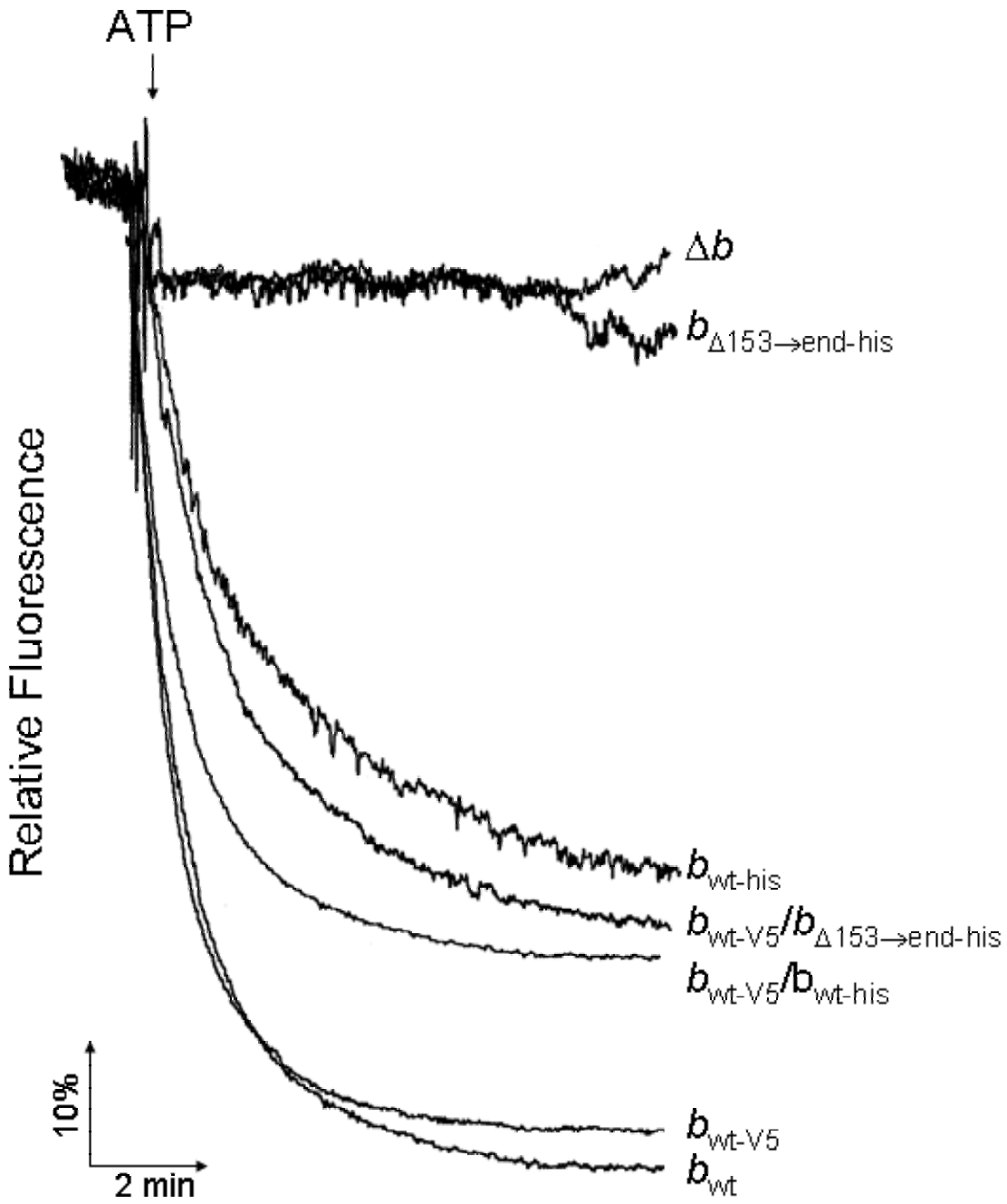

Figure 3-5. ATP-driven energization of membrane vesicles incorporated with F_1F_0 ATP synthase containing a *b* subunit carboxyl-terminal truncation. Membrane preparation and ATP-driven proton pumping was accomplished as described in Materials and Methods. The samples for each trace have been labeled according to the *b* subunit mutation and the epitope tag, so the strains used as the sources of the samples were as follows: Δ*b*, KM2/pBR322; b_{wt}, KM2/pKAM14; $b_{wt\text{-}V5}$, KM2/pTAM46; $b_{wt\text{-}his}$, KM2/pTAM37; $b_{\Delta153\rightarrow end\text{-}his}$, KM2/pTAM51; $b_{wt\text{-}his}/b_{wt\text{-}V5}$, KM2/pTAM37/pTAM46; $b_{wt\text{-}V5}/b_{\Delta153\rightarrow end\text{-}his}$, KM2/pTAM46/pTAM51.

($b_{\Delta 153 \rightarrow end\text{-}his}$) and pTAM46 ($b_{wt\text{-}V5}$) resulted in a specific activity of about 81% of the wild type strain (Table 3-1). An indication of coupled activity was shown by F_1F_0 ATP synthase-mediated ATP-driven proton pumping activity in membrane vesicles prepared from the epitope-tagged mutants (Figure 3-5). Membranes containing only the $b_{\Delta 153 \rightarrow end\text{-}his}$ subunit exhibited no coupled activity as expected. Membranes isolated from cells coexpressing pTAM51 ($b_{\Delta 153 \rightarrow end\text{-}his}$) and pTAM46 ($b_{wt\text{-}V5}$) displayed a slight reduction in coupled activity, of about 20%, compared to membranes from cells coexpressing $b_{wt\text{-}V5}$ and $b_{wt\text{-}his}$. It is feasible that the observed reductions in enzymatic activities were entirely due to formation of the mutant homodimeric species; this could not be directly demonstrated by these methods due to background activity from $b_{wt\text{-}V5}$ homodimeric F_1F_0 ATP synthases present in the membranes.

Heterodimer Formation of $b_{+124\text{-}130\text{-}his}$ Complemented with $b_{wt\text{-}V5}$

It has been shown by Dr. Deepa Bhatt that insertions or deletions constructed in a hydrophobic stretch corresponding to amino acids 124-130 (VAILAVA) of the *b* subunit results in loss of enzyme function (Bhatt *et al*., manuscript in preparation). Immunoblot analysis was performed in order to detect a heterodimer interaction between $b_{+124\text{-}130\text{-}his}$ and $b_{wt\text{-}V5}$ (Figure 3-6A and B). The *b* subunit was detected only in membranes prepared from strains expressing a functional *b* subunit (Figure 3-6A, Lanes 1-6). No *b* subunit was present in membranes when KM2 (Δb) was complemented with plasmid pTAM38 ($b_{+124\text{-}130\text{-}his}$). Immunoblot analysis using an anti-V5 antibody was performed on the membrane preparations and Ni-purified products (Figure 3-6B). Interestingly, coexpression of pTAM38 ($b_{+124\text{-}130\text{-}his}$) and pTAM46 ($b_{wt\text{-}V5}$) in the same cell resulted in the appearance of a signal representing $b_{wt\text{-}V5}$ in a Ni-resin purified sample (Figure 3-6B,

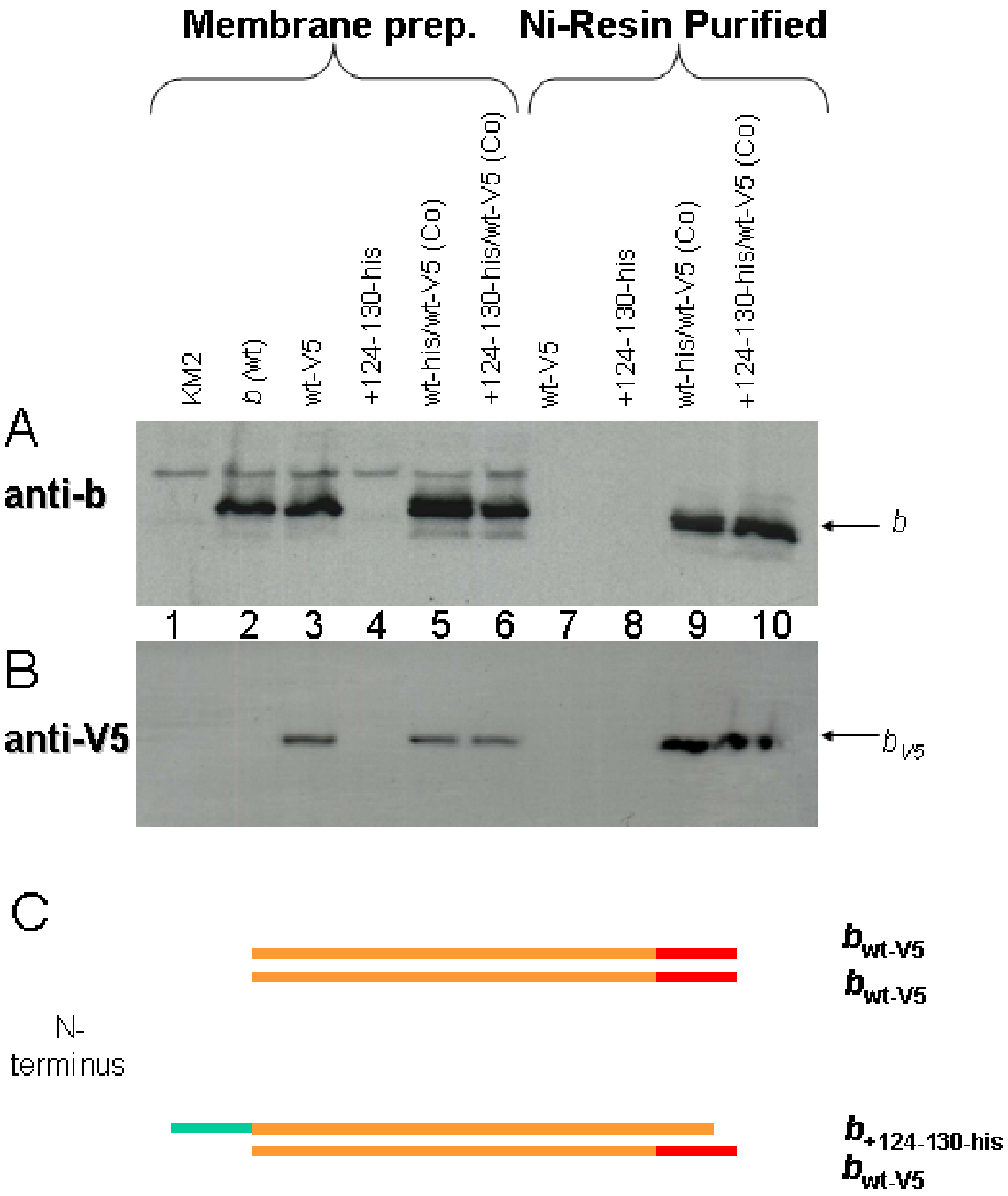

Figure 3-6. Ni-resin purification of membranes incorporated with $b_{+124\text{-}130\text{-}his}$ subunit mutation. Membrane preparation and Ni-resin purification and Western blot analysis were accomplished as described in Materials and Methods. A) Proteins were transferred to a nitrocellulose membrane and probed using a polyclonal anti-*b* antibody or B) an anti-V5 mouse monoclonal antibody. C) line diagram of the different *b* dimers found in the cell.

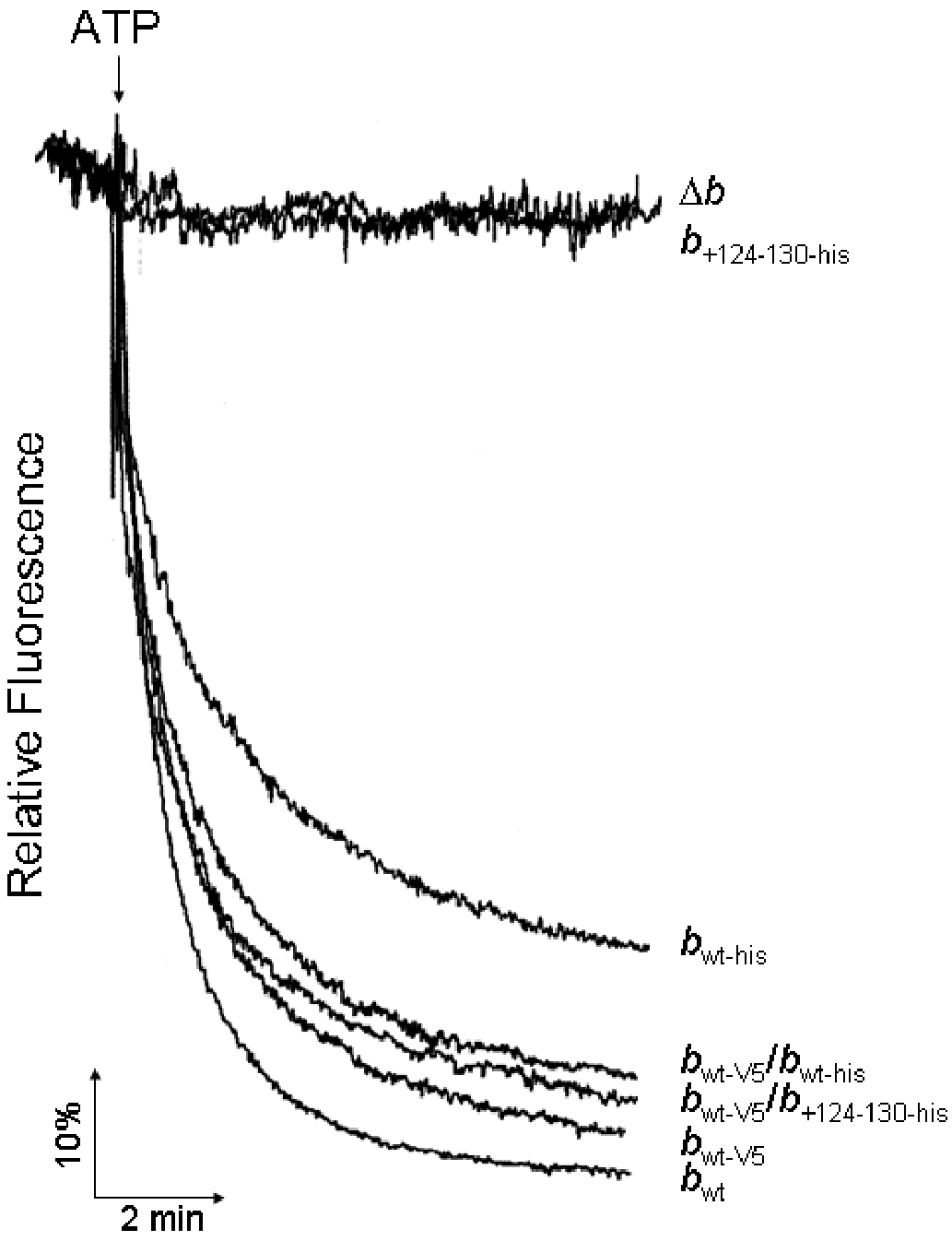

Figure 3-7. ATP-driven energization of membrane vesicles incorporated with a defective $b_{+124-130}$ subunit mutation. Membrane preparation and ATP-driven proton pumping was accomplished as described in Materials and Methods. The samples for each trace have been labeled according to the *b* subunit mutation and the epitope tag, so the strains used as the sources of the samples were as follows: Δ*b*, KM2/pBR322; b_{wt}, KM2/pKAM14; b_{wt-V5}, KM2/pTAM46; b_{wt-his}, KM2/pTAM37; $b_{+124-130-his}$, KM2/pTAM38; b_{wt-his}/b_{wt-V5}, KM2/pTAM37/pTAM46; $b_{wt-V5}/b_{+124-130-his}$, KM2/pTAM46/pTAM38.

Lane 10). The only mechanism for recovery of $b_{wt\text{-}V5}$ was through dimerization with $b_{+124\text{-}130\text{-}his}$, indicating that the $b_{wt\text{-}his}$ subunit rescued some of the defective *b* subunit and formed heterodimeric F_1F_0 ATP synthase complexes. Therefore, coexpression of the two different *b* subunits in the same cell led to two distinct interactions within an intact F_1F_0 ATP synthase complex (Figure 3-6C): 1) a homodimer of $b_{wt\text{-}V5}$ and 2) a heterodimer consisting of both the defective and wild type *b* subunit.

F_1-ATP hydrolysis activity of total membrane protein was used as a test of F_1F_0 ATP synthase assembly (Table 3-1). As expected, membranes with enzyme complexes incorporated with $b_{+124\text{-}130\text{-}his}$ displayed a specific activity similar to the negative control, indicating virtually no interaction with F_1. Coexpression of pTAM38 ($b_{+124\text{-}130\text{-}his}$) and pTAM46 ($b_{wt\text{-}V5}$) resulted in a specific activity similar to the wild type strain (Table 3-1). It was likely that the F_1F_0 ATP synthase complexes incorporated with the $b_{+124\text{-}130\text{-}his}/b_{wt\text{-}V5}$ were intact. An indication of coupled activity was shown by F_1F_0 ATP synthase-mediated ATP-driven proton pumping activity in membrane vesicles prepared from the epitope-tagged mutants (Figure 3-7). Membranes containing only the $b_{+124\text{-}130\text{-}his}$ subunit exhibited no coupled activity as expected. Membranes isolated from cells coexpressing pTAM38 ($b_{+124\text{-}130\text{-}his}$) and pTAM46 ($b_{wt\text{-}V5}$) displayed virtually the same amount of coupled activity as the membranes from cells coexpressing $b_{wt\text{-}V5}$ and $b_{wt\text{-}his}$. Since coexpression of the two different *b* subunits in the same cell led to only two distinct interactions, it was likely that the F_1F_0 ATP synthase complexes incorporated with the $b_{+124\text{-}130\text{-}his}/b_{wt\text{-}V5}$ were functional.

Mutual Complementation

In order to look for mutual complementation of *b* subunits with defects in different functional domains, $b_{arg36\rightarrow ile\text{-}V5}$ and $b_{arg36\rightarrow glu\text{-}V5}$ were coexpressed with $b_{\Delta 153\rightarrow end\text{-}his}$ in the absence of a functional wild type *b* subunit. Significantly, when $b_{\Delta 153\rightarrow end\text{-}his}$ and $b_{arg36\rightarrow ile\text{-}V5}$ were coexpressed in the same cell, KM2/pTAM51/pTAM53, small colonies were present after 5 days of growth. Expression of either $b_{arg36\rightarrow ile\text{-}V5}$ or $b_{\Delta 153\rightarrow end\text{-}his}$ alone in KM2 (Δ*b*) results in a completely defective enzyme complex, any F_1F_0 ATP synthase activity must necessarily have come from a heterodimer formed from two defective *b* subunits. Therefore, the $b_{arg36\rightarrow ile}$ and $b_{\Delta 153\rightarrow end}$ mutations qualified as intergenic second site suppressor mutations.

To determine whether there was a direct protein-protein interaction between two mutant subunits, we investigated the ability of $b_{\Delta 153\rightarrow end\text{-}his}$ to form an interaction with $b_{arg36\rightarrow ile\text{-}V5}$ or $b_{arg36\rightarrow glu\text{-}V5}$ by the standard immunoblot (Figure 3-8A and B). All of the controls provided on the first immunoblot were included and displayed similar results. An additional control was included to ensure complete solubilization of membrane vesicles was achieved and nonspecific aggregation of the *b* subunits was not a concern (Figure 3-8A and B, Lanes 10-11). Two independent membrane preparations were mixed together. Membrane vesicles derived from strains KM2/pTAM51 ($b_{\Delta 153\rightarrow end\text{-}his}$) and KM2/pTAM53 ($b_{arg36\rightarrow ile\text{-}V5}$) or KM2/pTAM54 ($b_{arg36\rightarrow glu\text{-}V5}$) were mixed and the membranes were solubilized with 0.2% tegamineoxide WS-35 prior to Ni-resin purification. Immunoblot analysis with anti-*b* antibodies showed normal levels of histidine-tagged *b* subunit upon Ni-resin purification (Figure 3-8A, Lanes 10-11). No V5-epitope was present after Ni-resin purification, indicating that neither non-specific

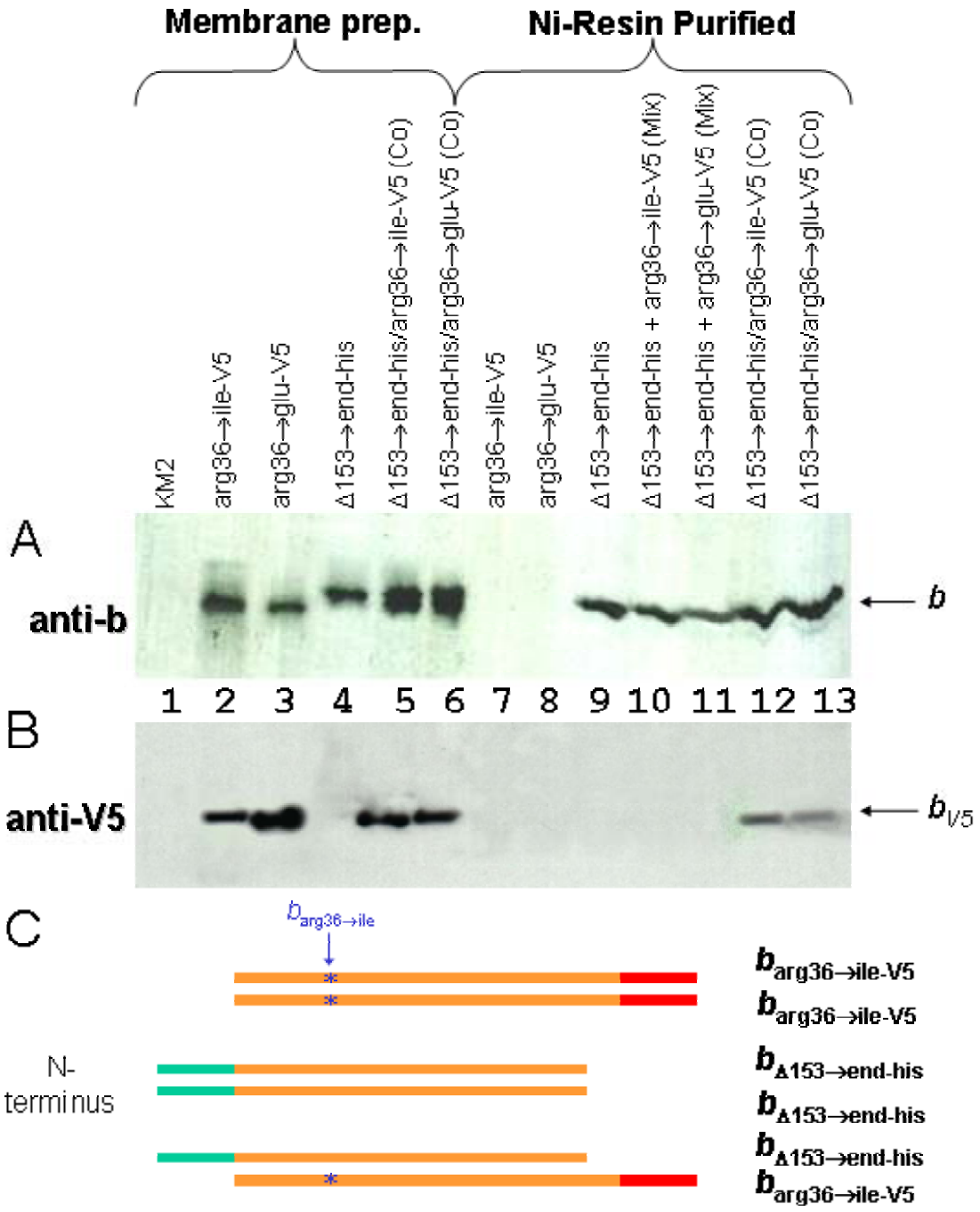

Figure 3-8. Ni-resin purification of F_1F_0 ATP synthase incorporated with complementing defective *b* subunits. Membranes preparation, Ni-resin purification and Western blot analysis was accomplished as described in Materials and Methods. A) Proteins were transferred to a nitrocellulose membrane and probed using a polyclonal anti-*b* antibody or B) an anti-V5 mouse monoclonal antibody. C) line diagram of the different *b* dimers found in the cell. Three interactions, $b_{arg36\rightarrow mut\text{-}V5}/b_{arg36\rightarrow mut\text{-}V5}$ and $b_{\Delta153\rightarrow end\text{-}his}/b_{\Delta153\rightarrow end\text{-}his}$ homodimers as well as $b_{arg36\rightarrow mut\text{-}V5}/b_{\Delta153\rightarrow end\text{-}his}$ heterodimers, existed in the cell.

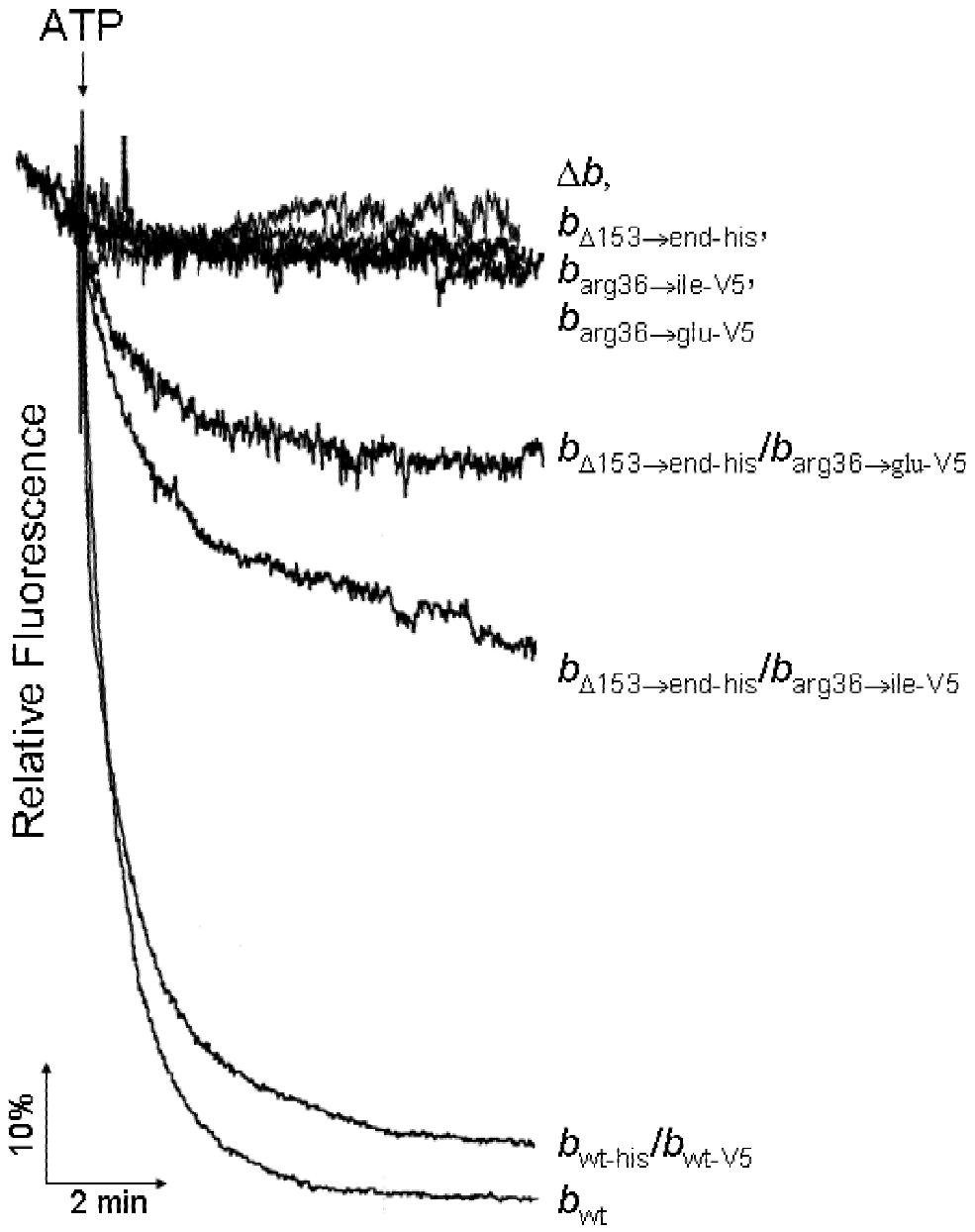

Figure 3-9. ATP-driven energization of membrane vesicles incorporated with F_1F_0 ATP synthase containing complementing defective *b* subunits. Membrane preparation and ATP-driven proton pumping was accomplished as described in Materials and Methods. The samples for each trace have been labeled according to the *b* subunit mutation and the epitope tag, so the strains used as the sources of the samples were as follows: Δ*b*, KM2/pBR322; b_{wt}, KM2/pKAM14; $b_{153\rightarrow end\text{-}his}$, KM2/pTAM51; $b_{arg36\rightarrow ile\text{-}V5}$, KM2/pTAM53; $b_{arg36\rightarrow glu\text{-}V5}$, KM2/pTAM54; $b_{wt\text{-}his}/b_{wt\text{-}V5}$, KM2/pTAM37/pTAM46; $b_{153\rightarrow end\text{-}his}/b_{arg36\rightarrow ile\text{-}V5}$, KM2/pTAM51/pTAM53; $b_{153\rightarrow end\text{-}his}/b_{arg36\rightarrow glu\text{-}V5}$, KM2/pTAM51/pTAM54.

aggregation was nor incomplete solubilization was a factor in the observed results (Figure 3-8B, lanes 10-11). Therefore, in cells expressing two different *b* subunits, any observed interactions of *b* subunits must have been due to heterodimers integrating into an intact F_1F_0 ATP synthase complex. Importantly, immunobotting using the anti-V5 antibody clearly detected V5 epitope-tagged *b* subunits in Ni-resin purified samples when two different *b* subunits, $b_{\Delta 153 \rightarrow \text{end-his}}$ and $b_{\text{arg36} \rightarrow \text{ile-V5}}$ or $b_{\text{arg36} \rightarrow \text{glu-V5}}$, were coexpressed (Figure 3-8B, Lanes 12-13). The data indicated that dimerization between the two defective *b* subunits could occur and the F_1F_0 ATP synthase complex accepted incorporation of a *b* heterodimer with mutations affecting two different domains.

Expression of two different defective *b* subunits yielded three distinct F_1F_0 ATP synthase complexes including the $b_{\text{arg36} \rightarrow \text{ile-V5}}$ or $b_{\text{arg36} \rightarrow \text{glu-V5}}$ homodimeric F_1F_0, a partially assembled $b_{\Delta 153 \rightarrow \text{end-his}}$ homodimer complex, and the heterodimeric F_1F_0 ATP synthase complexes. Total membrane associated F_1-ATP hydrolysis activity was used as a test of F_1F_0 ATP synthase complex assembly (Table 3-1). Membrane vesicles isolated from strains KM2/pTAM51/pTAM53 ($b_{\Delta 153 \rightarrow \text{end-his}}/b_{\text{arg36} \rightarrow \text{ile-V5}}$) and KM2/pTAM51/pTAM54 ($b_{\Delta 153 \rightarrow \text{end-his}}/b_{\text{arg36} \rightarrow \text{glu-V5}}$) yielded membrane associated specific activities of about 29% and 14%, respectively, which was intermediate between the specific activities if either of the mutants were expressed alone in the cell. An indication of coupled activity was obtained by F_1F_0 ATP synthase-mediated ATP-driven proton pumping activity in membrane vesicles prepared from the epitope-tagged mutants (Figure 3-9). As expected, membranes from all three strains expressing defective *b* subunits by themselves showed no proton pumping activity. Membranes isolated from cells expressing $b_{\Delta 153 \rightarrow \text{end-his}}/b_{\text{arg36} \rightarrow \text{ile-V5}}$ or $b_{\Delta 153 \rightarrow \text{end-his}}/b_{\text{arg36} \rightarrow \text{glu-V5}}$, KM2/pTAM51/pTAM53

or KM2/pTAM51/pTAM54, respectively, displayed coupled ATP-driven proton pumping of about 20% and 16%. Since either homodimer leads to a completely defective enzyme, any coupled activity observed necessarily came from an intact heterodimeric F_1F_0 ATP synthase. The data indicated that F_1F_0 ATP synthase complexes incorporated with heterodimers of two mutant *b* subunits were indeed functional. Furthermore, the results demonstrated that the roles of the two *b* subunits in the peripheral stalk were not equivalent.

Discussion

Historically the *b* subunit dimer has been viewed as a single functional unit. However, the asymmetric nature of the F_1F_0 ATP synthase enzyme complex suggested that the functional role of each *b* subunit should not necessarily be considered equivalent. Protein-protein contacts made by one *b* subunit cannot be made by the other. In the present work, a unique expression system that facilitates the production, purification and detection of F_1F_0 ATP synthase complexes incorporated with a *b* subunit heterodimer was utilize in order to study the functional roles of the two *b* subunits. The experiments involved a two-plasmid expression system that directed production of two different *b* subunits in the same cell and an epitope tag system that allowed detection of a *b* subunit heterodimeric F_1F_0 ATP synthase species. Three regions of the *b* subunit were considered. An evolutionarily conserved arginine, b_{arg36}, located near the interface between the membrane and tether domains had been found to be crucial for F_1F_0 ATP synthase function (215). Enzyme complexes incorporated with a $b_{arg36\rightarrow ile\text{-}V5}$ or $b_{arg36\rightarrow glu\text{-}V5}$ were found to be intact yet functionally defective. Second, the C-terminal last four amino acids had been shown to be essential for the F_1 binding domain (206, 288).

Enzyme complexes with a $b_{\Delta 153 \rightarrow end\text{-}his}$ were found to be only partially assembled. Thirdly, insertions and deletions in a hydrophobic stretch of amino acids in the *b* subunit corresponding to amino acids 124-130 (VAILAVA) resulted in a complete loss of enzyme function. The *b* dimer was not found in membranes when cells expressed only the $b_{+124\text{-}130}$ subunit. Heterodimerization was detected in cells expressing either *arg*36 mutation, $b_{arg36 \rightarrow ile\text{-}V5}$ or $b_{arg36 \rightarrow glu\text{-}V5}$, with $b_{wt\text{-}his}$, $b_{\Delta 153 \rightarrow end\text{-}his}/b_{wt\text{-}V5}$ and $b_{+124\text{-}130\text{-}his}/b_{wt\text{-}V5}$ (Figure 3-10).

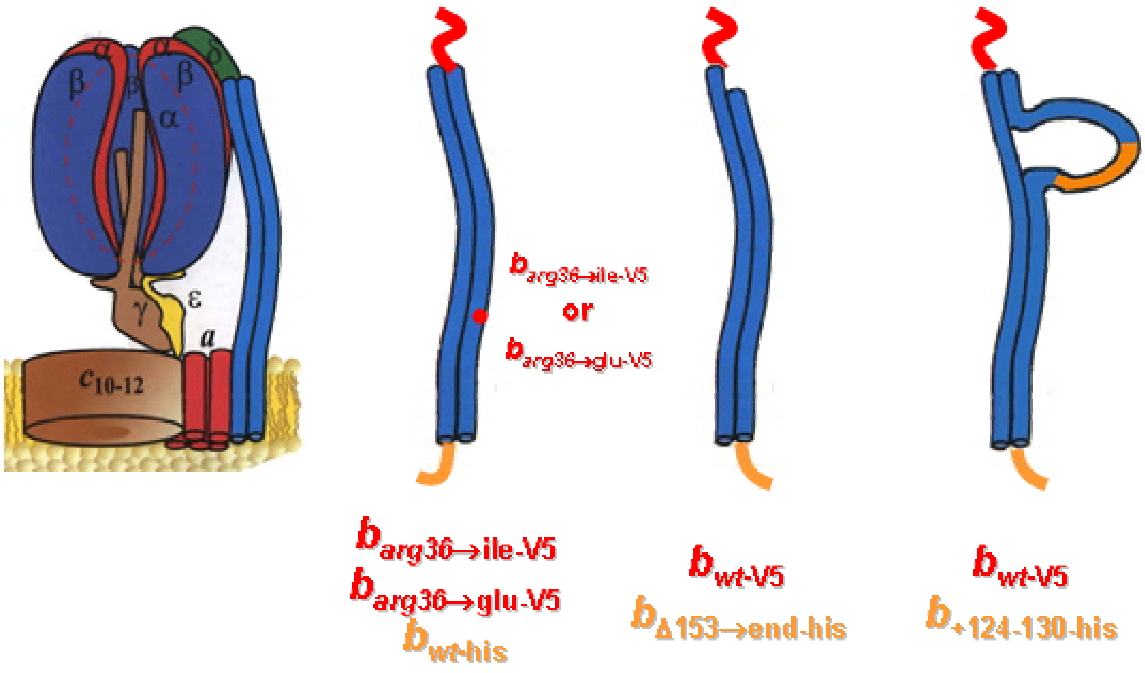

Figure 3-10. Interactions of defective *b* subunit with wild type *b* subunits found in intact F_1F_0 ATP synthase complexes. An epitope-tag system was used in order to determine if a defective *b* subunit could form a dimer with a wild type *b* subunit. A V5 epitope tag was constructed at the C-terminus of the *b* subunit (shown in red) or a histidine epitope tag was placed at the N-terminus of the *b* subunit. Four mutant *b* subunits were studied and all were found to form a dimer with a wild type *b* subunit – (1) $b_{arg36 \rightarrow ile\text{-}V5}$, (2) $b_{arg36 \rightarrow glu\text{-}V5}$, (3) $b_{\Delta 153 \rightarrow end\text{-}his}$ and (4) $b_{+124\text{-}130\text{-}his}$.

Dimerization was observed in membrane preparations from cells expressing both $b_{\Delta153\rightarrow end\text{-}his}/b_{arg36\rightarrow ile\text{-}V5}$ and $b_{\Delta153\rightarrow end\text{-}his}/b_{arg36\rightarrow glu\text{-}V5}$. More importantly, enzyme complexes incorporated with the mutant heterodimers were functionally active, suggesting that each of the *b* subunits were complementing the other to form an intact and functional enzyme complex. This observation demonstrated unambiguously that F_1F_0 ATP synthase complexes containing *b* heterodimers were active and provided evidence that each of the individual *b* subunits provide specialized functions within the peripheral stalk. Clearly, each of the mutant *b* subunits compensates for what the other is lacking.

This raises a question concerning the relative positions of the individual *b* subunits of the peripheral stalk. In order for F_1F_0 ATP synthase containing the two different mutant *b* subunits to be intact and functional, it is likely that the $b_{arg36\rightarrow ile\text{-}V5}$ (or $b_{arg36\rightarrow glu\text{-}V5}$) subunit must be positioned such that its extreme C-terminus forms the appropriate contacts with the δ subunit of F_1. Similarly, the $b_{\Delta153\rightarrow end\text{-}his}$ subunit must be positioned so that its b_{arg36} makes the appropriate contacts with the F_0 subunits (Figure 3-11). Incorrect positioning of the mutant *b* subunits during assembly might be expected to lead to an inactive or partially assembled enzyme complex.

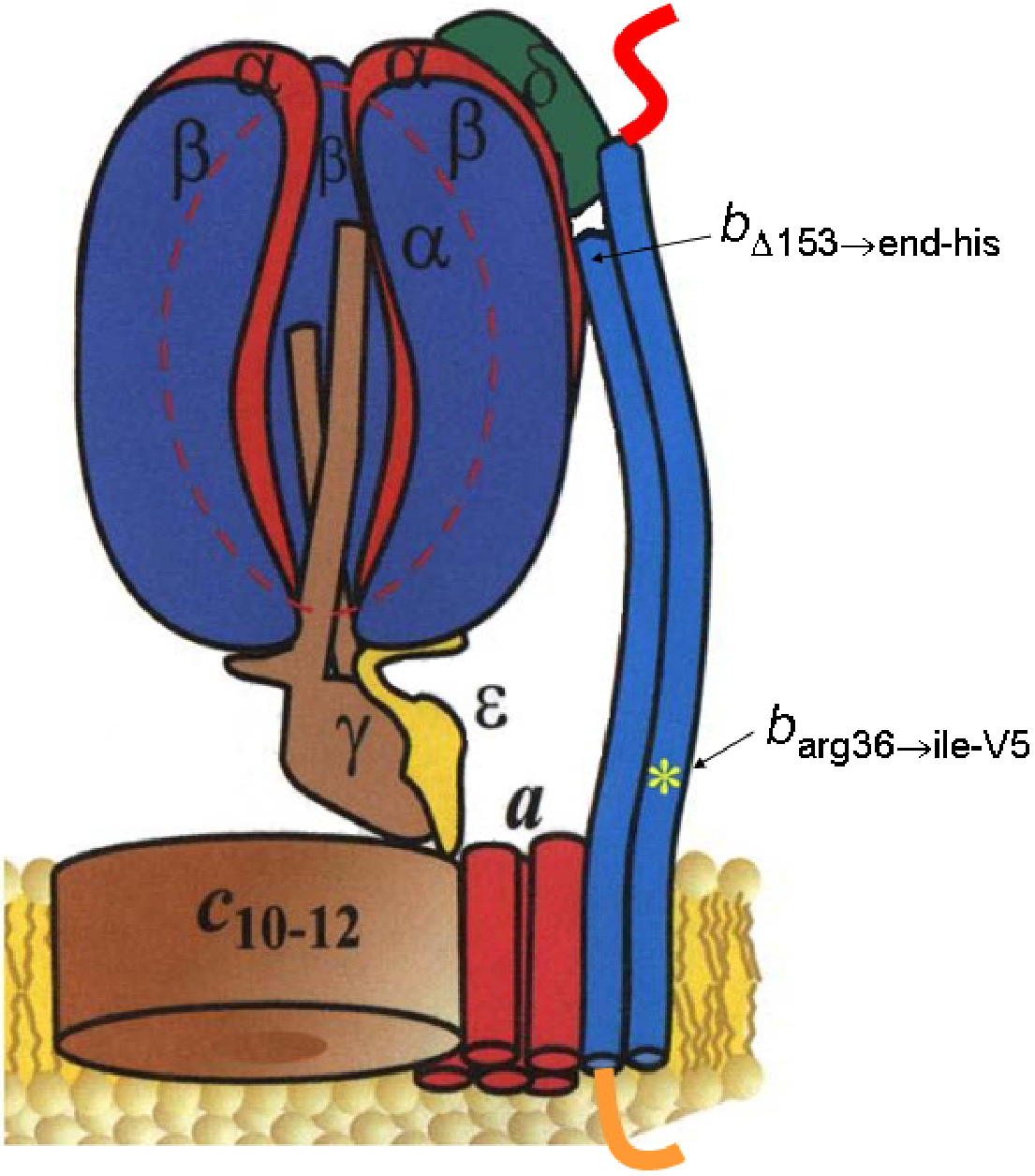

Figure 3-11. Model of F_1F_0 ATP synthase incorporated with complementing defective *b* subunits. The $b_{arg36 \rightarrow ile}$ subunit was expressed with a V5 epitope tag at its carboxyl terminus (represented by the "*S*"-shaped red line) and the $b_{153 \rightarrow end}$ subunit was expressed with a histidine tag at its amino terminus (represented by the orange curved line). Complexes incorporated with a *b* subunit heterodimer resulted in a functional enzyme complex. The $b_{arg36 \rightarrow ile\text{-}V5}$ subunit provides an intact F_1 binding domain for interaction with the δ subunit, and the $b_{153 \rightarrow end\text{-}his}$ subunit carries out the interaction with the *a* subunit.

CHAPTER 4
DEVELOPMENT OF CYSTEINE CHEMICAL MODIFICATIONS OF ALTERED *b* SUBUNITS

Introduction

F_1F_0 ATP synthases utilize the electrochemical gradient of protons across membranes to synthesize ATP from ADP and P_i (3, 290, 291). In *E. coli*, F_1F_0 ATP synthase is a multimeric enzyme composed of twenty-two polypeptides of eight different types (Figure 4-1). The F_1 portion is composed of the subunits $\alpha_3\beta_3\gamma\delta\varepsilon$ and is responsible for catalysis. The F_0 portion of the enzyme consists of the ab_2c_{10} subunits and conducts proton translocation through the membrane. Two stalk structures link the F_1 and F_0 sectors. Proton translocation drives the rotation of the central stalk, known as the "rotor", within the stationary $\alpha_3\beta_3$ hexamer, resulting in conformational changes within the catalytic sites (3, 15, 16, 63, 64). A second stalk structure, known as the peripheral stalk, consists of the δ and *b* subunits (Figure 4-1). The role of the peripheral stalk is thought to be that of a "stator", holding the hexamer in place against the rotation of the central stalk. The δ subunit can be chemically fixed to a single α subunit without loss of enzyme activity, which would be expected if δ was part of the peripheral stalk linking F_1 and F_0, supporting the "stator" concept (185). The carboxyl termini of the δ and *b* subunits have been shown to be in direct contact (3, 142, 200, 219, 220).

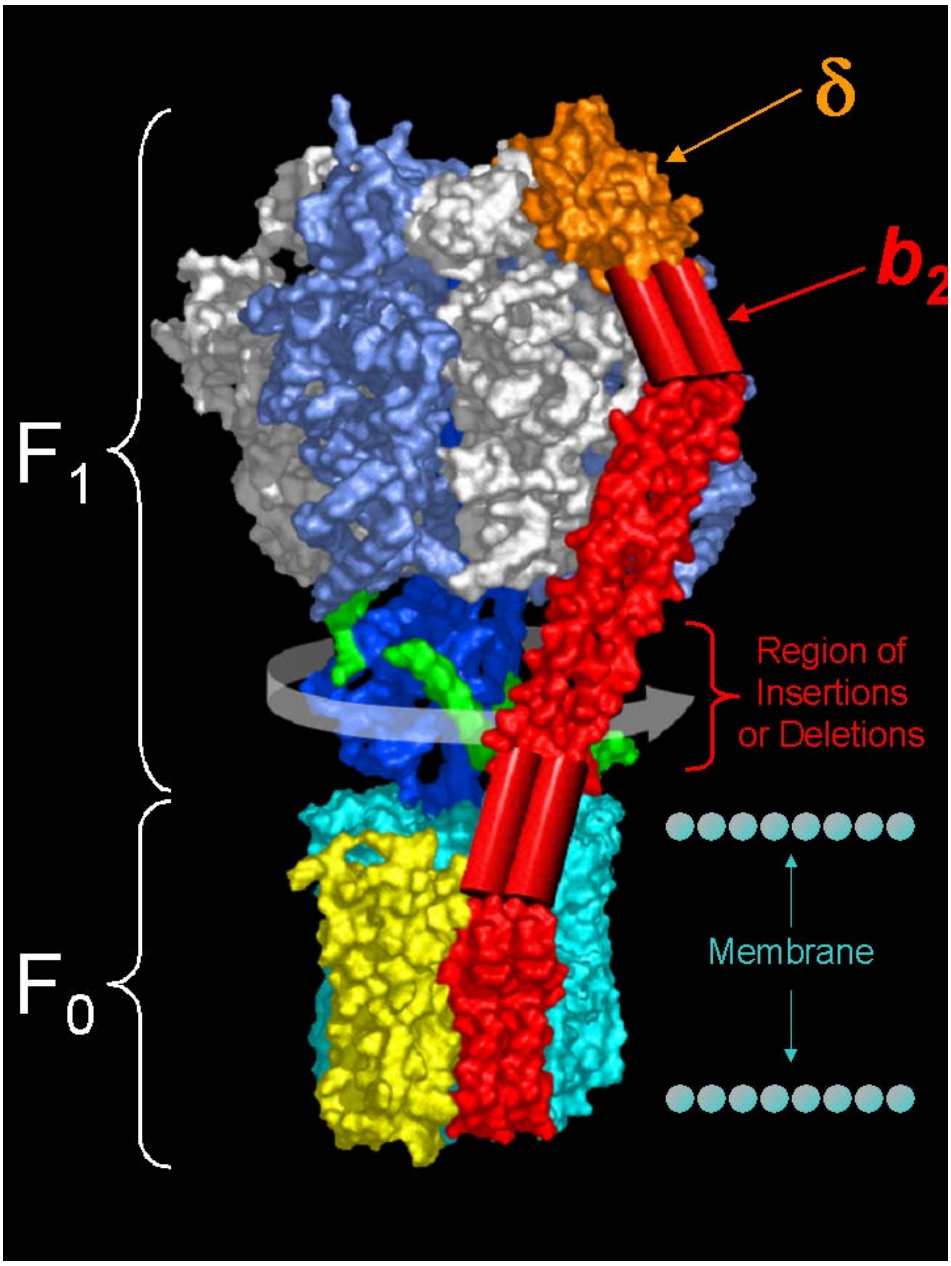

Figure 4-1. Model of *E. coli* F_1F_0 ATP synthase. The peripheral stalk of F_1F_0 ATP synthase is composed of the δ subunit of F_1 and the homodimer of *b* subunits of F_0. Shown in orange and red are the δ and *b* subunits, respectively. It has been shown previously that insertions and deletions of amino acids in the tether region of the *b* subunit do not affect enzyme activity. However, it was not known how the insertions or deletions were accommodated in the context of an intact enzyme. An understanding of the structure of the peripheral stalk can be obtained by investigating the apparent length of the peripheral stalk in shortened, lengthened and wild type *b* subunits.

A dimer of two *b* subunits is the major component of the peripheral stalk of F_1F_0 ATP synthase and is necessary for normal assembly and function. The *b* dimer spans the cytoplasmic membrane and reaches towards the topside of F_1 where it meets the δ subunit (Figure 4-1) (100, 141-143). A substantial amount of evidence suggests the *b* dimer to be at least 80% α-helical, with 14% β-turn, and exist in a parallel, elongated conformation, spanning about 45 Å from the top of the membrane to the bottom of the $\alpha_3\beta_3$ hexamer or about 100 Å to the top of the hexamer (12, 13, 166, 196, 292). Four domains comprise the *b* subunits: the amino-terminal membrane spanning, tether, dimerization and the carboxyl terminal δ-binding domains (Figure 4-5) (13). Despite the previous model of the *b* subunit dimer, describing it as a rigid structural feature of F_1F_0 ATP synthase, accumulating evidence suggests a more flexible stalk model (193-195, 202).

It has been shown by Dr. Paul Sorgen that F_1F_0 ATP synthase retains sufficient levels of activity upon relatively large deletions or insertions in the *b* subunit. An eleven amino acid deletion and a fourteen amino acid insertion in the region of the *b* subunit spanning the tether domain and the beginning of the dimerization domain was accommodated by the enzyme (Figure 4-5). Assuming α-helical structure, this 21 Å insertion and 16 Å deletion corresponds to well over a third of the length spanning from the top of the membrane to F_1, or right under a quarter of the length spanning towards the top of F_1. Furthermore, four amino acid insertions and deletions were successfully accommodated throughout most of the dimerization and δ-binding domains of the *b* subunit (manuscript in preparation). In contrast to the previously accepted role of the *b* subunit as a rigid "stator", these observations suggest that the role of the *b* dimer is more of a flexible or elastic structural feature during rotational catalysis. In the present

chapter, cysteine chemical modifications were created in the δ and *b* subunits to provide reactive thiols groups for future labeling studies.

Materials and Methods

A more thorough account of many of the procedures used in Chapter 6 can be found in previous chapters. Many of the techniques, including recombinant DNA techniques, site directed mutagenesis, crude membrane preparation procedures, western blotting, as well as assays of protein concentration and F_1F_0 ATP synthase activity have been described in detail in Chapter 2.

Materials

Molecular biology enzymes and mutagenic oligonucleotides were obtained from Invitrogen (Carlsbad, CA), Life Technologies, Inc. (Grand Island, NY), New England Biolabs (Beverly, MA) and Stratagene (La Jolla, CA). Reagents were obtained from Sigma (St. Louis, MO), BioRad Laboratories (Hercules, CA) and Fisher Scientific (Pittsburgh, PA). Plasmid purification kits were acquired from Qiagen Inc. (Valencia, CA). The anti-rabbit immunoglobulin horseradish peroxidase-linked whole antibody (from donkey), Hybond ECL Nitrocellulose membrane, electrochemiluminescence Western blotting reagents and high performance chemiluminescence film were purchased from Amersham Biosciences (Piscataway, NJ). Polyclonal antibodies against SDS-denatured *b* subunit (284, 285) were generously provided by Dr. Karlheinz Altendorf (Universität Osnabrück, Osnabrück, Germany.

Strains and Media

The bacterial strains used to create the cysteine chemical modifications in the *b* subunit include the wild type *b* subunit expression plasmid, pKAM14 (*b*, Ap^r), and plasmids used to express *b* subunits shortened or lengthened by 11 amino acids, pAUL5

($b_{\Delta 11}$, Ap^r) and pAUL47 (b_{+11}, Ap^r), respectively, and have been described previously (193, 194, 203). The plasmids encoding the *uncF*(*b*) gene were used to compliment *Escherichia coli* (*E. coli*) strain KM2 (Δ*b*) carrying a chromosomal deletion of the gene. Plasmid pJLG1 (*a*, *c*, *b*, Cm^r), generated by Dr. James Gardner in our lab, was used as a temporary vector in order to facilitate cloning due to its extra unique restriction enzyme sites. The wild type *unc* operon expression plasmid, pAES9 (αβγδε*abc,* Cm^r), was used to create a cysteine-less F_1F_0 ATP synthase complex and has been described previously (178). The plasmids encoding the *unc* operon (αβγδε*abc*) were used to compliment *E. coli* strain 1100ΔBC (Δαβγδε*abc*) carrying a chromosomal deletion for the entire operon. All strains were streaked onto plates containing Minimal A media supplemented with succinate (0.2% w/v), to determine enzyme viability. Cells harvested for membrane preparation were grown in Luria Broth supplemented with glucose (0.2% w/v) (LBG). Isopropyl-1-thio-β-D-galactopyranoside (IPTG)(40 μg/ml), ampicillin (Ap) (100μg/ml), and chloramphenicol (Cm) (25 μg/ml) were added to media as needed. All cultures were incubated at 37˚C for the appropriate duration.

Recombinant DNA Techniques

Plasmid DNA was purified with the Qiagen Mini-Prep and Maxi-Prep kits. Restriction endonuclease digestions, ligations, and transformations were performed according to the recommendations of the manufacturers (New England Biolabs, Stratagene and Life Technologies, Inc.). Site-directed mutagenesis was performed either by means of a Stratagene Quikchange kit or by ligation-mediated mutagenesis. DNA fragments were separated in 0.8 % agarose gel by electrophoresis and purified using a

Qiagen, Inc. QIAquick Gel Extraction kit. Plasmid sequences were determined by automated sequencing in the core facility of the University of Florida ICBR.

Mutagenesis and Strain Construction

Plasmids pKAM14 (*b*, Ap^r) (203), pAUL5 ($b_{\Delta 11}$, Ap^r) (194) or pAUL47 (b_{+11}, Ap^r) (193) and pJLG1 (*a*, *c*, *b*, Cm^r) (167) were used to construct cysteine mutant *b* subunits. Mutagenesis was performed in three different subunits; therefore, the ultimate goal was to express the entire *unc* operon containing the desired cysteine mutations from one plasmid. Plasmid pJLG1 (*a*, *c*, *b*, Cm^r) was used as a temporary vector in order to facilitate cloning due to its extra unique restriction enzyme sites.

***b* subunit mutations.** In order to construct the *b* subunit mutations, plasmids pAUL5 ($b_{\Delta 11}$, Ap^r), pAUL47 (b_{+11}, Ap^r) and pJLG1 (*a*, *c*, *b*, Cm^r) were first digested with restriction enzymes *Ppu*MI and *Nar*I in order to move the *b* subunit deletion and insertion into the pJLG1 plasmid. The resulting 204 and 270 bp cassettes isolated from pAUL5 ($b_{\Delta 11}$, Ap^r) and pAUL47 (b_{+11}, Ap^r), respectively, were subsequently ligated into the pJLG1 vector, resulting in pTAM1 ($b_{\Delta 11}$, Cm^r) and pTAM3 (b_{+11}, Cm^r) (Table 4-1). In order to site specifically label the *b* subunit in future experiments, a native amino acid was mutated to a cysteine. Two sites were chosen for replacement, b_{ser84} and b_{gly43}, located respectively above and below the region of length alteration. Furthermore, the *b* subunit had a native cysteine, b_{cys20}, located in the membrane-spanning portion of the subunit, which was mutated to a serine. The mutations were created in each of the plasmids using the Stratagene Quikchange kit. Sense and antisense mutagenic oligonucleotides were created for each of the desired *b* subunit mutations (Appendix A) (Figure 4-2A). First, the native cysteine was abolished by mutagenesis of codon 20

Table 4-1. Description of *uncF*(*b*) cysteine mutations

Plasmid	Description[1, 2]	*b* Length	$b_{cys20\rightarrow ser}$	$b_{gly43\rightarrow cys}$	$b_{ser84\rightarrow cys}$	Growth[3]
pKAM14	b_{wt}, Ap^r	wt	–	-	-	+++
pBR322	Δ*b*, Ap^r	-	NA	NA	NA	-
pTAM1	$b_{\Delta 11}$, Cm^r	Δ11	-	-	-	nd
pJLG1[4]	b_{wt}, Cm^r	wt	-	-	-	nd
pTAM3	b_{+11}, Cm^r	+11	-	-	-	nd
pTAM8	$b_{\Delta 11\text{-}cys20\rightarrow ser,\ gly43\rightarrow cys}$	Δ11	✓	✓	-	+++
pTAM9	$b_{cys20\rightarrow ser,\ gly43\rightarrow cys}$	wt	✓	✓	-	+++
pTAM10	$b_{+11\text{-}cys20\rightarrow ser,\ gly43\rightarrow cys}$	+11	✓	✓	-	+++
pTAM11	$b_{\Delta 11\text{-}cys20\rightarrow ser,\ ser84\rightarrow cys}$	wt	✓	-	✓	+++
pTAM12	$b_{cys20\rightarrow ser,\ ser84\rightarrow cys}$	Δ11	✓	-	✓	+++
pTAM13	$b_{+11\text{-}cys20\rightarrow ser,\ ser84\rightarrow cys}$	+11	✓	-	✓	+++

[1] Description as found in text.

[2] Plasmids pTAM1-pTAM13 all encode the *uncB*(*a*) and *c* genes, but for the sake of brevity, only the *b* subunit mutations are described.

[3] Plasmids were transformed into *E. coli* strain KM2 (Δ*b*) and grown aerobically on succinate minimal medium. Colony size was scored after 72-hr incubation at 37ºC as: +++, ≥ 1.0 mm; ++, 0.3-0.5 mm; +, ~0.1 mm; -, no growth.

[4] Plasmid courtesy of Dr. James Gardner.

of the *uncF*(*b*) gene to express $b_{cys20\rightarrow ser}$, $b_{\Delta 11\text{-}cys20\rightarrow ser}$ and $b_{+11\text{-}cys20\rightarrow ser}$. Then, a cysteine was introduced by mutagenesis of codon 43 ($b_{gly43\rightarrow cys}$) or codon 84 ($b_{ser84\rightarrow cys}$) of the *uncF*(*b*) gene to generate a set of six plasmids: pTAM9 ($b_{cys20\rightarrow ser,\ gly43\rightarrow cys}$), pTAM8 ($b_{\Delta 11\text{-}cys20\rightarrow ser,\ gly43\rightarrow cys}$), pTAM10 ($b_{+11\text{-}cys20\rightarrow ser,\ gly43\rightarrow cys}$), pTAM12 ($b_{cys20\rightarrow ser,\ ser84\rightarrow cys}$), pTAM11 ($b_{\Delta 11\text{-}cys20\rightarrow ser,\ ser84\rightarrow cys}$) and pTAM13 ($b_{+11\text{-}cys20\rightarrow ser,\ ser84\rightarrow cys}$) (Table 4-1). The existing unique restriction enzyme sites recognized by *SnaB*I, *Bsp1285*I and *Xba*I were abolished by silent mutation near the encoded $b_{cys20\rightarrow ser}$, $b_{gly43\rightarrow cys}$ and $b_{ser84\rightarrow cys}$ mutations, respectively, for an initial detection of mutations. Subsequently, the nucleotide sequence was subsequently confirmed by automated sequencing in the ICBR core facility (Figure 4-2A). The recombinant altered *b* subunits included the chloramphenicol resistance gene and the pACYA184 origin of replication.

Figure 4-2. Oligonucleotides for cysteine mutagenesis of the *unc* operon. Shown are the sense strands of the mutagenic primer pairs. The desired mutations are shown in color. Bold script indicates a change in nucleotide. Restriction enzyme recognition sequences that were silently added or abolished are underlined. Mutations were introduced as described in the Materials and Methods. A) Blue indicates the cysteine mutations constructed in *uncF*(*b*). The *SnaB*I, *Bsp1285*I and *Xba*I restriction sequences were knocked out along with the $b_{cys20\rightarrow ser}$, $b_{gly43\rightarrow cys}$ and $b_{ser84\rightarrow cys}$, respectively, to facilitate screening. B) Red indicates the cysteine mutations generated in *uncH*(δ). The *Cla*I sequence was knocked out and the *EcoR*I site was generated along with $\delta_{cys140\rightarrow ser}$ for screening purposes. C) Green indicates the cysteine mutation made in *unc*(α). The *BamH*I sequence was added to screen for the $\alpha_{cys90\rightarrow ser}$ mutation.

δ and α subunit mutations. The δ subunit has two indigenous cysteines, δ_{cys64} and δ_{cys140}, which have been shown to be highly reactive with maleimide reagents (293). We planned to chemically label both sites specifically, so plasmids were constructed which expressed only one of the two cysteines by mutating one, either $\delta_{cys64\rightarrow ser}$ or $\delta_{cys140\rightarrow ser}$, to a serine. Also, another cysteine located within the α subunit of F_1 has been shown to be highly reactive to maleimide reagents. This cysteine was mutated to a serine without loss of enzyme function (198). Plasmid pAES9 (αβγδε*abc,* Cm^r) was used to construct the cysteine mutant δ and α subunits. Due to the difficulty of performing Quikchange on a 10.9 kb plasmid, it was necessary temporarily move the genes encoding the δ and α subunits into plasmid pBluescript (pBS) by digesting pAES9 (αβγδε*abc,* Cm^r) with the restriction enzymes *BamH*I and *EcoR*I, flanking the genes of interest, and then ligating the 3.8 kb cassette into pBS, pTAM2. Sense and antisense mutagenic oligonucleotides were created for each of the desired δ and α subunit mutations (Figure 4-2B and C). First, each of the native cysteines found in the δ subunit were substituted with serines in two different plasmids by site-directed mutagenesis of codon 64 or 140 of the *unc* (δ) gene to express $\delta_{cys64\rightarrow ser}$ or $\delta_{cys140\rightarrow ser}$. Then the native cysteine found in the α subunit was changed to a serine by mutagenesis of codon 90 of the *unc* (α) gene to express $\alpha_{cys90\rightarrow ser}$. The *Cla*I sequence was silently knocked out and the *EcoR*I site was generated along with $\delta_{cys140\rightarrow ser}$ (Figure 4-2B) and the *BamH*I sequence was added along with the $\alpha_{cys90\rightarrow ser}$ mutation (Figure 4-2C) for initial screening purposes and then the nucleotide sequence was subsequently confirmed by automated sequencing in the ICBR core facility. The genes encoding the δ and α subunits with the generated cysteine

mutations were then shuttled back into pAES9 ($\alpha\beta\gamma\delta\varepsilon$*abc,* Cm^r) to create plasmids pTAM20 ($\alpha_{cys90\rightarrow ser}$ $\beta\gamma\delta_{cys64\rightarrow ser}\varepsilon$*abc,* Cm^r) and pTAM21 ($\alpha_{cys90\rightarrow ser}$ $\beta\gamma\delta_{cys140\rightarrow ser}\varepsilon$*abc,* Cm^r). The recombinant plasmids included the chloramphenicol resistance gene and the pACYA184 origin of replication.

Construction of intact mutant *unc* operons. The final step of plasmid construction was to move each of the previously generated *b* subunit cysteine mutants (Table 4-1) into both pTAM20 ($\alpha_{cys90\rightarrow ser}$ $\beta\gamma\delta_{cys64\rightarrow ser}\varepsilon$*abc,* Cm^r) and pTAM21 ($\alpha_{cys90\rightarrow ser}$ $\beta\gamma\delta_{cys140\rightarrow ser}\varepsilon$*abc,* Cm^r), generating plasmids pTAM22-pTAM33 (Table 4-2). Each of the plasmids encoded the entire *unc* operon with the $\alpha_{cys90\rightarrow ser}$ and $b_{cys20\rightarrow ser}$ mutations as well as every possible combination of shortened, lengthened or wild type length *b* subunits, $b_{gly43\rightarrow cys}$ or $b_{ser84\rightarrow cys}$ and $\delta_{cys64\rightarrow ser}$ or $\delta_{cys64\rightarrow ser}$. The final products included 12 plasmids that encoded 12 genetically different F_1F_0 ATP synthase complexes as well as the chloramphenicol resistance gene and the pACYA184 origin of replication (Table 4-2).

Crude Preparative Procedures

Inverted membrane vesicles from KM2 (Δb) or 1100ΔBC ($\Delta\alpha\beta\gamma\delta\varepsilon abc$) strains expressing the desired cysteine mutations were prepared essentially as described in Chapter 2 (194). Bacteria were grown in 500 mL LBG supplemented with the appropriate antibiotic, harvested, and passed through a French Pressure Cell one time at 14,000 psi. Membranes were then collected by differential centrifugation. Protein concentrations were determined by the bicinchoninic acid (BCA) assay (286).

Assays of F_1F_0 ATP Synthase Activity

Growth on a minimal succinate medium was used as an initial, *in vivo*, assay for enzyme viability. ATP hydrolysis activity was assayed by the acid molybdate method

(146). Membranes were assayed in buffer (50 mM Tris-HCl, 1 mM MgCl2, pH9.1) to determine the linearity with respect to time and enzyme concentration.

Immunoblot Analysis

Proteins were loaded on a 15% tris-glycine SDS gel and transferred onto nitrocellulose by electroblot. The *b* subunit antibody incubation was performed essentially as described previously, using a 1:25,000 dilution of the anti-*b* subunit antibodies. Secondary antibody incubation was performed with horseradish peroxidase-linked donkey anti-rabbit antibody (1:50,000), and the antibody was detected by enhanced chemiluminescence. Signals were visualized on high performance chemiluminescence film using a Kodak X-Omat.

Results

Construction and Growth Characteristics of Mutants

Single cysteines, which will provide reactive thiols for site-specific chemical modification, were strategically placed within the F_1F_0 ATP synthase enzyme complex. Several cysteine mutations were generated in the *unc* operon in a multi-step construction scheme to ultimately result in 12 plasmids encoding different combinations of six different amino acid substitutions as well as *b* subunits of altered length (Table 4-2) (Figure 4-3).

A previous analysis of F_1F_0 ATP synthase complexes with *b* subunits shortened and lengthened by 11 amino acids found the mutants to be essentially wild-type when expressed in the presence of 40 μM IPTG (193, 194). Functional F_1F_0 ATP synthase complexes have been studied with many different cysteine mutations;

Table 4-2. Description of the *unc* operon cysteine mutations[1]

Plasmid[2]	Length[3]	$\alpha_{cys90\rightarrow ser}$	$b_{cys20\rightarrow ser}$	$b_{gly43\rightarrow cys}$	$b_{ser84\rightarrow cys}$	$\delta_{cys140\rightarrow ser}$	$\delta_{cys64\rightarrow ser}$
pAES9	wt	–	–	-	-	-	-
pBR322	•	NA	NA	NA	NA	NA	NA
pTAM22	Δ11	✓	✓	✓	-	✓	-
pTAM23	wt	✓	✓	✓	-	✓	-
pTAM24	+11	✓	✓	✓	-	✓	-
pTAM25	Δ11	✓	✓	-	✓	✓	-
pTAM26	wt	✓	✓	-	✓	✓	-
pTAM27	+11	✓	✓	-	✓	✓	-
pTAM28	Δ11	✓	✓	✓	-	-	✓
pTAM29	wt	✓	✓	✓	-	-	✓
pTAM30	+11	✓	✓	✓	-	-	✓
pTAM31	Δ11	✓	✓	-	✓	-	✓
pTAM32	wt	✓	✓	-	✓	–	✓
pTAM33	+11	✓	✓	-	✓	–	✓

[1] Plasmids were designed to contain various combinations of the cysteine mutations in the *b* and δ subunits. Symbols: -, plasmid does not contain the listed mutation; ✓, plasmid encodes the mutation listed above.

[2] All plasmids, with the exception of pBR322, encoded the entire *unc* operon and conferred chloramphenicol resistance.

[3] Length of the tether domain of the *b* subunit. Symbols: •, empty plasmid vector; wt, normal length; Δ11, eleven amino acid deletion; +11, eleven amino acid insertion.

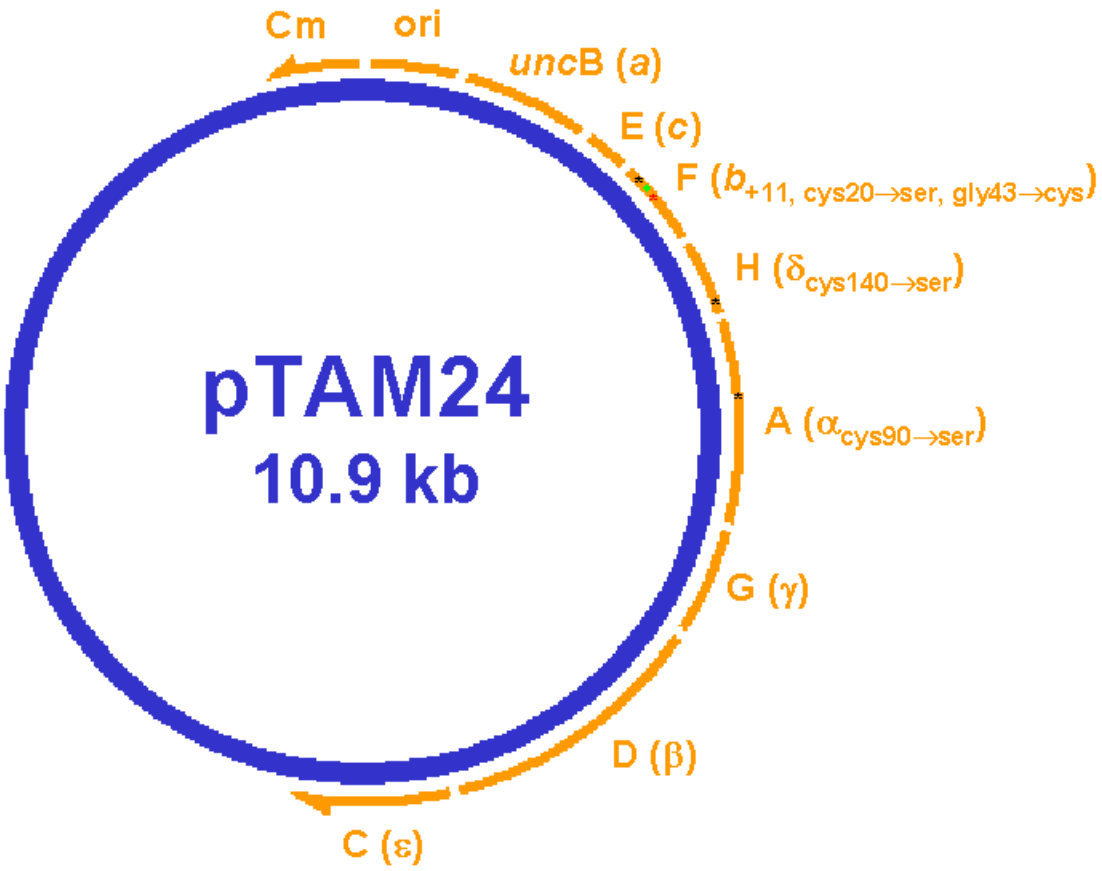

Figure 4-3. Expression plasmid of cysteine mutants. F_1F_0 ATP synthase complexes with site-specific cysteine mutations were designed to be expressed from a single plasmid encoding the entire *unc* operon. Plasmid pTAM24 is one of twelve of the constructed plasmids. The name of the *unc* gene is listed followed by the subunit it expresses in parenthesis. The black stars represents codons that expressed a native cysteine that had been substituted with a serine. The red star represents a glycine to cysteine substitution at codon 43 of the *uncF*(*b*) gene. The green dot represents an 11 amino acid insertion. Plasmid pTAM24 expresses the entire *unc* operon with the following mutations: $b_{+11,\ cys20\rightarrow ser,\ gly43\rightarrow cys}$, $\delta_{cys140\rightarrow ser}$, and $\alpha_{cys90\rightarrow ser}$. The plasmids confer chloramphenicol resistance and the pACYA184 origin of replication. Similar constructions include those listed in Table 4-2.

however, it was necessary to determine whether the mutations generated in the present study would have affect activity. The effects of the cysteine mutations were studied by the ability of the plasmids to complement either the *E. coli* strain KM2 (Δ*b*) (Table 4-1) or 1100ΔBC (Δαβγδε*abc*) (Table 4-3). Growth on succinate minimal medium was used

as an initial qualitative gauge of enzyme activity *in vivo* since *E. coli* strains lacking F_1F_0 ATP synthase cannot derive energy from nonfermentable sources. In each case, the strains expressing the different cysteine mutations grew comparable to the wild type strain (Table 4-3).

Table 4-3. Aerobic growth properties and membrane-associated ATP hydrolysis activity of mutants expressing cysteine

Strains[1]	Description[2]	Growth[3]	Activity[4]
pAES9	α, β, γ, δ, ε, *a, b, c,* Cm^r	+++	100%
pBR322	empty vector, Ap^r	-	12%
pAUL5[5]	$b_{\Delta 11}$, Ap^r	+++	90%
pAUL47[5]	b_{+11}, Ap^r	+++	87%
pTAM22	$\alpha_{cys90\rightarrow ser}$, $\delta_{cys140\rightarrow ser}$, $b_{\Delta 11,\ cys20\rightarrow ser,\ gly43\rightarrow cys}$	+++	89%
pTAM23	$\alpha_{cys90\rightarrow ser}$, $\delta_{cys140\rightarrow ser}$, $b_{cys20\rightarrow ser,\ gly43\rightarrow cys}$	+++	95%
pTAM24	$\alpha_{cys90\rightarrow ser}$, $\delta_{cys140\rightarrow ser}$, $b_{+11,\ cys20\rightarrow ser,\ gly43\rightarrow cys}$	+++	87%
pTAM25	$\alpha_{cys90\rightarrow ser}$, $\delta_{cys140\rightarrow ser}$, $b_{\Delta 11,\ cys20\rightarrow ser,\ ser84\rightarrow cys}$	+++	88%
pTAM26	$\alpha_{cys90\rightarrow ser}$, $\delta_{cys140\rightarrow ser}$, $b_{cys20\rightarrow ser,\ ser84\rightarrow cys}$	+++	101%
pTAM27	$\alpha_{cys90\rightarrow ser}$, $\delta_{cys140\rightarrow ser}$, $b_{+11,\ cys20\rightarrow ser,\ ser84\rightarrow cys}$	+++	89%
pTAM28	$\alpha_{cys90\rightarrow ser}$, $\delta_{cys64\rightarrow ser}$, $b_{\Delta 11,\ cys20\rightarrow ser,\ gly43\rightarrow cys}$	+++	92%
pTAM29	$\alpha_{cys90\rightarrow ser}$, $\delta_{cys64\rightarrow ser}$, $b_{cys20\rightarrow ser,\ gly43\rightarrow cys}$	+++	96%
pTAM30	$\alpha_{cys90\rightarrow ser}$, $\delta_{cys64\rightarrow ser}$, $b_{+11,\ cys20\rightarrow ser,\ gly43\rightarrow cys}$	+++	90%
pTAM31	$\alpha_{cys90\rightarrow ser}$, $\delta_{cys64\rightarrow ser}$, $b_{\Delta 11,\ cys20\rightarrow ser,\ ser84\rightarrow cys}$	+++	93%
pTAM32	$\alpha_{cys90\rightarrow ser}$, $\delta_{cys64\rightarrow ser}$, $b_{cys20\rightarrow ser,\ ser84\rightarrow cys}$	+++	99%
pTAM33	$\alpha_{cys90\rightarrow ser}$, $\delta_{cys64\rightarrow ser}$, $b_{+11,\ cys20\rightarrow ser,\ ser84\rightarrow cys}$	+++	91 %

[1] With the exception of pAUL5 and pAUL47, all plasmids were expressed in the 1100ΔBC cell line. Plasmids pAUL5 and pAUL47 encode only the *b* subunit and were expressed in the KM2 cell line.

[2] The description for plasmids pTAM22-pTAM33 only list the subunits with cysteine mutations for brevity; however, these plasmids also encode the wild type genes for the β, γ, ε, *a* and *c* subunits.

[3] *E. coli* strains were grown aerobically on succinate minimal medium supplemented with 40 μM IPTG. Colony size was scored after 72-hr incubation at 37ºC as: +++, ≥ 1.0 mm; ++, 0.3-0.5 mm; +, ~0.1 mm; -, no growth.

[4] *E. coli* strains were grown in LBG supplemented with the appropriate antibiotics and 40 μM IPTG. ATPase activities were measured as described under "Materials and Methods." Activity is listed as a percentage of the wild type strain (pAES9), which was set to 100%. Units were calculated from the slope of the line based on three measurements with incubations for 12 minutes.

[5] Plasmids courtesy of Dr. Paul Sorgen.

Effects of Cysteine Mutations

Membrane associated ATP hydrolysis activity. F_1 has very little affinity for the membrane in the absence of intact F_0, therefore, total membrane associated F_1-ATP hydrolysis activity was used as a test of F_1F_0 ATP synthase complex assembly. The cysteine mutations had very little, if any at all, affect on enzyme assembly. In general, membranes with the cysteine mutations incorporated into the F_1F_0 ATP synthase complex had specific activities ranging from about 88 to 95% of the wild types strain (Table 4-3). These values were comparable to the effect of the eleven amino acid deletion and insertions in the absence of the cysteine mutations. In fact, membranes with F_1F_0 ATP synthase complexes incorporated with *b* subunits that were wild type in length, yet carried all the cysteine mutations, ranged from 95 to 100% of the wild type strain. It was likely that the slight decrease in ATP hydrolysis activity was due to the change in length in the *b* subunits and not due to the cysteine mutations.

Western blot analysis. If the *b* subunit of F_1F_0 ATP synthase does not dimerize and become incorporated into an intact F_1F_0 ATP synthase complex, it is generally turned over and therefore absent from membrane preparations. Therefore the presence of the *b* subunit in the membrane preparations was detected by Western blot analysis. Proteins from membrane preparations generated from *E. coli* strain 1100ΔBD (Δαβγδε*abc*) complemented with pAES9 (αβγδε*abc*), pTAM31 ($\alpha_{cys90\rightarrow ser}$, β, γ, $\delta_{cys64\rightarrow ser}$,ε, *a*, $b_{\Delta 11,\ cys20\rightarrow ser,\ ser84\rightarrow cys}$, *c*), pTAM32 ($\alpha_{cys90\rightarrow ser}$, β, γ, $\delta_{cys64\rightarrow ser}$,ε, *a*, $b_{cys20\rightarrow ser,\ ser84\rightarrow cys}$, *c*) and pTAM33 ($\alpha_{cys90\rightarrow ser}$, β, γ, $\delta_{cys64\rightarrow ser}$,ε, *a*, $b_{+11,\ cys20\rightarrow ser,\ ser84\rightarrow cys}$, *c*) were separated by SDS-PAGE and detected with anti-*b* antibodes (Figure 4-4). The *b* subunit expressed from pTAM32 and pAES9 migrated to the same molecular weight as expected. The size

difference in the *b* subunit is clear between the Δ11 and +11, confirming the expression of unequal length *b* subunits.

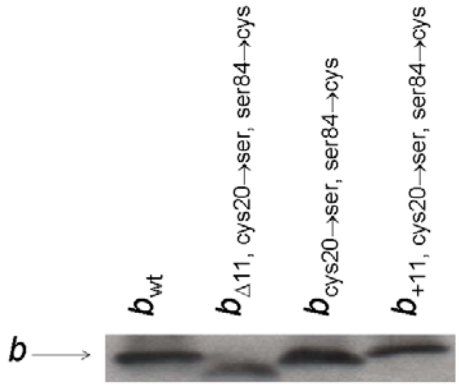

Figure 4-4. Western blot analysis of cysteine mutant *b* subunits of differing length. 1100DBC cells were transformed with plasmids pAES9 (αβγδε*abc*), pTAM31 ($\alpha_{cys90\rightarrow ser}$, β, γ, $\delta_{cys64\rightarrow ser}$,ε, *a*, $b_{\Delta 11,\ cys20\rightarrow ser,\ ser84\rightarrow cys}$, *c*), pTAM32 ($\alpha_{cys90\rightarrow ser}$, β, γ, $\delta_{cys64\rightarrow ser}$,ε, *a*, $b_{cys20\rightarrow ser,\ ser84\rightarrow cys}$, *c*) and pTAM33 ($\alpha_{cys90\rightarrow ser}$, β, γ, $\delta_{cys64\rightarrow ser}$,ε, *a*, $_{b+11,\ cys20\rightarrow ser,\ ser84\rightarrow cys}$, *c*). Proteins from a crude membrane preparation were separated on a 15% polyacrylamide Tris-HCl-SDS BioRad Ready gel and then transferred to a nitrocellulose membrane in order to probe with anti-*b* antibodies.

Discussion

In the current chapter, we have developed a set of twelve *unc* operon expression plasmids that encode amino acid substitutions to void the F_1F_0 ATP synthase complex of all known reactive thiols as well as generate strategically placed cysteines. Cysteines were chosen because the thiol side chain is highly reactive and can be modified by maleimide reagents. The cysteine mutations did not affect enzyme assembly or function. Plasmids were designed to express a single cysteine at one of two locations in the δ subunit as well as one position, either above or below the site of insertion or deletion, in the *b* subunit (Figure 4-5).

The idea for establishing a single reactive cysteine in both F_1 and F_0 is to use them as targets for labeling with fluorescence compounds. F_1 can readily be stripped from F_0,

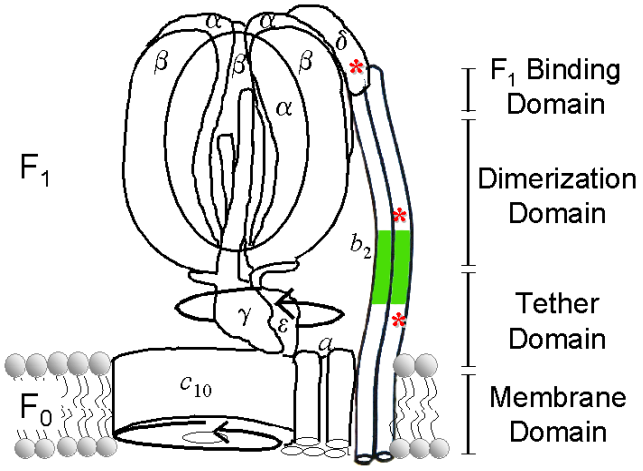

Figure 4-5. Model of F_1F_0 ATP synthase with cysteine substitutions in the *b* and δ subunits. The red stars indicate the approximate location of generated cysteines. The region colored green is the approximate location of the eleven amino acid insertion (b_{+11}) or deletion ($b_{\Delta 11}$). A set of twelve plasmids was designed to express one cysteine in the δ and unequally length *b* subunits.

each cysteine labeled separately with a "donor" and "acceptor" fluorescent compound, and then stoichiometrically reconstituted under conditions of high ionic strength (203). With a single fluorescent compound located above and below the region of insertion or deletion in the tether domain of the *b* subunit, physical measurements can be calculated and compared.

Comparing the length of the wild type, shortened and lengthened peripheral stalks will give some insight on the overall possible conformation of the altered F_1F_0 ATP synthase complex. The F_1F_0 ATP synthase enzyme complex must, in some way, adapt to the shortened or lengthened *b* subunits. This can occur in at least one of two ways: 1) distortion of F_1 to accommodate the change in length of the peripheral stalk or 2) distortion of the peripheral stalk itself. If the former was true, F_1 would become distorted by bending of the γε central stalk or compression of the $\alpha_3\beta_3$ hexamer and the rigid stalk hypothesis would gain favor. Since F_1F_0 ATP synthase function requires the ability of the central stalk to rotate freely while making specific interactions within the catalytic

hexamer, this mechanism is highly unlikely. If the latter situation were true, distortion would be limited to the *b* dimer and the flexible stalk hypothesis would hold true. This could occur by straightening or increasing the naturally occurring 20º bend in the shortened or lengthened peripheral stalk, respectively, or by stretching or compressing the secondary structure in the *b* dimer. The use of FRET will provide evidence as to which of the hypotheses is true.

One major limitation plagued this line of research. F_1F_0 ATP synthase is incorporated with a homodimer of *b* subunits, hence two *b* subunits, each with a reactive cysteine. Since FRET requires only one *b* subunit be labeled, a system necessarily had to be developed to allow purification of F_1F_0 ATP synthase complexes with two genetically different *b* subunits: one cysteine-less and one with a single cysteine. The system utilizes epitope tags placed on the *b* subunits and is discussed in detail in Chapter 2. Future FRET studies will use this epitope-tagged scheme in order to express F_1F_0 ATP synthase complexes with a *b* dimer containing only one cysteine.

CHAPTER 5
MUTAGENISIS OF THE AMINO AND CARBOXYL TERMINI OF THE *b* SUBUNIT IN F_1F_0 ATP SYNTHASE

Introduction

Two stalk structures have been shown to link the F_1 and F_0 sectors (11, 187). The central, or "rotary" stalk, extends within the $\alpha_3\beta_3$ hexamer. Protons diffuse through the membrane, via the *a* and *c* subunits of F_0, resulting in the rotation of the central stalk within the hexamer, ultimately generating ATP (4, 16, 189). The peripheral stalk, or "stator", is positioned to the side of the F_1F_0 ATP synthase complex and reaches from the periplasmic leaflet of the membrane up to near the top of F_1, in an α-helical highly extended conformation (12, 13, 166, 204, 294), where it makes contact with a single α subunit (100, 141-143). The primary function of the peripheral stalk is to prevent the rotation of the $\alpha_3\beta_3$ hexamer against the rotation of the central stalk.

The peripheral stalk consists of the δ subunit of F_1 and the *b* subunit dimer of F_0 (198, 288), which have been shown to be in direct contact with each other at their carboxyl termini (3, 4, 200, 219, 220). The *b* subunit dimer is the major component of the peripheral stalk, anchoring F_1 to the membrane. Despite attempts by several other laboratories, there is presently no high-resolution structure of the entire *b* subunit. Therefore, model polypeptides have been constructed in order to elucidate the structure of the *b* subunit by domain. Four domains comprise the *b* subunits: the amino terminal membrane-spanning, tether, dimerization and the carboxyl terminal δ-binding domains (Figure 5-1) (12, 13). A model polypeptide comparable to residues 1-34, which contains

the membrane-spanning domain, has been solved by nuclear magnetic resonance (NMR). The data revealed an α-helical monomeric structure with a 20º bend at residues 23-26 (136). A series of crosslinking studies led to a dimeric model in which the extreme

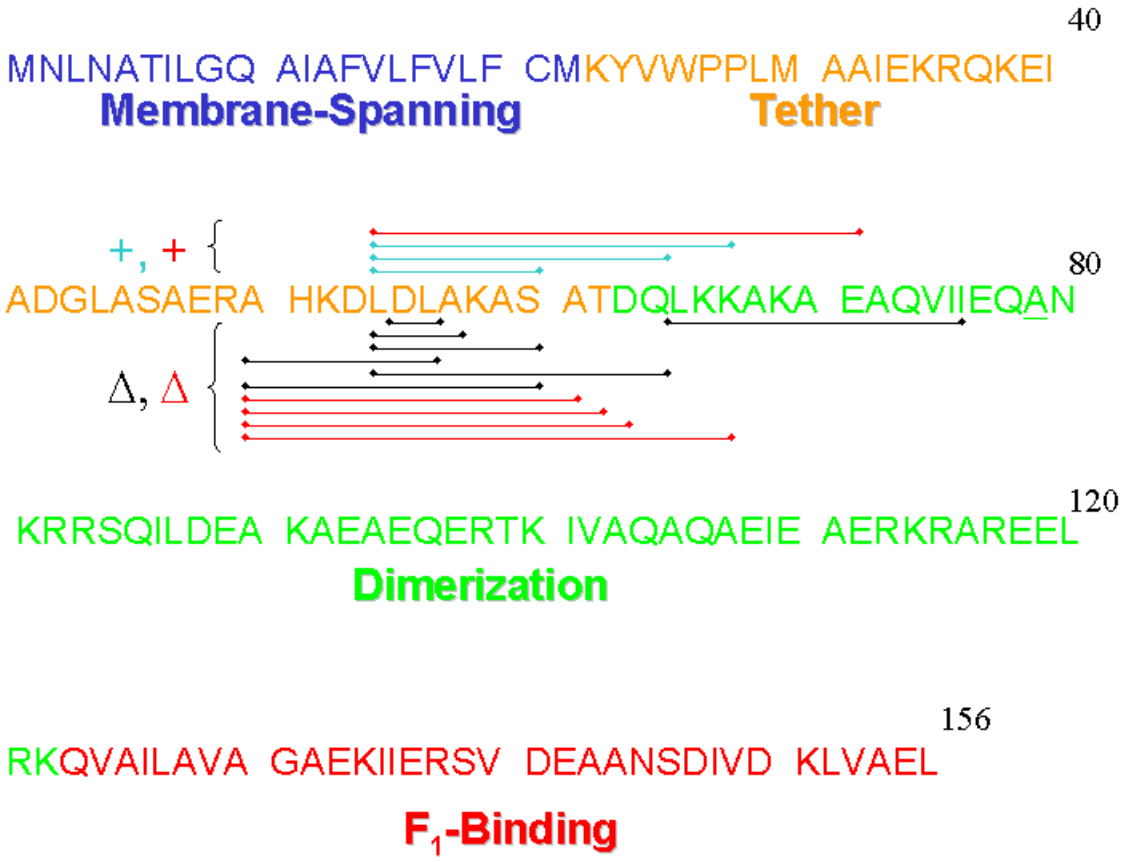

Figure 5-1 Amino acid sequence and domains of the *E. coli b* subunit. The *b* subunit is a 156 residue, 17,264 Dalton amphipathic polypeptide. Dunn and coworkers have defined four domains in the *b* subunit: the membrane spanning (blue), tether (orange), dimerization (green) and δ-binding domains (red). However, the boundaries of the dimerization domain are continually being refined. Dr. Paul Sorgen demonstrated that F_1F_0 ATP synthase could retain sufficient levels of activity upon relatively large deletions or insertions of up to eleven and fourteen amino acids, respectively, in the tether and beginning of the dimerization regions. The black lines indicate the amino acids deleted and the cyan indicates the amino acids duplicated that resulted in a functional F_1F_0 ATP synthase. Red lines indicate amino acids deleted (below sequence) or inserted (above sequence) that resulted in a loss of enzyme function.

amino-termini of the *b* subunits crossed each other in close proximity, the two *b* subunits then angled apart as they traverse the membrane towards the cytoplasmic side (136). The tether domain, contained within residues 23 and approximately 60, does not add significant stability to the dimerization of the *b* subunits and its role is the least distinct portion of the *b* subunit. This is the region of the *b* subunit that can be seen in electron micrographs (EM) of intact F_1F_0 ATP synthase complexes (11, 187). There is currently no high-resolution structure for this domain. The structural conformation of the tether domain is suggested to be that of an α-helical coiled-coil based on the heptad repeat which extends from the membrane surface to residue b_{Ala79} (138, 203). It has been shown by Dr. Paul Sorgen that F_1F_0 ATP synthase retains sufficient levels of activity upon relatively large deletions or insertions of up to eleven and fourteen amino acids, respectively, within the *b* subunit tether domain, suggesting that this domain contributes a significant degree of flexibility to the peripheral stalk (Figure 5-1) (193, 194). The dimerization domain is currently defined as residues 63-122 and is required for the *b* subunit to form a dimer. A crystal structure of a monomeric polypeptide, modeled from residues 62-122, has recently been solved and refined to 1.55 Å (138). Dunn and coworkers have constructed a model in which the two α-helices of the $b_{62\text{-}122}$ region form a right handed coiled coil. Finally, the carboxyl-terminal region, residues 123-156, forms the δ-binding domain. The extreme two to four amino acids of the carboxyl terminus are significantly important for the ability of the *b* subunit to form an interaction with the δ subunit. Deletion of these amino acids has been known to inhibit F_1F_0 ATP synthase function (205, 206).

This chapter focuses on the extreme amino and carboxyl termini of the *b* subunit. At the amino end, several mutational studies have been conducted in the membrane-spanning region; however, very few were known to produce a deficient F_1F_0 ATP synthase complex. A single amino acid mutation, $b_{gly9\rightarrow asp}$, has been suggested to have a strong negative influence proton conduction by the *a* and *c* subunits (209). A systematic mutational analysis of the membrane domain, performed by Andrew Hardy in our laboratory, supports the model predicted by Dmitriev *et al*. It appears the extreme amino termini of the *b* subunit dimer are in close contact with each other, accounting for most of the important *b*-*b* interactions in the membrane domain, and as the dimer traverses the membrane the two *b* subunits flares apart (202). Three amino acids that have been shown to exhibit the strongest crosslinking efficiency in the membrane-spanning domain were replaced with alanines ($b_{asn2\rightarrow ala,\ thr6\rightarrow ala,\ gln10\rightarrow ala}$), yielding a defecting F_1F_0 ATP synthase complex. Here, we demonstrate that mutation of only a single amino acid, at positions 2, 6 or 10, does not significantly affect the function of the enzyme.

Several insertions and deletions can be tolerated in the tether region of the *b* subunit dimer (Figure 5-1) (193, 194). Evidence that the *b* subunit may form specific interactions with an α subunit of F_1 suggested that length alterations may not be tolerated in regions of *b* running parallel to the F_1 αβ hexamer (198). Other members in our laboratory are currently studying a series of insertions and deletions throughout the dimerization and δ-binding domains. At the carboxyl terminal end of the *b* subunit, mutation of the last amino acid to a cysteine, $b_{leu156\rightarrow cys}$, and chemical crosslinking forms an uncoupled F_1F_0 ATP synthase complex (198). Furthermore, deletion of as few as two to four amino acids yields a completely defective enzyme (205, 206). However, an

insertion of amino acids had not been attempted. Here, we demonstrate that a four amino acid insertion at the *b* subunit carboxyl terminus does not affect the activity of the enzyme.

Materials and Methods

Many of the procedures utilized in Chapter 7 can be found in detail in the previous chapters. Many of the techniques, including recombinant DNA techniques, site directed mutagenesis, western blotting, as well as assays of protein concentration and F_1F_0 ATP synthase activity have been described in detail in Chapter 2.

Materials

Molecular biology enzymes and mutagenic oligonucleotides were obtained from Invitrogen (Carlsbad, CA), Life Technologies, Inc. (Grand Island, NY), New England Biolabs (Beverly, MA) and Stratagene (La Jolla, CA). Reagents were obtained from Sigma (St. Louis, MO), BioRad Laboratories (Hercules, CA) and Fisher Scientific (Pittsburgh, PA). Plasmid purification kits were acquired from Qiagen Inc. (Valencia, CA).

Strains and Media

The wild type *b* subunit expression plasmid, pKAM14, has been described previously (193, 194, 203). The plasmids encoding the *uncF*(*b*) gene were used to compliment *E. coli* strain KM2 (Δ*b*) carrying a chromosomal deletion of the gene (218). All strains were streaked onto plates containing Minimal A media supplemented with succinate (0.2% w/v), to determine enzyme viability. Cells harvested for membrane preparation were grown in Luria Broth supplemented with glucose (0.2% w/v) (LBG). Isopropyl-1-thio-β-D-galactopyranoside (IPTG)(40 μg/ml) and ampicillin (Ap)

(100μg/ml) were added to the media as needed. All cultures were incubated at 37˚C for the appropriate duration.

Recombinant DNA Techniques

Plasmid DNA was purified with the Qiagen Mini-Prep and Maxi-Prep kits. Restriction endonuclease digestions, ligations, and transformations were performed according to the recommendations of the manufacturers (New England Biolabs, Stratagene and Life Technologies, Inc.). Site-directed mutagenesis was performed either by means of a Stratagene Quikchange kit or by ligation-mediated mutagenesis. DNA fragments were separated in 0.8 % agarose gel by electrophoresis and purified using a Qiagen, Inc. QIAquick Gel Extraction kit. Plasmid sequences were determined by automated sequencing in the core facility of the University of Florida Interdisciplinary Center for Biotechnology Research (ICBR).

Mutagenesis and Strain Construction

Plasmid pKAM14 (*b*, Ap^r) (203) was used to construct all the *b* subunit mutants. The mutations were created in each of the plasmids using the Stratagene Quikchange kit.

Amino terminal mutations. An alanine scan at the amino terminus of the *b* subunit, producing $b_{asn2\rightarrow ala,\ thr6\rightarrow ala,\ gln10\rightarrow ala}$, was performed by Andrew Hardy, resulting in the expression of a defective F_1F_0 ATP synthase complex. Here, the individual sites were mutated, one at a time, to determine if the defect was the result of any particular amino acid. Sense and antisense mutagenic oligonucleotides were designed for each of the desired *b* subunit mutations (Appendix A) (Figure 5-2A). Three separate site-directed mutagenesis reactions were performed at codons 2, 6 and 10 of the *uncF*(*b*) gene in order to express mutant *b* subunits from plasmids pTAM43 ($b_{asn2\rightarrow ala}$), pTAM44 ($b_{thr6\rightarrow ala}$) and

Figure 5-2. Oligonucleotides for mutagenesis at the amino and carboxyl termini in the *unc* operon. Shown are the sense strands of the mutagenic primer pairs. The amino terminus mutations are depicted in orange and the carboxyl terminus insertion is shown in blue. Bold script indicates a change in nucleotide. Green and red indicate start and stop codons, respectively. Restriction enzyme sequences that were silently added are underlined. Mutations were introduced as described in the Materials and Methods. A) The *Dra*I, *Stu*I and *Mfe*I restriction sequences were added along with the $b_{asn2\rightarrow ala}$, $b_{thr6\rightarrow ala}$, and $b_{asn10\rightarrow ala}$, respectively, to facilitate screening. B) The codons expressing the last four amino acids of the *b* subunit (VAEL) were duplicated or deleted in order to insert or remove four amino acids at the extreme carboxyl terminus. The *Sac*I or *Hind*III restriction sequences were added, respectively, along with the mutations for screening purposes.

pTAM45 ($b_{gln10\rightarrow ala}$) (Table 5-1). The restriction enzyme sites recognized by *Dra*I, *Stu*I and *Mfe*I were silently added near the encoded $b_{asn2\rightarrow ala}$, $b_{thr6\rightarrow ala}$ and $b_{gln10\rightarrow ala}$ mutations (Figure 5-2A), respectively, for an initial detection of mutations, and then the nucleotide sequence was subsequently confirmed by automated sequencing in the ICBR core facility. The recombinant mutant *b* subunits included the ampicillin resistance gene and the pUC18 origin of replication.

Carboxyl terminal mutation. The *b* subunit dimer can tolerate relatively large insertions and deletions in the tether region (193, 194). Insertions have been generated throughout the dimerization and δ-binding domains, and the corresponding deletions are currently under construction by other members of the laboratory. Here, a four amino acid carboxyl-terminal truncation was accomplished by deletion of the final four codons of the *uncF*(*b*) gene to express $b_{\Delta 153\rightarrow end}$ from plasmid pTAM51 (Figure 5-2B). Likewise, a four amino acid insertion was constructed by duplication of the final four codons of the *uncF*(*b*) gene to express $b_{+153\text{-}156}$ (Figure 5-2B). The restriction endonuclease recognition sequence for *Hind*III or *Sac*I, respectively, was constructed near the deleted sequence for an initial detection of the truncation and deletion, and then the nucleotide sequence was later established by automated sequencing in the ICBR core facility (Figure 5-2B). The recombinant lengthened *b* subunit included the pUC18 origin of replication and conferred ampicillin resistance.

Crude Preparative Procedures

Inverted membrane vesicles from KM2 (Δ*b*) or 1100ΔBC (Δαβγδε*abc*) strains expressing the desired cysteine mutations were prepared essentially as described in Chapter 2 (194). Bacteria were grown in 500 mL LBG supplemented with the

appropriate antibiotic, harvested, and passed through a French Pressure Cell one time at 14,000 psi. Membranes were then collected by differential centrifugation. Protein concentrations were determined by the bicinchoninic acid (BCA) assay (286).

Assays of F_1F_0 ATP Synthase Activity

Growth on a minimal succinate medium was used as an initial, *in vivo*, assay for enzyme viability. ATP hydrolysis activity was assayed by the acid molybdate method (146). Membranes were assayed in buffer (50 mM Tris-HCl, 1 mM MgCl2, pH9.1) to determine the linearity with respect to time and enzyme concentration. Membrane energization was detected by the fluorescence quenching of 9-amino-6-chloro-2-methoxyacridine (ACMA) (271).

Results

This chapter focuses on the extreme amino and carboxyl termini of the *b* subunit. Work accomplished at the amino terminal was an extension of studies accomplished by Andrew Hardy. Work accomplished at the carboxyl terminal end was a contribution to an insertion and deletion analysis, currently in progress, of the *b* subunit dimerization and δ-binding domains.

Amino Terminal Mutations

Mutations simultaneously effecting amino acids b_{asn2}, b_{thr6} and b_{gln10} produces a completely deficient F_1F_0 ATP synthase complex (202). To investigate the mutations individually, the sites were each mutated one by one and then the effects were studied.

Construction and growth characteristics of mutants

A previous analysis of F_1F_0 ATP synthase complexes incorporated with *b* subunits including three mutations at codons 2, 6 and 10 ($b_{asn2\rightarrow ala,\ thr6\rightarrow ala,\ gln10\rightarrow ala}$) found the

Table 5-1. Aerobic growth properties and membrane-associated ATP hydrolysis activity of mutants expressing uncF(b) mutations at the amino terminus

Strains	Description	Growth[1]	Activity[2]
KM2/pKAM14 (+)	b_{wt}, Ap^r	+++	1.46 ± 0.03
KM2/pBR322 (-)	Δ*b*, Ap^r	-	0.17 ± 0.02
KM2/pAWH24[3]	$b_{asn2\rightarrow ala,\ thr6\rightarrow ala,\ gln10\rightarrow ala}$, Ap^r	-	0.83 ± 0.09
KM2/pTAM43	$b_{asn2\rightarrow ala}$, Ap^r	+++	1.49 ± 0.09
KM2/pTAM44	$b_{thr6\rightarrow ala}$, Ap^r	+++	1.13 ± 0.07
KM2/pTAM45	$b_{gln10\rightarrow ala}$, Ap^r	+++	1.15 ± 0.04

[1] *E. coli* strains were grown aerobically on succinate minimal medium supplemented with 40 μM IPTG. Colony size was scored after 72-hr incubation at 37ºC as: +++, ≥ 1.0 mm; ++, 0.3-0.5 mm; +, ~0.1 mm; -, no growth.

[2] *E. coli* strains were grown in LBG supplemented with the appropriate antibiotics and 40 μM IPTG. ATPase activities were measured as described under "Materials and Methods." Units were calculated from the slope of the line based on three measurements with incubations for 12 minutes.

[3] Work accomplished by Andrew W. Hardy.

mutant to be completely defective; however, membrane-associated ATP hydrolysis activity and immunoblot analysis revealed that the triple mutant was forming intact F_1F_0 ATP synthase complexes, suggesting that the mutant was incapable of performing coupled proton translocation (202). As a result of these observations, the alanine substitutions were studied individually. The amino acids expressed by codons 2, 6 and 10 were individually mutated to express an alanine, resulting in plasmids pTAM43 ($b_{asn2\rightarrow ala}$), pTAM44 ($b_{thr6\rightarrow ala}$), and pTAM45 ($b_{gln10\rightarrow ala}$) (Table 5-1). The effects of the mutations were studied by the ability of the plasmids to compliment *E. coli* strain KM2 (Δ*b*) (218). Growth on succinate minimal media was used as an initial qualitative gauge of enzyme activity *in vivo* since *E. coli* strains lacking F_1F_0 ATP synthase cannot derive energy from nonfermentable sources. In each case, the strains expressing the different alanine substitutions grew comparably to the wild type strain (Table 5-1).

Effects of amino terminal mutations

Since F_1 has little affinity for the membrane in the absence of intact F_0, total membrane associated F_1-ATP hydrolysis activity was used as a test of F_1F_0 ATP synthase complex assembly. Under conditions of high pH, F_1 can be released from the influence of F_0 (146), so the amount of ATPase activity in the solution was used as a measure of the amount of intact enzyme complex located in the membrane vesicles. The $b_{asn2\rightarrow ala}$ substitution, expressed from KM2/pTAM43, had no effect on enzyme assembly (Table 5-1). The $b_{thr6\rightarrow ala}$ and $b_{gln10\rightarrow ala}$, expressed from KM2/pTAM44 and KM2/pTAM45, had a slight, but not vitally significant effect on enzyme assembly. Membranes with a $b_{thr6\rightarrow ala}$ or $b_{gln10\rightarrow ala}$ incorporated into the F_1F_0 ATP synthase complex had specific activities of about 77% of the wild type strain.

F_1F_0 ATP synthase-mediated ATP-driven proton pumping activity in membrane vesicles prepared from the mutants was used as an indication of coupled activity. Acidification of inverted membrane vesicles was examined by fluorescence of ACMA (Figure 5-3). The level of NADH-driven fluorescence quenching was monitored for all membrane preparations to demonstrate that the vesicles were intact and closed. The levels of NADH-driven fluorescence quenching were strong and directly comparable in every case (data not shown, for a representative figure, see Figure 2-10). Membranes isolated from cells expressing $b_{asn2\rightarrow ala}$, KM2/pTAM43, displayed an insignificant reduction, approximately 1.6 %, in coupled activity, correlating with the wild-type-like F_1-ATP hydrolysis activity (Figure 5-2 and Table 5-1). A larger reduction in coupled activity, of about 11%, was observed in membrane vesicles isolated from cells in which a $b_{the6\rightarrow ala}$ or $b_{gln10\rightarrow ala}$, expressed from KM2/pTAM44 or KM2/pTAM45, respectively, was

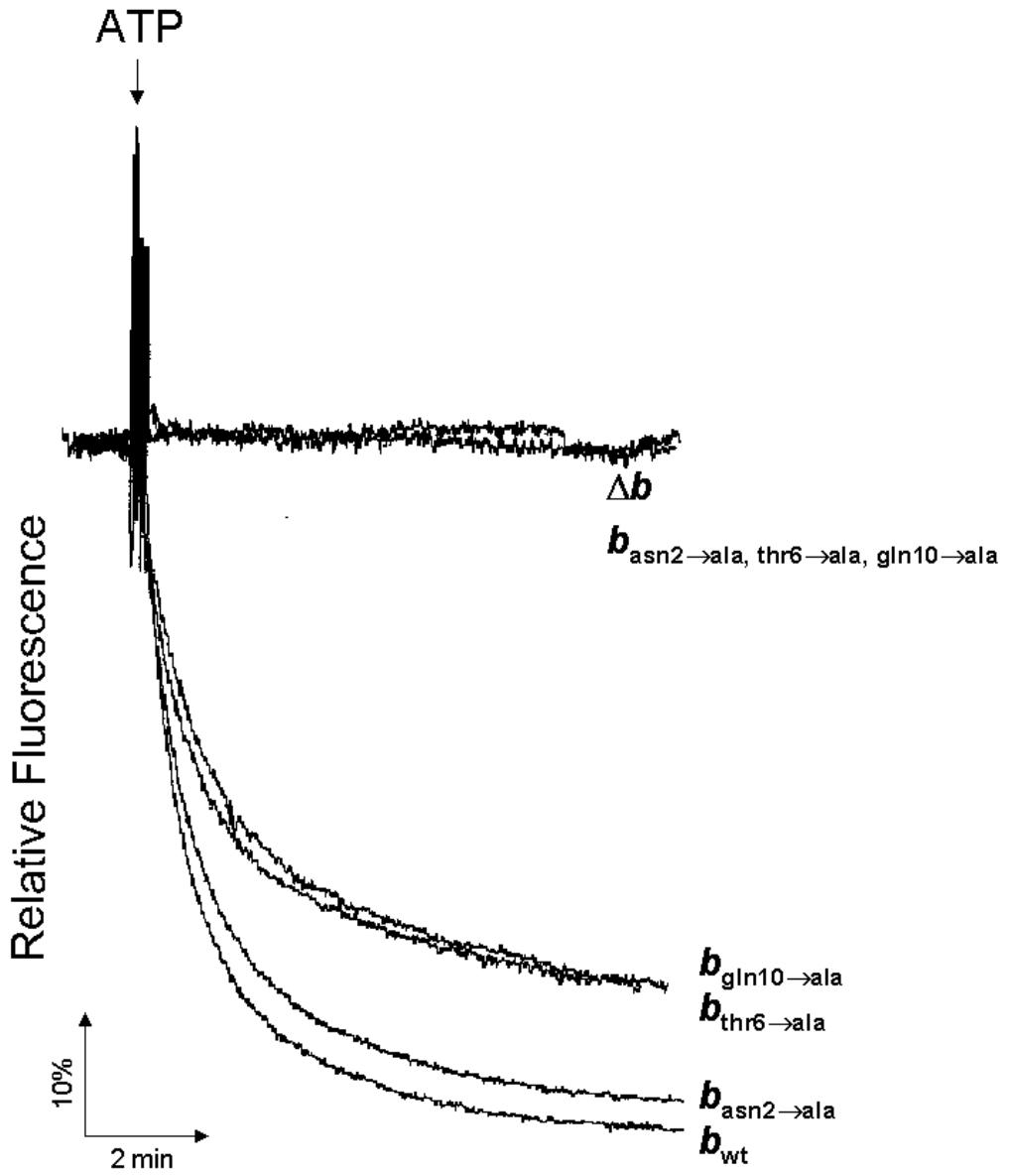

Figure 5-3. ATP-driven energization of membrane vesicles prepared from *b* subunit membrane domain mutants. Cell membrane vesicles were prepared by differential centrifugation (see Materials and Methods). Membrane protein (200 μg) was suspended in 3 mL of assay buffer (50 mM MOPS, 10 mM $MgCl_2$, pH 7.3). The fluorescent dye ACMA was added to a final concentration of 1 mM and fluorescence was recorded with excitation at 410 nm and emission at 490 nm. ATP was added as indicated to a final concentration of 1 mM. The samples for each trace have been labeled according to the mutation, so the strains used are as follows: Δ*b*, membranes from strain KM2/pBR322; b_{wt}, KM2/pKAM14; $b_{asn2\rightarrow ala,\ thr6\rightarrow ala,\ gln10\rightarrow ala}$, KM2/pAWH24; $b_{asn2\rightarrow ala}$, KM2/pTAM43; $b_{thr6\rightarrow ala}$, KM2/pTAM44; $b_{gln10\rightarrow ala}$, KM2/pTAM45.

incorporated into F_1F_0 ATP synthase (Figure 5-3). The decrease in coupled activity paralleled the reduction seen in F_1-ATP hydrolysis activity (Table 5-1).

Carboxyl Terminal Mutations

Since the original insertions and deletions constructed by Dr. Paul Sorgen in the in the tether region, a collaborative effort has been made by other members of the laboratory to study the remainder of the *b* subunit (Figure 5-4). Insertions and deletions constructed in a hydrophobic region of the *b* subunit in the F_1 binding domain , $b_{124\text{-}130}$, was accomplished by Dr. Deepa Bhatt. Four amino acid duplications, scattered throughout the dimerization and F_1 binding domains, were constructed by an undergraduate in the laboratory Stephanie Cole and the corresponding deletions are currently underway by another undergraduate, Megan Greenlee. Here, a four amino acid insertion and deletion was constructed at the extreme carboxyl terminus of the *b* subunit.

Construction and growth characteristics of mutants

The C-terminal region of the *b* dimer is in direct contact with the extreme C-terminal end of the δ subunit (3, 185, 200, 219, 220). Small deletions at the extreme C-terminal end of the *b* subunit had been shown to inhibit F_1F_0 ATP synthase function (206, 288). Two plasmids were generated to study the affects of deleting or duplicating the final four amino acids of the *b* subunit. Plasmids pTAM51 and pTAM52 were expressed in the *E. coli* KM2 (Δ*b*) cell line to express $b_{\Delta 153 \rightarrow end}$ or $b_{+153\text{-}156}$, respectively (Table 5-2). Since *E. coli* strains lacking functional F_1F_0 ATP synthase cannot derive energy from nonfermentable sources, growth on succinate minimal medium was used as an initial determination of enzyme activity *in vivo*. As expected, KM2 cells complemented with

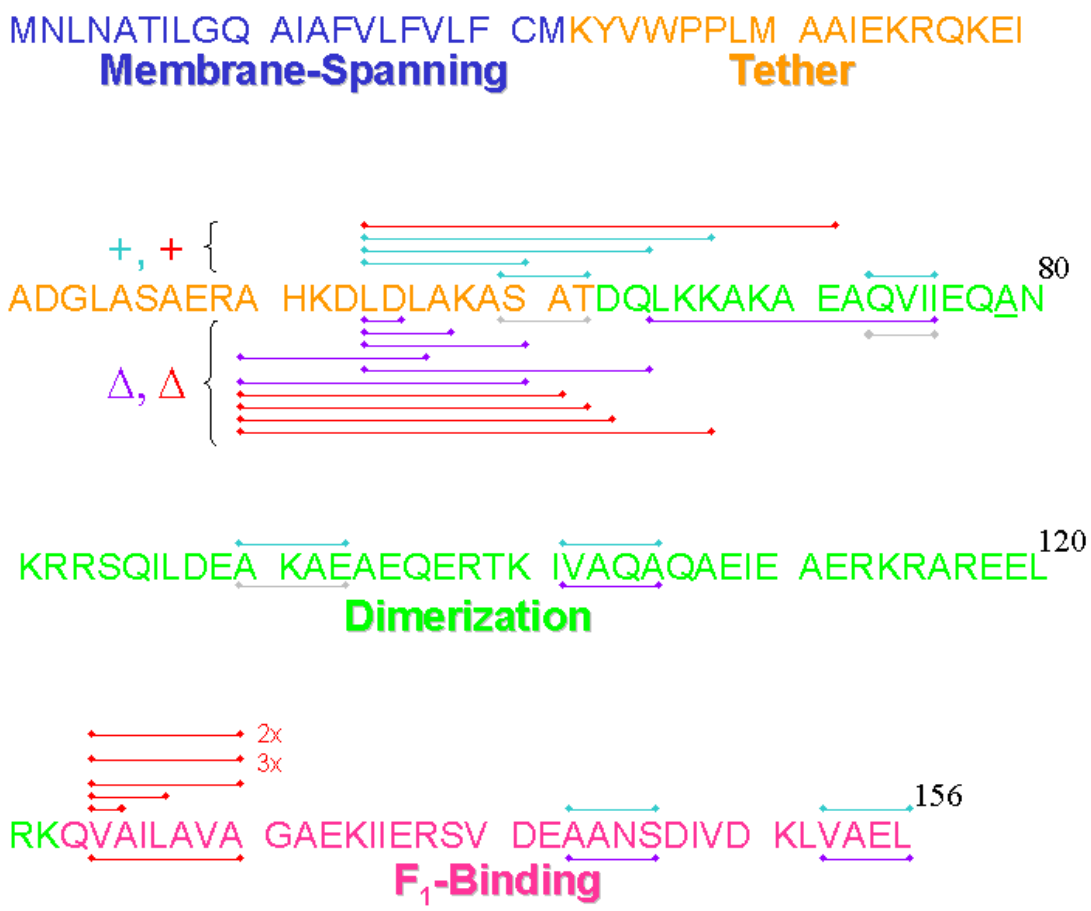

Figure 5-4. Amino acid insertion and deletion analysis of the *E. coli b* subunit. Dunn and coworkers have defined four domains in the *b* subunit: the membrane spanning (blue), tether (orange), dimerization (green) and δ-binding domains (pink). Dr. Paul Sorgen demonstrated that F_1F_0 ATP synthase could retain sufficient levels of activity upon relatively large deletions or insertions in the tether and beginning of the dimerization regions. An analysis of the remainder of the *b* subunit is currently underway. Lines drawn below the sequence correspond to deletions, lines drawn above the sequence correspond to a duplication (insertion). The purple lines indicate the amino acids deleted and the cyan indicates the amino acids duplicated that resulted in a functional F_1F_0 ATP synthase. Red lines indicate amino acids deleted (below sequence) or inserted (above sequence) that resulted in a loss of enzyme function. Grey lines indicate deletions that are currently under construction.

plasmid pTAM51 ($b_{\Delta 153 \rightarrow end}$) failed to grow on a succinate medium (Table 5-2). In contrast, the strain expressing $b_{+153\text{-}156}$, KM2/pTAM52, grew comparably to the wild type strain. Hence, even though deletion of only four amino acids affected the ability of the *b*

dimer to interact with the F_1 δ subunit, addition of four amino acids to the carboxyl terminus did not interfere with the interaction of the *b* and δ subunits.

Effects of carboxyl terminal mutation

Total membrane associated F_1-ATP hydrolysis activity was used as a test of F_1F_0 ATP synthase complex assembly (Table 5-2). As expected, membranes with enzyme complexes incorporated with $b_{\Delta 153 \rightarrow end}$ displayed a specific activity similar to the negative control, indicating virtually no interaction with F_1. On the other hand, membranes with

Table 5-2. Aerobic growth properties and membrane-associated ATP hydrolysis activity of mutants expressing *uncF*(*b*) insertions or deletions throughout the *b* subunit

Strains	Description	Growth[1]	% Activity[2]
KM2/pKAM14 (+)	b_{wt}, Ap^r	+++	100
KM2/pBR322 (-)	Δ*b*, Ap^r	-	13
KM2/pSC1[3]	$b_{+59\text{-}62}$, Ap^r	+++	82
KM2/pSC2[3]	$b_{+73\text{-}76}$, Ap^r	+++	89
KM2/pSC3[3]	$b_{+90\text{-}93}$, Ap^r	+++	103
KM2/pSC4[3]	$b_{+102\text{-}105}$, Ap^r	+++	90
KM2/pMMG2[4]	$b_{\Delta 102\text{-}105}$, Ap^r	+++	nd
KM2/pDB20[5]	$b_{\Delta 124\text{-}125}$, Ap^r	-	12
KM2/pDB21[5]	$b_{+124\text{-}125}$, Ap^r	-	19
KM2/pDB22[5]	$b_{+124\text{-}127}$, Ap^r	-	19
KM2/pDB23[5]	$b_{+124\text{-}130}$, Ap^r	(+)	21
KM2/pDB24[5]	$b_{2x(+124\text{-}125)}$, Ap^r	(+)	16
KM2/ pDB25[5]	$b_{3x(+124\text{-}125)}$, Ap^r	(+)	11
KM2/pSC5[3]	$b_{+143\text{-}146}$, Ap^r	+++	87
KM2/pMMG1[4]	$b_{\Delta 143\text{-}146}$, Ap^r	+++	nd
KM2/pTAM52	$b_{+153\text{-}156}$, Ap^r	+++	108
KM2/pTAM51	$b_{\Delta 153\text{-}156\text{-}his}$, Ap^r	-	12

[1] *E. coli* strains were grown aerobically on succinate minimal medium supplemented with 40 μM IPTG. Colony size was scored after 72-hr incubation at 37ºC as: +++, ≥ 1.0 mm; ++, 0.3-0.5 mm; +, ~0.1 mm; -, no growth; (+), sporadic colonies from reversions.

[2] *E. coli* strains were grown in LBG supplemented with the appropriate antibiotics and 40 μM IPTG. ATPase activities were measured as described under "Materials and Methods." Units were calculated from the slope of the line based on three measurements with incubations for 12 minutes. Value presented as percentage (%) of the wild type control (KM2/pKAM14).

[3] Work accomplished by Stephanie Cole.

[4] Work accomplished by Megan Greenlee.

[5] Work accomplished by Dr. Deepa Bhatt.

enzyme complexes incorporated with $b_{+153\text{-}156}$ displayed a specific activity similar to the wild type strain.

An indication of coupled activity was shown by F_1F_0 ATP synthase-mediated ATP-driven proton pumping activity in membrane vesicles prepared from the mutants (data not shown, work accomplished by Stephanie Cole). Membranes containing the $b_{\Delta 153 \rightarrow end}$ subunit exhibited no coupled activity as expected. Membranes isolated from cells expressing pTAM52 ($b_{+153\text{-}156}$) exhibited coupled activity comparable to the wild type strain. The levels of NADH-driven fluorescence quenching were strong and comparable in every case (data not shown). The coupled activities observed reflected the observations from the F_1-ATP hydrolysis activities (Table 5-2).

Discussion

In a collaborative effort, members of the laboratory have conducted an extensive mutational study of the entire length of the *b* subunit (Figure 5-5). At the amino terminal end of the *b* subunit, Andrew Hardy conducted a systematic mutational analysis of the membrane-spanning domain. His work established that there were specific sequence requirements in the *b* subunit membrane spanning domain and supported a model in which the extreme amino-termini of the two *b* subunits are in close contact with one another, accounting for most of the important *b*-*b* interactions in the membrane domain, and then flares apart as they cross the membrane (202). Here, an alanine scan was performed on three amino acids that had been shown to exhibit the strongest crosslinking efficiency in the membrane-spanning domain ($b_{asn2 \rightarrow ala,\ thr6 \rightarrow ala,\ gln10 \rightarrow ala}$), yielding a defecting yet intact F_1F_0 ATP synthase complex (202). It appears that there were adequate *b*-*b* interactions to support assembly of the enzyme, but the proton channel of F_0

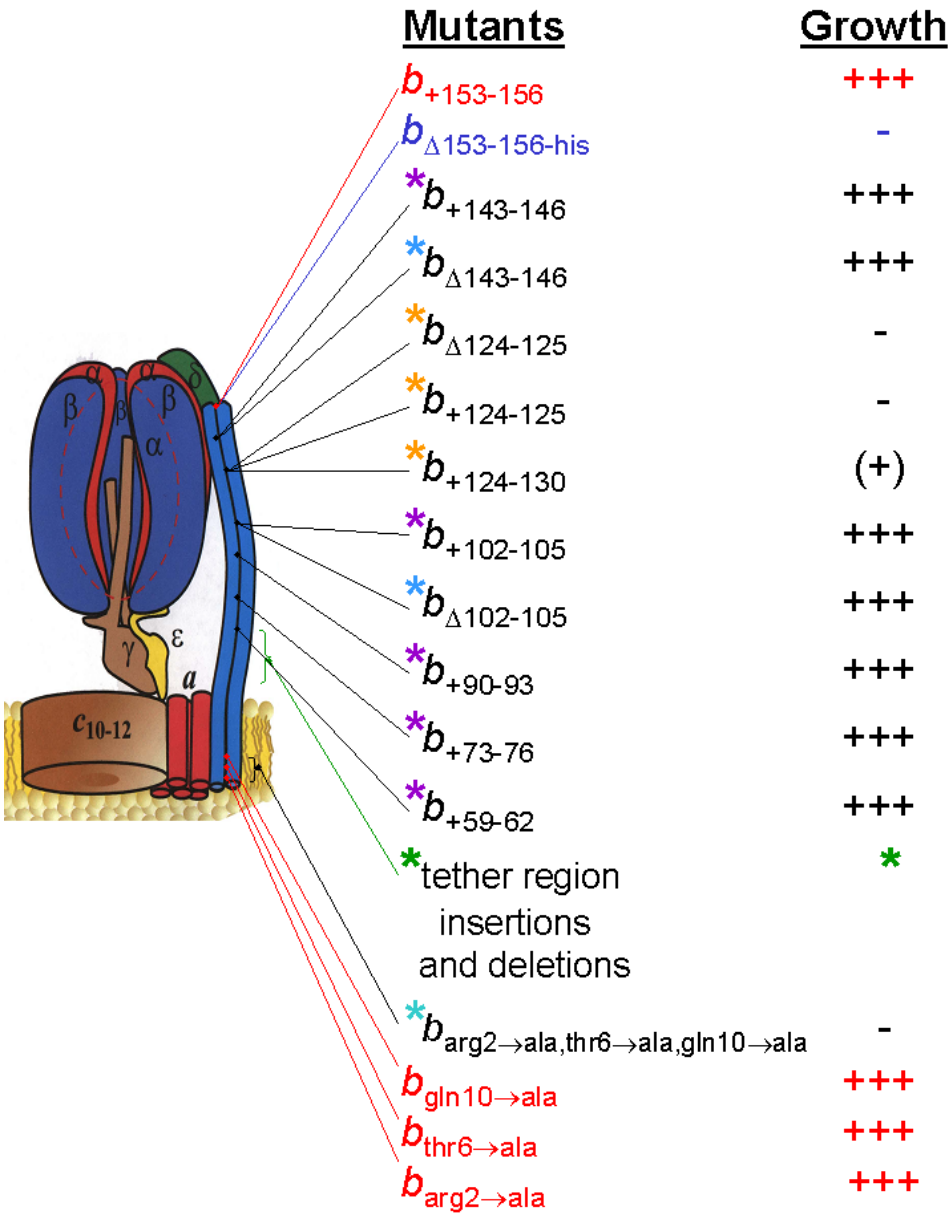

Figure 5-5. Mutations constructed throughout the *b* subunit. Shown are the approximate locations of the expressed *b* subunit mutants constructed and studied in our laboratory. Red indicates mutants constructed and studied in the present chapter. Shown in blue is the mutant created and studied in Chapter 3. The purple stars indicate mutants constructed and studied by Stephanie Cole. The blue stars indicate mutants constructed and studied by Megan Greenlee. The orange stars indicate a select few of the mutants constructed and studied by Dr. Deepa Bhatt. The green star designates the region of insertions and deletions studied by Dr. Paul Sorgen. The cyan star shows a mutant constructed and studied by Andrew Hardy. Growth indicates the ability of the strain to compliment the *E. coli* KM2 (Δ*b*) cell line and grow on minimal succinate media. Symbols are as follows: +++, colonies >1.5 mm; -, no growth; (+), sporatic colonies from reversions.

was not functional, suggesting that the *b* subunit membrane spanning domain may have a role in allowing the proton channel of the *a* and *c* subunits to align correctly (202). Here, we demonstrated that mutation of only a single amino acid, at positions 2, 6 or 10 ($b_{asn2\rightarrow ala,}$ $b_{thr6\rightarrow ala}$ or $b_{gln10\rightarrow ala}$), did not significantly affect the function of the enzyme. In fact, the minimal loss of enzyme activity associated from any of the single mutations did not nearly add up to the total defect of all three mutations combined. The results support the idea that although no single amino acid is necessary for the arrangement of a functional proton channel, several sites contribute synergistically to the formation of a functional F_1F_0 ATP synthase enzyme complex.

In the tether region of the *b* subunit, Dr. Paul Sorgen had constructed a series of insertions and deletions and observed that the altered *b* subunits were capable of forming the peripheral stalk of a functional F_1F_0 ATP synthase complex (193, 194). It was not known whether similar insertions or deletions could be accommodated in other regions of the *b* subunit where crucial interactions with F_1 subunits are believed to occur. Dr. Deepa Bhatt observed that neither insertions nor deletions were tolerated in a small stretch of hydrophobic amino acids found in the F_1 binding domain, $b_{124\rightarrow 130}$ (Figure 5-5). Four amino acid insertions, as well as the corresponding deletions, scattered throughout the remainder of the soluble portion of the *b* dimer were constructed by Stephanie Cole and Megan Greenlee and were found to result in a functional F_1F_0 ATP synthase complex (Figure 5-5). In the present chapter, we confirmed that a four amino acid truncation at the extreme carboxyl terminus of the *b* subunit ($b_{\Delta 153\rightarrow end}$) results in a partially assembled defective enzyme complex. However, duplication of the last four amino acids ($b_{+153\text{-}156}$) had no appreciable affect on enzyme assembly or function.

The research presented here suggests the importance of the extreme amino and caborxyl termini. Although it was believed that the dimerization domain provided the majority of the protein-protein interactions by allowing the formation of the *b* subunit dimer (12, 13), our studies indicated that other regions of the *b* subunit are required for normal assembly of a functional F_1F_0 ATP synthase complex due to contacts made with other subunits in the enzyme. Though the three amino acid substitutions at the amino terminus allowed dimerization and assembly of an intact F_1F_0 ATP synthase, it appears that it's sequence is crucial for the correct alignment of the proton channel formed by the *a* and *c* subunits. Likewise, the final four amino acids at the carboxyl terminus is not critical for the dimerization and partial assembly of the enzyme, however it is essential for the binding of F_1 due to it's contacts with the δ subunit.

CHAPTER 6
CONCLUSIONS AND FUTURE DIRECTIONS

Conclusions

The work presented in the preceding chapters had a considerable impact on the way the b_2 homodimer of the *E. coli* F_1F_0 ATP synthase is viewed and may provide some implications concerning the genetically dissimilar *b*-type subunit heterodimers found in higher organisms. A previous analysis of the *b* subunit performed in Dr. Cain's laboratory had suggested that the b_2 dimer has a flexible characteristic in its tether region (193, 194). A two plasmid expression system novel to the studies of the *E. coli b* subunit was developed in Chapter 2 in order to determine if the apparent flexibility extended to the dimerization of the *b* subunit. This work provided interesting information concerning the tether region of the peripheral stalk. The two plasmid expression system was also utilized in Chapter 3 to study the function of individual *b* subunits in the peripheral stalk by exploiting *b* subunits with known defective mutations. From this work, a model has been developed concerning the positioning of the two *b* subunits relative to the F_1F_0 ATP synthase complex and the intersubunit contacts made by the individual *b* subunits. On another note, Chapter 4 describes single cysteine substitutions that were generated in different length *b* subunits with the ultimate goal of studying the apparent flexibility of the b_2 dimer. And finally, Chapter 5 describes mutagenesis work performed on the extreme amino- and carboxyl-termini of the b_2 dimer in contribution to ongoing experiments performed by others in the laboratory. The following sections will summarize and discuss the implications of the results from Chapters 2, 3, 4 and 5 and

then discuss the future directions that will be taken as a direct result of the work accomplished in this dissertation.

Chapter 2: Integration of Unequal Length *b* Subunits into F_1F_0 ATP Synthase

The work presented in Chapter 2 stemmed from observations made by Dr. Paul Sorgen in our laboratory that *b* subunits with deletions of up to eleven amino acids and insertions of up to fourteen amino acids, corresponding to approximately 16 Å and 21 Å, respectively, formed intact and functional F_1F_0 ATP synthase complexes (193, 194). This work had suggested that the tether region of the *b* subunit possesses a certain degree of flexibility. However, it was not known whether this flexibility extended to the dimerization of two *b* subunits of unequal lengths and their incorporation into an enzyme complex. An experimental system was developed to allow expression of two different *b* subunit genes and determine whether the differing *b* subunits were assembled into an F_1F_0 ATP synthase complex. The experiments involved an epitope tag system that allowed us to determine if the different *b* subunits segregated into homodimers, or alternatively, if a heterodimer of long and short *b* subunits can be incorporated into an F_1F_0 ATP synthase complex. The histidine and V5 epitope tags introduced into the *b* subunits did not appreciably affect enzyme assembly or function. Expression of two different wild-type length *b* subunits led to three distinct F_1F_0 ATP synthase complexes in the same cell; 1) a homodimer of histidine-tagged *b* subunits, 2) a homodimer of V5-tagged *b* subunits and 3) a heterodimer consisting of a histidine-tagged *b* and a V5-tagged *b* subunit.

More importantly, three different F_1F_0 ATP synthase complexes were present even when the *b* subunits were not of identical length. We observed dimerization of *b*

subunits between $b_{+7\text{-his}}$ and both $b_{\text{wt-V5}}$ and $b_{\Delta 7\text{-V5}}$. This demonstrates that *b* subunits that differ in length by at least 14 amino acids can be incorporated into an enzyme complex. Given that the tether domain is likely an α–helix, the difference in length between the *b* subunits would be approximately 21 Å. Dimerization could occur in two ways. First, assuming that the transmembrane domains were in parallel, the hydrophilic domains could be out of register. Alternatively, we favor a conformation in which both the transmembrane domains and the dimerization domains as defined by Dunn and coworkers (13) exist in parallel. This would require that a section of the tether domain in the longer *b* subunit be out of contact with the shorter *b* subunit (Figure 2-14). It is likely that a parallel alignment of the dimerization domain is required for enzyme assembly. Recent electron microscopy and NMR studies have revealed a distinctive 20º bend in the *b* dimer within the tether domain (27, 136, 196). The research presented here suggests the possibility of straightening or further bending of the two *b* subunits within the peripheral stalk and lends support to the concept of a flexible peripheral stalk.

This raises the question, why should the tether domain be so flexible as to allow insertions, deletions and dimerization of *b* subunits of unequal lengths? If one views the peripheral stalk to be a rope-like structure linking F_1 to F_0, then its position holding F_1 against the rotation of the central stalk would not be expected to be the same for counterclockwise and clockwise rotation. Flexibility of the tether domain might facilitate reorienting the peripheral stalk to act as a stator for rotation in either direction during ATP synthesis and ATP hydrolysis (Figure 1-7).

The ability to generate and purify F_1F_0 complexes with two genetically different *b* subunits provides a potentially useful experimental tool. It is now feasible to specifically

label a single *b* subunit within a purified complex. This will facilitate biochemical modification experiments and the use of physical methods in future experiments.

Chapter 3: Genetic Complementation between Mutant *b* Subunits in F_1F_0 ATP synthase

The work documented in Chapter 3 directly stemmed from the experimental system developed in Chapter 2. Our ability to genetically express two different *b* subunits in the same cell and detect heterodimer formation provided us with the unique opportunity to study each of the *b* subunits in the peripheral stalk as an individual *b* subunit rather than a dimer forming a single entity. A major problem that had plagued all previous mutagenesis studies of the *b* subunit was that mutations constructed in the *uncF*(*b*) gene affected both subunits of the *b* homodimer. One missense mutation led to two amino acid replacements. However, the asymmetric nature of the F_1F_0 ATP synthase enzyme complex suggested that the functional role of each *b* subunit should not necessarily be considered equivalent. Protein-protein contacts made by one *b* subunit cannot be made by the other. The work presented Chapter 3 exploited three *b* subunit mutations that had already been characterized and shown to result in completely defective F_1F_0 ATP synthase complexes when expressed in both *b* subunits. An evolutionarily conserved arginine, b_{arg36}, located near the interface between the membrane and tether domains had been found to be crucial for F_1F_0 ATP synthase function (215). Enzyme complexes incorporated with a $b_{arg36\rightarrow ile\text{-}V5}$ or $b_{arg36\rightarrow glu\text{-}V5}$ were found to be intact yet functionally defective. Second, the C-terminal last four amino acids had been shown to be essential for the F_1 binding domain (206, 288). Enzyme complexes with a $b_{\Delta 153\rightarrow end\text{-}his}$ were found to be only partially assembled. Thirdly, insertions and deletions in a hydrophobic stretch of amino acids in the *b* subunit corresponding to residues $b_{124\text{-}130}$ (VAILAVA) resulted in

a complete loss of enzyme function. The *b* subunit dimer was not found in membranes when cells expressed only the $b_{+124\text{-}130}$ subunit. Heterodimerization was detected in cells expressing either *arg*36 mutation, $b_{arg36\rightarrow ile\text{-}V5}$ or $b_{arg36\rightarrow glu\text{-}V5}$, with $b_{wt\text{-}his}$, $b_{\Delta 153\rightarrow end\text{-}his}/b_{wt\text{-}V5}$ and $b_{+124\text{-}130\text{-}his}/b_{wt\text{-}V5}$ (Figure 3-10).

Dimerization was also observed in membrane preparations from cells expressing both $b_{\Delta 153\rightarrow end\text{-}his}/b_{arg36\rightarrow ile\text{-}V5}$ and $b_{\Delta 153\rightarrow end\text{-}his}/b_{arg36\rightarrow glu\text{-}V5}$. More importantly, enzyme complexes incorporated with the mutant heterodimers were functionally active, suggesting that each of the *b* subunits were complementing the other to form an intact and functional enzyme complex. This observation demonstrated unambiguously that F_1F_0 ATP synthase complexes containing *b* heterodimers were active and provided evidence that each of the individual *b* subunits provide specialized functions within the peripheral stalk. Clearly, each of the mutant *b* subunits compensates for what the other is lacking.

The work accomplished in this chapter raises a question concerning the relative positions of the individual *b* subunits of the peripheral stalk. In order for F_1F_0 ATP synthase containing the two different mutant *b* subunits to be intact and functional, it is likely that the $b_{arg36\rightarrow ile\text{-}V5}$ (or $b_{arg36\rightarrow glu\text{-}V5}$) subunit must be positioned such that its extreme C-terminus forms the appropriate contacts with the δ subunit of F_1. Similarly, the $b_{\Delta 153\rightarrow end\text{-}his}$ subunit must be positioned so that its b_{arg36} makes the appropriate contacts with the F_0 subunits (Figure 3-11). Incorrect positioning of the mutant *b* subunits during assembly might be expected to lead to an inactive or partially assembled enzyme complex. An answer to this question will be a goal discussed in “Future Directions”.

Chapter 4: Development of Cysteine Chemical Modifications of Altered *b* Subunits

The work described in Chapter 4 was performed in order to examine the nature of the apparent flexibility of the tether region. It has been shown by Dr. Paul Sorgen that an eleven amino acid deletion and a fourteen amino acid insertion in the the *b* subunit spanning the tether domain and the beginning of the dimerization domain was accommodated by the enzyme (Figure 4-5). Assuming α-helical structure, this 21 Å insertion and 16 Å deletion corresponds to well over a third of the length spanning from the top of the membrane to F_1, or right under a quarter of the length spanning towards the top of F_1. In contrast to the previously accepted role of the *b* subunit as a rigid "stator", these observations suggested that the role of the *b* dimer is more of a flexible or elastic structural feature during rotational catalysis. In Chapter 4, cysteine chemical modifications were created in the δ and *b* subunits to provide reactive thiols groups for future labeling and measurement studies. A set of twelve *unc* operon expression plasmids that encode amino acid substitutions were developed to void the F_1F_0 ATP synthase complex of all known reactive thiols as well as generate strategically placed cysteines. Cysteines were chosen because the thiol side chain is highly reactive and can be modified by maleimide reagents. The cysteine mutations did not affect enzyme assembly or function. Plasmids were designed to express a single cysteine at one of two locations in the δ subunit, δ_{cys64}or δ_{cys140}, as well as one position, either above or below the site of insertion or deletion in the *b* subunit, b_{cys84} or b_{cys43} (Figure 4-5). The idea for establishing a single reactive cysteine in both F_1 and F_0 is to use them as targets for labeling with fluorescence compounds (see "Future Directions"). One major limitation plagued this line of research. F_1F_0 ATP synthase is incorporated with a homodimer of *b*

subunits, hence two *b* subunits, each with a reactive cysteine. Since only one *b* subunit was desired to be labeled, a system necessarily had to be developed to allow purification of F_1F_0 ATP synthase complexes with two genetically different *b* subunits: one cysteine-less and one with a single cysteine. With the epitope-tag system developed in Chapter 2, this should not be a problem for future studies.

Chapter 5: Mutagenesis of the Amino and Carboxyl Termini of the *b* subunit in F_1F_0 ATP Synthase

In a collaborative effort, members of the laboratory have conducted an extensive mutational study of the entire length of the *b* subunit (Figure 5-5). The work illustrated in Chapter 5 was achieved in order to contribute to two other projects in the lab. The chapter focuses on the extreme amino- and carboxyl-termini of the *b* subunit. At the amino end, a systematic mutational analysis of the membrane domain was performed by Andrew Hardy in our laboratory. His work established that there were specific sequence requirements in the *b* subunit membrane spanning domain and supported a model in which the extreme amino-termini of the two *b* subunits are in close contact with one another, accounting for most of the important *b*-*b* interactions in the membrane domain, and then flares apart as they cross the membrane (202). Three amino acids that have been shown to exhibit the strongest crosslinking efficiency in the membrane-spanning domain were replaced with alanines ($b_{asn2\rightarrow ala,\ thr6\rightarrow ala,\ gln10\rightarrow ala}$), yielding a defecting F_1F_0 ATP synthase complex. It appeared that there were adequate *b*-*b* interactions to support assembly of the enzyme, but the proton channel of F_0 was not functional, suggesting that the *b* subunit membrane spanning domain may have a role in allowing the proton channel of the *a* and *c* subunits to align correctly (202). Work performed in contribution to this dissertation demonstrated that mutation of only a single amino acid, at positions 2, 6 or

10 ($b_{asn2\rightarrow ala,}$ $b_{thr6\rightarrow ala}$ or $b_{gln10\rightarrow ala}$), did not significantly affect the function of the enzyme. In fact, the minimal loss of enzyme activity associated from any of the single mutations did not nearly add up to the total defect of all three mutations combined. The results support the idea that although no single amino acid is necessary for the arrangement of a functional proton channel, several sites contribute synergistically to the formation of a functional F_1F_0 ATP synthase enzyme complex.

In the other line of research described in Chapter 5, mutations were constructed at the extreme carboxyl-terminus of the *b* subunit in contribution to an extensive insertion and deletion analysis. In the tether region of the *b* subunit, Dr. Paul Sorgen had constructed a series of insertions and deletions and observed that the altered *b* subunits were capable of forming the peripheral stalk of a functional F_1F_0 ATP synthase complex (193, 194). It was not known whether similar insertions or deletions could be accommodated in other regions of the *b* subunit where crucial interactions with F_1 subunits are believed to occur. Dr. Deepa Bhatt observed that neither insertions nor deletions were tolerated in a small stretch of hydrophobic amino acids found in the F_1 binding domain, $b_{124\rightarrow 130}$ (Figure 5-5). Four amino acid insertions, as well as the corresponding deletions, scattered throughout the remainder of the soluble portion of the *b* dimer were constructed by Stephanie Cole and Megan Greenlee and were found to result in a functional F_1F_0 ATP synthase complex (Figure 5-5). Work described in this dissertation confirmed that a four amino acid truncation at the extreme carboxyl terminus of the *b* subunit ($b_{\Delta 153\rightarrow end}$) results in a partially assembled defective enzyme complex. However, duplication of the last four amino acids ($b_{+153\text{-}156}$) had no appreciable affect on enzyme assembly or function.

The research presented here suggests the importance of the extreme amino and carboxyl termini. Although it was believed that the dimerization domain provided the majority of the protein-protein interactions by allowing the formation of the *b* subunit dimer (12, 13), our studies indicated that other regions of the *b* subunit are required for normal assembly of a functional F_1F_0 ATP synthase complex due to contacts made with other subunits in the enzyme. Though the three amino acid substitutions at the amino terminus allowed dimerization and assembly of an intact F_1F_0 ATP synthase, it appears that its sequence is crucial for the correct alignment of the proton channel formed by the *a* and *c* subunits. Likewise, the final four amino acids at the carboxyl terminus is not critical for the dimerization and partial assembly of the enzyme, however it is essential for the binding of F_1 due to its contacts with the δ subunit.

Future Directions

One of the major objectives for the field as a whole is to obtain a high-resolution structure of an intact F_1F_0 ATP synthase complex, or at least a complete F_0. The high resolution structure of F_1 confirmed many existing views and it was also a valuable tool used to assist a plethora of experimental planning that concerned F_1. We believe the same will hold true for F_0. A high-resolution structure will help to unveil many of the mysteries of F_0 such as proton translocation, and the mechanism in which the c_{10} ring rotates while the adjacent *a* and *b* subunits remain in place. Although the work illustrated in this dissertation has contributed a great deal of novel information concerning the *b* subunit of the *E. coli* F_1F_0 ATP synthase, it also left many open questions for future investigators. The following section discusses some of the future directions that directly resulted from work accomplished in this dissertation.

Complementing Mutant *b* Subunits

The data presented in Chapter 3 leads to the immediate question, do additional pairs of mutant *b* subunits exist that can mutually complement each other? The asymmetric nature of the F_1F_0 ATP synthase complex suggests that only one *b* subunit must make the appropriate contact within the enzyme. However, this trait may sometimes be restricted by the quaternary structure of the *b* subunit dimer. In other words, due to the coiled coil arrangement of the two *b* subunits, one region of a particular *b* subunit may make a contact near the amino terminal end and then that same *b* subunit may also align to make an additional important contact up towards the carboxyl terminal end. Pairs of plasmids encoding a mutant *unc*F(*b*) gene, which expresses a defective *b* subunit, are currently being cotransformed into KM2 (Δ*b*) cells and studied for their ability to grow on succinate. Since the expression system requires one plasmid to carry the ampicillin resistance gene and the second to carry the chloramphenicol resistance gene, an undergraduate in the laboratory, Stacia Howard, is currently cloning some of the other *unc*F(*b*) gene mutants in the laboratory's possession into chloramphenicol resistant plasmids. Table 6-1 describes preliminary evidence of ATP-driven proton pumping of various combinations of mutant *b* subunits. Indeed it appears that at least one pair of *b* mutants, $b_{N2A,\ T6A,\ Q10A}/b_{arg83\rightarrow pro}$, do not mutually suppress each other (Table 6-1). Furthermore, it appears that some of the complementing pairs have more activity than the other. Whether the apparent reduction in activity is due to a smaller percentage of heterodimeric F_1F_0 or whether the assembled heterodimeric species are still impaired will require purification of the heterodimeric complexes to homogeneity (described next).

Table 6-1. Preliminary data of coexpressed mutant *b* subunits.

	$b_{+124\text{-}130}$	$b_{\Delta 153 \rightarrow end}$	$b_{arg83 \rightarrow pro}$
$b_{arg36 \rightarrow ile}$	***	***	*
$b_{arg36 \rightarrow glu}$	***	***	***
$b_{N2A,\ T6A,\ Q10A}$	*	*	-
$b_{+124\text{-}125}$	nd	nd	***
$b_{+124\text{-}127}$	-	*	*
$b_{\Delta 124\text{-}127}$	-	*	nd
$b_{ala79 \rightarrow lys}$	***	***	***

Defective *b* subunits were coexpressed in the KM2 (Δb) cell line. Membrane preparation and preliminary ATP-driven proton pumping were accomplished as described in Chapter 2 "Materials and Methods". Symbols: ***, proton-pumping activity at least 20% of samples prepared from wild type strains; *, <10% activity; -, no activity; nd, no data.

Function of F_1F_0 ATP Synthase Incorporated with *b* Subunit Heterodimers

Work discussed in Chapters 2 and 3 have provided evidence that F_1F_0 ATP synthase complexes can be incorporated with *b* subunit heterodimers. Although it was unambiguously demonstrated that the heterodimeric F_1F_0 ATP synthase complexes were functional, a direct confirmation of activity will be pursued by performing activity assays on homogeneous enzyme preparations. These assays will also allow us to directly determine the activity of the complementing, double *b* subunit mutants (Chapter 3) relative to wild type F_1F_0 complexes. A detailed account of a developing protocol for purifying the F_1F_0 ATP synthase complexes with *b* subunit heterodimers can be found in Appendix B.

Positions of the Individual *b* Subunits in F_1F_0 ATP Synthase

The two *b* subunits of F_1F_0 ATP synthase have traditionally been viewed as a single functional entity. However, work described in Chapter 3 indicated that this may not be the case. F_1F_0 ATP synthase complexes incorporated with a heterodimeric *b* subunit in which each *b* subunit contains a defective mutation were functional. This observation suggested that the individual *b* subunits have specialized roles within the enzyme

complex. Furthermore, the asymmetric nature of the enzyme suggests that the two *b* subunits cannot participate in the exact same interactions. For example, the *b* subunit cannot have the same contacts with the single *a* in the membrane-spanning region and likewise with the δ subunit at the carboxyl-terminus. The unique experimental system described in Chapters 2 and 3 will be used to investigate the individual roles and positions of each *b* subunit. The experiments will heavily rely on the use of defective *b* subunits along with very efficient and well characterized chemical crosslinking techniques.

Length of the Peripheral Stalk in F_1F_0 ATP Synthase Complexes Incorporated with Shortened and Lengthened *b* Subunits

FRET. Relatively large insertions and deletions in the tether region of the *b* subunit were accommodated by the F_1F_0 ATP synthase complex and allowed retention of function (193, 194). Comparing the length of the wild type, shortened and lengthened peripheral stalks will give some insight on the overall possible conformation of the altered F_1F_0 ATP synthase complex. The F_1F_0 ATP synthase enzyme complex must, in some way, adapt to the shortened or lengthened *b* subunits. This can occur in at least one of two ways: i) distortion of F_1 to accommodate the change in length of the peripheral stalk or ii) distortion of the peripheral stalk itself. If the former was true, F_1 could become distorted by bending of the γε central stalk or compression of the $\alpha_3\beta_3$ hexamer and the rigid stalk hypothesis would gain favor. Since F_1F_0 ATP synthase function requires the ability of the central stalk to rotate freely while making specific interactions within the catalytic hexamer, this mechanism is highly unlikely. If the latter situation were true, distortion would be limited to the *b* dimer and the flexible stalk hypothesis would hold true. This could occur by straightening or increasing the naturally occurring

20º bend in the shortened or lengthened peripheral stalk, respectively, or by stretching or compressing the secondary structure in the *b* dimer. The use of fluorescence resonance energy transfer (FRET) will provide evidence as to which of the hypotheses is true.

The flexible stalk hypothesis suggests that the overall conformation of the F_1F_0 ATP synthase complex is maintained regardless of the alterations in the length of the *b* subunit and the changes in length are accommodated by changes in the tether region. If the flexible stalk hypothesis holds true, two predictions can be made based on the relative measured length of the shortened, lengthened and wild type length *b* subunits: i) the altered length of the tether region will not effect on the measured distance between a fixed site in F_1 and a site in the dimerization domain of the *b* subunit and ii) the distance between a fixed site in F_1 and a site below the tether region alteration will vary by only a few Å due to the bending or straightening of the tether region. On the other hand, if the rigid stalk hypothesis holds true a change in distance from a fixed site in F_1 and a site below the alteration would result in an approximately 16 Å difference between the wild type length *b* and $b_{\Delta 11}$.

The length of the peripheral stalks with altered length *b* subunits will be measured by FRET. FRET requires the introduction of single donor and acceptor fluorophores into a purified F_1F_0 ATP synthase complex. A common approach to performing FRET is to advantageously place a single cysteine at each end of the distance to be measured. Fluorescent maleimide derivatives are highly and specifically reactive with cysteine side chains. In order to perform FRET, single cysteines were strategically placed within the δ subunit of F_1 and *b* subunit of F_0. This work has been accomplished and is discussed in Chapter 4. These cysteines will be used to donor- and acceptor-label F_1 and F_0 with

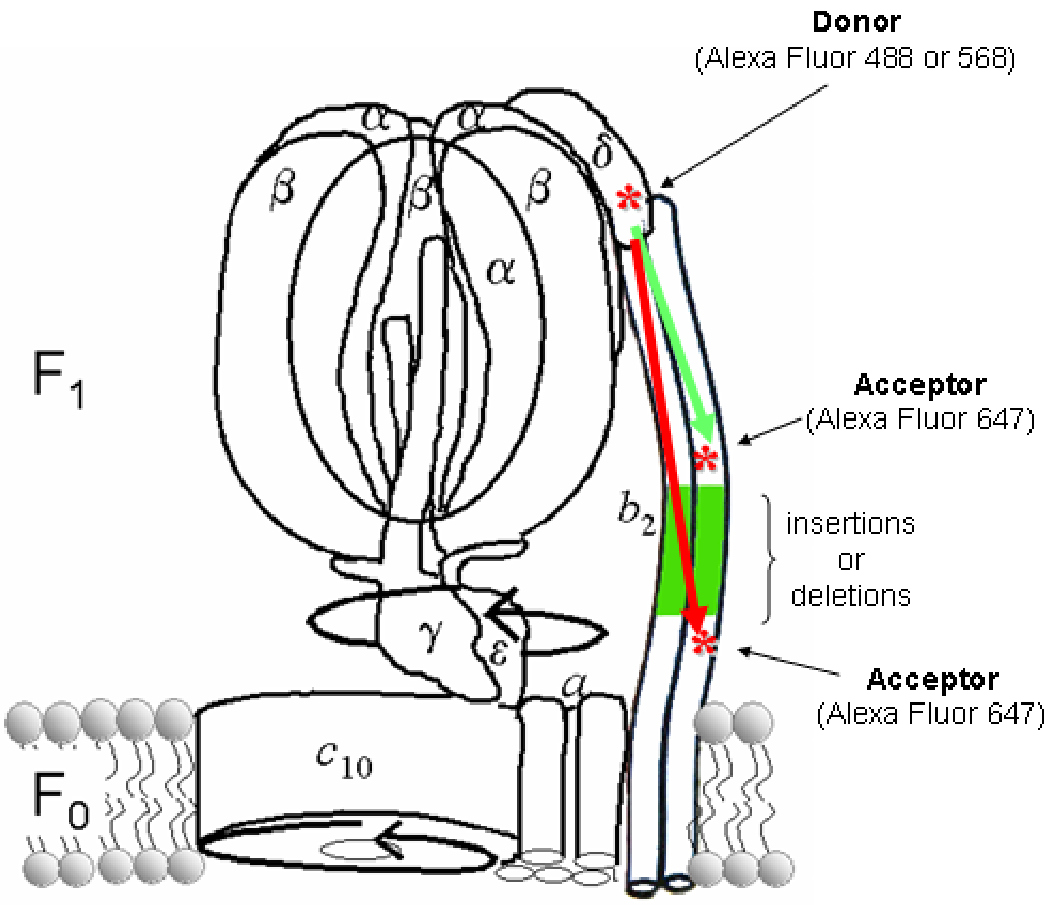

Figure 6-1. Design of FRET experiments to measure the peripheral stalk. The fluorophores will be added to the thiol side chains of the cysteines generated in Chapter 4. The stars indicate the approximate positions of the d_{cys140}, b_{cys84} and b_{cys43}. The green shaded area of the *b* subunit represents the location of the insertions or deletions.

maleimide reagents for the FRET studies (Figure 6-1). F_1 can readily be stripped from F_0, each cysteine labeled separately with a "donor" and "acceptor" fluorescent compound, and then stoichiometrically reconstituted under conditions of high ionic strength (203). With a single donor fluorophore positioned in the δ subunit and a single acceptor fluorescent compound located above or below the region of insertion or deletion in the tether domain of the *b* subunit, physical measurements can be calculated and compared (Figure 6-1).

One major limitation plagued this line of research. F_1F_0 ATP synthase is incorporated with a homodimer of *b* subunits, hence two *b* subunits, each with a reactive cysteine. Since FRET requires only one *b* subunit be labeled, a system necessarily had to be developed to allow purification of F_1F_0 ATP synthase complexes with two genetically different *b* subunits: one cysteine-less and one with a single cysteine. The system utilizes epitope tags placed on the *b* subunits and was discussed in detail in Chapter 2. Future FRET studies will use this epitope-tagged scheme in order to express F_1F_0 ATP synthase complexes with a *b* dimer containing only one cysteine.

Alternative approach. Another approach for the investigation of a potentially flexible peripheral stalk may also be attempted in future experiments. An innovative set of experiments conducted by members of the Dunn laboratory made use of different sized fluorescent proteins, ranging from the 12 kDa cytochrome b_{562} protein to the 30 kDa flavodoxin reductase protein with a 20 residue linker (100). The proteins were fused to the ε subunit of the central rotor stalk. If the fusion protein were small enough, one would expect the central stalk to rotate freely. If the fusion protein were too bulky, one could imagine that the protein would run into the peripheral stalk during rotational catalysis. As the fusion proteins became larger, an inhibition of activity resulted due to the bulky fluorescent protein running into the peripheral stalk during rotation. The growth curve of the bacteria was also monitored and revealed that the larger fusion proteins inhibited growth more than the smaller proteins. If this same technique were to be applied to F_1F_0 ATP synthases incorporated with $b_{\Delta 11}$ and compared to the activity of complexes incorporated with b_{+14}, conclusions could be made concerning the flexibility of the peripheral stalk. For example, if the 20° bend in the *b* subunit were straightened in

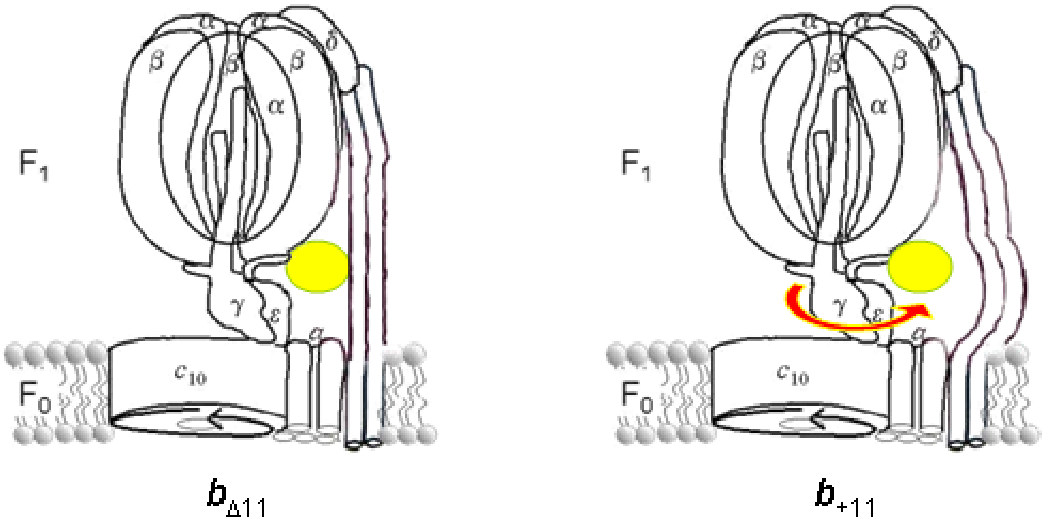

Figure 6-2. Model of rotation inhibition due to a fusion protein on the ε subunit. A natural 20° bend in the *b* subunit has been observed near the surface of the membrane (136). Shortening the *b* subunit by 11 amino acids (left panel) or lengthing by 14 amino acids(right panel) may be accompanied by the straightening or further bending, respectively, of this 20° bend. Genetic fusion proteins on the ε subunit have been described by Cipriano *et al.* (represented by the yellow oval) (100). The larger the fusion protein, the greater the inhibition of activity due to the inability of the central stalk to rotate during catalysis. We propose a model in which F_1F_0 ATP synthase complexes incorporated with shorten or lengthened *b* subunits may accommodate smaller or larger fusion proteins, respectively.

the shortened *b* subunit, inhibition of growth might become apparent with the smaller fusion proteins (Figure 6-2). Conversely, in complexes incorporated with the lengthened *b* subunit, the tether region may bend further, allowing the larger fusion proteins to pass between the central and peripheral stalks. Comparison of the growth properties of the two extreme tolerable lengths of the *b* subunit could lend support to the flexible stalk model.

Other Implications

How does the work presented in this dissertation affect the way in which the *b* subunit homologues of F_1F_0 ATP synthase are currently viewed? This work suggests that the importance of the *b* subunit dimer may be reflected in the fact that higher organisms

evolved to encode multiple *b* subunit equivalents. The *b* subunit is the least conserved subunit of F_1F_0 ATP synthase. In *E. coli*, the peripheral stalk of the F_1F_0 ATP synthase complex exists as a dimer of identical *b* subunits expressed from a single gene. However, the equivalent of the bacterial *b* subunit in photosynthetic bacteria and plants exists as two different subunits, referred to as *b* and *b'*, and the mammal counterpart exists as at least four subunits, expressed from two and four separate genes, respectively (Figure 1-8). The second non-identical *b*-type subunit found in photosynthetic organisms has been assumed to appear in order to gain additional functions in connection with photophosphorylation, though there is no direct evidence of this proposal (295, 296). Here, I would like to propose a different view concerning the multiple *b*-type subunit genes found in higher organisms. Work described in this dissertation suggested that the bacterial enzyme does not require two identical *b* subunits to form the dimer. Two different length *b* subunits, with a size difference of at least14 amino acids, were capable of forming the *b* dimer of an intact F_1F_0 ATP synthase complex. Interestingly, the *b* and *b'* subunits of photosynthetic organisms are rarely of equal length, with size differences ranging from about 4 to 40 amino acids due to extensions at either the amino- or carboxyl-termini or sometimes due to gaps found within the center of a *b* subunit. Also, in work presented in this dissertation, a defective mutation in one region of the *b* subunit has been shown to be overcome by dimer formation with a second *b* subunit that contained defective mutation in a different region but had a wild-type sequence in the region of the former defective *b* subunit. This observation has implications concerning the two individual *b* subunits in which each *b* subunit makes individual contacts within the enzyme complex. I believe the presence of the two *b* subunits are required for the

structural stability of the peripheral stalk. However, I would like to take this observation a step further and ask the following question: Why do bacteria encode only one *b* subunit gene, whereas higher organisms encode multiple *b*-type subunit genes, if single amino acid mutations are capable of destroying the enzyme function? One could speculate that bacteria do not require a functional F_1F_0 ATP synthase in order to survive. Though growth would be slow, bacteria can persist via glycolysis until environmental pressures either cause death, a reversion of the *unc*F(*b*) back to a wild-type gene, or a second site suppressor mutation. Higher organisms, on the other hand, do not have the luxury of solely surviving from glycolysis due to their higher energy needs. Selective pressures may have caused higher organisms to evolve to encode two different *b* subunit genes, where important amino acids may occur in only the *b* subunit or the *b'* subunit. This is reflected in my finding that the *b* or the *b'* subunits in plants have only about 15-20% identity with the *E. coli b* subunit, but the amino acids conserved in the chloroplast *b* and *b'* subunits generally occur at different residues, suggesting that the *b* dimer, as a whole, actually contains a larger number of conserved residues that are involved in making the functional contacts (Figure 6-3A, C). In fact, when the sequences of the *b* and *b'* sequences were manually merged together, such that identical or similar amino acids replaced the nonconserved residues, the percent identity and similarity of the fictional "merged" *b* subunit nearly doubled (Figure 6-3B, C). It appears the actual number of conserved residues is actually higher than believed to be, the difference being, the conserved residue need only to be in one or the other *b* subunit. This proposal may account for why the *b*-type subunits are the least conserved of all the F_1F_0 ATP synthase. If only one of the *b*-type subunits is required to make the appropriate contacts, mutations

occurring in the other *b*-type subunits of the organism would not have a dramatic affect on the enzyme function.

A

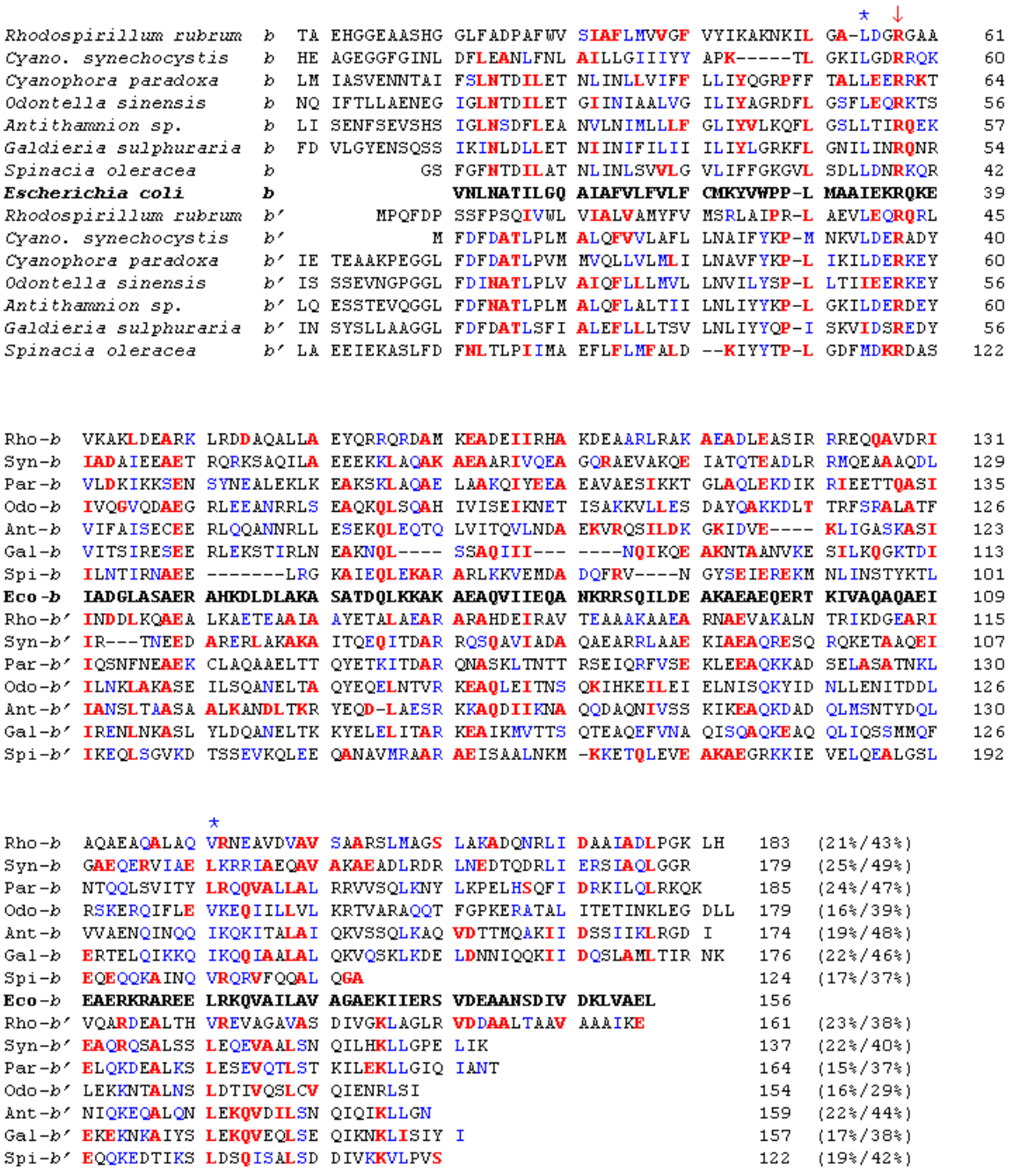

B

```
                                                 *         *              ↓↓     ** ↓*  ↓
Escherichia coli                b          VNLNATILGQ AIAFVLFVLF CMKYVWPPLM AAIEKRQKEI   40
Rhodospirillum rubrum  merged b's   FDP SSFPSQIVWL SIAFVMMVFF MSRLAIRPLL EALEQRQRLI   46
Cyano. synechocystis   merged b's   INL DDLDATLFNL AILFVIIIYY APKY--PPLG KALEERRKKI   61
Cyanophora paradoxa    merged b's   GGL FDLNATILVM MVQLLLLMLF LLAYFYKPLI KILDERKEYI   61
Odontella sinensis     merged b's   NEG IDLNATILET AIIFILALVG ILIYLYRPLG SFIEQRKTSI   57
Antithamnion sp.       merged b's   SHS IDLNATLLEA AVLFIMLLLF GLIYVYKPLG SLLDERQEKI   58
Galdieria sulphuraria  merged b's   QSS IDINATLLET AIIFILILII ILIYLYRPLG NILDNRQNRI   55
Spinacia oleracea      merged b's   LFD FNLTLPILMA EFLFVLFALD --KIYYTPLG DFMDKRKQSI  123

          *  ↓↓                  *↓ ***      *   *       *       * **         *
Eco-b  ADGLASAERA HKDLDLAKAS ATDQLKKAKA EAQVIIEQAN KRRSQILDEA KAEAEQERTK IVAQAQAEIE  110
Rho-b  NDDLKQAEAL KADTEAAIAA YETRLREARA RAHDIIRAAT EAAAKLAEKA EAEVEKALNR RIKQAEARIV  116
Syn-b  ADAIENAETA QRRLAQAKAE EEEQLAQAKA EAQRIIQEAG QRAERLKQEI AAEAERELRR MQEAAAQEIE  130
Par-b  QDNINEAEKS YAEAAELTTQ AETKLTQARQ NAKKITEQAR SEIQRIVSEK LAEAEKKADR ILAQATNKIE  131
Odo-b  VNGLADAEGR LEEANRRLAE AQKQLSQARI EAQLIINESI KAKKELLESD AYQAKKDLTT RFSRALATFR  127
Ant-b  ANALSAAEEA LKQADLRKLE SEDQLEQSQL KAQQIIKDAE KVRQSILDKG KIEAEKDRTK LISASKAQIV  124
Gal-b  IESLREAEER LEKSNIRLNE AKNQLKRARS EAQIIITTSQ TEANQIVNEA KSQAQKEKEQ ILKQSKTDIE  114
Spi-b  KEQLSNAEDT SSEVKQLEEQ ANEQLRKARA EIKAVLNKAN KKRTQLEVEA KAEGEKEIEV LLQEALGSLE  193

          *     * ***   * *                    *
Eco-b  AERKRAREEL RKQVAILAVA GAEKIIERSV DEAANSDIVD KLVAEL          156
Rho-b  QARDQALTQV REEAGAVAVS IAGKLMGLSV DDAALTALVD AAIAEL          161   (35%/61%)
Syn-b  AERERAIAEL KRRVAALAVA KAEADLRDRL NEDTQDRLIE RSIAQLGGR      179   (40%/64%)
Par-b  LQKDEALKSL RQQVAILSLK ILEKLLKIQI ANTLHSQFID RKILQL         184   (35%/65%)
Odo-b  SKERQIFLEV KEQIILLVLK RTVARAQQTF GPKERATALI TETINKLEG DLL  179   (23%/53%)
Ant-b  VQKEQANQQL KKQVTILAIQ KVSSQLKAQV DTTMQAKIID SSIIKLRGD I   174   (38%/69%)
Gal-b  RELKQAKKQL KKQVAILALQ KVQKLIKDEL DNNIQQKIID QSLAMLTIR NK  176   (35%/67%)
Spi-b  QEKEKAIKQL RQQVSALALD GAKKVLPVS                           122   (31%/57%)
```

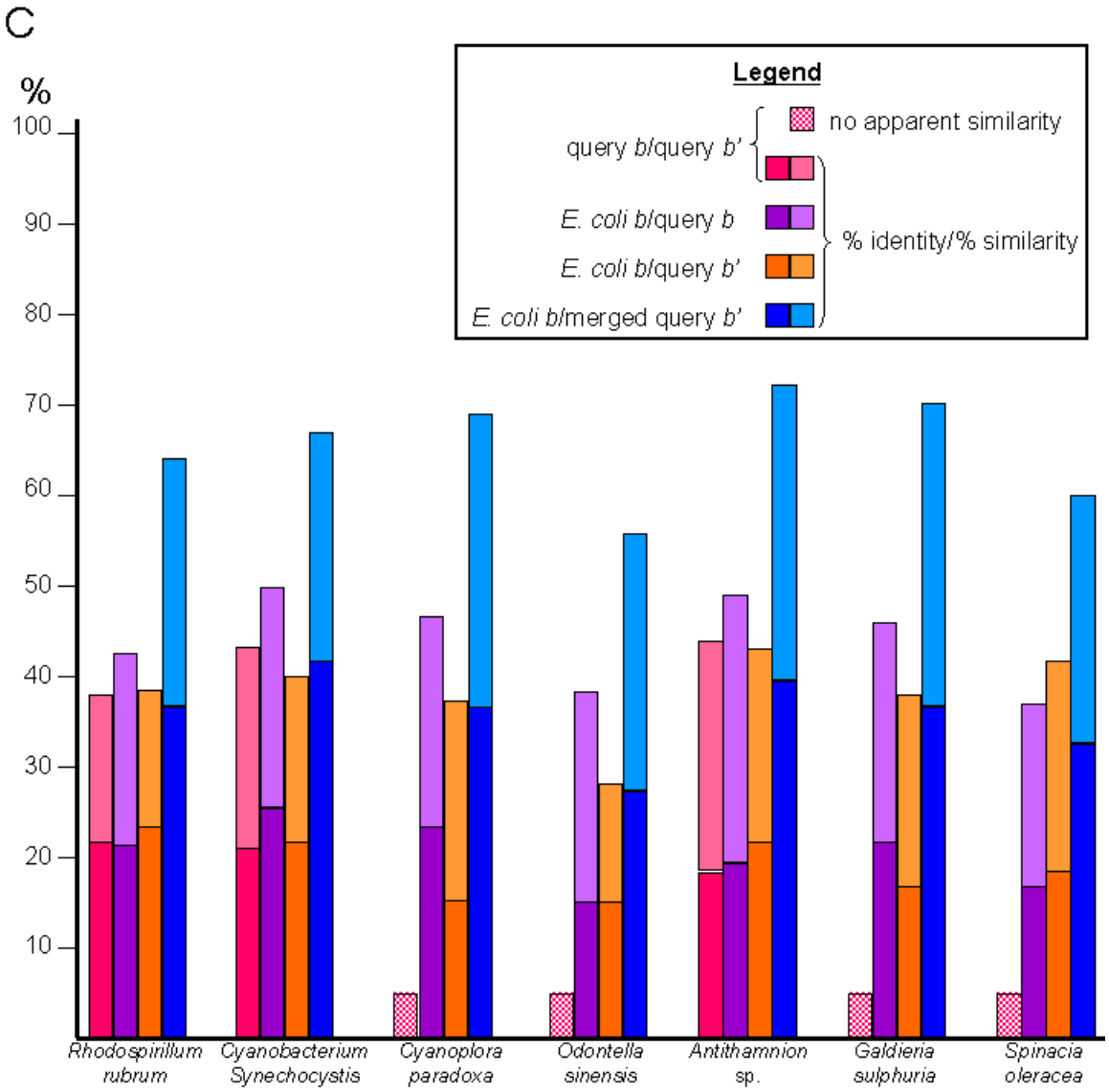

Figure 6-3. Sequence alignments of subunits *b* and *b'* from various species with the *b* subunit of *E. coli*. The *E. coli* sequence is entirely in bold script. The blue star indicates residues that are similar across all of the species. The red arrow indicates residues that are identical across all of the species. The hyphen indicates gaps. Sequences were randomly chosen from the National Center for Biotechnology Information (NCBI) database. Residues indicated in red bold script in the *b* and *b'* subunits of the various species are identical to the corresponding residue in the *E. coli b* subunit. Residues indicated in blue are similar to the *E. coli b* subunit. In parenthesis are the percent identity followed by the percent similarity. A) Sequence alignment of subunits *b* and *b'* of other species with the *b* subunit of *E. coli*. B) The *b* and *b'* subunits of each species were merged together so that the identical or most similar amino acid (relative to *E. coli*) replaced nonconserved amino acids. C) Graphical representation of sequence alignments.

APPENDIX A
MUTAGENIC OLIGONULCEOTIDES

Many of the mutations created during the course of this dissertation were via site-directed mutagenesis, performed either by means of a Stratagene Quikchange XL kit or by ligation-mediated mutagenesis. For the Quikchange XL procedure, oligonucleotides containing the desired mutation(s) were designed to anneal to the same sequence on opposite strands of the plasmid (sense and antisense primers). When possible, a silent mutation was encoded to add or delete a restriction endonuclease recognition sequence to allow for easy screening of the mutation. Primers were optimally designed by ensuring the mutation was in the middle of the sequence, a cytosine (C) or guanine (G) flanked both ends of the sequence, and the melting temperature (T_m) was greater than or equal to 78 ºC. The T_m was calculated as T_m=81.5+0.41(%GC)-675/N-%mismatch, where N was the primer length (bases). When introducing insertions or deletions, "%mismatch" was dropped from the formula. For a detailed description of the reaction, see Chatper 2 “Recombinant DNA Techniques” under “Materials and Methods”. The resulting plasmids that carried the desired mutation were then transformed into competent DH5α cells, purchased from Life Technologies, and grown on LBG plates supplemented with the appropriate antibiotic. Plasmids carrying the desired mutation(s) were screened for by restriction endonuclease analysis and then the nucleotide sequences were directly determined by automated sequencing in the core facility of the University of Florida Interdisciplinary Center for Biotechnology Research (ICBR). A description of the oligonucleotides follows. All oligonucleotides are listed in the 5’ to 3’ direction.

Table A-1. Oligonucleotide sequences.

Primer	Sequence
TB1	5’ ctaaatagaagcatgctgctgtgcaccaccaccaccaccacaatcttaacgcaacaatcctcggc 3’
TB2	5’ gccgaggattgttgcgttaagattgtggtggtggtggtggtgcacagcagcatgcttctatttag 3’
TB3	5’ ctaaatagaggcattgtgctatgtacccatatgacgtgccggactacgcgaatcttaacgcaacaatcctcggc
TB4	5’ gccgaggattgttgcgttaagattcgcgtagtccggcacgtcatatgggtacatagcacaatgcctctatttag
TB5	5’ ctgtaaggagggaggggcatgcgtctgaattttattacg 3’
TB6	5’ cgtaataaaattcagacgcatgcccctccctccttacag 3’
TB7	5’ ggagggaggggggaggctgctgtgc 3’
TB8	5’ gcacagcagcctccccctccctcc 3’
TB10	5’ cgtctgtcacgcaaagttaagctgaattcgaaaattgataagtctgtaatggcagg 3’
TB11	5’ cctgccattacggacttatcaattttcgaattcagcttaactttgcgtgacagacg 3’
TB12	5’ ctgttcgttctgttctccatgaagtacgtttggccgcc 3’
TB13	5’ ggcggccaaacgtacttcatggagaacagaacgaacag 3’
TB14	5’ gaaattgctgactgccttgcttccgcagaacgagcacataag 3’
TB15	5’ ccttatgggctcgttctgcggaagcaaggcagtcagcaatttc 3’
TB16	5’ gcgaacaaacgccgctgccagattctcgacgaagc 3’
TB17	5’ gcttcgtcgagaatctggcagcggcgtttgttcg 3’
TB18	5’ gccgagtcgtttatcgcagtttctggtgagcaactggac 3’
TB19	5’ ccagttgctcaccagaaaccgcgataaacgactc 3’
TB20	5’ ctgtacgtgatgttcgctgtcgc 3’
TB21	5’ gctcgcccctacgccaaagcagc 3’
TB23	5’ ggcatgaaagttaagtctactggccggatcctggaag 3’
TB24	5’ cttccaggatccggccagtagacttaactttcatgcc 3’
TB25	5’ ctgctgcgatggaaaaacgtctgtcac 3’
TB27	5’ gggaggggggaggcagatatgcaccaccacc 3’
TB28	5’ ggtggtggtgcatatctgcctccccctccc 3’
TB29	5’ gtcctgccagcgttctacactttggtg 3’
TB30	5’ gaggcattgtgctgtgtggccgccattaatggc 3’
TB31	5’ gccattaatggcggccacacagcacaatgcctc 3’
TB32	5’ gaggcattgtgctgtgcaccaccaccaccaccaccaccaccaccactggccgccattaatggc 3’
TB33	5’ gccattaatggcggccagtggtggtggtggtggtggtggtggtgcacagcacaatgcctc 3’
TB36	5’ ggagggaggggctgatgcaccaccac 3’
TB37	5’ gtggtgcatcagcccctccctcc 3’
TB38	5’ cgtggataaacttgtcgctgagctcggtaaaccgatcccgaacccg ctgctgggtctggactctacctaaggagggaggggctgatgtct 3’
TB39	5’catcagcccctccctccttaggtagagtccagacccagcagcgg gttcgggatcggtttaccgagctcagcgacaagtttatccacg 3’
TB40-	5’ catcgtggataagctttaaggagggaggggctg 3’
TB41-	5’ cagcccctccctccttaaagcttatccacgatg 3’
TB40+	5’ gataaacttgtcgctgaactggtcgctgagctctaaggagggaggg 3’
TB41+	5’ ccctccctccttagagctcagcgaccagttcagcgacaagtttatc 3’

Table A-2. Oligonucleotide description.

Primer	Conc.[1]	Sense[2]	Description	T_m[3]
TB1	0.892	S	addition of histidine-epitope tag (HHHHHH) to the N-terminus of the *b* subunit; +*Sph*I	85
TB2	0.606	A		
TB3	0.329	S	addition of HA-epitope tag (YPYDVPDYA) to the N-terminus of the *b* subunit; +*Nde*I	85
TB4	0.414	A		
TB5	2.846	S	addition of *Sph*I site 3' of the *b* subunit for cloning purposes; + *Sph*I	78
TB6	2.236	A		
TB7	1.951	S	mutation of *Sph*I site 3' of the *b* subunit and addition of a favorable "ATG" prior to next gene; -*Sph*I	78
TB8	1.593	A		
TB10	0.308	S	$\delta_{cys140\rightarrow ser}$ mutation; +*EcoR*I; -*Cla*I	80
TB11	0.650	A		
TB12	0.977	S	$b_{cys20\rightarrow ser}$ mutation; -*SnaB*I	79
TB13	1.538	A		
TB14	1.151	S	$b_{gly43\rightarrow cys}$ mutation; -*Bsp1285*I	77
TB15	1.446	A		
TB16	1.100	S	$b_{ser84\rightarrow cys}$ mutation; -*Xba*I	75
TB17	1.290	A		
TB18	1.366	S	$\delta_{cys64\rightarrow ser}$ mutation	82
TB19	1.242	A		
TB20	2.684	S	sequences *b* in the sense (not a good one)	75
TB21	2.422	S	sequences δ in the sense direction	81
TB23	1.380	S	$\alpha_{cys90\rightarrow ser}$ mutation; +*BamH*I	77
TB24	1.640	A		
TB25	5.016	S	sequences α in the sense direction	78
TB27	0.886	S	mutations to create Shine Delgarno sequence upstream of the 2nd *b* gene in "mix" plasmids	76
TB28	1.235	A		
TB29	5.279	A	sequences *b* in the inverse complement direction	79
TB30	4.334	S	deletion of residues 1-24 of *b* subunit to create "b_{sol}"	85
TB31	4.608	A		
TB32	8.301	S	addition of histidine-epitope tag (HHHHHHHHHH) to the N-terminus of the "b_{sol}" subunit	78
TB33	7.618	A		
TB36	0.439	S	mutations to create a better Shine Delgarno sequence upstream of the 2nd *b* gene in "mix" plasmids	78
TB37	0.477	A		
TB38	12.33	S	addition of V5-epitope tag (GKPIPNPLLGLDST) to the C-terminus of the *b* subunit; +*Sac*I	79
TB39	9.310	A		
TB40-	4.522	S	deletion of last 4 amino acids at the C-terminus of the *b* subunit; +*Hind*III	76
TB41-	4.891	A		
TB40+	1.109	S	duplication of last 4 amino acids at the C-terminus of the *b* subunit; +*Sac*I	78
TB41+	0.983	A		

[1] Concentration of stock oligonucleotide in μg/μl, stored in the -20°C.
[2] Direction of the primer: S, sense; A, antisense.
[3] Melting temperature in °C.

APPENDIX B
DEVELOPING PROTOCOL FOR PURIFYING F_1F_0 ATP SYNTHASE

Purification of Enzyme Complexes Incorporated with *b* Subunit Heterodimers

The purification procedure described below has been attempted one time; therefore a detailed account of the current protocol is given here. Once the particulars of the procedure are optimized, the same protocol will be applied to all the F_1F_0 ATP synthases incorporated with different combinations of heterodimeric mutant *b* subunits. For the sake of simplicity, the different *b* subunits are simply referred to as b_{V5} and b_{his}.

Culture

Inverted membrane vesicles from KM2(Δ*b*) strains expressing the desired *b* subunits will be prepared essentially as described previously and optimized for large-scale membrane preparations (199, 297). One of the advantages of studying a bacterial enzyme is the practically unlimited amount of bacteria that may be grown and harvested. The following can be scaled up or down to meet the experimental needs. The bacteria will grown by inoculating 20 mL starter culture, grown overnight, into a 2 L Erlenmeyer flask holding 1 L LBG supplemented with both ampicillin (Ap) (100 μg/mL) and chloramphenicol (Cm) (25 μg/mL). Similarly, 1 mL of the starter culture will be inoculated into a nephalo flask containing 50 mL LBG (Ap and/or Cm) to monitor growth. For the purposes of the large-scale purification, a total of 10 L LBG-Ap-Cm, contained in 10 flasks, will be grown. The bacteria will be grown at 37 ºC in a New Brunswick Scientific incubator shaker (220 rpm) and the turbidity monitered using a Klett-Summerson photoelectric colorimeter. IPTG (40 μM) will be added when the

turbidity reaches 75 Klett units and the cells will subsequently be collected when the turbidity reaches 150 Klett units. The bacteria will be harvested by centrifugation for 10 minutes at 8,000Xg in a Sorvall GSA rotor. The pellets will be rinsed once with TM buffer (50 mM tris-HCl, 10 mM $MgSO_4$, pH 7.5), weighed, and then stored at –20 ºC until the following day. Typically, a 10 L culture will yielded approximately 25 g bacteria.

Disruption of Bacteria

The 25 g frozen bacteria will be allowed to thaw at room temperature and resuspended in a final volume of 200 mL TM buffer. Resuspension requires rigorous vortexing, until the bacterial clumps dislodge from the walls of the bottles, and then continuously pipetted with a 25 mL pipette until no cell clumps are apparent. It is important to sufficiently break all clumps of bacteria in order to efficiently break open the cells. The bacteria will be treated with lysozyme in order to disrupt the bacterial cell wall. Prior to lysozyme treatment, the cells will be prepared by dissolving 0.91 g ethylenediamine tetra acetic acid (EDTA) in the suspension. The 200 mL bacterial suspension should be stirred with a magnetic stir bar at room temperature throughout the lysozyme treatment. 200 mL of 200 mM Tris-HCl, pH 7.5 and 1 M sucrose will be added and stirred for 3 minutes. Lysozyme (0.6 mg per g cells) will be added and stirred for 5 minutes. The bacterial cell walls may then be broken by osmotically shocking with 400 mL ddH_2O. The suspension will be stirred for an additional 5-10 minutes. Hereafter, all samples, reagents and equipment should be kept at 4 ºC unless otherwise specified. The bacteria will be harvested by centrifugation and the viscous supernatant may be discarded. The pellet will be resuspended in a final volume of 125 mL TM buffer by pipetting. Notably, in a trial attempt at purification, the bacterial pellet was extremely

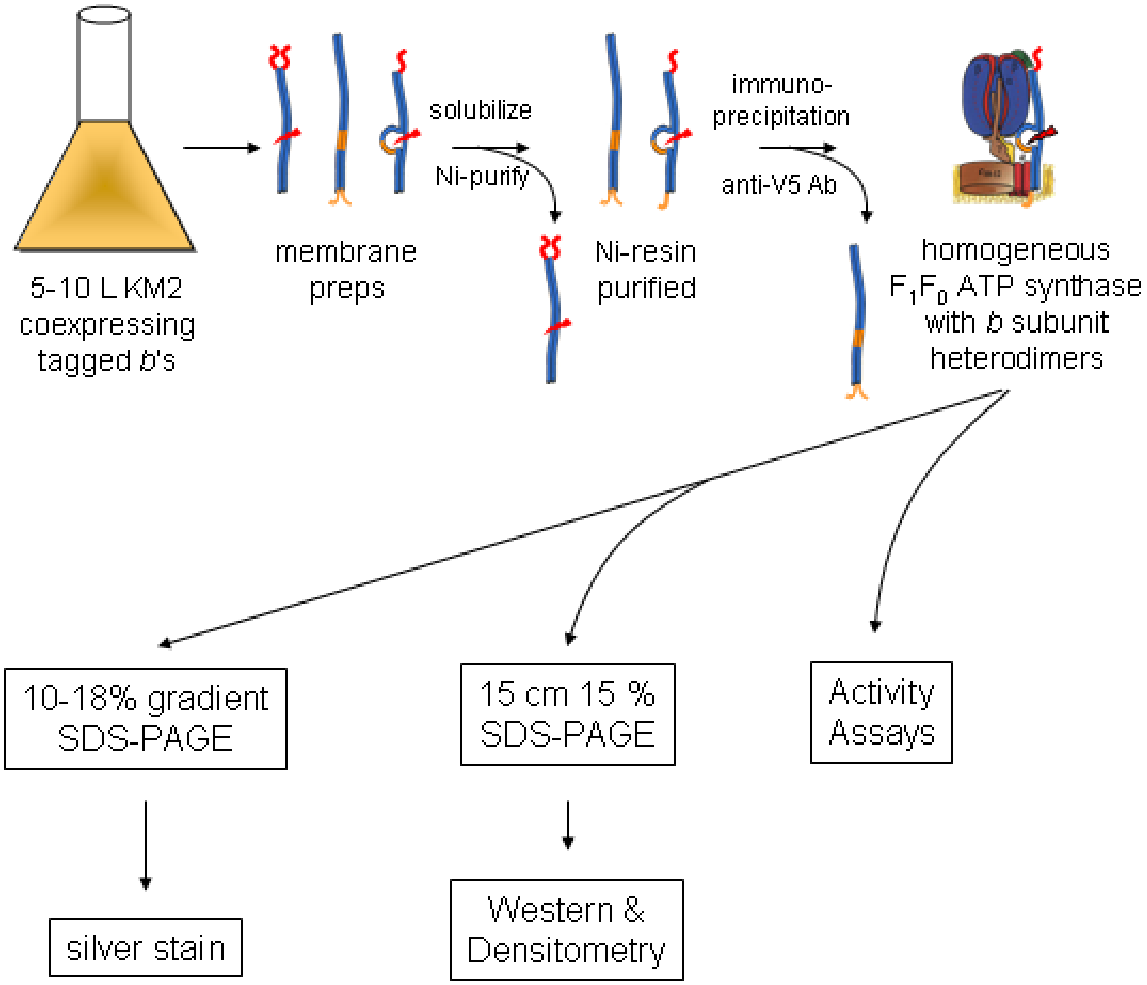

Figure B-1. Diagram of purification procedures for homogeneous heterodimeric b_{V5}/b_{his} F_1F_0 ATP synthase complexes. The *b* subunit dimers represents intact F_1F_0 ATP synthase. Basically, membrane preparations will be solubilized in 0.2% tegamineoxide WS-35. The solubilized proteins will then be Ni-resin purified in order to remove the homodimeric b_{V5}/b_{V5} F_1F_0 complexes. This will be followed by a V5 immunoprecipitation step to remove the homodimeric b_{his}/b_{his} F_1F_0 complexes, leaving only the heterodimeric b_{V5}/b_{his} complexes in solution. A battery of tests will then be run in order to determine the success of the purification procedures and then ultimately activity assays will be performed.

viscous and resuspension required about 30 minutes. DnaseI (10 mg/mL) will be added to help decrease the viscosity during resuspension. The bacteria will be broken by a single pass through the French Pressure Cell at 20,000 psi. Cellular debris and unbroken cells will be removed by centrifuging twice at 10,000Xg for 10 minutes each. Membranes will then be collected by ultracentrifugation at 150,000Xg in a Beckman 70.1 Ti rotor for 1.5 hours. The membranes pellets will be rinsed once with Tm buffer and then resuspended in a final volume of 30 mL Tm buffer using a 30 mL Wheaton tissue grinder. Total membrane protein concentration will be determined by the bicinchoninic acid (BCA) assay (Markwell et al., 1978).

Ni-Resin Purification

The crude membrane preparation described above will contain all membrane proteins, including homodimeric b_{V5}/b_{V5} F_1F_0 complexes, homodimeric b_{his}/b_{his} F_1F_0 complexes and heterodimeric b_{V5}/b_{his} F_1F_0 complexes (Figure B-1). The membrane preparation will be solubilized in 0.2% tegamineoxide WS-35 and then the homodimeric b_{his}/b_{his} F_1F_0 complexes and heterodimeric b_{V5}/b_{his} F_1F_0 complexes will be isolated using the Ni-CAM resin purification procedure (see Chapter 2 "Materials and Methods"). The homodimeric b_{V5}/b_{V5} F_1F_0 complexes will be eliminated at this step due to the lack of a histidine epitope tag. Preliminary experiments showed that Ni-CAM resin overloaded with membrane protein only produced the homodimeric b_{his}/b_{his} F_1F_0 complexes and the heterodimeric complexes were washed away. This can be explained by the fact that the heterodimeric b_{V5}/b_{his} complexes only contain one histidine epitope tag where the homodimeric b_{his}/b_{his} enzyme complexes are incorporated with two histidine epitope tags. Therefore, an optimization of the ratio of membrane protein to Ni-CAM resin will be

necessary. The optimized ratio will lie somewhere around 1.0 mg membrane protein to 0.2 mL packed Ni-CAM resin.

V5-Epitope Iimmunoprecipitation

The mixture of the homodimeric b_{his}/b_{his} F_1F_0 ATP synthase complexes and the heterodimeric b_{V5}/b_{his} F_1F_0 complexes will then be separated by a second epitope-mediated purification (Figure B-1). Immunoprecipitation of the heterodimeric b_{V5}/b_{his} F_1F_0 will be accomplished by immobilizing mouse monoclonal anti-V5 antibody (purchased from Invitrogen) on a resin using the Seize Primary Immunoprecipitation Kit (Purchased from Pierce Biotechnology). This kit has been successfully used several times by Dr. Michelle Gumz in our laboratory and consistently gave high yields of purified proteins.

Detection of Purified Enzyme Complexes

Once the purified heterodimeric b_{V5}/b_{his} F_1F_0 ATP synthase complexes are eluted from the V5-affinity resin, the eluant will be tested for the presence of intact and pure enzyme complexes (Figure B-1). The product will be ran on a 10-18% gradient SDS PAGE gel and then silver stained in order to examine the subunit content of the purified product. All eight subunits should be distinguishable in the stained gel, indicating the presence of intact F_1F_0 ATP synthase complexes. The homogeneity of the purified product will then be examined by immunoblot analysis. The b_{V5} and b_{his} were separable on a 15 cm 15% SDS PAGE gel when ran at 100 mamp, with current held constant, until the dye reached the stacker and then at 24 mamp for 12 hours (see Figure 2-13 for a representative figure). It was necessary to double the amperage when two gels were running at the same time. Upon transfer to a nitrocellulose membrane, immunoblot analysis using anti-*b* antibodies will be performed in order to determine if the

heterodimeric b_{V5}/b_{his} F_1F_0 has been purified to homogeneity. Densitometry will be used to determine the relative amounts of the b_{V5} and b_{his} subunits. If the product is indeed pure, the b_{V5} and b_{his} subunits should be present in a 1:1 ratio.

Assays of F_1F_0 ATP Synthase Activity

Once the purified heterodimeric b_{V5}/b_{his} F_1F_0 ATP synthase complexes are obtained, the battery of traditional activity assays will be performed. ATP hydrolysis assays will be performed by the standard procedure described in Chapter 2 ("Materials and Methods") in both the presence and absence of DCCD. ATP hydrolysis activity will be used both as an assay of yield of intact complexes and of functional coupling. DCCD is a *c* subunit specific inhibitor of F_1F_0 ATP hydrolysis; therefore, DCCD sensitivity can be used as an indication of functional coupling.

ATP-driven proton pumping assays will require reconstitution of the solubilized F_1F_0 ATP synthase into liposomes. This will be accomplished by a protocol described by Aggeler *et al.* (60) and modified by Dr. James Garder for use in our laboratory (167, 297). ATP-driven proton pumping will then be assayed by the standard method routinely used in the laboratory (Chapter 2, "Materials and Methods").

LIST OF REFERENCES

1. Mitchell P, Keilin's respiratory chain concept and its chemiosmotic consequences. *Science* 1979, 206(4423):1148-1159.

2. Mitchell P, Chemiosmotic coupling in oxidative and photosynthetic phosphorylation. *Biol Rev Camb Philos Soc* 1966, 41(3):445-502.

3. Senior AE, Nadanaciva S, Weber J, The molecular mechanism of ATP synthesis by F1F0-ATP synthase. *Biochim Biophys Acta* 2002, 1553(3):188-211.

4. Senior AE, Weber J, Happy motoring with ATP synthase. *Nat Struct Mol Biol* 2004, 11(2):110-112.

5. Nath S, The molecular mechanism of ATP synthesis by F1F0-ATP synthase: a scrutiny of the major possibilities. *Adv Biochem Eng Biotechnol* 2002, 74:65-98.

6. Fillingame RH, Divall S, Proton ATPases in bacteria: comparison to Escherichia coli F1F0 as the prototype. *Novartis Found Symp* 1999, 221:218-229; discussion 229-234.

7. Pedersen PL, Ko YH, Hong S, ATP synthases in the year 2000: evolving views about the structures of these remarkable enzyme complexes. *J Bioenerg Biomembr* 2000, 32(4):325-332.

8. Belogrudov GI, Tomich JM, Hatefi Y, Membrane topography and near-neighbor relationships of the mitochondrial ATP synthase subunits e, f, and g. *J Biol Chem* 1996, 271(34):20340-20345.

9. Devenish RJ, Prescott M, Roucou X, Nagley P, Insights into ATP synthase assembly and function through the molecular genetic manipulation of subunits of the yeast mitochondrial enzyme complex. *Biochim Biophys Acta* 2000, 1458(2-3):428-442.

10. Velours J, Paumard P, Soubannier V, Spannagel C, Vaillier J, Arselin G, Graves PV, Organisation of the yeast ATP synthase F(0):a study based on cysteine mutants, thiol modification and cross-linking reagents. *Biochim Biophys Acta* 2000, 1458(2-3):443-456.

11. Wilkens S, F1F0-ATP synthase-stalking mind and imagination. *J Bioenerg Biomembr* 2000, 32(4):333-339.

12. Dunn SD, McLachlin DT, Revington M, The second stalk of *Escherichia coli* ATP synthase. *Biochim Biophys Acta* 2000, 1458(2-3):356-363.

13. Dunn SD, Revington M, Cipriano DJ, Shilton BH, The b subunit of Escherichia coli ATP synthase. *J Bioenerg Biomembr* 2000, 32(4):347-355.

14. Fillingame RH, Jiang W, Dmitriev OY, Jones PC, Structural interpretations of F(0) rotary function in the Escherichia coli F(1)F(0) ATP synthase. *Biochim Biophys Acta* 2000, 1458(2-3):387-403.

15. Noji H, Yasuda R, Yoshida M, Kinosita K, Jr., Direct observation of the rotation of F_1-ATPase [see comments]. *Nature* 1997, 386(6622):299-302.

16. Noji H, Yoshida M, The rotary machine in the cell, ATP synthase. *J Biol Chem* 2001, 276(3):1665-1668.

17. Fernandez-Moran H, Cell-membrane ultrastructure. Low-temperature electron microsopy and x-ray diffraction studies of lipoprotein components in lamellar systems. *Circulation* 1962, 26:1039-1065.

18. Kagawa Y, Reconstitution of oxidative phosphorylation. *Biochim Biophys Acta* 1972, 265(3):297-338.

19. Catterall WA, Coty WA, Pedersen PL, Adenosine triphosphatase from rat liver mitochondria. 3. Subunit composition. *J Biol Chem* 1973, 248(21):7427-7431.

20. Abrahams JP, Leslie AG, Lutter R, Walker JE, Structure at 2.8 A resolution of F_1-ATPase from bovine heart mitochondria [see comments]. *Nature* 1994, 370(6491):621-628.

21. Bianchet MA, Hullihen J, Pedersen PL, Amzel LM, The 2.8-A structure of rat liver F_1-ATPase: configuration of a critical intermediate in ATP synthesis/hydrolysis. *Proc Natl Acad Sci U S A* 1998, 95(19):11065-11070.

22. Soper JW, Pedersen PL, Isolation of an oligomycin-sensitive ATPase complex from rat liver mitochondria. *Methods Enzymol* 1979, 55:328-333.

23. Boekema EJ, Berden JA, van Heel MG, Structure of mitochondrial F1-ATPase studied by electron microscopy and image processing. *Biochim Biophys Acta* 1986, 851(3):353-360.

24. Gogol EP, Lucken U, Capaldi RA, The stalk connecting the F1 and F0 domains of ATP synthase visualized by electron microscopy of unstained specimens. *FEBS Lett* 1987, 219(2):274-278.

25. Tsuprun VL, Orlova EV, Mesyanzhinova IV, Structure of the ATP-synthase studied by electron microscopy and image processing. *FEBS Lett* 1989, 244(2):279-282.

26. Bottcher B, Schwarz L, Graber P, Direct indication for the existence of a double stalk in CF0F1. *J Mol Biol* 1998, 281(5):757-762.

27. Wilkens S, Capaldi RA, Electron microscopic evidence of two stalks linking the F_1 and F_0 parts of the *Escherichia coli* ATP synthase. *Biochim Biophys Acta* 1998, 1365(1-2):93-97.

28. Wilkens S, Capaldi RA, Solution structure of the epsilon subunit of the F_1-ATPase from *Escherichia coli* and interactions of this subunit with beta subunits in the complex. *J Biol Chem* 1998, 273(41):26645-26651.

29. Karrasch S, Walker JE, Novel features in the structure of bovine ATP synthase. *J Mol Biol* 1999, 290(2):379-384.

30. Futai M, Noumi T, Maeda M, ATP synthase (H+-ATPase): results by combined biochemical and molecular biological approaches. *Annu Rev Biochem* 1989, 58:111-136.

31. Futai M, Noumi T, Maeda M, Molecular genetics of F1-ATPase from Escherichia coli. *J Bioenerg Biomembr* 1988, 20(1):41-58.

32. Weber J, Senior AE, Catalytic mechanism of F_1-ATPase. *Biochim Biophys Acta* 1997, 1319(1):19-58.

33. Senior AE, Catalytic sites of Escherichia coli F1-ATPase. *J Bioenerg Biomembr* 1992, 24(5):479-484.

34. Sato K, Mori H, Yoshida M, Mizushima S, Characterization of a potential catalytic residue, Asp-133, in the high affinity ATP-binding site of Escherichia coli SecA, translocation ATPase. *J Biol Chem* 1996, 271(29):17439-17444.

35. Weidenhaupt M, Bruckert F, Satre M, Identification of the Dictyostelium discoideum homolog of the N-ethylmaleimide-sensitive fusion protein. *Gene* 1998, 207(1):53-60.

36. Yu D, Weller SK, Herpes simplex virus type 1 cleavage and packaging proteins UL15 and UL28 are associated with B but not C capsids during packaging. *J Virol* 1998, 72(9):7428-7439.

37. Ovchinnikov Yu A, Luneva NM, Arystarkhova EA, Gevondyan NM, Arzamazova NM, Kozhich AT, Nesmeyanov VA, Modyanov NN, Topology of Na+,K+-ATPase. Identification of the extra- and intracellular hydrophilic loops of the catalytic subunit by specific antibodies. *FEBS Lett* 1988, 227(2):230-234.

38. Milburn MV, Tong L, deVos AM, Brunger A, Yamaizumi Z, Nishimura S, Kim SH, Molecular switch for signal transduction: structural differences between active and inactive forms of protooncogenic ras proteins. *Science* 1990, 247(4945):939-945.

39. Shen H, Yao BY, Mueller DM, Primary structural constraints of P-loop of mitochondrial F1-ATPase from yeast. *J Biol Chem* 1994, 269(13):9424-9428.

40. Story RM, Weber IT, Steitz TA, The structure of the E. coli recA protein monomer and polymer. *Nature* 1992, 355(6358):318-325.

41. Kjeldgaard M, Nissen P, Thirup S, Nyborg J, The crystal structure of elongation factor EF-Tu from Thermus aquaticus in the GTP conformation. *Structure* 1993, 1(1):35-50.

42. Noel JP, Hamm HE, Sigler PB, The 2.2 A crystal structure of transducin-alpha complexed with GTP gamma S. *Nature* 1993, 366(6456):654-663.

43. Aggeler R, Zhang YZ, Capaldi RA, Labeling of the ATP synthase of Escherichia coli from the head-group region of the lipid bilayer. *Biochemistry* 1987, 26(22):7107-7113.

44. Abrahams JP, Buchanan SK, Van Raaij MJ, Fearnley IM, Leslie AG, Walker JE, The structure of bovine F1-ATPase complexed with the peptide antibiotic efrapeptin. *Proc Natl Acad Sci U S A* 1996, 93(18):9420-9424.

45. van Raaij MJ, Abrahams JP, Leslie AG, Walker JE, The structure of bovine F1-ATPase complexed with the antibiotic inhibitor aurovertin B. *Proc Natl Acad Sci U S A* 1996, 93(14):6913-6917.

46. Orriss GL, Runswick MJ, Collinson IR, Miroux B, Fearnley IM, Skehel JM, Walker JE, The delta- and epsilon-subunits of bovine F1-ATPase interact to form a heterodimeric subcomplex. *Biochem J* 1996, 314 (Pt 2):695-700.

47. Braig K, Menz RI, Montgomery MG, Leslie AG, Walker JE, Structure of bovine mitochondrial F(1)-ATPase inhibited by Mg(2+) ADP and aluminium fluoride. *Structure Fold Des* 2000, 8(6):567-573.

48. Gibbons C, Montgomery MG, Leslie AG, Walker JE, The structure of the central stalk in bovine F(1)-ATPase at 2.4 A resolution. *Nat Struct Biol* 2000, 7(11):1055-1061.

49. Lobau S, Weber J, Senior AE, Nucleotide occupancy of F1-ATPase catalytic sites under crystallization conditions. *FEBS Lett* 1997, 404(1):15-18.

50. Menz RI, Walker JE, Leslie AG, Structure of bovine mitochondrial F(1)-ATPase with nucleotide bound to all three catalytic sites: implications for the mechanism of rotary catalysis. *Cell* 2001, 106(3):331-341.

51. Shirakihara Y, Leslie AG, Abrahams JP, Walker JE, Ueda T, Sekimoto Y, Kambara M, Saika K, Kagawa Y, Yoshida M, The crystal structure of the nucleotide-free alpha 3 beta 3 subcomplex of F1-ATPase from the thermophilic Bacillus PS3 is a symmetric trimer. *Structure* 1997, 5(6):825-836.

52. Hausrath AC, Gruber G, Matthews BW, Capaldi RA, Structural features of the gamma subunit of the Escherichia coli F(1) ATPase revealed by a 4.4-A resolution map obtained by x-ray crystallography. *Proc Natl Acad Sci U S A* 1999, 96(24):13697-13702.

53. Senior AE, ATP synthesis by oxidative phosphorylation. *Physiol Rev* 1988, 68(1):177-231.

54. Weber J, Senior AE, ATP synthase: what we know about ATP hydrolysis and what we do not know about ATP synthesis. *Biochim Biophys Acta* 2000, 1458(2-3):300-309.

55. Issartel JP, Dupuis A, Garin J, Lunardi J, Michel L, Vignais PV, The ATP synthase (F0-F1) complex in oxidative phosphorylation. *Experientia* 1992, 48(4):351-362.

56. Perlin DS, Latchney LR, Wise JG, Senior AE, Specificity of the proton adenosinetriphosphatase of Escherichia coli for adenine, guanine, and inosine nucleotides in catalysis and binding. *Biochemistry* 1984, 23(21):4998-5003.

57. Nakamoto RK, Ketchum CJ, al-Shawi MK, Rotational coupling in the F_0F_1 ATP synthase. *Annu Rev Biophys Biomol Struct* 1999, 28:205-234.

58. Stock D, Leslie AG, Walker JE, Molecular architecture of the rotary motor in ATP synthase [see comments]. *Science* 1999, 286(5445):1700-1705.

59. Capaldi RA, Schulenberg B, Murray J, Aggeler R, Cross-linking and electron microscopy studies of the structure and functioning of the Escherichia coli ATP synthase. *J Exp Biol* 2000, 203 Pt 1:29-33.

60. Aggeler R, Haughton MA, Capaldi RA, Disulfide bond formation between the COOH-terminal domain of the beta subunits and the gamma and epsilon subunits of the *Escherichia coli* F_1- ATPase. Structural implications and functional consequences. *J Biol Chem* 1995, 270(16):9185-9191.

61. Aggeler R, Capaldi RA, Nucleotide-dependent movement of the epsilon subunit between alpha and beta subunits in the *Escherichia coli* F_1F_0-type ATPase. *J Biol Chem* 1996, 271(23):13888-13891.

62. Sabbert D, Engelbrecht S, Junge W, Intersubunit rotation in active F-ATPase. *Nature* 1996, 381(6583):623-625.

63. Sabbert D, Engelbrecht S, Junge W, Functional and idling rotatory motion within F_1-ATPase. *Proc Natl Acad Sci U S A* 1997, 94(9):4401-4405.

64. Duncan TM, Bulygin VV, Zhou Y, Hutcheon ML, Cross RL, Rotation of subunits during catalysis by *Escherichia coli* F_1-ATPase. *Proc Natl Acad Sci U S A* 1995, 92(24):10964-10968.

65. Kato-Yamada Y, Noji H, Yasuda R, Kinosita K, Jr., Yoshida M, Direct observation of the rotation of epsilon subunit in F_1-ATPase. *J Biol Chem* 1998, 273(31):19375-19377.

66. Sambongi Y, Iko Y, Tanabe M, Omote H, Iwamoto-Kihara A, Ueda I, Yanagida T, Wada Y, Futai M, Mechanical rotation of the *c* subunit oligomer in ATP synthase (F_0F_1): direct observation [see comments]. *Science* 1999, 286(5445):1722-1724.

67. Panke O, Gumbiowski K, Junge W, Engelbrecht S, F-ATPase: specific observation of the rotating c subunit oligomer of EF(o)EF(1). *FEBS Lett* 2000, 472(1):34-38.

68. Itoh H, Takahashi A, Adachi K, Noji H, Yasuda R, Yoshida M, Kinosita K, Mechanically driven ATP synthesis by F1-ATPase. *Nature* 2004, 427(6973):465-468.

69. Wilkens S, Dahlquist FW, McIntosh LP, Donaldson LW, Capaldi RA, Structural features of the epsilon subunit of the *Escherichia coli* ATP synthase determined by NMR spectroscopy [see comments]. *Nat Struct Biol* 1995, 2(11):961-967.

70. Uhlin U, Cox GB, Guss JM, Crystal structure of the epsilon subunit of the proton-translocating ATP synthase from *Escherichia coli*. *Structure* 1997, 5(9):1219-1230.

71. Weiss MA, McCarty RE, Cross-linking within a subunit of coupling factor 1 increases the proton permeability of spinach chloroplast thylakoids. *J Biol Chem* 1977, 252(22):8007-8012.

72. Moroney JV, McCarty RE, Reversible uncoupling of photophosphorylation by a new bifunctional maleimide. *J Biol Chem* 1979, 254(18):8951-8955.

73. Moroney JV, Andreo CS, Vallejos RH, McCarty RE, Uncoupling and energy transfer inhibition of photophosphorylation by sulfhydryl reagents. *J Biol Chem* 1980, 255(14):6670-6674.

74. Aggeler R, Chicas-Cruz K, Cai SX, Keana JF, Capaldi RA, Introduction of reactive cysteine residues in the epsilon subunit of Escherichia coli F1 ATPase, modification of these sites with tetrafluorophenyl azide-maleimides, and examination of changes in the binding of the epsilon subunit when different nucleotides are in catalytic sites. *Biochemistry* 1992, 31(11):2956-2961.

75. Aggeler R, Capaldi RA, Cross-linking of the gamma subunit of the Escherichia coli ATPase (ECF1) via cysteines introduced by site-directed mutagenesis. *J Biol Chem* 1992, 267(30):21355-21359.

76. Aggeler R, Cai SX, Keana JF, Koike T, Capaldi RA, The gamma subunit of the Escherichia coli F1-ATPase can be cross-linked near the glycine-rich loop region

of a beta subunit when ADP + Mg2+ occupies catalytic sites but not when ATP + Mg2+ is bound. *J Biol Chem* 1993, 268(28):20831-20837.

77. Aggeler R, Capaldi RA, ATP hydrolysis-linked structural changes in the N-terminal part of the gamma subunit of Escherichia coli F1-ATPase examined by cross-linking studies. *J Biol Chem* 1993, 268(20):14576-14578.

78. Moroney JV, McCarty RE, Light-dependent cleavage of the gamma subunit of coupling factor 1 by trypsin causes activation of Mg2+-ATPase activity and uncoupling of photophosphorylation in spinach chloroplasts. *J Biol Chem* 1982, 257(10):5915-5920.

79. Turina P, Capaldi RA, ATP hydrolysis-driven structural changes in the gamma-subunit of Escherichia coli ATPase monitored by fluorescence from probes bound at introduced cysteine residues. *J Biol Chem* 1994, 269(18):13465-13471.

80. Gogol EP, Johnston E, Aggeler R, Capaldi RA, Ligand-dependent structural variations in Escherichia coli F1 ATPase revealed by cryoelectron microscopy. *Proc Natl Acad Sci U S A* 1990, 87(24):9585-9589.

81. Bullough DA, Ceccarelli EA, Roise D, Allison WS, Inhibition of the bovine-heart mitochondrial F1-ATPase by cationic dyes and amphipathic peptides. *Biochim Biophys Acta* 1989, 975(3):377-383.

82. Zhuo S, Paik SR, Register JA, Allison WS, Photoinactivation of the bovine heart mitochondrial F1-ATPase by [14C]dequalinium cross-links phenylalanine-403 or phenylalanine-406 of an alpha subunit to a site or sites contained within residues 440-459 of a beta subunit. *Biochemistry* 1993, 32(9):2219-2227.

83. Jackson PJ, Harris DA, Sites of protein-protein interaction on the mitochondrial F1-ATPase inhibitor protein. *Biochem J* 1986, 235(2):577-583.

84. Greene MD, Frasch WD, Interactions among gamma R268, gamma Q269, and the beta subunit catch loop of Escherichia coli F1-ATPase are important for catalytic activity. *J Biol Chem* 2003, 278(51):51594-51598.

85. Hausrath AC, Capaldi RA, Matthews BW, The conformation of the epsilon- and gamma-subunits within the Escherichia coli F(1) ATPase. *J Biol Chem* 2001, 276(50):47227-47232.

86. Sternweis PC, The epsilon subunit of Escherichia coli coupling factor 1 is required for its binding to the cytoplasmic membrane. *J Biol Chem* 1978, 253(9):3123-3128.

87. Sternweis PC, Smith JB, Characterization of the inhibitory (epsilon) subunit of the proton-translocating adenosine triphosphatase from Escherichia coli. *Biochemistry* 1980, 19(3):526-531.

88. Mendel-Hartvig J, Capaldi RA, Catalytic site nucleotide and inorganic phosphate dependence of the conformation of the epsilon subunit in Escherichia coli adenosinetriphosphatase. *Biochemistry* 1991, 30(5):1278-1284.

89. Mendel-Hartvig J, Capaldi RA, Nucleotide-dependent and dicyclohexylcarbodiimide-sensitive conformational changes in the epsilon subunit of *Escherichia coli* ATP synthase. *Biochemistry* 1991, 30(45):10987-10991.

90. Kuki M, Noumi T, Maeda M, Amemura A, Futai M, Functional domains of epsilon subunit of Escherichia coli H+-ATPase (F0F1). *J Biol Chem* 1988, 263(33):17437-17442.

91. Dunn SD, Zadorozny VD, Tozer RG, Orr LE, Epsilon subunit of Escherichia coli F1-ATPase: effects on affinity for aurovertin and inhibition of product release in unisite ATP hydrolysis. *Biochemistry* 1987, 26(14):4488-4493.

92. Aggeler R, Ogilvie I, Capaldi RA, Rotation of a gamma-epsilon subunit domain in the Escherichia coli F1F0-ATP synthase complex. The gamma-epsilon subunits are essentially randomly distributed relative to the alpha3beta3delta domain in the intact complex. *J Biol Chem* 1997, 272(31):19621-19624.

93. Tozer RG, Dunn SD, The epsilon subunit and inhibitory monoclonal antibodies interact with the carboxyl-terminal region of the beta subunit of Escherichia coli F1-ATPase. *J Biol Chem* 1987, 262(22):10706-10711.

94. Bragg PD, Hou C, Role of minor subunits in the structural asymmetry of the Escherichia coli F1-ATPase. *Biochem Biophys Res Commun* 1990, 166(1):431-435.

95. Cox GB, Cromer BA, Guss JM, Harvey I, Jeffrey PD, Solomon RG, Webb DC, Formation in vivo, purification and crystallization of a complex of the gamma and epsilon subunits of the F0F1-ATPase of Escherichia coli. *J Mol Biol* 1993, 229(4):1159-1162.

96. Tang C, Capaldi RA, Characterization of the interface between gamma and epsilon subunits of *Escherichia coli* F_1-ATPase. *J Biol Chem* 1996, 271(6):3018-3024.

97. Sawada K, Watanabe H, Moritani-Otsuka C, Kanazawa H, Subunit interactions of Escherichia coli F1-ATPase: mutants of the gamma subunits defective in interaction with the epsilon subunit isolated by the yeast two-hybrid system. *Arch Biochem Biophys* 1997, 348(1):183-189.

98. Zhang Y, Oldenburg M, Fillingame RH, Suppressor mutations in F1 subunit epsilon recouple ATP-driven H+ translocation in uncoupled Q42E subunit c mutant of Escherichia coli F1F0 ATP synthase. *J Biol Chem* 1994, 269(14):10221-10224.

99. Zhang Y, Fillingame RH, Subunits coupling H+ transport and ATP synthesis in the *Escherichia coli* ATP synthase. Cys-Cys cross-linking of F_1 subunit epsilon to the polar loop of F_0 subunit *c*. *J Biol Chem* 1995, 270(41):24609-24614.

100. Cipriano DJ, Bi Y, Dunn SD, Genetic fusions of globular proteins to the epsilon subunit of the Escherichia coli ATP synthase: Implications for in vivo rotational catalysis and epsilon subunit function. *J Biol Chem* 2002, 277(19):16782-16790.

101. Rodgers AJ, Wilce MC, Structure of the gamma-epsilon complex of ATP synthase. *Nat Struct Biol* 2000, 7(11):1051-1054.

102. Tsunoda SP, Rodgers AJ, Aggeler R, Wilce MC, Yoshida M, Capaldi RA, Large conformational changes of the epsilon subunit in the bacterial F1F0 ATP synthase provide a ratchet action to regulate this rotary motor enzyme. *Proc Natl Acad Sci U S A* 2001, 98(12):6560-6564.

103. Capaldi RA, Aggeler R, Wilkens S, Gruber G, Structural changes in the gamma and epsilon subunits of the Escherichia coli F1F0-type ATPase during energy coupling. *J Bioenerg Biomembr* 1996, 28(5):397-401.

104. Harris DA, Das AM, Control of mitochondrial ATP synthesis in the heart. *Biochem J* 1991, 280 (Pt 3):561-573.

105. Jiang W, Hermolin J, Fillingame RH, The preferred stoichiometry of c subunits in the rotary motor sector of Escherichia coli ATP synthase is 10. *Proc Natl Acad Sci U S A* 2001, 98(9):4966-4971.

106. Hoppe J, Brunner J, Jorgensen BB, Structure of the membrane-embedded F0 part of F1F0 ATP synthase from Escherichia coli as inferred from labeling with 3-(Trifluoromethyl)-3-(m-[125I]iodophenyl)diazirine. *Biochemistry* 1984, 23(23):5610-5616.

107. Girvin ME, Hermolin J, Pottorf R, Fillingame RH, Organization of the F0 sector of Escherichia coli H+-ATPase: the polar loop region of subunit c extends from the cytoplasmic face of the membrane. *Biochemistry* 1989, 28(10):4340-4343.

108. Hensel M, Deckers-Hebestreit G, Schmid R, Altendorf K, Orientation of subunit c of the ATP synthase of Escherichia coli--a study with peptide-specific antibodies. *Biochim Biophys Acta* 1990, 1016(1):63-70.

109. Hoppe J, Schairer HU, Sebald W, Identification of amino-acid substitutions in the proteolipid subunit of the ATP synthase from dicyclohexylcarbodiimide-resistant mutants of Escherichia coli. *Eur J Biochem* 1980, 112(1):17-24.

110. Fillingame RH, Oldenburg M, Fraga D, Mutation of alanine 24 to serine in subunit c of the Escherichia coli F1F0-ATP synthase reduces reactivity of aspartyl 61 with dicyclohexylcarbodiimide. *J Biol Chem* 1991, 266(31):20934-20939.

111. Miller MJ, Oldenburg M, Fillingame RH, The essential carboxyl group in subunit c of the F1F0 ATP synthase can be moved and H(+)-translocating function retained. *Proc Natl Acad Sci U S A* 1990, 87(13):4900-4904.

112. Hermolin J, Fillingame RH, H+-ATPase activity of *Escherichia coli* F_1F_0 is blocked after reaction of dicyclohexylcarbodiimide with a single proteolipid (subunit *c*) of the F_0 complex. *J Biol Chem* 1989, 264(7):3896-3903.

113. Dmitriev OY, Altendorf K, Fillingame RH, Reconstitution of the Fo complex of Escherichia coli ATP synthase from isolated subunits. Varying the number of essential carboxylates by co-incorporation of wild-type and mutant subunit c after purification in organic solvent. *Eur J Biochem* 1995, 233(2):478-483.

114. Fraga D, Fillingame RH, Conserved polar loop region of Escherichia coli subunit c of the F1F0 H+-ATPase. Glutamine 42 is not absolutely essential, but substitutions alter binding and coupling of F1 to F0. *J Biol Chem* 1989, 264(12):6797-6803.

115. Fraga D, Fillingame RH, Essential residues in the polar loop region of subunit c of Escherichia coli F1F0 ATP synthase defined by random oligonucleotide-primed mutagenesis. *J Bacteriol* 1991, 173(8):2639-2643.

116. Fraga D, Hermolin J, Fillingame RH, Transmembrane helix-helix interactions in F0 suggested by suppressor mutations to Ala24-->Asp/Asp61-->Gly mutant of ATP synthase subunit. *J Biol Chem* 1994, 269(4):2562-2567.

117. Miller MJ, Fraga D, Paule CR, Fillingame RH, Mutations in the conserved proline 43 residue of the uncE protein (subunit c) of Escherichia coli F1F0-ATPase alter the coupling of F1 to F0. *J Biol Chem* 1989, 264(1):305-311.

118. Watts SD, Zhang Y, Fillingame RH, Capaldi RA, The gamma subunit in the Escherichia coli ATP synthase complex (ECF1F0) extends through the stalk and contacts the c subunits of the F0 part. *FEBS Lett* 1995, 368(2):235-238.

119. Fillingame RH, Subunit c of F1F0 ATP synthase: structure and role in transmembrane energy transduction. *Biochim Biophys Acta* 1992, 1101(2):240-243.

120. Fillingame RH, H+ transport and coupling by the F0 sector of the ATP synthase: insights into the molecular mechanism of function. *J Bioenerg Biomembr* 1992, 24(5):485-491.

121. Hatch LP, Cox GB, Howitt SM, The essential arginine residue at position 210 in the alpha subunit of the Escherichia coli ATP synthase can be transferred to position 252 with partial retention of activity. *J Biol Chem* 1995, 270(49):29407-29412.

122. Girvin ME, Rastogi VK, Abildgaard F, Markley JL, Fillingame RH, Solution structure of the transmembrane H+-transporting subunit *c* of the F_1F_0 ATP synthase. *Biochemistry* 1998, 37(25):8817-8824.

123. Jones PC, Fillingame RH, Genetic fusions of subunit c in the F0 sector of H+-transporting ATP synthase. Functional dimers and trimers and determination of stoichiometry by cross-linking analysis. *J Biol Chem* 1998, 273(45):29701-29705.

124. Jones PC, Jiang W, Fillingame RH, Arrangement of the multicopy H+-translocating subunit c in the membrane sector of the Escherichia coli F1F0 ATP synthase. *J Biol Chem* 1998, 273(27):17178-17185.

125. Assadi-Porter FM, Fillingame RH, Proton-translocating carboxyl of subunit c of F1Fo H(+)-ATP synthase: the unique environment suggested by the pKa determined by 1H NMR. *Biochemistry* 1995, 34(49):16186-16193.

126. Singh S, Turina P, Bustamante CJ, Keller DJ, Capaldi R, Topographical structure of membrane-bound *Escherichia coli* F_1F_0 ATP synthase in aqueous buffer. *FEBS Lett* 1996, 397(1):30-34.

127. Wilkens S, Dunn SD, Capaldi RA, A cryoelectron microscopy study of the interaction of the *Escherichia coli* F_1-ATPase with subunit *b* dimer. *FEBS Lett* 1994, 354(1):37-40.

128. Girvin ME, Fillingame RH, Helical structure and folding of subunit c of F1F0 ATP synthase: 1H NMR resonance assignments and NOE analysis. *Biochemistry* 1993, 32(45):12167-12177.

129. Girvin ME, Fillingame RH, Hairpin folding of subunit c of F1Fo ATP synthase: 1H distance measurements to nitroxide-derivatized aspartyl-61. *Biochemistry* 1994, 33(3):665-674.

130. Girvin ME, Fillingame RH, Determination of local protein structure by spin label difference 2D NMR: the region neighboring Asp61 of subunit c of the F1F0 ATP synthase. *Biochemistry* 1995, 34(5):1635-1645.

131. von Ballmoos C, Meier T, Dimroth P, Membrane embedded location of Na+ or H+ binding sites on the rotor ring of F1F0 ATP synthases. *Eur J Biochem* 2002, 269(22):5581-5589.

132. Fillingame RH, Jones PC, Jiang W, Valiyaveetil FI, Dmitriev OY, Subunit organization and structure in the F_0 sector of *Escherichia coli* F_1F_0 ATP synthase. *Biochim Biophys Acta* 1998, 1365(1-2):135-142.

133. Ruppert C, Kavermann H, Wimmers S, Schmid R, Kellermann J, Lottspeich F, Huber H, Stetter KO, Muller V, The proteolipid of the A(1)A(0) ATP synthase from Methanococcus jannaschii has six predicted transmembrane helices but only

two proton-translocating carboxyl groups. *J Biol Chem* 1999, 274(36):25281-25284.

134. Kashket ER, Stoichiometry of the H+-ATPase of growing and resting, aerobic Escherichia coli. *Biochemistry* 1982, 21(22):5534-5538.

135. Lehninger AL, Nelson DL, Cox MM, Lehninger principles of biochemistry. In., 3rd edn. New York: Worth Publishers; 2000.

136. Dmitriev O, Jones PC, Jiang W, Fillingame RH, Structure of the membrane domain of subunit *b* of the *Escherichia coli* F_0F_1 ATP synthase. *J Biol Chem* 1999, 274(22):15598-15604.

137. Wilkens S, Dunn SD, Chandler J, Dahlquist FW, Capaldi RA, Solution structure of the N-terminal domain of the delta subunit of the *E. coli* ATPsynthase [letter]. *Nat Struct Biol* 1997, 4(3):198-201.

138. Del Rizzo PA, Bi Y, Dunn SD, Shilton BH, The "second stalk" of Escherichia coli ATP synthase: structure of the isolated dimerization domain. *Biochemistry* 2002, 41(21):6875-6884.

139. Sternweis PC, Smith JB, Characterization of the purified membrane attachment (beta) subunit of the proton translocating adenosine triphosphatase from Escherichia coli. *Biochemistry* 1977, 16(18):4020-4025.

140. Fillingame RH, Molecular Mechanics of ATP Synthesis by F_1F_0-Type H+-Transporting ATP Synthases. In: *The Bacteria.* Edited by Krulwich TA, vol. XII. New York: Academic Press; 1990: 345-391.

141. Prescott M, Nowakowski S, Gavin P, Nagley P, Whisstock JC, Devenish RJ, Subunit gamma-green fluorescent protein fusions are functionally incorporated into mitochondrial F1F0-ATP synthase, arguing against a rigid cap structure at the top of F1. *J Biol Chem* 2003, 278(1):251-256.

142. Weber J, Wilke-Mounts S, Senior AE, Identification of the F1-binding surface on the delta-subunit of ATP synthase. *J Biol Chem* 2003.

143. Weber J, Muharemagic A, Wilke-Mounts S, Senior AE, F1Fo-ATP synthase: Binding of delta subunit to a 22-residue peptide mimicking the N-terminal region of alpha subunit. *J Biol Chem* 2003.

144. Hartzog PE, Cain BD, Second-site suppressor mutations at glycine 218 and histidine 245 in the alpha subunit of F_1F_0 ATP synthase in *Escherichia coli*. *J Biol Chem* 1994, 269(51):32313-32317.

145. Lightowlers RN, Howitt SM, Hatch L, Gibson F, Cox GB, The proton pore in the *Escherichia coli* F_0F_1-ATPase: a requirement for arginine at position 210 of the *a* subunit. *Biochim Biophys Acta* 1987, 894(3):399-406.

146. Cain BD, Simoni RD, Proton translocation by the F_1F_0 ATPase of *Escherichia coli*. Mutagenic analysis of the *a* subunit. *J Biol Chem* 1989, 264(6):3292-3300.

147. Eya S, Maeda M, Futai M, Role of the carboxyl terminal region of H(+)-ATPase (F0F1) a subunit from Escherichia coli. *Arch Biochem Biophys* 1991, 284(1):71-77.

148. Schneider E, Altendorf K, All three subunits are required for the reconstitution of an active proton channel (F0) of Escherichia coli ATP synthase (F1F0). *Embo J* 1985, 4(2):515-518.

149. von Meyenburg K, Jorgensen BB, Michelsen O, Sorensen L, McCarthy JE, Proton conduction by subunit a of the membrane-bound ATP synthase of Escherichia coli revealed after induced overproduction. *Embo J* 1985, 4(9):2357-2363.

150. Hermolin J, Fillingame RH, Assembly of F_0 sector of *Escherichia coli* H+ ATP synthase. Interdependence of subunit insertion into the membrane. *J Biol Chem* 1995, 270(6):2815-2817.

151. Akiyama Y, Kihara A, Ito K, Subunit a of proton ATPase F0 sector is a substrate of the FtsH protease in Escherichia coli. *FEBS Lett* 1996, 399(1-2):26-28.

152. Vik SB, Dao NN, Prediction of transmembrane topology of F0 proteins from Escherichia coli F1F0 ATP synthase using variational and hydrophobic moment analyses. *Biochim Biophys Acta* 1992, 1140(2):199-207.

153. Wang S, Vik SB, Single amino acid insertions probe the alpha subunit of the Escherichia coli F1F0-ATP synthase. *J Biol Chem* 1994, 269(4):3095-3099.

154. Valiyaveetil FI, Fillingame RH, Transmembrane topography of subunit *a* in the *Escherichia coli* F_1F_0 ATP synthase. *J Biol Chem* 1998, 273(26):16241-16247.

155. Long JC, Wang S, Vik SB, Membrane topology of subunit *a* of the F_1F_0 ATP synthase as determined by labeling of unique cysteine residues. *J Biol Chem* 1998, 273(26):16235-16240.

156. Wada T, Long JC, Zhang D, Vik SB, A novel labeling approach supports the five-transmembrane model of subunit *a* of the *Escherichia coli* ATP synthase. *J Biol Chem* 1999, 274(24):17353-17357.

157. Jiang W, Fillingame RH, Interacting helical faces of subunits *a* and *c* in the F_1F_0 ATP synthase of *Escherichia coli* defined by disulfide cross-linking. *Proc Natl Acad Sci U S A* 1998, 95(12):6607-6612.

158. Patterson AR, Wada T, Vik SB, His(15) of subunit a of the Escherichia coli ATP synthase is important for the structure or assembly of the membrane sector F(o). *Arch Biochem Biophys* 1999, 368(1):193-197.

159. Vik SB, Long JC, Wada T, Zhang D, A model for the structure of subunit a of the Escherichia coli ATP synthase and its role in proton translocation. *Biochim Biophys Acta* 2000, 1458(2-3):457-466.

160. Jager H, Birkenhager R, Stalz WD, Altendorf K, Deckers-Hebestreit G, Topology of subunit a of the Escherichia coli ATP synthase. *Eur J Biochem* 1998, 251(1-2):122-132.

161. Lewis MJ, Chang JA, Simoni RD, A topological analysis of subunit alpha from Escherichia coli F1F0-ATP synthase predicts eight transmembrane segments. *J Biol Chem* 1990, 265(18):10541-10550.

162. Yamada H, Moriyama Y, Maeda M, Futai M, Transmembrane topology of Escherichia coli H(+)-ATPase (ATP synthase) subunit a. *FEBS Lett* 1996, 390(1):34-38.

163. Lewis MJ, Simoni RD, Deletions in hydrophilic domains of subunit a from the Escherichia coli F1F0-ATP synthase interfere with membrane insertion or F0 assembly. *J Biol Chem* 1992, 267(5):3482-3489.

164. Vik SB, Lee D, Marshall PA, Temperature-sensitive mutations at the carboxy terminus of the alpha subunit of the Escherichia coli F1F0 ATP synthase. *J Bacteriol* 1991, 173(14):4544-4548.

165. Cain BD, Simoni RD, Impaired proton conductivity resulting from mutations in the a subunit of F_1F_0 ATPase in *Escherichia coli*. *J Biol Chem* 1986, 261(22):10043-10050.

166. Cain BD, Mutagenic analysis of the F0 stator subunits. *J Bioenerg Biomembr* 2000, 32(4):365-371.

167. Gardner JL, Cain BD, Amino acid substitutions in the *a* subunit affect the epsilon subunit of F_1F_0 ATP synthase from *Escherichia coli*. *Arch Biochem Biophys* 1999, 361(2):302-308.

168. Valiyaveetil FI, Fillingame RH, On the role of Arg-210 and Glu-219 of subunit *a* in proton translocation by the *Escherichia coli* F_0F_1-ATP synthase. *J Biol Chem* 1997, 272(51):32635-32641.

169. Rastogi VK, Girvin ME, Structural changes linked to proton translocation by subunit *c* of the ATP synthase [see comments]. *Nature* 1999, 402(6759):263-268.

170. Hatch LP, Cox GB, Howitt SM, Glutamate residues at positions 219 and 252 in the a-subunit of the Escherichia coli ATP synthase are not functionally equivalent. *Biochim Biophys Acta* 1998, 1363(3):217-223.

171. Cain BD, Simoni RD, Interaction between Glu-219 and His-245 within the a subunit of F1F0-ATPase in Escherichia coli. *J Biol Chem* 1988, 263(14):6606-6612.

172. Hartzog PE, Cain BD, Mutagenic analysis of the a subunit of the F1F0 ATP synthase in Escherichia coli: Gln-252 through Tyr-263. *J Bacteriol* 1993, 175(5):1337-1343.

173. Kuo PH, Nakamoto RK, Intragenic and intergenic suppression of the Escherichia coli ATP synthase subunit a mutation of Gly-213 to Asn: functional interactions between residues in the proton transport site. *Biochem J* 2000, 347 Pt 3:797-805.

174. Angevine CM, Herold KA, Fillingame RH, Aqueous access pathways in subunit a of rotary ATP synthase extend to both sides of the membrane. *Proc Natl Acad Sci U S A* 2003, 100(23):13179-13183.

175. Smith JB, Sternweis PC, Heppel LA, Partial purification of active delta and epsilon subunits of the membrane ATPase from escherichia coli. *J Supramol Struct* 1975, 3(3):248-255.

176. Angov E, Ng TC, Brusilow WS, Effect of the delta subunit on assembly and proton permeability of the F0 proton channel of Escherichia coli F1F0 ATPase. *J Bacteriol* 1991, 173(1):407-411.

177. Jounouchi M, Takeyama M, Chaiprasert P, Noumi T, Moriyama Y, Maeda M, Futai M, Escherichia coli H(+)-ATPase: role of the delta subunit in binding Fl to the Fo sector. *Arch Biochem Biophys* 1992, 292(2):376-381.

178. Stack AE, Cain BD, Mutations in the delta subunit influence the assembly of F_1F_0 ATP synthase in *Escherichia coli*. *J Bacteriol* 1994, 176(2):540-542.

179. Hazard AL, Senior AE, Mutagenesis of subunit delta from Escherichia coli F1F0-ATP synthase. *J Biol Chem* 1994, 269(1):418-426.

180. Hazard AL, Senior AE, Defective energy coupling in delta-subunit mutants of Escherichia coli F1F0-ATP synthase. *J Biol Chem* 1994, 269(1):427-432.

181. Tozer RG, Dunn SD, Column centrifugation generates an intersubunit disulfide bridge in Escherichia coli F1-ATPase. *Eur J Biochem* 1986, 161(2):513-518.

182. Bragg PD, Hou C, Effect of disulfide cross-linking between alpha and delta subunits on the properties of the F1 adenosine triphosphatase of Escherichia coli. *Biochim Biophys Acta* 1986, 851(3):385-394.

183. Bragg PD, Hou C, Chemical crosslinking of alpha subunits in the F1 adenosine triphosphatase of Escherichia coli. *Arch Biochem Biophys* 1986, 244(1):361-372.

184. Lill H, Hensel F, Junge W, Engelbrecht S, Cross-linking of engineered subunit δ to $(\alpha\beta)_3$ in chloroplast F-ATPase. *J Biol Chem* 1996, 271(51):32737-32742.

185. Ogilvie I, Aggeler R, Capaldi RA, Cross-linking of the delta subunit to one of the three alpha subunits has no effect on functioning, as expected if delta is a part of the stator that links the F_1 and F_0 parts of the *Escherichia coli* ATP synthase. *J Biol Chem* 1997, 272(26):16652-16656.

186. Bottcher B, Bertsche I, Reuter R, Graber P, Direct visualisation of conformational changes in EF(0)F(1) by electron microscopy. *J Mol Biol* 2000, 296(2):449-457.

187. Wilkens S, Zhou J, Nakayama R, Dunn SD, Capaldi RA, Localization of the delta subunit in the *Escherichia coli* F_1F_0 ATPsynthase by immuno electron microscopy: the delta subunit binds on top of the F_1. *J Mol Biol* 2000, 295(3):387-391.

188. Ormo M, Cubitt AB, Kallio K, Gross LA, Tsien RY, Remington SJ, Crystal structure of the Aequorea victoria green fluorescent protein. *Science* 1996, 273(5280):1392-1395.

189. Weber J, Senior AE, ATP synthesis driven by proton transport in F1F0-ATP synthase. *FEBS Lett* 2003, 545(1):61-70.

190. Schneider E, Altendorf K, Subunit b of the membrane moiety (F0) of ATP synthase (F1F0) from Escherichia coli is indispensable for H+ translocation and binding of the water-soluble F1 moiety. *Proc Natl Acad Sci U S A* 1984, 81(23):7279-7283.

191. Walker JE, Saraste M, Gay NJ, *E. coli* F_1-ATPase interacts with a membrane protein component of a proton channel. *Nature* 1982, 298(5877):867-869.

192. Revington M, McLachlin DT, Shaw GS, Dunn SD, The dimerization domain of the *b* subunit of the *Escherichia coli* F_1F_0-ATPase. *J Biol Chem* 1999, 274(43):31094-31101.

193. Sorgen PL, Bubb MR, Cain BD, Lengthening the second stalk of F_1F_0 ATP synthase in *Escherichia coli*. *J Biol Chem* 1999, 274(51):36261-36266.

194. Sorgen PL, Caviston TL, Perry RC, Cain BD, Deletions in the second stalk of F_1F_0-ATP synthase in *Escherichia coli*. *J Biol Chem* 1998, 273(43):27873-27878.

195. Grabar TB, Cain BD, Integration of b subunits of unequal lengths into F1F0-ATP synthase. *J Biol Chem* 2003, 278(37):34751-34756.

196. Greie JC, Deckers-Hebestreit G, Altendorf K, Secondary structure composition of reconstituted subunit b of the Escherichia coli ATP synthase. *Eur J Biochem* 2000, 267(10):3040-3048.

197. Dunn SD, The polar domain of the *b* subunit of *Escherichia coli* F_1F_0-ATPase forms an elongated dimer that interacts with the F_1 sector. *J Biol Chem* 1992, 267(11):7630-7636.

198. Rodgers AJ, Capaldi RA, The second stalk composed of the *b*- and delta-subunits connects F_0 to F_1 via an alpha-subunit in the *Escherichia coli* ATP synthase. *J Biol Chem* 1998, 273(45):29406-29410.

199. Sorgen PL, Bubb MR, McCormick KA, Edison AS, Cain BD, Formation of the *b* subunit dimer is necessary for interaction with F_1- ATPase. *Biochemistry* 1998, 37(3):923-932.

200. Rodgers AJ, Wilkens S, Aggeler R, Morris MB, Howitt SM, Capaldi RA, The subunit delta-subunit *b* domain of the *Escherichia coli* F_1F_0 ATPase. The *b* subunits interact with F_1 as a dimer and through the delta subunit. *J Biol Chem* 1997, 272(49):31058-31064.

201. Hoppe J, Montecucco C, Friedl P, Labeling of subunit b of the ATP synthase from Escherichia coli with a photoreactive phospholipid analogue. *J Biol Chem* 1983, 258(5):2882-2885.

202. Hardy AW, Grabar TB, Bhatt D, Cain BD, Mutagenesis studies of the F1F0 ATP synthase b subunit membrane domain. *J Bioenerg Biomembr* 2003, 35(5):389-397.

203. McCormick KA, Deckers-Hebestreit G, Altendorf K, Cain BD, Characterization of mutations in the *b* subunit of F_1F_0 ATP synthase in *Escherichia coli*. *J Biol Chem* 1993, 268(33):24683-24691.

204. Revington M, Dunn SD, Shaw GS, Folding and stability of the b subunit of the F(1)F(0) ATP synthase. *Protein Sci* 2002, 11(5):1227-1238.

205. McLachlin DT, Bestard JA, Dunn SD, The *b* and δ subunits of the *Escherichia coli* ATP synthase interact via residues in their C-terminal regions. *J Biol Chem* 1998, 273(24):15162-15168.

206. Takeyama M, Noumi T, Maeda M, Futai M, F_0 portion of *Escherichia coli* H+-ATPase. Carboxyl-terminal region of the *b* subunit is essential for assembly of functional F_0. *J Biol Chem* 1988, 263(31):16106-16112.

207. McLachlin DT, Dunn SD, Dimerization interactions of the *b* subunit of the *Escherichia coli* F_1F_0-ATPase. *J Biol Chem* 1997, 272(34):21233-21239.

208. Dunn SD, Bi Y, Revington M, A re-examination of the structural and functional consequences of mutation of alanine-128 of the b subunit of Escherichia coli ATP synthase to aspartic acid. *Biochim Biophys Acta* 2000, 1459(2-3):521-527.

209. Porter AC, Kumamoto C, Aldape K, Simoni RD, Role of the *b* subunit of the *Escherichia coli* proton-translocating ATPase. A mutagenic analysis. *J Biol Chem* 1985, 260(13):8182-8187.

210. Kumamoto CA, Simoni RD, Genetic evidence for interaction between the a and b subunits of the F0 portion of the Escherichia coli proton translocating ATPase. *J Biol Chem* 1986, 261(22):10037-10042.

211. Kumamoto CA, Simoni RD, A mutation of the c subunit of the Escherichia coli proton-translocating ATPase that suppresses the effects of a mutant b subunit. *J Biol Chem* 1987, 262(7):3060-3064.

212. Cox GB, Fimmel AL, Gibson F, Hatch L, The mechanism of ATP synthase: a reassessment of the functions of the b and a subunits. *Biochim Biophys Acta* 1986, 849(1):62-69.

213. Tiburzy HJ, Berzborn RJ, Subunit II (b') and not subunit I (b) of photosynthetic ATP synthases is equivalent to subunit b of the ATP synthases from nonphotosynthetic eubacteria. Evidence for a new assignment of b-type F0 subunits. *Z Naturforsch [C]* 1997, 52(11-12):789-798.

214. Blair A, Ngo L, Park J, Paulsen IT, Saier MH, Jr., Phylogenetic analyses of the homologous transmembrane channel-forming proteins of the F0F1-ATPases of bacteria, chloroplasts and mitochondria. *Microbiology* 1996, 142 (Pt 1):17-32.

215. Caviston TL, Ketchum CJ, Sorgen PL, Nakamoto RK, Cain BD, Identification of an uncoupling mutation affecting the b subunit of F1F0 ATP synthase in Escherichia coli. *FEBS Lett* 1998, 429(2):201-206.

216. McLachlin DT, Coveny AM, Clark SM, Dunn SD, Site-directed cross-linking of *b* to the alpha, beta, and a subunits of the *Escherichia coli* ATP synthase. *J Biol Chem* 2000, 275(23):17571-17577.

217. Long JC, DeLeon-Rangel J, Vik SB, Characterization of the first cytoplasmic loop of subunit a of the Escherichia coli ATP synthase by surface labeling, cross-linking, and mutagenesis. *J Biol Chem* 2002, 277(30):27288-27293.

218. McCormick KA, Cain BD, Targeted mutagenesis of the *b* subunit of F_1F_0 ATP synthase in *Escherichia coli*: Glu-77 through Gln-85. *J Bacteriol* 1991, 173(22):7240-7248.

219. Sawada K, Kuroda N, Watanabe H, Moritani-Otsuka C, Kanazawa H, Interaction of the delta and *b* subunits contributes to F_1 and F_0 interaction in the *Escherichia coli* F_1F_0-ATPase. *J Biol Chem* 1997, 272(48):30047-30053.

220. Dunn SD, Chandler J, Characterization of a $b_2$delta complex from *Escherichia coli* ATP synthase. *J Biol Chem* 1998, 273(15):8646-8651.

221. McLachlin DT, Dunn SD, Disulfide linkage of the b and delta subunits does not affect the function of the Escherichia coli ATP synthase. *Biochemistry* 2000, 39(12):3486-3490.

222. Cherepanov DA, Mulkidjanian AY, Junge W, Transient accumulation of elastic energy in proton translocating ATP synthase. *FEBS Lett* 1999, 449(1):1-6.

223. Kersten MV, Dunn SD, Wise JG, Vogel PD, Site-directed spin-labeling of the catalytic sites yields insight into structural changes within the F_0F_1-ATP synthase of *Escherichia coli*. *Biochemistry* 2000, 39(13):3856-3860.

224. Walker JE, Saraste M, Gay NJ, The *unc* operon. Nucleotide sequence, regulation and structure of ATP- synthase. *Biochim Biophys Acta* 1984, 768(2):164-200.

225. Dunn SD, Heppel LA, Properties and functions of the subunits of the Escherichia coli coupling factor ATPase. *Arch Biochem Biophys* 1981, 210(2):421-436.

226. Schneider E, Altendorf K, Bacterial adenosine 5'-triphosphate synthase (F1F0): purification and reconstitution of F0 complexes and biochemical and functional characterization of their subunits. *Microbiol Rev* 1987, 51(4):477-497.

227. Fromme P, Graber, P., Salnikow, J., *FEBS Lett* 1987, 218:27-30.

228. Collinson IR, Fearnley IM, Skehel JM, Runswick MJ, Walker JE, ATP synthase from bovine heart mitochondria: identification by proteolysis of sites in F0 exposed by removal of F1 and the oligomycin-sensitivity conferral protein. *Biochem J* 1994, 303 (Pt 2):639-645.

229. Walker JE, Collinson IR, The role of the stalk in the coupling mechanism of F1F0-ATPases. *FEBS Lett* 1994, 346(1):39-43.

230. Lutter R, Saraste M, van Walraven HS, Runswick MJ, Finel M, Deatherage JF, Walker JE, F1F0-ATP synthase from bovine heart mitochondria: development of the purification of a monodisperse oligomycin-sensitive ATPase. *Biochem J* 1993, 295 (Pt 3):799-806.

231. Miki J, Maeda M, Mukohata Y, Futai M, The gamma-subunit of ATP synthase from spinach chloroplasts. Primary structure deduced from the cloned cDNA sequence. *FEBS Lett* 1988, 232(1):221-226.

232. Nalin CM, McCarty RE, Role of a disulfide bond in the gamma subunit in activation of the ATPase of chloroplast coupling factor 1. *J Biol Chem* 1984, 259(11):7275-7280.

233. Pan W, Ko YH, Pedersen PL, Delta subunit of rat liver mitochondrial ATP synthase: molecular description and novel insights into the nature of its association with the F1-moiety. *Biochemistry* 1998, 37(19):6911-6923.

234. Walker JE, Fearnley IM, Gay NJ, Gibson BW, Northrop FD, Powell SJ, Runswick MJ, Saraste M, Tybulewicz VL, Primary structure and subunit stoichiometry of F1-ATPase from bovine mitochondria. *J Mol Biol* 1985, 184(4):677-701.

235. Ovchinnikov Yu A, Modyanov NN, Grinkevich VA, Aldanova NA, Kostetsky PV, Trubetskaya OE, Hundal T, Ernster L, Oligomycin sensitivity-conferring protein (OSCP) of beef heart mitochondria. Internal sequence homology and structural relationship with other proteins. *FEBS Lett* 1984, 175(1):109-112.

236. Ovchinnikov YA, Modyanov NN, Grinkevich VA, Aldanova NA, Trubetskaya OE, Nazimov IV, Hundal T, Ernster L, Amino acid sequence of the oligomycin sensitivity-conferring protein (OSCP) of beef-heart mitochondria and its homology with the delta-subunit of the F1-ATPase of Escherichia coli. *FEBS Lett* 1984, 166(1):19-22.

237. Uh M, Jones D, Mueller DM, The gene coding for the yeast oligomycin sensitivity-conferring protein. *J Biol Chem* 1990, 265(31):19047-19052.

238. Van Walraven HS, Lutter R, Walker JE, Organization and sequences of genes for the subunits of ATP synthase in the thermophilic cyanobacterium Synechococcus 6716. *Biochem J* 1993, 294 (Pt 1):239-251.

239. Devenish RJ, Papakonstantinou T, Galanis M, Law RH, Linnane AW, Nagley P, Structure/function analysis of yeast mitochondrial ATP synthase subunit 8. *Ann N Y Acad Sci* 1992, 671:403-414.

240. Walker JE, Runswick MJ, Poulter L, ATP synthase from bovine mitochondria. The characterization and sequence analysis of two membrane-associated sub-units and of the corresponding cDNAs. *J Mol Biol* 1987, 197(1):89-100.

241. Walker JE, Lutter R, Dupuis A, Runswick MJ, Identification of the subunits of F1F0-ATPase from bovine heart mitochondria. *Biochemistry* 1991, 30(22):5369-5378.

242. Torok K, Joshi S, Cross-linking of bovine mitochondrial H+-ATPase by copper--o-phenanthroline. Interaction of the oligomycin-sensitivity-conferring protein with a 24-kDa protein. *Eur J Biochem* 1985, 153(1):155-159.

243. Houstek J, Kopecky J, Zanotti F, Guerrieri F, Jirillo E, Capozza G, Papa S, Topological and functional characterization of the F0I subunit of the membrane moiety of the mitochondrial H+-ATP synthase. *Eur J Biochem* 1988, 173(1):1-8.

244. Kimura T, Nakamura K, Kajiura H, Hattori H, Nelson N, Asahi T, Correspondence of minor subunits of plant mitochondrial F_1 ATPase to F_1F_0ATPase subunits of other organisms. *J Biol Chem* 1989, 264(6):3183-3186.

245. Manson MD, Tedesco P, Berg HC, Harold FM, Van der Drift C, A protonmotive force drives bacterial flagella. *Proc Natl Acad Sci U S A* 1977, 74(7):3060-3064.

246. Boyer PD, The binding change mechanism for ATP synthase--some probabilities and possibilities. *Biochim Biophys Acta* 1993, 1140(3):215-250.

247. Yasuda R, Noji H, Kinosita K, Jr., Yoshida M, F1-ATPase is a highly efficient molecular motor that rotates with discrete 120 degree steps. *Cell* 1998, 93(7):1117-1124.

248. Ariga T, Masaike T, Noji H, Yoshida M, Stepping rotation of F(1)-ATPase with one, two, or three altered catalytic sites that bind ATP only slowly. *J Biol Chem* 2002, 277(28):24870-24874.

249. Yasuda R, Noji H, Yoshida M, Kinosita K, Jr., Itoh H, Resolution of distinct rotational substeps by submillisecond kinetic analysis of F1-ATPase. *Nature* 2001, 410(6831):898-904.

250. Nagle JF, Tristram-Nagle S, Hydrogen bonded chain mechanisms for proton conduction and proton pumping. *J Membr Biol* 1983, 74(1):1-14.

251. Deckers-Hebestreit G, Altendorf K, The Fo complex of the proton-translocating F-type ATPase of Escherichia coli. *J Exp Biol* 1992, 172:451-459.

252. Dimroth P, Sodium ion transport decarboxylases and other aspects of sodium ion cycling in bacteria. *Microbiol Rev* 1987, 51(3):320-340.

253. Fillingame RH, Coupling H+ transport and ATP synthesis in F_1F_0-ATP synthases: glimpses of interacting parts in a dynamic molecular machine. *J Exp Biol* 1997, 200(Pt 2):217-224.

254. Junge W, ATP synthase and other motor proteins. *Proc Natl Acad Sci U S A* 1999, 96(9):4735-4737.

255. Vik SB, Antonio BJ, A mechanism of proton translocation by F1F0 ATP synthases suggested by double mutants of the a subunit. *J Biol Chem* 1994, 269(48):30364-30369.

256. Inesi G, Kirtley MR, Structural features of cation transport ATPases. *J Bioenerg Biomembr* 1992, 24(3):271-283.

257. Mosher ME, White LK, Hermolin J, Fillingame RH, H+-ATPase of Escherichia coli. An uncE mutation impairing coupling between F1 and Fo but not Fo-mediated H+ translocation. *J Biol Chem* 1985, 260(8):4807-4814.

258. Fraga D, Hermolin J, Oldenburg M, Miller MJ, Fillingame RH, Arginine 41 of subunit *c* of *Escherichia coli* H(+)-ATP synthase is essential in binding and coupling of F_1 to F_0. *J Biol Chem* 1994, 269(10):7532-7537.

259. Shin K, Nakamoto RK, Maeda M, Futai M, F0F1-ATPase gamma subunit mutations perturb the coupling between catalysis and transport. *J Biol Chem* 1992, 267(29):20835-20839.

260. Nakamoto RK, Maeda M, Futai M, The gamma subunit of the Escherichia coli ATP synthase. Mutations in the carboxyl-terminal region restore energy coupling to the amino-terminal mutant gamma Met-23-->Lys. *J Biol Chem* 1993, 268(2):867-872.

261. Nakamoto RK, al-Shawi MK, Futai M, The ATP synthase gamma subunit. Suppressor mutagenesis reveals three helical regions involved in energy coupling. *J Biol Chem* 1995, 270(23):14042-14046.

262. Dunn SD, Futai M, Reconstitution of a functional coupling factor from the isolated subunits of Escherichia coli F1 ATPase. *J Biol Chem* 1980, 255(1):113-118.

263. Boyer PD, A perspective of the binding change mechanism for ATP synthesis. *Faseb J* 1989, 3(10):2164-2178.

264. Futai M, Kanazawa H, Structure and function of proton-translocating adenosine triphosphatase (F_0F_1): biochemical and molecular biological approaches. *Microbiol Rev* 1983, 47(3):285-312.

265. Gibson F, Downie JA, Cox GB, Radik J, Mu-induced polarity in the *unc* operon of *Escherichia coli*. *J Bacteriol* 1978, 134(3):728-736.

266. Nielsen J, Jorgensen BB, van Meyenburg KV, Hansen FG, The promoters of the atp operon of *Escherichia coli* K12. *Mol Gen Genet* 1984, 193(1):64-71.

267. Kasimoglu E, Park SJ, Malek J, Tseng CP, Gunsalus RP, Transcriptional regulation of the proton-translocating ATPase (atpIBEFHAGDC) operon of Escherichia coli: control by cell growth rate. *J Bacteriol* 1996, 178(19):5563-5567.

268. McCarthy JE, Expression of the *unc* genes in *Escherichia coli*. *J Bioenerg Biomembr* 1988, 20(1):19-39.

269. Brusilow WS, Porter AC, Simoni RD, Cloning and expression of uncI, the first gene of the unc operon of Escherichia coli. *J Bacteriol* 1983, 155(3):1265-1270.

270. Brusilow WS, Assembly of the Escherichia coli F1F0 ATPase, a large multimeric membrane-bound enzyme. *Mol Microbiol* 1993, 9(3):419-424.

271. Aris JP, Klionsky DJ, Simoni RD, The F_0 subunits of the *Escherichia coli* F_1F_0-ATP synthase are sufficient to form a functional proton pore. *J Biol Chem* 1985, 260(20):11207-11215.

272. Cox GB, Jans, D., Fimmel, A., Gibson, F., Hatch, L., The role of the *b* subunit in the integrated assembly of the F_1F_0 ATP synthase. *Biochim Biophys Acta* 1984, 768:201-208.

273. Klionsky DJ, Brusilow WS, Simoni RD, In vivo evidence for the role of the epsilon subunit as an inhibitor of the proton-translocating ATPase of Escherichia coli. *J Bacteriol* 1984, 160(3):1055-1060.

274. Xiong H, Vik SB, Alanine-scanning mutagenesis of the epsilon subunit of the F1-F0 ATP synthase from Escherichia coli reveals two classes of mutants. *J Biol Chem* 1995, 270(40):23300-23304.

275. Xiong H, Vik SB, Construction and plasmid-borne complementation of strains lacking the epsilon subunit of the Escherichia coli F1F0 ATP synthase. *J Bacteriol* 1995, 177(3):851-853.

276. Xiong H, Zhang D, Vik SB, Subunit epsilon of the Escherichia coli ATP synthase: novel insights into structure and function by analysis of thirteen mutant forms. *Biochemistry* 1998, 37(46):16423-16429.

277. Pati S, Brusilow WS, Deckers-Hebestreit G, Altendorf K, Assembly of the F0 proton channel of the Escherichia coli F1F0 ATPase: low proton conductance of reconstituted Fo sectors synthesized and assembled in the absence of F1. *Biochemistry* 1991, 30(19):4710-4714.

278. Pati S, Brusilow WS, The roles of the alpha and gamma subunits in proton conduction through the Fo sector of the proton-translocating ATPase of Escherichia coli. *J Biol Chem* 1989, 264(5):2640-2644.

279. Monticello RA, Angov E, Brusilow WS, Effects of inducing expression of cloned genes for the F0 proton channel of the Escherichia coli F1F0 ATPase. *J Bacteriol* 1992, 174(10):3370-3376.

280. Grabar TB, Cain BD, Genetic complementation between mutant b subunits in F1F0 ATP synthase. *J Biol Chem* 2004.

281. Bulygin VV, Duncan TM, Cross RL, Rotation of the epsilon subunit during catalysis by Escherichia coli FOF1-ATP synthase. *J Biol Chem* 1998, 273(48):31765-31769.

282. Turina P, Structural changes during ATP hydrolysis activity of the ATP synthase from Escherichia coli as revealed by fluorescent probes. *J Bioenerg Biomembr* 2000, 32(4):373-381.

283. Altendorf K, Stalz W, Greie J, Deckers-Hebestreit G, Structure and function of the F(o) complex of the ATP synthase from Escherichia coli. *J Exp Biol* 2000, 203 Pt 1:19-28.

284. Deckers-Hebestreit G, Altendorf K, Accessibility of F_0 subunits from *Escherichia coli* ATP synthase. A study with subunit specific antisera. *Eur J Biochem* 1986, 161(1):225-231.

285. Deckers-Hebestreit G, Simoni RD, Altendorf K, Influence of subunit-specific antibodies on the activity of the F_0 complex of the ATP synthase of *Escherichia coli*. I. Effects of subunit *b*-specific polyclonal antibodies. *J Biol Chem* 1992, 267(17):12364-12369.

286. Markwell MA, Haas SM, Bieber LL, Tolbert NE, A modification of the Lowry procedure to simplify protein determination in membrane and lipoprotein samples. *Anal Biochem* 1978, 87(1):206-210.

287. Tamarappoo BK, Handlogten ME, Laine RO, Serrano MA, Dugan J, Kilberg MS, Identification of the protein responsible for hepatic system N amino acid transport activity. *J Biol Chem* 1992, 267(4):2370-2374.

288. McLachlin DT, Bestard JA, Dunn SD, The b and delta subunits of the Escherichia coli ATP synthase interact via residues in their C-terminal regions. *J Biol Chem* 1998, 273(24):15162-15168.

289. Smith PK, Krohn RI, Hermanson GT, Mallia AK, Gartner FH, Provenzano MD, Fujimoto EK, Goeke NM, Olson BJ, Klenk DC, Measurement of protein using bicinchoninic acid. *Anal Biochem* 1985, 150(1):76-85.

290. Boyer PD, The ATP synthase--a splendid molecular machine. *Annu Rev Biochem* 1997, 66:717-749.

291. Capaldi RA, Aggeler R, Mechanism of the F(1)F(0)-type ATP synthase, a biological rotary motor. *Trends Biochem Sci* 2002, 27(3):154-160.

292. Greie JC, Deckers-Hebestreit G, Altendorf K, Subunit organization of the stator part of the F0 complex from Escherichia coli ATP synthase. *J Bioenerg Biomembr* 2000, 32(4):357-364.

293. Ziegler M, Xiao R, Penefsky HS, Close proximity of Cys64 and Cys140 in the delta subunit of Escherichia coli F1-ATPase. *J Biol Chem* 1994, 269(6):4233-4239.

294. Vogel PD, Insights into ATP synthase structure and function using affinity and site-specific spin labeling. *J Bioenerg Biomembr* 2000, 32(4):413-421.

295. Berzborn RJ, Klein-Hitpass L, Otto J, Schunemann S, Oworah-Nkruma R, Meyer HE, The "additional subunit" CF0II of the photosynthetic ATP-synthase and the thylakoid polypeptide, binding ferredoxin NADP reductase: are they different? *Z Naturforsch [C]* 1990, 45(7-8):772-784.

296. Lill H, Steinemann D, Nelson N, Mutagenesis of the b'-subunit of Synechocystis sp. PCC 6803 ATP-synthase. *Biochim Biophys Acta* 1994, 1184(2-3):284-290.

297. Gardner JL, Cain BD, The *a* subunit ala-217 --> arg substitution affects catalytic activity of F_1F_0 ATP synthase. *Arch Biochem Biophys* 2000, 380(1):201-207.

BIOGRAPHICAL SKETCH

Tammy Weng Bohannon Grabar, daughter of William and Chu Shia Bohannon, was born in Altus, Oklahoma, on February 6, 1977. She lived in Okinawa, Japan, Patrick Air Force Base, Florida, Selfridge Air National Guard Base, Michigan, and Orange Park, Florida, before settling with her family in Melbourne, Florida. In her youth she participated in a variety of extracurricular activities and sports. She graduated in the top 1% of her class from Eau Gallie High School in June 1995. The following August she attended the University of Florida where she majored in microbiology. She received a Bachelor of Science degree with honors from the College of Agriculture in May 1999. During the summer of 1999 Tammy joined Dr. Brian Cain's laboratory in the Department of Biochemistry and Molecular Biology at the University of Florida to gain her first experiences in scientific research. The following Fall semester she was accepted to the University of Florida graduate program in the Department of Biochemistry and Molecular Biology. She joined the laboratory of Dr. Brian Cain in February 2000 where she began the work described in this dissertation. During her graduate career Tammy married her high school sweetheart and boyfriend of 11 years, Charles Raymond Grabar, Jr., on May 11, 2002. Their daughter, Kaia Mae Grabar, was born on August 16, 2003.